CELLULAR MECHANISMS OF G PROTEIN-COUPLED RECEPTOR SIGNALING IN THE MODULATION OF ANXIETY, FEAR, AND PAIN

by

Mee Jung Ko

A Dissertation

Submitted to the Faculty of Purdue University

In Partial Fulfillment of the Requirements for the degree of

Doctor of Philosophy

Department of Medicinal Chemistry and Molecular Pharmacology

West Lafayette, Indiana

May 2020

THE PURDUE UNIVERSITY GRADUATE SCHOOL
STATEMENT OF COMMITTEE APPROVAL

Dr. Richard M. van Rijn, Chair

Department of Medicinal Chemistry and Molecular Pharmacology

Dr. Julia A. Chester

Department of Psychological Sciences

Dr. Riyi Shi

Department of Basic Medical Sciences

Dr. Edward L. Bartlett

Department of Biomedical Engineering

Approved by:

Dr. Zhong-Yin Zhang

Head of the Graduate Program

To my parents,

without whose love, encouragement, support, and prayers,

none of these would have been possible.

ACKNOWLEDGMENTS

First and foremost, I would like to express my utmost gratitude to my Ph.D. mentor, Dr. Richard van Rijn for his endless support, guidance, and mentorship for the past four and a half years. With his support, I was able to overcome countless challenges that I encountered as a Ph.D. student. Not only has he been a great mentor to me, but he has taught me how to become a good mentor to others. I feel privileged to have him as my Ph.D. mentor, and I truly appreciate his support and guidance.

I am also grateful for my thesis committee members including Dr. Julia Chester, Dr. Riyi Shi, and Dr. Edward Bartlett for their guidance since I came to Purdue. Especially, I am very thankful for Dr. Chester's kind support and guidance for our collaboration.

It would have been much difficult for me to come this far without the support of my labmates and friends: Terrance Chiang, Dr. Meridith Robins, Dr. Doungkamol Alongkronrusmee, Robert Cassell, Anna Gutridge, Arryn Blaine, Dr. Alex French, Chelsea Theisen, Aswathy Chandran, and Saranya Radhakrishnan. I am thankful for their support and friendship.

I also acknowledge three students who helped me complete my research. Arbaaz Mukadam, Grace Mulia, and Angel Lin started as an undergraduate research assistant in Dr. van Rijn's lab respectively in 2016, 2017 and 2018. Without their help, I wouldn't have achieved this far or be a mentor of three wonderful students. From the perspective of teaching, I am also grateful to Dr. Jean-Christophe Rochet for giving me an opportunity to assist him for MCMP544 and to serve as a graduate teaching assistant where I gain substantial teaching experience.

Finally, without hesitation, I would like to express my deepest gratitude to my parents, Dr. Young Tae Ko and Yan Ja Woo, and my fiancé, Logan Ganzen, for their unconditional love, encouragement, support, inspiration, and prayers. Without them, none of these would have been possible.

TABLE OF CONTENTS

LIST OF TABLES

LIST OF FIGURES

LIST OF ABBREVIATIONS

AC	Adenylyl cyclase
AIP4	Atrophin 1-interacting protein 4
AITC	Allyl isothiocyanate
ANOVA	Analysis of Variance
AUC	Area under the curve
BLA	Basolateral amygdala
BNST	Bed nucleus of the stria terminalis
CaMKII	Ca^{2+}/calmodulin-dependent protein kinase II
cAMP	cyclic adenosine monophosphate
CaV	Voltage-dependent Ca2+ channels
CeA	Central amygdala
CFA	Complete Freund's Adjuvant
CGRP	Calcitonin gene related peptide
CHO	Chinese Hamster Ovarian
CREB	cAMP response element-binding protein
CS	Conditioned stimulus
DAG	Diacyl glycerol
EGFR	Epidermal growth factor receptor
EPAC	Exchange protein directly activated by cAMP
EPM	Elevated plus maze
ERK1/2	Extracellular signal-regulated kinases 1 and 2
GIRK	G protein-activating inwardly rectifying K+ channels
GPCR	G protein-coupled receptor
Grb2	Growth factor receptor-bound-2
GRK	G protein-receptor kinase
ICD	International Classification of Diseases
IEGs	Immediate early genes
IP3	Inositol trisphosphate
ISAP	International Association for the Study of Pain

IκBα	Inhibitor of NFkB
JNK	c-Jun N-terminal kinase
KO	Knockout
lCeA	Lateral CeA
LTD	Long-term depression
LTP	Long-term potentiation
mAchR	Muscarinic acetylcholine receptor
MAPK	Mitogen-activated protein kinase
mCeA	Medial CeA
NAC	Nucleus accumbens
NFkB	Nuclear factor kappa-light-chain-enhancer of activated B cells
NMDA	N-methyl-D-aspartate
NR2B	NMDA receptor subtype 2B
NSAIDS	Non-steroidal anti-inflammatory drugs
PAG	Periaqueductal grey
PDE4D5	Phosphodiesterase 4D5
PI3K	Phosphatidylinositide 3-kinase
PIP2	Phospholipid phosphatidylinositol 4,5-bisphosphate
PKC	Protein kinase C
PKCδ	Protein kinase C δ
PLC	Phospholipase C
PTSD	Post-traumatic stress disorder
Pyk2	Pyruvate kinase 2
RFU	Relative fluorescence units
Rho-GEFs	Rho guanine-nucleotide exchange factors
RSK	Ribosomal protein kinase
RTK	Receptor tyrosine kinase
SEM	Standard error of the mean
SNARE	Soluble N-Ethylmaleimide-Sensitive Factor Attachment Protein Receptor
Sos	Son of sevenless
SRE	Serum response element

TRP	Transient receptor potential
US	Unconditioned stimulus
WHO	World Health Organization
WT	Wildtype
δORs	δ-opioid receptors
κORs	κ-opioid receptors
μORs	μ-opioid receptors

ABSTRACT

G protein-coupled receptors (GPCRs) are a large family of seven-transmembrane domain receptors that can be activated by endogenous and exogenous ligands including neuropeptides, hormones, and neurotransmitters. Approximately 30% of clinically marketed drugs are targeting GPCRs. Various GPCRs are involved in modulation of neurophysiological responses in the brain, suggesting that GPCRs serve as an important drug target for neurological disorders. Traditional GPCR pharmacology has focused on the canonical G protein-mediated signaling pathway of GPCRs, but increasing cellular evidence suggests that β-arrestin-mediated signaling pathways are also modulating GPCR signaling and affecting pathophysiological responses. Here, the present thesis aims to interrogate cellular mechanisms of β-arrestin-mediated signaling and its downstream kinase activity in behavioral modulation. I will also briefly examine β-arrestin-mediated ion channel modulation and developing in vivo tools for this unique modulation. Altogether, these studies advance understanding of GPCR signaling in distinct behavioral modulation and provide novel insights to therapeutic developments for neurological disorders targeting GPCRs.

CHAPTER 1. INTRODUCTION

1.1 G protein-coupled receptor (GPCR) signal transduction in the central nervous system

1.1.1 Canonical G protein-mediated pathways

Of hundreds of clinically marketed drugs, approximately 30 % of the drugs are targeting GPCRs (Hauser et al., 2017). GPCRs mediate various physiological responses of endogenous hormones, chemokines, neurotransmitters, and sensory stimuli in the brain (Pierce et al., 2002). An early concept of GPCRs as a 'receptive substance' was first asserted by the British pharmacologist, John N. Langley in 1905 (Langley, 1905). Yet Langley's idea was not recognized until the concept was further developed by his student Sir Henry H. Dale forty years after Langley's initial assertion (Hill, 2006; Lefkowitz, 2013). The concept of GPCR as well as its mechanisms have been dramatically advanced in part due to the development of radioligand binding studies in the late 1960s and 70s (Hill, 2006). These advances have helped recognize GPCRs not only as a key regulator for physiological responses, but also as an attractive therapeutic target. When endogenous and exogenous ligands target GPCRs, downstream intracellular signaling pathways are primarily mediated via heterotrimeric G proteins (**Figure 1.1**). Heterometric G proteins consist of three subunits including alpha, beta and gamma subunit. Of these three subunits, the Gα subunit can be further subclassified into four distinct subunit families: $G\alpha_s$, $G\alpha_q$, $G\alpha_{i/o}$, and $G\alpha_{12/13}$, which will be referred as G_s, G_q, G_i and $G_{12/13}$ from here on. The G_s proteins can stimulate the downstream adenylyl cyclase (AC) and increase subsequent cyclic adenosine monophosphate (cAMP) levels, whereas G_i proteins opposingly modulate AC decreasing subsequent cAMP levels (Ritter & Hall, 2009). Generated cAMP subsequently activates downstream protein kinase A (PKA), which regulates cellular dynamics including differentiation, proliferation, and cell cycle in tissue- and organ-specific manner through its effector mitogen-activated protein kinase (MAPK) (Lefkowitz et al., 2002; Tasken & Aandahl, 2004). For instance, PKA activation in neurons is required for neuronal survival and synaptic plasticity via downstream extracellular signal-regulated kinase 1 and 2 (ERK1/2) signaling, one of three MAPK signaling pathways (Martin et al., 1997; Villalba et al., 1997). In contrast to G_s and G_i-protein modulation of AC, G_q proteins activate phospholipase Cβ (PLCβ) and modulate protein kinase C (PKC) and intracellular calcium levels through inositol 1,4,5-trisphosphate (IP3) production (Ritter & Hall, 2009). Additionally, PLCβ also cleaves

membrane-bound phospholipid phosphatidylinositol 4,5-bisphosphate (PIP2) into diacyl glycerol (DAG) and IP3, which can further increase intracellular calcium levels. Intracellular calcium levels play a critical role in neuronal excitability (Yamamoto et al., 2002) as well as neuronal proliferation (Hasbi et al., 2009), and changes in neuronal functions have been heavily implicated in various neuropsychiatric and neurodegenerative disorders. $G_{12/13}$ proteins are the fourth Gα subunit that activates Rho guanine-nucleotide exchange factors (Rho-GEFs) and mediate physiological responses of the cells (Siehler, 2009); however, detailed molecular signaling in the CNS has not been fully understood.

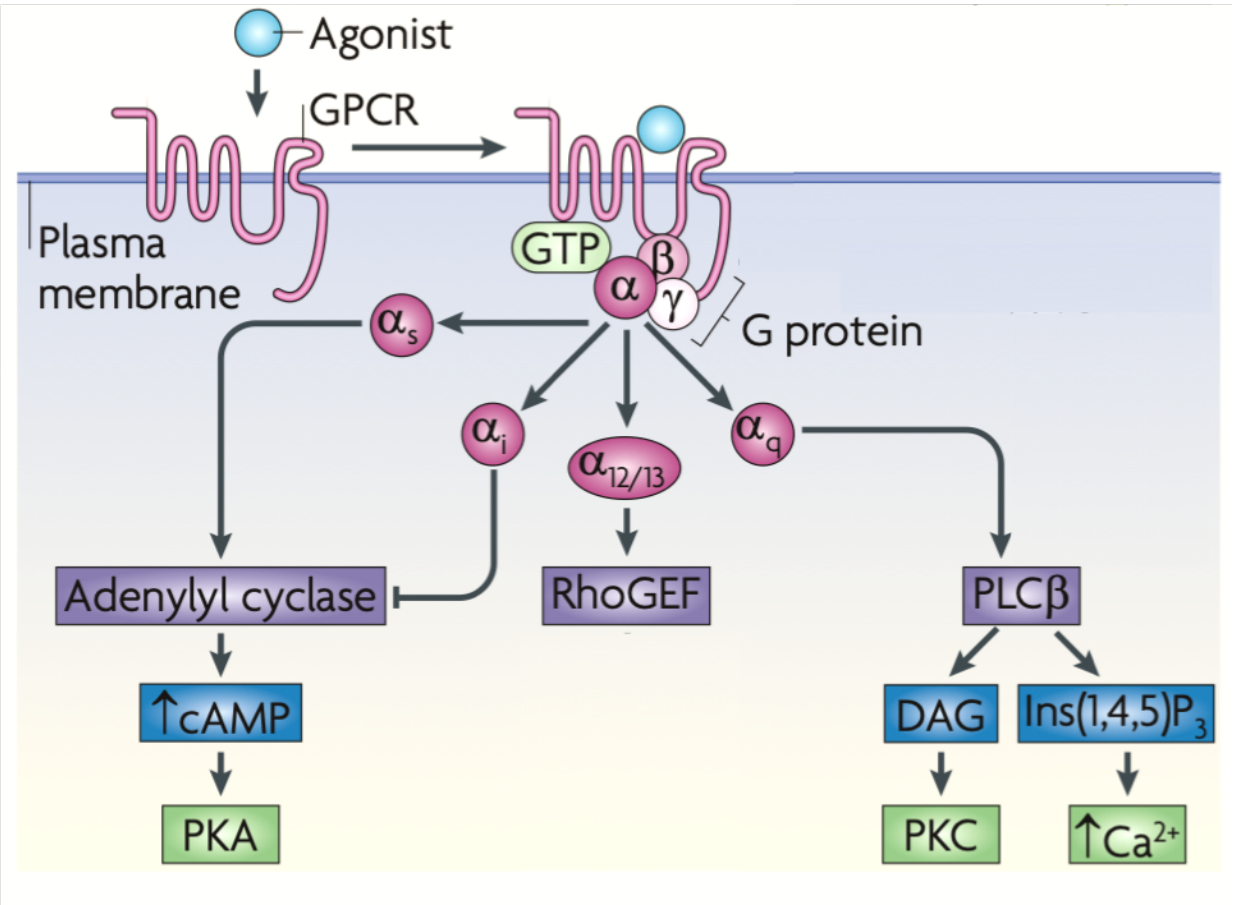

Figure 1.1 Diagram depicting GPCR signal transduction through canonical G protein-mediated pathways

Upon binding of receptor ligands, heterometric G proteins consisting of three subunits, including alpha, beta and gamma subunits, are recruited to the receptor. Depending on the subtypes of G alpha subunit, GPCRs can initiate different intracellular signaling pathways. The current diagram is adapted from (Ritter & Hall, 2009).

1.1.2 Non-canonical β-arrestin-mediated pathways

Upon activation of GPCRs, the heterotrimeric G protein dissociate from the receptor, and G protein-receptor kinase (GRK)-mediated phosphorylation prevents further activation of GPCRs (**Figure 1.2**) (Zhang et al., 1997). The phosphorylation triggers a cascading event of receptor desensitization and internalization upon recruitment of β-arrestin, which has a high affinity for phosphorylated GPCRs (Freedman & Lefkowitz, 1996). Two isoforms of β-arrestin (i.e. β-arrestin 1, 2 equals Arrestin 2, 3) – there are also highly homologous visual arrestins (Arrestin 1 and 4) that interact with rhodopsin GPCRs – were first characterized as a downstream effector of β2-adrenergic receptors, which limits G protein receptor signaling (Lohse et al., 1990; Wilden et al., 1986). Non-canonical β-arrestin-mediated GPCRs signaling pathways were previously known as a key modulator for receptor desensitization and internalization of the receptor signaling (Freedman & Lefkowitz, 1996). Upon binding of β-arrestin to GPCRs, β-arrestin further assists the interaction of receptors with clathrin that further accelerates internalization of the receptor into endosomes or helps the receptor recycle back to the membranes. Depending on binding affinity of β-arrestin to the receptors, GPCRs can be classified into two groups: Class A and Class B (Pierce & Lefkowitz, 2001). For Class A GPCRs such as β2-adrenoceptors, β-arrestin 2 translocates to receptors, internalizes receptors, but before they reach to endosome, β-arrestin 2 rapidly dissociates from receptors, resulting the receptors to be recycled back to membranes (Oakley et al., 2000). For Class B GPCRs such as angiotensin receptor AT1A or the vasopressin V2 receptor, β-arrestin 1 and 2 equally translocate to receptors, internalize them, but stay co-localized until the receptors reach the endosome (Oakley et al., 2000), allowing distinctive receptor trafficking profile in cells. In addition to their function as chaperones in receptor trafficking, both β-arrestin isoforms can scaffold with various downstream effectors and kinase (Luttrell & Miller, 2013), and thereby contribute to G-protein-independent signal transduction. For instance, β-arrestin can scaffold with extracellular signal-regulated kinases 1 and 2 (ERK1/2) upstream, cRaf-1-MEK1/2 to promote MAPK signaling (Morrison & Davis, 2003). Depending on the receptor, ERK1/2 can be activated upon binding with β-arrestin in the clathrin-coated pits or when β-arrestin-clathrin complex is internalized as a form of vesicle (Ranjan et al., 2016). Activated ERK1/2 can modulate basic dynamics of cells such as differentiation and proliferation through transcriptional modulation, and thus it plays a key role in cellular functions (Cassier et al., 2017; Cruz & Cruz, 2007). Besides

cRaf-1-MEK1/2-ERK1/2 signaling, β-arrestin can also scaffold with a wide range of proteins including mouse double minute 2 homolog (MDM2) and E3 ligase, leading to proteasome-dependent destruction (**Figure 1.5**) (Girnita et al., 2007). Alternatively, β-arrestin can scaffold with inhibitor (IκBα) of nuclear factor kappa-light-chain-enhancer of activated B cells (NF-κB) and modulate NF-κB-mediated gene regulation (Witherow et al., 2004), resulting in inflammatory responses or cell survivals. β-arrestin can also serve itself as a downstream effector and affect cellular functions at transcriptional levels (Cassier et al., 2017; Cruz & Cruz, 2007; Witherow et al., 2004). Therefore, given β-arrestin's ability to ubiquitously modulate cellular functions, it is clear that β-arrestin serves as an attractive drug target for future drug development.

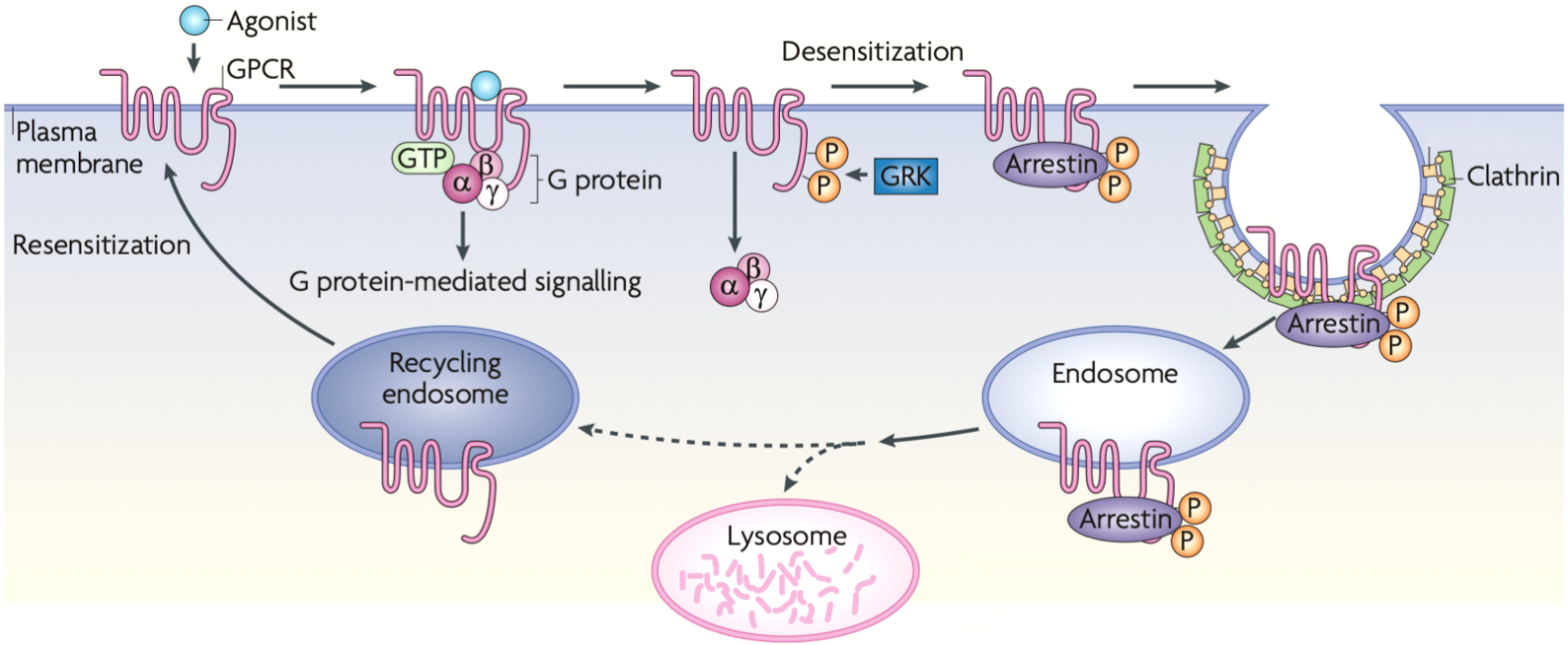

Figure 1.2 Diagram depicting GPCR signal transduction through non-canonical β-arrestin-mediated pathway

Once the receptor is activated, heterometric G proteins are dissociated from the receptor and C terminals of the receptor can be phosphorylated by GRK. This phosphorylation further desensitizes the receptor as β-arrestin proteins are recruited to the receptor. Together with other vesicle complex proteins such as clathrin, β-arrestin internalizes the receptor. Depending on the interaction between receptor and β-arrestin, the receptor can be either depredated in lysosome or recycle back to the membrane. The current diagram is adapted from (Ritter & Hall, 2009).

1.1.3 Signal bias of GPCR: Implication for drug discovery

In classical pharmacology, drugs have been characterized by two important properties: 1) affinity, the ability of a drug to bind to a receptor, and 2) efficacy, the ability of a drug to produce responses upon binding to a receptor (Urban et al., 2007). Based on these two properties, GPCR-targeted ligands have been categorized as full agonists, partial agonists, inverse agonists, or antagonists. For instance, in this concept, a drug characterized as an agonist is expected to activate overall signaling pathways linked to a target receptor to the same degree, whereas a drug characterized as an antagonist, is expected to inhibit overall signaling pathways linked to a target receptor to the same degree (Urban et al., 2007). However, accumulating studies have identified that a drug does not always activate or inhibit all signaling pathways of a target GPCRs at the same degree, meaning that a drug can equally activate signaling pathways in an unbiased (balanced) manner or activate one or the other in a biased (unbalanced) manner (Whalen et al., 2011), which is later referred as 'signal bias' or 'functional selectivity' (Rankovic et al., 2016). An example of signal bias was first found by ligands that target muscarinic acetylcholine receptor (mAchR). The mAchR ligand, carbachol, activates both G_s-mediated cAMP and G_q-mediated PLC signaling at mAchR, whereas studies have also found that other ligands of mAchR such as pilocarpine do not activate G_s-mediated cAMP, yet only activate PLC signaling (Fisher et al., 1993; Gurwitz et al., 1994; Rajagopal et al., 2010). These findings first introduced a concept that a ligand can preferably activate one signaling over another signaling pathway. Later studies further expanded the concept of signaling bias to non-canonical β-arrestin signaling (Lewis et al., 1998; Whistler & von Zastrow, 1998). The concept of signal bias has further helped researchers identify detailed molecular mechanisms of a ligand. For instance, carvedilol – a small-molecule ligand of β1- and β2-adrenergic receptors – was previously known as an antagonist or inverse agonist due to carvedilol's properties of lowering cAMP levels in cells expressing β-adrenergic receptors. Yet, a later study discovered that carvedilol in fact activates β-arrestin-mediated pathways, whereas it inhibit G protein-mediated pathways in a biased manner (Wisler et al., 2007).

Modern pharmacology has begun to utilize signal bias concept to avoid adverse effects linked to distinct GPCR signaling pathways. An early example of the potential power of a strategy focused on developing biased agonists came from a study by Bohn *et al.,* which identified that mice lacking β-arrestin 2 show significantly high analgesic effects of morphine (Bohn et al., 1999).

A follow-up study by Raehal *et al.* reported a potential link between β-arrestin 2 and adverse effects of morphine such as constipation and respiratory suppression by morphine usage (Raehal et al., 2005). Morphine is a powerful analgesic drug targeting μ-opioid receptor, but upon binding to μORs it recruits β-arrestin, albeit weaker than the endogenous opioids (Martini & Whistler, 2007). Under the hypothesis that β-arrestin recruitment by μOR agonist reduces potency and increases the likelihood of side effects, a G protein-biased opioid, TRV130, was produced. which provided more potent analgesic effects together with low on-target adverse effects in humans (Soergel et al., 2014).

1.1.4 Developing β-arrestin-targeting therapeutics for neurological disorders

For the past two decades, our knowledge on the roles of the non-canonical β-arrestin pathways in GPCR signaling has been dramatically expanded (Bond et al., 2019; Schmid & Bohn, 2009; Shukla et al., 2011). While studies have suggested a potential link between β-arrestin pathways and adverse effects of a drug such as morphine, accumulating studies have also demonstrated therapeutic effects of β-arrestin-biased ligands. An intriguing example that provides evidence of the therapeutic potentials of β-arrestin pathways comes from the study of dopamine D2 receptors. It was originally thought that clinically effective anti-psychotic drugs exerted their therapeutic effects by inhibiting the interaction of D2-β-arrestin (Masri et al., 2008), but subsequent discoveries found that β-arrestin pathways are essential for more effective therapeutic effects of antipsychotic drugs (Allen et al., 2011; Beaulieu et al., 2008). Moreover, a later study by Urs *et al.* revealed that cellular responses to β-arrestin-biased D2 ligands are not equal across the brain (Urs et al., 2016). Their new biased D2 agonist, UNC9994A, exhibited anti-psychotic effects by promoting β-arrestin-D2 interaction in the mouse prefrontal cortex while inhibiting β-arrestin-D2 interaction in the mouse striatum (Urs et al., 2016). This can be due to distinct expression levels of β-arrestin isoforms and associated GRK isoforms across the brain regions (Attramadal et al., 1992; Bjork et al., 2008; Reiter & Lefkowitz, 2006). The authors demonstrated differences in expression levels of GRK2 and β-arrestin 2 in the mouse prefrontal cortex and striatum (Urs et al., 2016). It is noteworthy that β-arrestin 1 has higher expression levels than β-arrestin 2 expressions in striatal regions (Attramadal et al., 1992; Bjork et al., 2008; Gurevich et al., 2002), whereas β-arrestin 2 is highly expressed in the dorsal hippocampus and amygdala (Attramadal et al., 1992; Bjork et al., 2008), and thus the unique differences in expression levels of the two isoforms need

to be considered when developing β-arrestin-biased drugs. Several studies have indeed reported how distinct β-arrestin isoforms affect different types of behavioral responses. The absence of β-arrestin 2 isoform significantly impaired consolidation of object recognition memory and spatial memory, and expression of β-arrestin 2 in the entorhinal cortex recovered the impaired memory function, suggesting a role of β-arrestin 2 in memory consolidation (Liu et al., 2015). β-arrestin 2 is also involved in the pathogenesis of Alzheimer's disease by interacting with γ-secretase that can increase generation of amyloid-β peptides (Thathiah et al., 2013). Studies have also reported a protective role of β-arrestin 1 against SNC80 (δ-opioid receptor agonist)-induced convulsion in rodents (Vicente-Sanchez et al., 2018), and increased alcohol consumption in females mice (Robins, Chiang, Berry, et al., 2018). It is clear that both isoforms have unique roles in the pathophysiology and behavioral phenotypes linked to various neuropsychiatric and neurodevelopmental disorders, and thus these differences in expression levels and behavioral modulation need to be taken into consideration for future drug development targeting β-arrestin pathways.

1.2 Crosstalk between GPCRs and ion channels

1.2.1 G protein-mediated ion channel modulation

Ion channels are a member of membrane proteins that direct flux of ions. Activation of ion channels in cellular membranes determines intrinsic membrane potentials, and activation of ion channels in the axon modulates axonal propagation and synaptic transmission in the brain. While ion channels can be activated by direct binding with ligands or changes in membrane potentials, they can also be activated by downstream effectors of GPCRs. It has been suggested that ion channels engage with several unique signaling pathways such as G protein- or β-arrestin-mediated pathways (**Figure 1.3**). For instance, two main ion channel families modulated by G protein pathways include voltage-dependent Ca^{2+} channels (Ca_v) and G protein-activating inwardly rectifying K^+ channels (GIRKs or Kir). The involvement of G proteins in the inhibition of Ca_v was first shown by Holz *et al.* and McFadzean *et al.* who demonstrated that inhibition of Ca_v current was blocked by pertussis toxin, a known inhibitor of G protein activity (Holz et al., 1986; McFadzean et al., 1989). Further studies identified that the Gβγ subunit of G proteins is in fact a distinct regulator that modulates Ca_v currents when Gβγ subunit dissociates from the receptor

(Herlitze et al., 1996). The Gβγ interacts with multiple binding sites of Ca_v, including their C-terminus of the α1 subunit, N-terminus, and I-II linker, and binding of these sites allows for a conformational change of the channel in order for them to be inactive (Mochida, 2019). Modulation of intracellular calcium levels via Ca_v is particularly vital for maintaining the synaptic functions. The Ca_v2 families expressed heavily in the presynaptic terminals of neurons control synchronous neurotransmitter release from synaptic vesicles by facilitating presynaptic Ca^{2+} entry and synaptic plasticity between neurons (Mochida, 2019), and thus play a pivotal role in functional dynamics of neural circuits. The G protein also regulates Kir3 channels in a similar mode of action. Upon binding of Gβγ to the N-terminus of the GIRK channels, Gβγ results in the channels to open (Ivanina et al., 2003). This mechanism seems to be specific to $G_{i/o}$ not to G_s or G_q, which can be explained by the fact that the opening of the channel allows efflux of potassium ions, which results in hyperpolarization of the cell membrane, and this mechanism of action ultimately leads to the inhibitory modulation to intrinsic properties of the cells (Lujan et al., 2014). Clearly, GPCRs have the ability to impact ion channel function through their G protein-dependent downstream signaling. To what degree β-arrestins modulate ion channel activity will be further discussed in the following section.

1.2.2 β-arrestin-mediated ion channel modulation

Besides G protein-mediated modulation of ion channels, increasing evidence implicates β-arrestin in the modulation of ion channels (Lefkowitz et al., 2006). β-arrestin-mediated ion channel modulation can be characterized as either direct modulation by β-arrestin itself or indirect modulation by β-arrestin-mediated downstream effectors. The first discovery of a direct interaction between β-arrestin and ion channels was found by a proteomics study on β-arrestin-interacting proteins (interactome) that elucidated the interaction between β-arrestin and transient receptor potential (TRP) channels (Xiao et al., 2007). TRP channels are calcium-permeable channels known to mediate thermal, chemical, and mechanical sensation to noxious stimuli by expressing in various neurons including the primary sensory neurons (Clapham et al., 2001). Both β-arrestin isoforms have been linked to the modulation of a particular TRP channel; β-arrestin 1 has been found to directly interact with TPRV4 by ubiquitinating the channels via recruitment of atrophin 1-interacting protein 4 (AIP4), an E3 ubiquitin ligase for TRPV4 (Shukla et al., 2010), whereas β-arrestin 2 desensitizes TRPV1 channels by dephosphorylating TRPV1 channels through

phosphodiesterase 4D5 (PDE4D5) (Por et al., 2012). A later study by Rowan *et al.* further reported that β-arrestin 2-dependent crosstalk between μ-opioid receptors (μORs) and TRPV1 has a physiological consequence in that it increases thermal sensitivity of mice (Rowan, Bierbower, et al., 2014). Upon activation of μORs by morphine, β-arrestin 2 is recruited away from TRPV1 channels and the absence of β-arrestin 2 results in phosphorylation and activation of TRPV1 that can lead to increases in thermal sensitivity (Rowan, Bierbower, et al., 2014). This mechanism of action on β-arrestin 2-mediated interaction between μORs and TRPV1 may also explain previously known opioid-induced hyperalgesia – increase in sensitivity to painful stimuli (Chen et al., 2008; Vardanyan et al., 2009). Interactions between GPCRs and TRP channels also affect synaptic transmission in neurons. Activation of angiotensin II receptor that recruits β-arrestin 1 away from TRPC3 channels has shown to activate TRPC3 channels via conformational changes and subsequently increase the intracellular calcium influx during the activation of the channels (Liu et al., 2017). Calcium ions play a crucial role in vesicle release by facilitating the release (Borst & Sakmann, 1996), and thus the increases in calcium in these TRPC3-expression neurons can facilitate catecholamine vesicle release (Liu et al., 2017). β-arrestin can mediate the interaction between GPCRs and ion channels via an indirect mechanism of action. A study by Tzingounis *et al.* reported β-arrestin 2 mediates modulation of $Ca_v3.2$ through ERK1/2 signaling at β-adrenergic receptor in hippocampal pyramidal cells (Tzingounis et al., 2010). A later study by Yang *et al.* elaborated that β-arrestin 2-mediated ERK1/2 signaling at dopamine D3 receptor also mediate $Ca_v3.2$ modulation at axon initial segment of cartwheel cells in the dorsal cochlear nucleus (Yang et al., 2016). These results demonstrate that β-arrestin plays a role not only in the direct modulation of ion channels, but also in the indirect modulation of ion channels through downstream kinases.

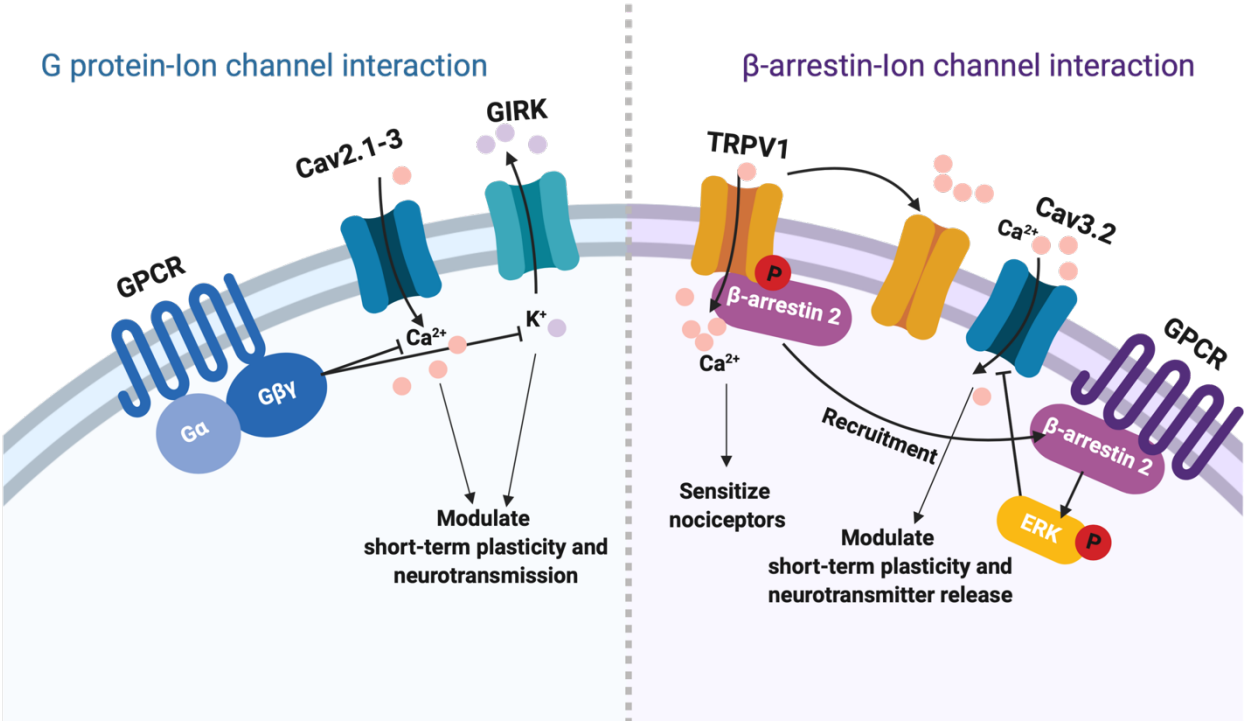

Figure 1.3 Crosstalk between GPCRs and ion channels through canonical and non-canonical GPCR signaling pathways

GPCRs can crosstalk with various ion channels such as $Ca_v2.1$-3 and GIRK channels through canonical G protein-mediated pathways or $Ca_v3.2$ and TRPV1 channels through non-canonical β-arrestin-mediated pathways.

1.3 Mitogen-activated protein kinases (MAPK) signaling

1.3.1 RTK-dependent (trans)activation of MAPK signaling

As stated earlier, MAPK phosphorylation is a common and an important downstream effector of GPCR activation. Extracellular signals are transmitted into the intracellular targets via multiple tiers of regulatory signaling molecules known as MAPK signaling. These signaling networks are also involved in the transmission of cytoplasmic signals to the nucleus that can further affect cellular function and dynamics (Seger & Krebs, 1995). There are three major families of MAPK signaling: ERK1/2, c-Jun N-terminal kinase (JNK), and p38 pathways. MAPKs signaling can be initiated by two large receptor category including receptor tyrosine kinase (RTKs) and GPCRs. The RTKs are a cell-surface receptor family that is comprised of ligand-binding domains in the extracellular regions, protein kinase domains with additional carboxy terminal in the cytoplasmic regions, and additional regions. Various signaling proteins (e.g. Epidermal growth factor, insulin, nerve growth factor, and others) can activate the RTKs and further transform the 'inactive' monomeric or oligomeric RTKs into 'active' ligand-induced dimerization (Schlessinger, 2000). Active status recruits various adapters and effectors such as growth factor receptor-bound-2 (Grb2) and son of sevenless (Sos) that can further activate Ras and its downstream Raf-MEK1/2-ERK1/2 signaling (Wetzker & Bohmer, 2003). In the early 90s, the RTK-mediated activation of ERK1/2 was thought to be linear and Ras-dependent, but later studies discovered that Ras and ERK1/2 activation can be initiated by various intracellular signaling pathways (McKay & Morrison, 2007). Ras-independent pathways were initially reported by Daub *et al*. (Daub et al., 1996). In this study, the authors demonstrated that GPCRs can modulate activation of RTK subtype, epidermal growth factor receptor (EGFR) (Daub et al., 1996). This phenomenon that an activated receptor activates a heterologous receptor signaling was referred to as 'transactivation' (Daub et al., 1996). During the transactivation, various mediators of GPCRs such as phosphatidylinositide 3-kinase (PI3K), PKC, and Rap1 affect RTKs signaling, in particular MAPK signaling (Wetzker & Bohmer, 2003). Multiple physiological events such as proliferation, differentiation, migration, and survival are mediated by the transactivation (Shah & Catt, 2004). For instance, δORs activate ERK1/2 signaling via integrin-stimulated RTKs signaling (Eisinger & Ammer, 2008), which is thought to be involved in opioid-induced neurogenesis in neuronal cells. However, at the same time, accumulating studies have also suggested that ERK1/2 can be activated in a RTK-independent

manner through unique GPCR-mediated intracellular signaling pathways (Belcheva et al., 2005; Kramer et al., 2002), which will be introduced in the next section.

1.3.2 GPCR-dependent activation of MAPK signaling

The initiation of the MAPK cascade is not restricted to RTKs-mediated activation or transactivation. Various GPCR signaling pathways themselves also serve as key modulators for MAPK signaling. Two main GPCR signaling pathways – G protein- and β-arrestin-mediated pathways – are involved in ERK1/2/MAPK activation. For G protein-mediated pathways, Gα subunit families have been implicated in initiating ERK1/2 activation. As previously described, G_s and $G_{i/o}$ subunits can respectively stimulate or inhibit AC-dependent cAMP production through PKA activation (**Figure 1.4**) (Ritter & Hall, 2009). Subsequent increase in cAMP production leads to direct activation of exchange protein directly activated by cAMP (EPAC), which activates Rap1 as well as BRaf, both are upstream of MEK1/2-ERK1/2 signaling (Jain et al., 2018). On the contrary, activation of PKA by G_s protein can also inhibit cRaf1 as well as subsequent MEK1/2-ERK1/2 signaling, whereas decrease in activation of PKA by $G_{i/o}$ activates cRaf1 as well as subsequent MEK1/2-ERK1/2 signaling (Jain et al., 2018). G_q subunit, however, has unique signaling mechanisms through PLCβ, upstream of PKC, which interacts with cRaf1 and increases the downstream MEK1/2-ERK1/2 activity (Goldsmith & Dhanasekaran, 2007). While underlying mechanisms are unclear, Gβγ subunit can activate MEK1/2-ERK1/2 signaling though PLCβ and its various downstream signaling molecules such as pyruvate kinase 2 (Pyk2), Src, and Ras, which can further activate cRaf1 and MEK1/2-ERK1/2 signaling pathways (Goldsmith & Dhanasekaran, 2007). In comparison to G protein subunits, β-arrestin activates downstream MAPKs signaling as a form of scaffolding (**Figure 1.5**). β-arrestin recruits downstream effectors (cRaf1-MEK1/2-ERK1/2) and stabilize the structure to activate the downstream effectors (Morrison & Davis, 2003; Strungs & Luttrell, 2014). More detailed mechanisms by which ERK1/2 is activated by β-arrestin were further elucidated by Cassier *et al*. where they demonstrated phosphorylation of β-arrestin 2 at Thr^{383} by MEK1/2 further creates a binding pocket for ERK1/2 in the C-terminal domain of β-arrestin, and ultimately allows ERK1/2 activation (Cassier et al., 2017). Traditional models of GPCRs envisioned β-arrestin signaling as a terminator of receptor signaling, but a series of evidence clearly suggests that both G protein and β-arrestin signaling pathways participate in a

meaningful interaction with downstream kinases and effectors, and thus present a possibility to serve as unique GPCR-mediated signaling regulators.

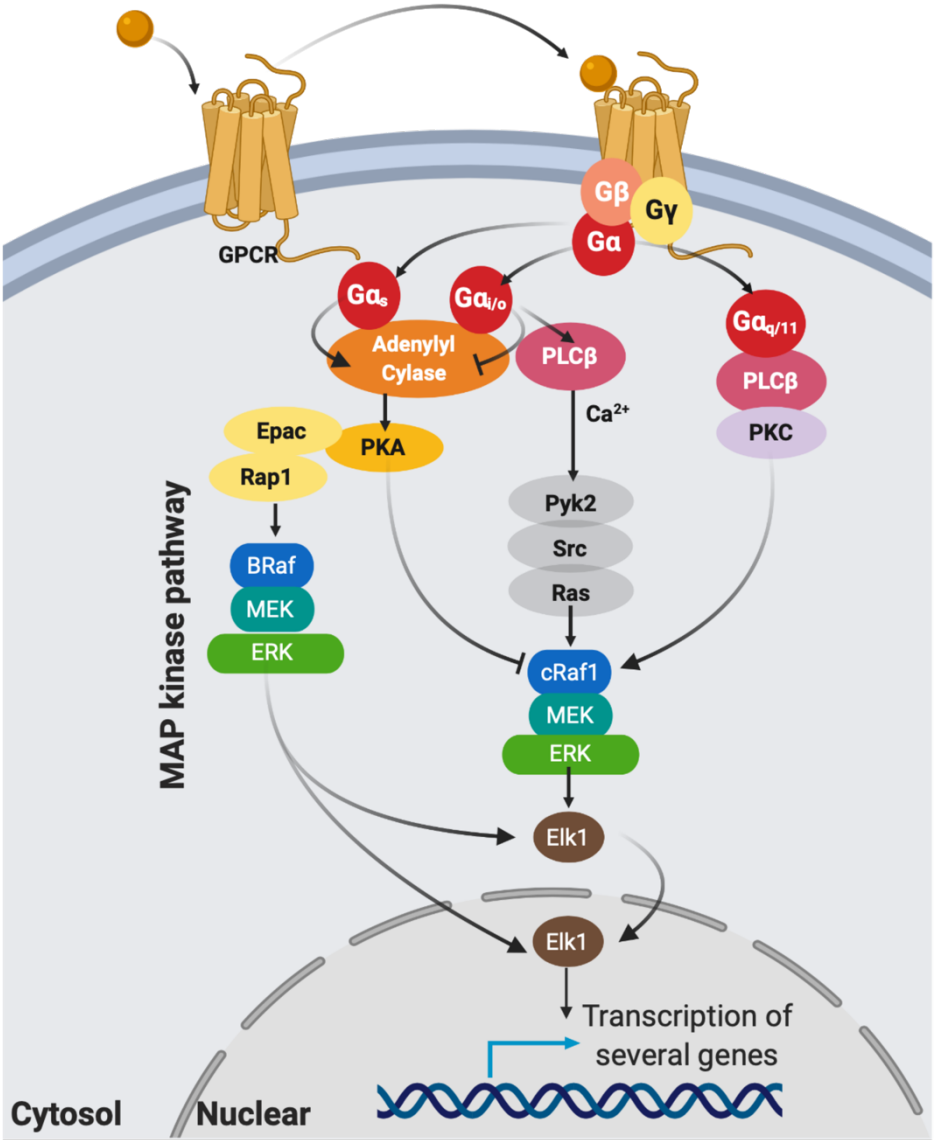

Figure 1.4 Detailed downstream signaling pathways of G protein subfamily and their subsequent transcriptional modulation

Upon activation of GPCR, G alpha protein can initiate various signaling pathways depending on their subtypes coupled with GPCRs. Gi/o and Gs protein can opposingly modulate adenylyl cyclase and its downstream PKA can activate Epac and Rap1, upstream of BRaf-MEK1/2-ERK1/2 signaling, whereas Gq protein can interact with PLC and PKC, subsequently activating cRaf1-MEK1/2-ERK1/2 signaling. Activation of ERK1/2 can further phosphorylate a transcriptional factor, Elk-1, which can further facilitate transcriptions of several genes.

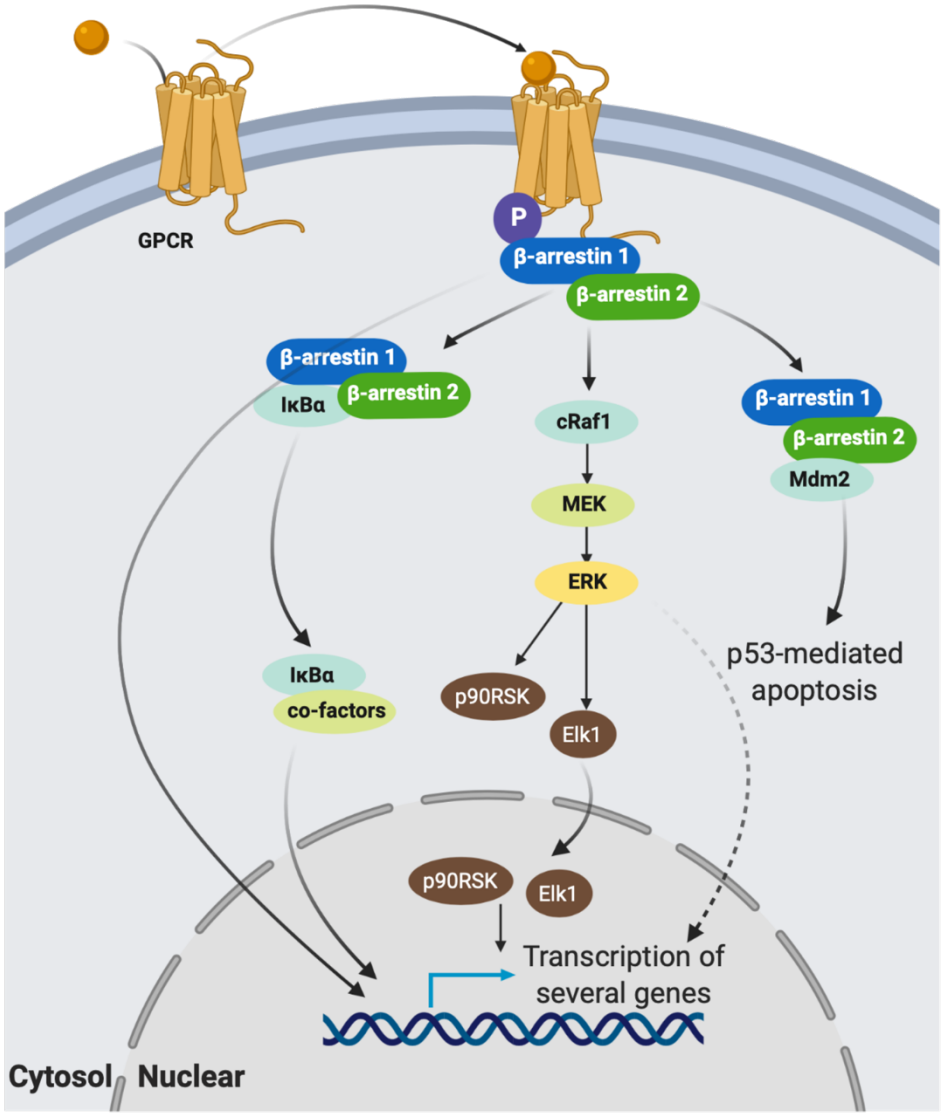

Figure 1.5 Detailed downstream signaling pathways of β-arrestin signaling and their subsequent transcriptional modulation

β-arrestin signaling can activate cRaf1-MEK1/2-ERK1/2 and further phosphorylate transcriptional factors Elk-1 as well as p90RSK. These transcriptional factors or β-arrestin itself can further facilitate transcription of several genes including IEGs and C-fos. For detailed modulation at transcriptional levels, see Chapter 5.4. β-arrestin can also interact with other downstream effectors such as IkBa and Mdm2 that can further affect cellular functions such as survivals or cell death.

1.4 Neural basis of emotion and pain

1.4.1 Behavioral paradigms for investigating anxiety and fear

In the present thesis, a major focus is placed on the investigation of GPCR signaling of β-arrestin and ERK1/2 in the modulation or control of behavior. As the thesis primarily utilizes δ-opioid receptors (δORs) as a model GPCR, the research described in this thesis utilizes behavioral endpoints related to δORs-mediated behaviors: emotion (Dripps & Jutkiewicz, 2018; Pradhan et al., 2011) and pain (Pradhan et al., 2011; Wang et al., 2018). In the following section, I will explain the circuitry of these behaviors as well as description of preclinical models to investigate these behaviors. Anxiety is a state of emotion that can occur in response to potential danger. While anxiety helps an organism be prepared for an imminent threat, excessive anxiety to specific objects or situations even in the absence of true danger can be defined as an anxiety disorder (Shin & Liberzon, 2010). According to a national survey, the lifetime prevalence of the anxiety disorder is approximately 30 % (Kessler et al., 2005), suggesting the potential impact to the society. In an attempt to model the human anxiety behavior, various animal behavioral paradigms have been developed. These paradigms integrate the contrasting tendency of an animal to engage in exploratory environment against the aversive properties such as an open area (open field test), bright light (dark-light box test) and elevated space (elevated plus maze or zeromaze) (Carola et al., 2002; Crawley, 1985). A more complex form of anxiety (i.e. fear) requires learning components. A pioneered work of learning behaviors was initially reported by Ivan Pavlov in 1927. He found that ringing a bell before a dog was fed can associate the bell with the food and a dog would even salivate to the bell sound alone. This behavior was later characterized as associative learning or as Pavlovian conditioning (Pavlov, 2010; Pearson, 2012). Ever since, the Pavlovian conditioning has been further developed into various form of associative learning behavioral paradigms including a paradigm that evaluate fear-related behaviors.

Fear is also a complex anxiety-related behavior that requires memory components. While fear can be evoked by stimuli that elicit the status of threat, excessive fear in the absence of the threat can be characterized as pathological symptoms of post-traumatic stress disorder (PTSD). In a classical fear conditioning paradigm, when the aversive event represented as an unconditioned stimulus (US) is paired with the neutral stimulus (e.g. sound or light) through an associative learning process, the US becomes the conditioned stimulus (CS) (Maren, 2001). When the CS is presented alone, it can evoke aversive responses that can be measured by increased defensive

behavior such as freezing behaviors of an animal (Fendt & Fanselow, 1999; LeDoux, 2000). In this paradigm, various memory acquisition phases (e.g. acquisition, consolidation and retrieval phases) and different associative memories (e.g. cued or contextual) can be evaluated using different protocols. For instance, if the cued CS such as sound or light is paired with an aversive event (such as foot-shock or loud noise), this can establish cued fear conditioning. If the context of the fear conditioning chamber is utilized to pair the US, this can establish contextual fear conditioning during the memory acquisition period (Maren, 2001). Alternatively, varying the time to reintroduce the CS after the primary conditioning period can particularly evaluate memory retrieval phases (Maren, 2001).

1.4.2 Neural circuits of anxiety and fear

Different brain circuits are involved in executing varied behavioral phenotypes. A complex network of the brain structures such as the basal ganglia (e.g. striatum, nucleus accumbens) and limbic systems (e.g. amygdala and hippocampus) have been implicated in emotional behaviors (**Figure 1.6**). In particular, a unique case of human patient S.M. depicts the importance of the amygdala in emotional behaviors. S.M. was a patient with a focal bilateral amygdala lesion (Adolphs et al., 1994) who was unable to read facial expression of fear of others and did not exhibit fear to exposures of the patient to fear-evoking stimuli such as snakes and a haunted house (Feinstein et al., 2011). While the role of amygdala in fear has been well-documented, it is important to understand microcircuits of fear and anxiety that incorporate the amygdala in order to fully evaluate the circuits involved in emotion (**Figure 1.7**). The amygdala is anatomically and functionally divided into two sub-regions including the basolateral amygdala (BLA) and the central amygdala (CeA) that receives sensory inputs from the thalamus and the primary sensory cortex. The BLA is comprised of 80 % glutamatergic spiny neurons that projects to the CeA and 20 % GABAergic neurons (McDonald, 1982b, 1985; Rainnie et al., 2006). The CeA is sub-divided into the lateral CeA (lCeA) and medial CeA (mCeA) and mostly comprised of GABAergic neurons (McDonald, 1982a; Oka et al., 2008). The mCeA neurons can project into other brain regions that are involved in freezing behaviors such as the periaqueductal grey (PAG) (Duvarci et al., 2009) or in anxiety such as the bed nucleus of the stria terminalis (BNST) for anxiety-related behavior (Dong et al., 2001). Recent optical and electrophysiological studies have further identified two functional neuronal groups in the lCeA that are involved in the fear learning. One subpopulation

is lCeA^{off} cells that expresses protein kinase C δ (PKCδ) and another subpopulation is lCeA^{on} cells without PKCδ (Ciocchi et al., 2010; Haubensak et al., 2010). Haubensak and colleagues further identified that the PKCδ-positive lCeA^{off} cells directly inhibits mCeA neurons that projects to the PAG and modulate freezing behaviors following the fear conditioning (Haubensak et al., 2010).

The amygdala alone, however, cannot fully function or process emotion without the help of other brain regions such as striatum. It has been suggested that unidirectional output from the BLA to the striatum, the nucleus accumbens (NAC), and the BNST is crucial to translate the BLA signal to behaviors (Janak & Tye, 2015). The striatum is anatomically divided into the dorsal striatum and the ventral striatum also known as the NAC, which further differentiates into shell and core (Deutch & Cameron, 1992; Zahm & Heimer, 1990). Inactivation of both shell and core of the NAC showed an impairment in acquisition and expression of fear-potentiated startle response in mice, and it has suggested that increased dopamine levels are correlated with NAC shell in contrast to the core during fear conditioning (Pezze et al., 2002). In humans, the NAC has been known to receive strong afferents from the BLA (Pezze & Feldon, 2004; Sturm et al., 2003). Studies revealed that synthesis of dopamine in the NAC and the BLA are both crucial in the formation of fear conditioning (Fadok et al., 2010; Pezze & Feldon, 2004). Given that the NAC shells has high expression of D1 and D3 receptors together with dense distribution of various neuropeptides including enkephalin, substance P and neurotensin (Heimer, 2000), it is likely that the NAC shells may be involved in the fear conditioning process through these various inputs.

Besides the NAC, the hippocampus also plays a key role in fear conditioning as a form of associative learning. Anatomical and functional studies have suggested that the hippocampus is segregated into the dorsal hippocampus that mediate spatial memory (Moser & Moser, 1998; Swanson & Cowan, 1977) and the ventral hippocampus that mediate emotional behaviors (Fanselow & Dong, 2010; Jimenez et al., 2018). Yet, pharmacological studies targeting GABAergic, serotonergic, and cholinergic systems in the dorsal hippocampus have suggested that the dorsal hippocampus is also involved in the modulation of anxiety-related behaviors (Engin & Treit, 2007; File et al., 2000). More recently, it has also been proposed that the functional domains of the hippocampus are organized as a long-axis gradient (Strange et al., 2014). Multiple research groups are currently investigating the discrete transition of anatomical, molecular, and functional organization of the long-axis gradient to better define the functional organization of the hippocampus.

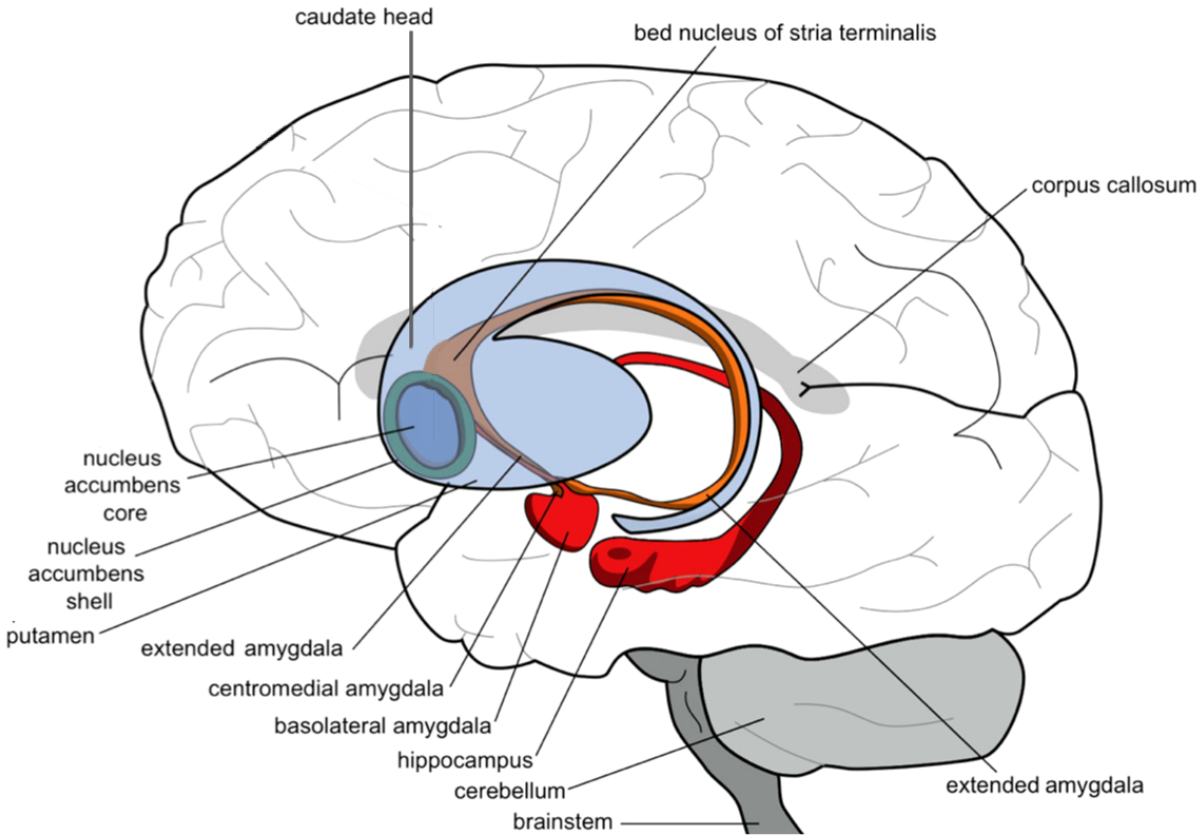

Figure 1.6 Sagittal view of the brain and anatomical regions linked to the modulation of anxiety and fear-related behaviors

Various brain regions and circuits are involved in the modulation of anxiety- and fear-related behaviors. Among many, basal ganglia (e.g. striatum, nucleus accumbens) and limbic systems (e.g. hippocampus, amygdala) are well-known anatomical structures that have been suggested for their roles in emotional behaviors. The current figure is adapted from (Loonen & Ivanova, 2015).

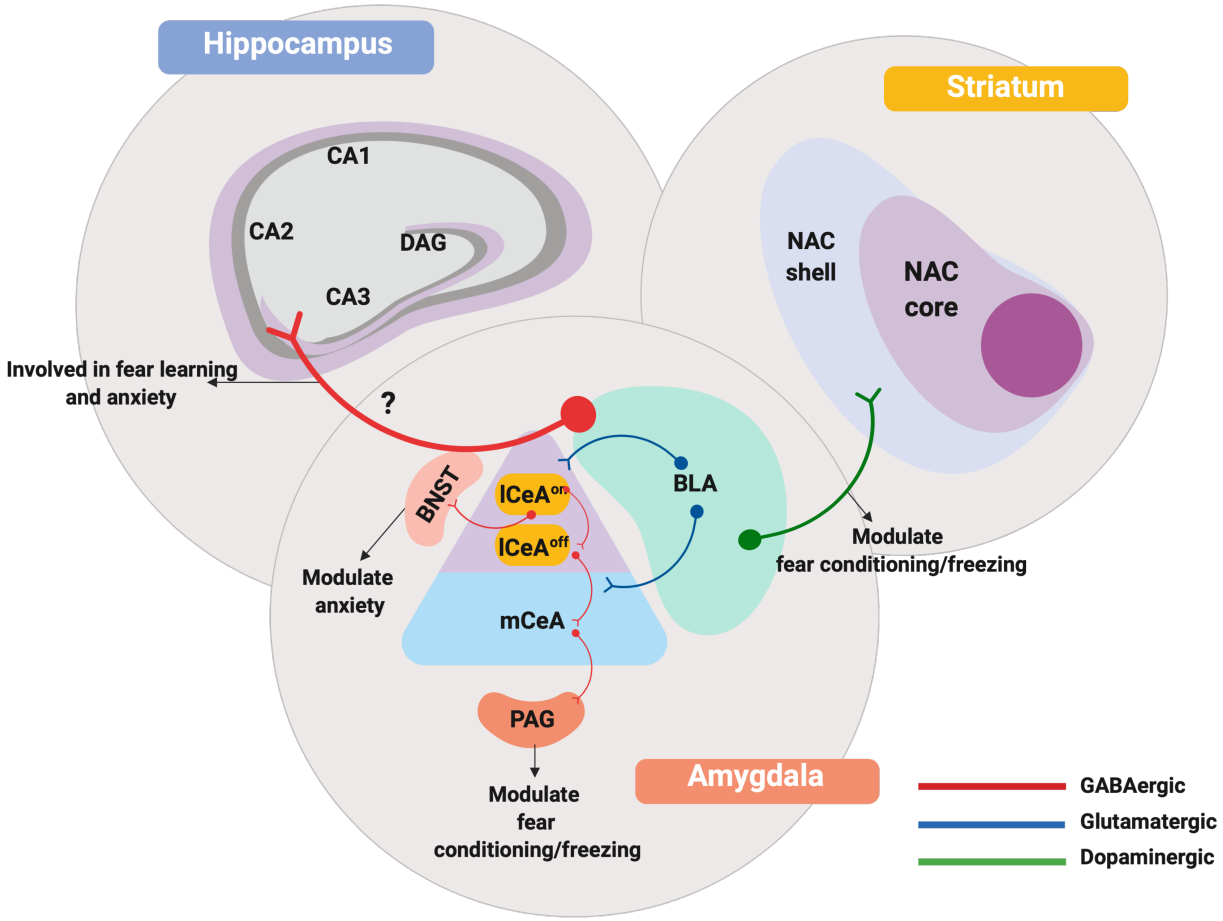

Figure 1.7 Striatal-amygdalar-hippocampal circuits involved in the modulation of anxiety and fear

Amygdala microcircuits are composed of the lCeA, mCeA, BLA, BNST, and PAG regions. Glutamatergic neurons in BLA projects to both on and off cells of lCeA, which further projects to BNST or to PAG through mCeA and mediate anxiety-like behaviors or freezing fear-related behaviors. Alternative BLA projections to NAC shell and the hippocampus have also been implicated in the modulation of anxiety- and fear-related behaviors, yet detailed neural mechanisms remain unknown.

1.4.3 Definition and neural mechanisms of chronic pain

δORs play an important role not only in emotions but also in chronic pain, and thus the present section will cover definition, neural circuits and current treatment options for chronic pain. Pain serves as a physiological nociception that can warn us from danger. Yet, exacerbated pain that lasts between 1 month to 3 months can be characterized as an acute pain syndrome and exacerbated pain that persists over 3 months can be further characterized as a chronic pain syndrome. Depending on the location and types of pain, various neural pathways are involved in mediating chronic pain. First, ascending pain pathways are initiated by noxious stimuli or peptides that can activate nociceptors located in the peripheral endings of primary sensory neurons (Basbaum et al., 2009). The cell bodies of the primary sensory neurons are clustered in the dorsal root ganglia or in the trigeminal ganglia, which innervates their target organs or the dorsal horn of the spinal cord (Basbaum et al., 2009; Peirs & Seal, 2016). Depending on its function or its anatomical feature, primary sensory neurons can largely be characterized into the following groups: unmyelinated C fiber (mechanical, thermal, and chemical pain), myelinated Aδ fiber (mechanical, thermal pain), and Aβ fiber (touch sensation) (Bourinet et al., 2014). Various nociceptors expressed in the periphery of these primary sensory neurons mediate different types of sensation. For instance, calcitonin gene related peptide (CGRP) is a 37-amino acid peptide that binds to various peptidic receptors in unmyelinated C and myelinated Aδ fiber (Benemei et al., 2009). Alternatively, various chemical and thermal stimuli activate TRP channels, as previously introduced in Chapter 1.2.2. Multiple subfamilies of TRP channels are expressed in one fiber such as C fiber and Aδ fiber of the dorsal root ganglia and trigeminal ganglia (Cavanaugh et al., 2009) and modulate both thermo- and chemo-sensation of the receptive fields. One example is TRPV1 channels, which originally described as chemically activated vanilloid receptor (Holzer, 1991), but later discovered that TRPV1 is also sensitive to thermal stimuli (Szallasi & Blumberg, 1999; Tominaga et al., 1998). As predicted, the absence of TRPV1 channels affects thermal sensation in mice, resulting in inflammation-mediated thermal hyperalgesia – increased sensitivity to painful stimuli (Caterina et al., 2000; J. B. Davis et al., 2000). Another type of TRP channel, TRPA1 channels, has an intriguing structural feature in that extended ankyrin repeats in the N-terminus of mammalian TRPA1 channels have been hypothesized as a mechanical gating of the ion entry (Howard & Bechstedt, 2004). TRPA1 channels have been known to be expressed in unmyelinated C fibers and to mediate chemical and mechanical nociception, yet the mechanisms by which TRPA1

channels mediate chemical and mechanical nociception are poorly understood (Kerstein et al., 2009). Due to the complex neural circuits and targets involved in chronic pain, there are multiple ways of treating the syndrome which will be introduced in the following section.

1.4.4 Current treatment options of chronic pain syndrome

Approximately 20 % of world population suffers from a chronic pain syndrome (Goldberg & McGee, 2011). For the clinicians, to effectively treat chronic pain, it is crucial to properly diagnose and suggest treatment options based on the diagnosis. The 11th version of the International Classification of Diseases (ICD-11) jointly created by the World Health Organization (WHO) and the International Association for the Study of Pain (IASP) defines chronic pain based on the perceived location, etiology, or the affected/damaged anatomical system (Treede et al., 2015). Unlike acute pain, chronic pain often accompanies negative emotions such as depression and anxiety (Corder et al., 2019). Due to this reason, various first- and second-line treatment options for chronic pain syndromes are also being used as antidepressants and anxiolytics. For instance, an inhibitor of endocannabinoid degradation, which has its role in anxiety-reducing effects, has proven to be effective in stress-induced hyperalgesia in mice (Lomazzo et al., 2015). Besides, benzodiazepines, commonly used as anxiolytics, have also demonstrated positive effects in chronic pain syndrome (Dellemijn & Fields, 1994).

Among many analgesic agents, opioids (e.g. morphine, buprenorphine, and fentanyl) have been considered as the most powerful treatment options for treating pain. Earliest literature on opioids was on opium poppy cultivated by the Sumerians in the lower Mesopotamia. The Sumerians referred opium poppy as 'hul gil', plant of joy, and used it as a euphoric agent during religious rituals. In 1806, a German pharmacist, Friedrich Serturner isolated an active compound in opium, which is currently referred as morphine (Brownstein, 1993). Three opioid receptors including μ-, δ- and κ-opioid receptors are present in the central nervous system (Mansour et al., 1988): μORs are involved in euphoria, δORs are involved in moods, whereas κ-opioid receptors (κORs) are involved in dysphoria (Lutz & Kieffer, 2013). Due to the role of these receptors in modulating both pain and moods, various opioid receptor agonists such as morphine have been utilized as a potent analgesic for chronic pain syndromes. However, severe potential side effects have been accompanied by the usage of opioids such as addiction, tolerance, and respiratory

depression, which has raised a serious concern over the opioid usages in clinical settings (Kolodny et al., 2015; Rosenblum et al., 2008).

In an attempt to develop more effective yet safe opioids for chronic pain syndromes, studies have identified distinct cellular pathways that are linked to adverse effects of the opioid usage. Bohn *et al.* and Raehal *et al.* pointed out that the absence of β-arrestin 2 not only enhances analgesic effects of morphine (Bohn et al., 1999) but also decreases respiratory depression, a side effect linked to an opioid usage (Raehal et al., 2005). Using this trait, two G protein-biased μORs selective agonists – TRV130 (Soergel et al., 2014) and PZM21(Manglik et al., 2016) – have been developed, respectively, in 2014 and 2016. However, despite their ability to void β-arrestin 2 recruitment, both drugs still raised concerns regarding adverse effects of morphine such as respiratory depression and addictive potential (Hill et al., 2018). Notably, δORs have low rewarding properties and analgesic properties (Filliol et al., 2000; Gaveriaux-Ruff & Kieffer, 2011). Furthermore, genetic and pharmacological studies have identified involvement of δORs in mood regulation (Pradhan et al., 2011; Saitoh et al., 2004; van Rijn et al., 2010), suggesting δORs as an attractive alternative for current μORs-targeting opioid analgesics.

1.5 Scope of Dissertation

To further investigate the topics introduced in previous sections, first, Chapter 2 will focus on δOR signaling in modulation of emotional behaviors, particularly on to what degree G protein and β-arrestin signaling pathways are involved in emotional modulation, and what types of downstream kinases and effectors are involved in this modulation of the mouse brain. Chapter 2 particularly targets δORs given their role in both pain and emotion. Detailed molecular and cellular mechanisms by which δORs mediate emotional behaviors provides great significance to the development of future analgesics for patients with chronic pain syndrome and mood disorders. In Chapter 3, kinase activities by different anesthetic approaches are evaluated. Given the role of downstream kinase activities in behavioral modulation, it is crucial to identify potential impacts caused by technical approaches to increase rigor and reproducibility in future studies. As previously described in Chapter 1.2, GPCR and ion channel modulation is one of the key mechanisms of action of how GPCRs manipulate intrinsic properties of the cells. Therefore, in Chapter 4, I will briefly examine high-throughput in vivo tools to screen drugs for TRPA1-δORs crosstalk in vertebrates. Overall, the ultimate goal of the current thesis is to provide novel insights

to the developments of drugs that may potentially aid in patients with both chronic pain syndrome and mood disorders by investigating detailed cellular mechanisms of GPCR-mediated signaling in distinct brain regions as well as by developing in vivo tools to investigate the crosstalk between GPCR and other ion channels in vertebrate.

CHAPTER 2. NON-CANONICAL GPCR SIGNALING POSITIVELY CORRELATES WITH REDUCED ANXIETY-LIKE AND CONDITIONED FEAR-RELATED BEHAVIOR IN MICE

2.1 Introduction

Anxiety- and fear-related behaviors are evolutionary adaptive behaviors important for human survival. However, excessive stimulation of the neural circuits that regulate anxiety- and fear-related behaviors can lead to harmful psychiatric disorders. The expression of anxiety- and fear-related behaviors is regulated by complex integration of both internal and external physiological and sensory cues that influence reflexive behavior, cognitive control, and executive functions. Accordingly, behavioral correlates of anxiety and fear are regulated by a harmonious activity of neurotransmitters and cellular actions across many overlapping and distinct neural circuits (Tovote et al., 2015).

With regard to cellular actions underlying (patho-)physiological behavior, GPCRs play an important role in neuronal signaling. GPCRs bind neurotransmitters and initiate intracellular signal transduction pathways which ultimately affect neuronal excitability, neurotransmitter release and synaptic plasticity. GPCRs, including serotonergic (Akimova et al., 2009), dopaminergic (de la Mora et al., 2010), adrenergic (Kindt et al., 2009), opioidergic (Land et al., 2009) and corticotropin-releasing factor receptors (Takahashi, 2001) have well-documented roles in the modulation of anxiety and fear.

Traditionally, drug development at GPCRs has focused on the canonical G protein pathways; however, the prior two decades have introduced arrestin-dependent signaling as a new concept of GPCR signal transduction. In particular, the 'non-visual' arrestins 2 and 3, referred here as β-arrestin 1 and 2, respectively, have been associated with specific and unique drug effects. The primary role of β-arrestins is to desensitize GPCRs, for example, HIV1-tat infection increases β-arrestin 2 expression in mice amygdala, leading to significant reduction in morphine efficacy in this region (Hahn et al., 2016). Beyond desensitization, β-arrestin 2 may also partake in receptor signaling by scaffolding with various kinases. For example, β-arrestin 2 p38 MAP kinase signaling has been linked to the aversive effects of κOR agonists (Bruchas et al., 2006; Land et al., 2009), whereas a β-arrestin 2-GSK3β/AKT scaffold appears to be driving the antipsychotic effects of dopamine D_2 receptors agonists (Allen et al., 2011; Beaulieu et al., 2005). Currently, few studies

have investigated how signaling scaffolds involving the β-arrestin isoforms may influence anxiety- and fear-like behavior. It is important to begin to address this gap in our current knowledge of the GPCR modulation of psychiatric behavior, especially since the majority of medications that target GPCRs were developed without consideration of the potential adverse or therapeutic effects of β-arrestin signaling. Yet, it is now possible to develop molecules that preferentially activate or avoid β-arrestin signaling and thus have the potential to treat psychiatric disorders more effectively and with a wider therapeutic window.

Here, we describe our efforts to elucidate the roles of β-arrestin isoforms in mediating GPCR signaling in relation to the modulation of anxiety and fear-like behavior. We chose to utilize the δOR as a model GPCR. Previous studies have shown that the δOR selective agonist SNC80 is an efficacious recruiter of β-arrestin 1 and 2 proteins (Chiang et al., 2016; Pradhan et al., 2016; Vicente-Sanchez et al., 2018), and has anxiolytic-like (Saitoh et al., 2004; Saitoh et al., 2018) and fear-reducing effects (Li et al., 2009; Saitoh et al., 2004). Moreover, the δOR-selective agonist TAN67, which is a poor β-arrestin 2 recruiter does not reduce anxiety-like behavior in naïve mice (van Rijn et al., 2010), providing further support for the correlation between β-arrestin 2 signaling and anxiety-like behavior.

Mitogen activated protein kinases (MAPKs) have been implicated with mood disorders and can scaffold with β-arrestin (Coyle & Duman, 2003; Lefkowitz & Shenoy, 2005). Studies have suggested that MAPK signaling, specifically ERK1/2, in the hippocampus and the basolateral amygdala is required for the acquisition and extinction of fear memory (Atkins et al., 1998; Herry et al., 2006). Therefore, we hypothesized that β-arrestin-dependent MAPK signaling may contribute to anxiety-like and fear-related behavior. To test our hypothesis, we assessed the degree to which β-arrestin isoforms and MAPK activation were involved in δOR agonist-mediated modulation of unconditioned anxiety-related behavior and cued-induced fear-related behavior. Our results suggest that ERK1/2 activity is differentially modulated by G protein and β-arrestin signaling and is correlated with anxiety-like and fear-related responses in C57BL/6 mice. We noted that different β-arrestin isoforms were involved in the activation of ERK1/2 across various brain regions, including the striatum, hippocampus and amygdala.

2.2 Materials and Methods

2.2.1 Animals

Wild-type (WT) C57BL/6 male mice were purchased from Envigo (Indianapolis, IN), and β-arrestin 1 or 2 global knockout (KO) mice were bred in our facility (Chiang et al., 2016; Robins, Chiang, Berry, et al., 2018). Adult mice (8-10 weeks, 24 ± 2g) were group housed (3-5 mice) in a single ventilated Plexiglas cage. Mice were maintained at ambient temperature (21°C) in an animal housing facility approved by the Association for Assessment and Accreditation of Laboratory Animal Care and animals were kept on a reversed 12-hour dark-light cycle (lights off at 10:00, lights on at 22:00). Food and water were provided ad libitum. Purchased mice were acclimated for one week prior to the experiments. All animal protocols (#1305000864 by RMvR) were preapproved by Purdue Animal Care and Use Committee and were in accordance with the National Institutes of Health's Guide for the Care and Use of Laboratory Animals.

2.2.2 Drug preparation and administration

SNC80 (#076410, Tocris, Thermo Fisher Scientific, Waltham, MA) was diluted in slightly acidic saline pH5-6. TAN67 (#092110, Tocris, Thermo Fisher Scientific) was diluted in saline, and SL327 (#19691, Tocris, Thermo Fisher Scientific) was diluted in 5% DMSO, 10% Cremophore (Millipore Sigma, Burlington, MA) and 85% saline. 20 mg/kg SNC80 was subcutaneously administered 30 minutes prior to the tests in **Figure 2.3 d-g, Figure 2.5 b and Figure 2.2**, and 50 mg/kg SL327 was subcutaneously administered 60 minutes prior to the administration of SNC80 for **Figure 2.5**. For **Figure 2.2-2.7 and Figure 2.10** either 20 mg/kg SNC80 or 25 mg/kg TAN67 was intraperitoneally administered at the indicated timepoint prior to the testing. The dose of SNC80 and TAN67 was determined based on our previous study (van Rijn et al., 2010) and our preliminary studies (data not shown). Separate batches of mice with no prior history of drug injection were used for the brain collection and behavioral tests to test earlier time-points of ERK1/2 signaling (such as 10 minutes).

2.2.3 Elevated-plus maze test

The elevated-plus maze test was performed as previously described (van Rijn et al., 2010). Mice were allowed to explore the maze for 5 minutes, and arm entries and time spent in each arm were recorded with a camera positioned above the maze.

2.2.4 Dark–light transition box test

The test was performed based on previously established protocols (Robins, Chiang, Berry, et al., 2018; van Rijn et al., 2010) Testing was conducted without a habituation session to the boxes and a 1/2 area dark insert was placed in the locomotor boxes, leaving the remaining 1/2 of the area lit as described previously (Bourin & Hascoet, 2003). Two LED lights were inserted above the light portion of the testing chamber where the lux of the light region ranged from 390-540 lumens and dark chamber lux ranged from 0-12 lumens. For testing, animals were placed in the light portion of the chamber and testing began upon animal entry. Time spent in the dark and light chambers as well as their locomotor activity was recorded for 5 minutes with a photobeam-based tracking system.

2.2.5 Fear potentiated startle (FPS) test

Startle reflexes of mice were recorded in the startle reflex chambers (25.8 x 25 x 26.5 cm) using the Hamilton Kinder Startle Monitor system (Kinder Scientific, Poway, CA). Mice groups were counterbalanced, such that no significant differences between startle reflexes were observed between groups (**Figure 2.10**). On the conditioning day, all subjects were conditioned with 40 conditioning trials by a fixed 2 minute inter-trial interval (ITI), and FPS responses were tested on the following day. The fear conditioning and FPS parameters were based on a previously established protocol (Barrenha & Chester, 2007).

2.2.6 Preparation of tissue homogenates

After drug injections, mice were euthanized by carbon dioxide asphyxiation and rapidly decapitated. Based on our previous studies, we have particularly chosen carbon dioxide asphyxiation over other euthanasia methods that may potentially increase basal ERK1/2 activity in the brain (Ko, Mulia, et al., 2019). The collected brains were first sliced as coronal sections (1.5-2.0 mm) with a brain matrix (#RBMS-205C, Kent scientific, Torrington, CT), and then flash-frozen in dry-ice-chilled 2-methylbutane (-40 °C) (#03551-4, Fisher Scientific). Regions of interest were collected from these slices using a 1 mm biopsy micropunch (#15110-10, Miltex, Plainsboro, NJ) as follows: dorsal striatum and nucleus accumbens (A/P: +0.5 mm to +1.5 mm), dorsal hippocampus and amygdala (A/P: -1 mm to -2 mm), and ventral hippocampus (A/P: -2 mm to -4 mm) (Paxinos & Franklin, 2004). The punches targeted a specific region and produced

enough tissue to run several blots. However, it is noteworthy that the extracted tissue may contain small amounts of tissue from neighboring regions. For example, while the punches for the amygdala primarily consisted of the BLA, the tissue will also have included a small portion of the central amygdala. Collected tissues were further homogenized with a tissue grinder (#357535 & 357537, DWK Life Sciences, Millville, NJ) in RIPA buffer mixed Halt™ Protease and Phosphatase Inhibitor Cocktail (#1861280, Thermo Fisher Scientific). Samples were further prepared based on previously established protocols (Ko, Mulia, et al., 2019). Data depicted in **Figure 2.3 i-m** also includes the data collected for SNC80 at the 0 min or 10 min time points in the experiment depicted in **Figure 2.5 c,d** to represent the full range of observed SNC80 induced ERK1/2 activation in mice tested in separate cohorts at different occasions.

2.2.7 Cell culture

Chinese hamster ovarian CHO-δOR-βArr2 cells (DiscoverX, Fremont, CA) U2OS-δOR-βArr1 (DiscoverX), and NG-108-15 cells (HB-12317™, ATCC®, Manassas, VA) were cultured as recommended by the manufacturer and maintained at 37° C/5 % CO_2. Cells were seeded in a clear 6 well plate (Corning™, Thermo Fisher Scientific) with 250,000 cells/2 mL/well. On the following day, all growth media was aspirated and changed into 1 mL serum-free Opti-MEM (#31985070, Gibco®, Thermo Fisher Scientific). The next day, cells were challenged with 10 µM drugs (SNC80) for a specific duration (0, 3, 6, 20, and 60 minutes). All drugs were diluted in Opti-MEM prior to administration. The media was aspirated following the challenge and 100 µL RIPA buffer was added to collect the samples on ice. Using cell scrapers (#353089, Thermo Fisher Scientific), all samples were dislodged from the 6 well plate, collected and stored at -30° C until usage. For the Western blot, the collected samples were quantified with the Bradford assay and samples were prepared with 4 x Laemmli and boiled at 95° C for 5 minutes. The CHO-δOR-βArr2 cells were also used to measure β-arrestin recruitment using the DiscoverX PathHunter Assay as previously described (Chiang et al., 2016).

2.2.8 SDS-Page and Western blot

Samples (20 µL containing 10 µg protein) were loaded per well of a NuPage 4-12 % Bis-Tris gradient gels (#NP0336BOX, Thermo Fisher Scientific), and the SDS-Page gel was subsequently transferred to nitrocellulose membranes (#1620115, BioRad) by the Western blot. Membranes

were incubated following previously established protocols (Ko, Mulia, et al., 2019). For reproducibility, detailed information regarding the antibodies used in the study are listed in **Table 2.1**. Prepared samples were scanned using the LiCor Odyssey® CLx Scanner (Li-Cor, Lincoln, NE). By utilizing the Li-Cor secondary antibodies, we were able to detect the MAPK, pMAPK, and α-Tubulin on the same blot without the need of stripping/reblotting. In the same membrane, each band was cut based on their size. For instance, ERK1/2 and pERK1/2 bands were collected around 42/44 kDa and α-Tubulin band was collected around 50 kDa in the same membrane. For statistical analysis, we normalized the pMAPK/MAPK ratio to α-Tubulin in case drug treatment changed ERK1/2 levels.

2.2.9 Preparation of tissue for immunofluorescence

To preserve the intact ERK1/2 activity in vivo for fluorescence microscopy, mice were transcardially perfused before isolation of brain tissue. Thirty minutes prior to transcardiac perfusion, mice were administered with 100/10 mg/kg Ketamine/Xylazine. Ten minutes prior to perfusion, 20 mg/kg SNC80 (i.p.) or a corresponding volume of saline was administered to the mice. Mice were then perfused with 30 mL of cold PBS and 4% paraformaldehyde (#100503-916, VWR, Radnor, PA) and were immediately decapitated to collect the brains. The brains were fixated in 4% paraformaldehyde overnight, dehydrated in 30% sucrose, and then embedded in Frozen Section Compound (#3801480, Leica, Wetzlar, Germany). Frozen brains were sliced at a width of 30 μm using the Leica cryostat and permeabilized in 100% methanol at - 20 °C for 10 minutes. The slices were blocked in 5 % Normal goat serum (#S26-100ml, Millipore Sigma) for an hour then stained with primary antibodies as listed in **Table 2.1**. For immunofluorescence labeling, the sections were incubated in the secondary antibodies according to the previously established protocol (Kim et al., 2018) and as listed in **Table 2.1**. After the final washing, the nuclei of the sections were stained and the slices were mounted on a glass slide with Vectashield® (#H-1200, Vector lab, Burlingame, CA). Images were acquired with a Nikon confocal microscope and assembled in Adobe Photoshop CS6 (Adobe).

Table 2.1. Antibody information for the Western blot

Lists of primary and secondary antibodies that were used in the study were included in the table.

Name of primary	*Company*	*Molecular*	*Source*	*Dilution ratio*	*Catalog number*	*Lot number*
p44/42 MAPK (Erk1/2) (L34F12)	Cell Signaling, MA	42, 44	Mouse	1:2,000 for WB; 1:250 for IF	4696S	22
phospho-ERK1/2 (Tyr 204)	Santa Cruz Biotechnology, Dallas, TX	42, 44	Rabbit	1:2,000 for WB	7976-R	C1113
Phospho-p44/42 MAPK (Erk1/2) (Thr202/Tyr204)	Cell Signaling, MA	42, 44	Rabbit	1:2,000 for WB; 1:200 for IF	4370S	24
p38 MAPK (D13E1) XP®	Cell Signaling, MA	38	Rabbit	1:2,000	8690S	6
Phospho-p38 MAPK (Thr180/Tyr182)	Cell Signaling, MA	38	Rabbit	1:2,000	9211S	23
JNK (D-2)	Santa Cruz Biotechnology, Dallas, TX	46, 54	Mouse	1:2,000	7345	L3015
p-JNK (G-7)	Santa Cruz Biotechnology, Dallas, TX	46, 54	Mouse	1:2,000	6254	B2117
α-Tubulin	Santa Cruz Biotechnology, Dallas, TX	50	Mouse	1:2,000	5286	G3117
Name of	*Company*	*Molecular*	*Source*	*Dilution ratio*	*Catalog number*	*Lot number*
IRDye® 680LT	Li-Cor, Lincoln, NE	-	Mouse	1:5,000	926-68020	60824-02
IRDye® 800CW	Li-Cor, Lincoln, NE	-	Rabbit	1:5,000	926-32211	C61103-06
Alexa fluor 594 Goat Anti-Rabbit IgG (H+L) Antibody	Life Technologies (Thermo Fisher), Waltham, MA	-	Rabbit	1:1,000	A-11012	-
Alexa Fluor 488 Goat Anti-Mouse IgG (H+L) Antibody	Life Technologies (Thermo Fisher), Waltham, MA	-	Mouse	1:1,000	A11001	-

2.2.10 Statistics

The maximum amplitude of the startle response was measured from the average of all responses for each trial type (12 noise-alone, 12 light+noise) of each mouse. Fear-potentiated startle response was analyzed using raw (maximum) startle amplitudes and proportional changes of each trial type (noise-alone, light+noise), which is shown as % FPS in the graphs. The proportional change score (% FPS) was calculated as follows: (startle response to light and noise – startle response to noise)/startle response to noise x 100. Thus, %FPS is a sensitive measure that adjusts for individual and group differences (e.g., possible non-specific effects of drug treatment) in startle response magnitude that may be observed on noise-alone and light + noise trials (Walker & Davis, 2002).

All data are presented as individual data points (or means) ± standard error of the mean (S.E.M.). Assays with one independent variable were analyzed for statistical significance using a one-way Analysis of Variance (ANOVA), whereas assays with two independent variables were analyzed using a two-way ANOVA. If a significant deviation of the mean was identified, an appropriate post-hoc analysis was performed as indicated in the supplemental table or the corresponding figure legends. Gaussian distribution of our datasets was assessed using the D'augostino and Pearson analysis. We excluded one outlier in our wild-type cohort that received SNC80 and one that received TAN67 in the FPS assay based on the Grubbs' test ($\alpha = 0.05$). In the dark-light and elevated plus maze tests we excluded subjects that were frozen/stationary for >95% of the experimental time. All statistical analysis was conducted using GraphPad Prism 7 (GraphPad Software, La Jolla, CA).

2.3 Results

2.3.1 Involvement of β-arrestin 2 in the modulation of anxiety-like behavior

In 2016, Astra Zeneca revealed that their novel δOR selective agonist AZD2327 (**Figure 2.1 a, Left**) was capable of reducing anxiety-like behavior in mice (Richards et al., 2016). AZD2327 is not commercially available, but is structurally similar to SNC80, a commercially available δOR selective agonist (**Figure 2.1 a, Right**). SNC80 is a known super-recruiter of β-arrestin 2 (Chiang et al., 2016) (**Figure 2.1 b**) and similar to AZD2327 exhibits anxiolytic-like effects in rodents (Saitoh et al., 2004; van Rijn et al., 2010). These previous findings led us to hypothesize that β-

arrestin 2 may be required for the anxiolytic effects of SNC80 and AZD2327. Using two models of anxiety-like behavior, the elevated plus maze (EPM) test and dark-light box transition test (**Figure 2.1 c**), we measured the behavioral effects of SNC80 in β-arrestin 2 KO mice, at a dose known to produce anxiolytic-like effects in wild-type (WT) mice (van Rijn et al., 2010). As expected, systemic administration of SNC80 (20 mg/kg, s.c.) significantly increased the time WT mice spent in the open arm of the elevated plus maze (**Figure 2.1 d**; see **Table 2.1** for two-way ANOVA and post-hoc multiple comparison) and the light chamber of dark-light transition box (**Figure 2.1 e**; see **Table 2.1** for two-way ANOVA and post-hoc multiple comparison). As we predicted, the anxiolytic effects of SNC80 were attenuated in β-arrestin 2 KO mice (**Figure 2.1 d and e**; see **Table 2.1** for two-way ANOVA and post-hoc multiple comparison). Although the total movement in the elevated plus maze was slightly lower in β-arrestin 2 KO mice than WT mice, no drug effects were observed in both genotypes (**Figure 2.1 f**; see **Table 2.1** for two-way ANOVA and post-hoc multiple comparison). Likewise, no statistical difference in total transition was observed in the dark light transition box test (**Figure 2.1 g** see **Table 2.1** for two-way ANOVA and post-hoc multiple comparison); however, as previously described, SNC80 produced hyperlocomotive behavior in mice ((Chiang et al., 2016), **Figure 2.2**).

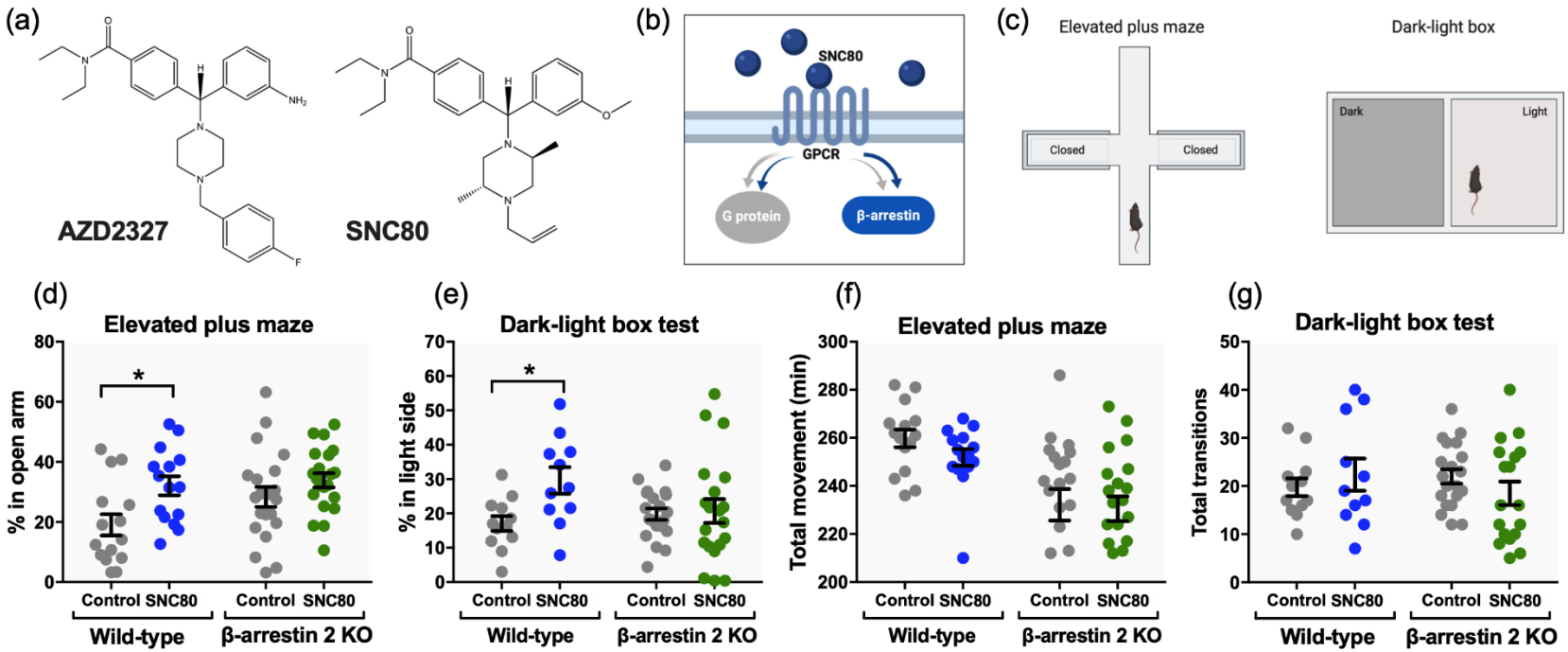

Figure 2.1 Beneficial role for β-arrestin 2 in reducing anxiety-like behavior

(a) Chemical similarity between AZD2327, a δOR agonist used in phase II clinical trials for anxious major depressive disorder and SNC80. **(b)** Scheme highlighting that SNC80 is δOR selective agonist, that activates Gi proteins but also strongly recruits β-arrestin 2. **(c)** Schematic diagram of the elevated plus maze test and dark-light box test. **(d)** The β-arrestin-biased δOR agonist, SNC80 (20 mg/kg, s.c.), significantly increased percentage of time spent in open arms in WT mice (n=15). but not β-arrestin 2 KO mice (n=21). **(e)** SNC80 increased percentage of time spent in light box in WT mice (control: n=12, SNC80: n=11), but not in β-arrestin 2 KO mice (n=20). **(f)** The total time of movements were equal between drug treatments. **(g)** No statistical significance was observed in the total transitions between light and dark chambers. (Significance was calculated by two-way ANOVA followed by a Sidak's multiple comparison; *$p<0.05$; all values are shown as individaul data points ± S.E.M.).

Table 2.2. Statistical analysis of anxiety-like behavior upon systemic administration of SNC80 in WT and β-arrestin 2 KO mice

Statistical differences of anxiety-like behaviors in WT or β-arrestin 2 KO mice shown in Fig. 2.1. Significance between groups was calculated by two-way ANOVA followed by a Sidak's multiple comparison (*p<0.05, and ns=not significant).

Subfigure	Behavior test	Genotype	Drug	# of samples	Test	Source of Variation	F-value	p-value	Post hoc analysis	Group Comparison	Mean Diff.	p-value	Significance
Figure 2.1-d	Elevated plus maze test	WT & βarr2 KO	SNC80 (20 mg/kg, s.c.)	WT-Control: 15 WT-SNC80: 15 B2-Control: 21 B2-SNC80: 21	Two-Way ANOVA test	Interaction Genotype factor Drug factor	F(1,68) = 1.429 F(1,68) = 3.15 F(1.68) = 8.781	0.236 0.0804 0.0042	Sidak's Multiple Comparison Test	WT: Con vs. SNC80	-13.0400	0.0164	*
										B2 KO: Con vs. SNC80	-5.5450	0.3200	ns
Figure 2.1-e	Dark-light box test	WT & βarr2 KO	SNC80 (20 mg/kg, s.c.)	WT-Control: 12 WT-SNC80: 11 B2-Control: 20 B2-SNC80: 20	Two-Way ANOVA test	Interaction Genotype factor Drug factor	F(1,59) = 3.677 F(1,59) = 1.039 F(1.59) = 4.978	0.06 0.3122 0.0295	Sidak's Multiple Comparison Test	WT: Con vs. SNC80	-12.5200	0.0232	*
										B2 KO: Con vs. SNC80	-0.9467	0.9584	ns
Figure 2.1-f	Elevated plus maze test	WT & βarr2 KO	SNC80 (20 mg/kg, s.c.)	WT-Control: 15 WT-SNC80: 15 B2-Control: 21 B2-SNC80: 21	Two-Way ANOVA test	Interaction Genotype factor Drug factor	F(1,68) = 0.3392 F(1,68) = 20.7 F(1.68) = 0.796	0.5622 <0.0001 0.3754	Sidak's Multiple Comparison Test	WT: Con vs. SNC80	7.9330	0.5615	ns
										B2 KO: Con vs. SNC80	1.6670	0.9643	ns
Figure 2.1-g	Dark-light box test	WT & βarr2 KO	SNC80 (20 mg/kg, s.c.)	WT-Control: 12 WT-SNC80: 11 B2-Control: 20 B2-SNC80: 18	Two-Way ANOVA test	Interaction Genotype factor Drug factor	F(1,57) = 1.754 F(1,57) = 0.1222 F(1.57) = 0.03687	0.1907 0.728 0.8484	Sidak's Multiple Comparison Test	WT: Con vs. SNC80	-2.6140	0.7254	ns
										B2 KO: Con vs. SNC80	3.5000	0.3949	ns

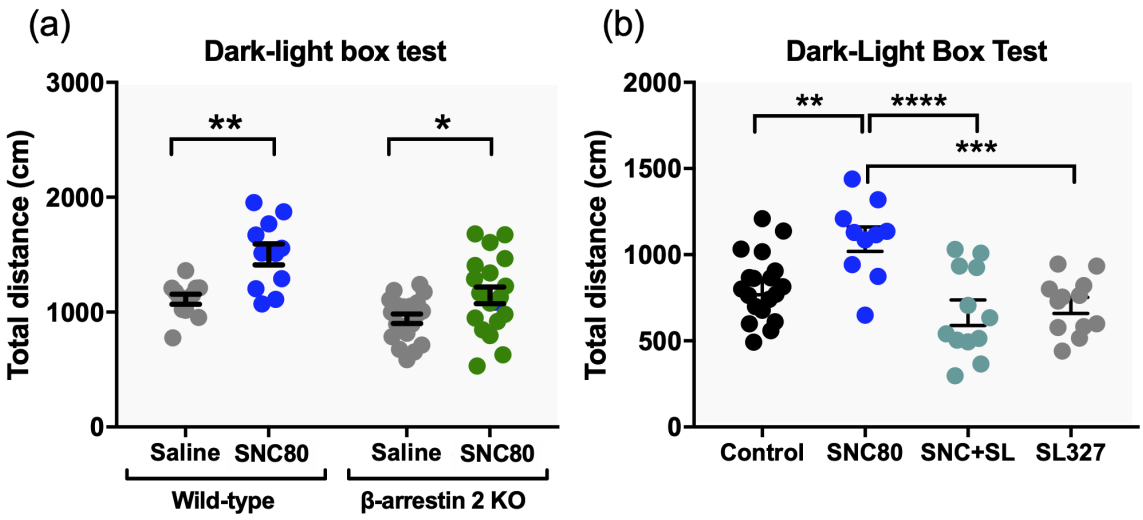

Figure 2.2 Locomotor effects of drug/vehicle treatment in the WT or β-arrestin 2 KO mice in the dark light upon administration of drugs

(a) Traveled distance of WT (control: n=12, SNC80: n=11) and β-arrestin 2 KO mice (control: n=20, SNC80: n=20) upon administration of 20 mg/kg SNC80 (i.p.) in dark light box test shown in Fig. 4 b, d. **(b)** Traveled distance of WT mice upon administration of 20 mg/kg SNC80 (i.p.) (control: n=8, SNC80: n=12, SNC+SL: n=12, SL327: n=12) in presence or absence of 50 mg/kg SL327 in dark light box test shown in Fig. 4 f. SNC80-induced hyperlocomotion corresponds with a previous report (Chiang et al., 2016). (For (a), Significance was calculated by two-way ANOVA $F_{1,59}$=1.949, p=0.1670, WT p=0.0011, β-arrestin 2 KO p=0.0283 after Sidak's multiple comparison; for (b), one-way ANOVA $F_{3,49}$=9.037, p<0.001, control vs. SNC80 p=0.007, SNC80 vs. SNC+SL p<0.0001, SNC+SL vs. SL327 p<0.0004 followed by a Tukey's multiple comparison; *p<0.05, **p<0.01, ***p<0.001, ****p<0.0001; all values are shown as individual data points ± S.E.M.).

2.3.2 The β-arrestin recruiting δOR agonist SNC80 strongly activates ERK1/2 in vitro and in vivo

Activation of κOR has been associated with β-arrestin 2-mediated p38 phosphorylation (Bruchas et al., 2006). To determine if δOR agonism similarly stimulates mitogen-activated protein kinases (MAPKs), we measured p38, JNK, and ERK1/2 activation in Chinese Hamster Ovarian cells stably expressing δOR and β-arrestin 2 (CHO-δOR-βArr2) following stimulation with 10 μM SNC80, a concentration that will fully activate G-protein signaling and induce β-arrestin 2 recruitment (Robins, Chiang, Mores, et al., 2018). We found that SNC80 led to a rapid increase in ERK1/2 phosphorylation within 3 minutes in CHO-δOR-βArr2 cells, which lasted until 60 minutes, in agreement with previous δOR-mediated ERK activation in CHO cells (Rozenfeld & Devi, 2007). We did not observe strong activation of p38 and JNK by SNC80 (**Figure 2.3 a**). The δOR mediated ERK1/2 signaling in these cells were not an artifact of the recombinant overexpression of δOR and β-arrestin 2 in the CHO cells as we observed a similar profile for ERK1/2 activation in NG108-15 neuroblastoma cells endogenously expressing δOR and β-arrestin (Cen et al., 2001; Eisinger et al., 2002; Klee et al., 1982) (**Figure 2.3 b**). We similarly found ERK1/2 activation in several mouse brain regions, known to express δORs, including the dorsal hippocampus, the amygdala and the striatum (Chu Sin Chung et al., 2015; Erbs et al., 2015) (**Figure 2.3 c-e**). The SNC80-induced ERK1/2 activation in these regions was confirmed and quantified by the Western blot analysis of flash-frozen tissue punches upon collection (**Figure 2.3 f**). Here, we observed that SNC80 (20 mg/kg, i.p.) significantly increased ERK1/2 phosphorylation at the 10-minute time-point in all tested brain regions except for the ventral hippocampus of WT mice (**Figure 2.3 g-k**; see **Table 2.3** for one-way ANOVA and post-hoc multiple comparison), and these activations returned to basal levels 30 minutes after the SNC80 administration.

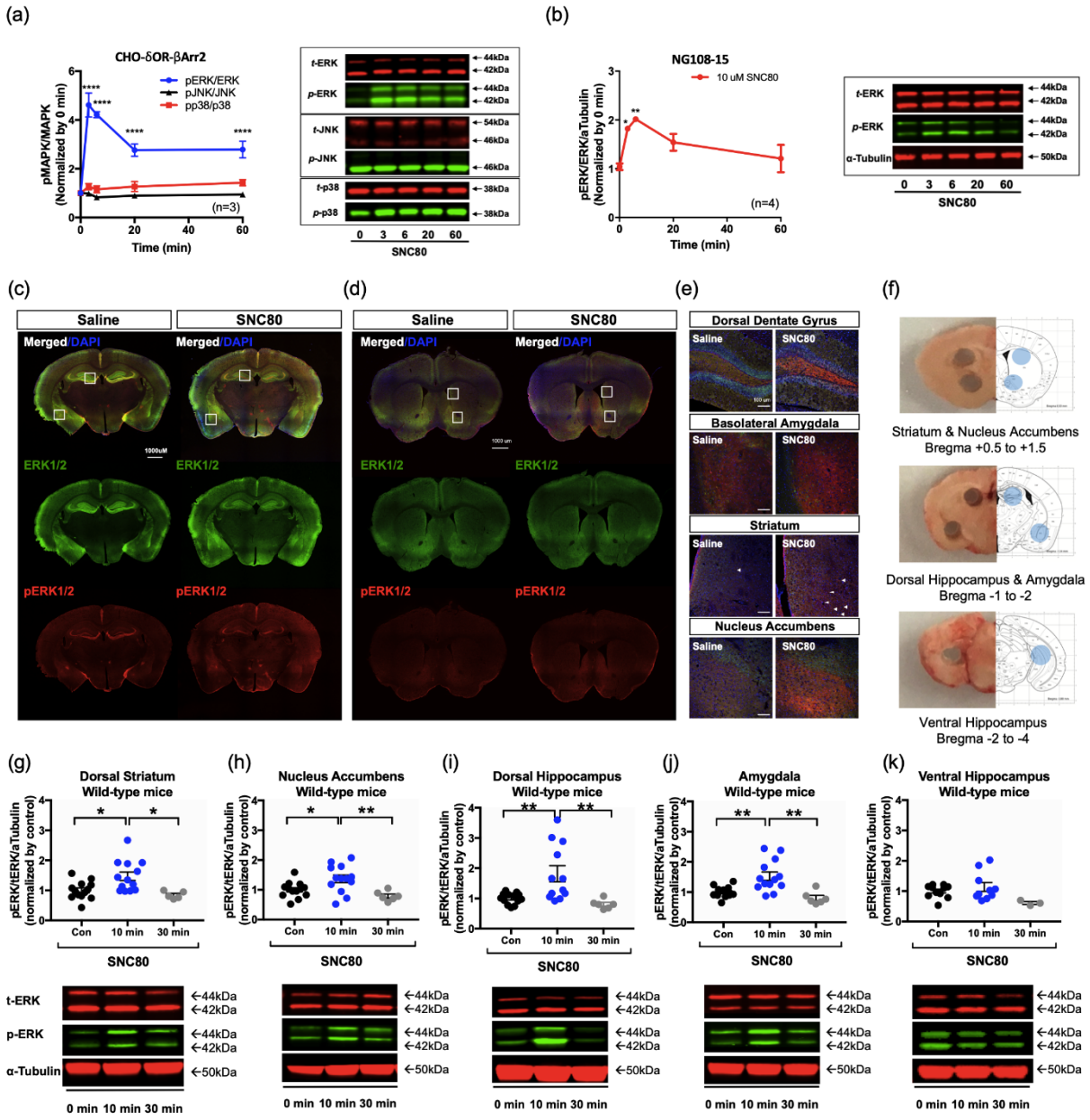

Figure 2.3 ERK1/2 activation in the amygdala and the dorsal hippocampus are β-arrestin 2 dependent

(a) Schematic diagram of the cellular context in β-arrestin 2 genetic KO mice. SNC80 (20 mg/kg, i.p.) induced ERK1/2 activation in the dorsal striatum (**b**) and nucleus accumbens (**c**). β-arrestin 2 KO ablated the SNC80-induced ERK1/2 activation in the dorsal hippocampus (**d**) and the amygdala (**e**) with no effects in the ventral hippocampus. **(f)** Representative Western blot images are shown tothe right of the related bar graph. (Significance was analyzed by one-way ANOVA followed by a Tukey's multiple comparison; *p < 0.05, **p<0.01; all values are shown as individual data points ± S.E.M.).

Table 2.3. Statistical analysis of ERK1/2 expression levels upon time-series administration of SNC80 in WT and β-arrestin 2 KO mouse brain

Statistical differences of ERK1/2 expression levels in WT mice shown in Figure 2.3 and β-arrestin 2 KO mice in Figure 2.4. Significance between groups was calculated by one-way ANOVA followed by a Tukey's multiple comparison (*p<0.05, **p<0.01, and ns=not significant).

Subfigure	Brain region	Genotype	Drug	# of samples	Test	F-value	p-value	Group	Mean	Post hoc analysis	Group Comparison	Mean Diff.	p-value	Significance
Figure 2.3-i	Dorsal Striatum	WT	SNC80 (20 mg/kg, i.p)	Con: 13 10 min: 13 30 min: 5	One-Way ANOVA test	F (2,28) = 6.776	P=0.0040	Con 10 min 30 min	1 1.472 0.8466	Tukey's Multiple Comparison Test	Con vs. 10 min Con vs. 30 min 10 min vs. 30 min	-0.4718 0.1534 0.6253	0.0128 0.7398 0.0140	* ns *
Figure 2.3-j	Nucleus Acumbens	WT	SNC80 (20 mg/kg, i.p)	Con: 13 10 min: 13 30 min: 6	One-Way ANOVA test	F (2,29) = 6.645	P=0.0042	Con 10 min 30 min	1 1.363 0.793	Tukey's Multiple Comparison Test	Con vs. 10 min Con vs. 30 min 10 min vs. 30 min	-0.3632 0.2070 0.5702	0.0317 0.4563 0.0064	* ns **
Figure 2.3-k	Dorsal Hippocampus	WT	SNC80 (20 mg/kg, i.p)	Con: 13 10 min: 12 30 min: 6	One-Way ANOVA test	F (2,28) = 8.252	P=0.0015	Con 10 min 30 min	1 1.819 0.8082	Tukey's Multiple Comparison Test	Con vs. 10 min Con vs. 30 min 10 min vs. 30 min	-0.8194 0.1918 1.0110	0.0051 0.7923 0.0056	** ns **
Figure 2.3-l	Amygdala	WT	SNC80 (20 mg/kg, i.p)	Con: 13 10 min: 13 30 min: 6	One-Way ANOVA test	F (2,29) = 10.82	P=0.0003	Con 10 min 30 min	1 1.526 0.806	Tukey's Multiple Comparison Test	Con vs. 10 min Con vs. 30 min 10 min vs. 30 min	-0.5264 0.1940 0.7204	0.0024 0.5284 0.0010	** ns **
Figure 2.3-m	Ventral Hippocampus	WT	SNC80 (20 mg/kg, i.p)	Con: 11 10 min: 10 30 min: 3	One-Way ANOVA test	F (2,21) = 2.82	P=0.0823	Con 10 min 30 min	1 1.138 0.6108	Tukey's Multiple Comparison Test	Con vs. 10 min Con vs. 30 min 10 min vs. 30 min	-0.1379 0.3892 0.5271	0.6248 0.2039 0.0676	ns ns ns
Figure 2.4-b	Dorsal Striatum	βarr2 KO	SNC80 (20 mg/kg, i.p)	Con: 5 10 min: 5 30 min: 6	One-Way ANOVA test	F (2,13) = 2.484	P=0.1220	Con 10 min 30 min	1 2.136 1.417	Tukey's Multiple Comparison Test	Con vs. 10 min Con vs. 30 min 10 min vs. 30 min	-1.1360 -0.4171 0.7194	0.1085 0.6837 0.3435	ns ns ns
Figure 2.4-c	Nucleus Acumbens	βarr2 KO	SNC80 (20 mg/kg, i.p)	Con: 5 10 min: 4 30 min: 6	One-Way ANOVA test	F (2,12) = 7.984	P=0.0062	Con 10 min 30 min	1 2.465 1.396	Tukey's Multiple Comparison Test	Con vs. 10 min Con vs. 30 min 10 min vs. 30 min	-1.4650 -0.3959 1.0690	0.0055 0.4935 0.0298	** ns *
Figure 2.4-d	Dorsal Hippocampus	βarr2 KO	SNC80 (20 mg/kg, i.p)	Con: 5 10 min: 4 30 min: 6	One-Way ANOVA test	F (2,12) = 0.02711	P=0.9733	Con 10 min 30 min	1 1.012 0.9664	Tukey's Multiple Comparison Test	Con vs. 10 min Con vs. 30 min 10 min vs. 30 min	-0.0115 0.0336 0.0451	0.9985 0.9840 0.9747	ns ns ns
Figure 2.4-e	Amygdala	βarr2 KO	SNC80 (20 mg/kg, i.p)	Con: 5 10 min: 5 30 min: 6	One-Way ANOVA test	F (2,13) = 2.502	P=0.1204	Con 10 min 30 min	1 1.471 0.9424	Tukey's Multiple Comparison Test	Con vs. 10 min Con vs. 30 min 10 min vs. 30 min	-0.4705 0.0576 0.5281	0.2149 0.9719 0.1315	ns ns ns
Figure 2.4-f	Ventral Hippocampus	βarr2 KO	SNC80 (20 mg/kg, i.p)	Con: 5 10 min: 4 30 min: 6	One-Way ANOVA test	F (2,12) = 1.474	P=0.2677	Con 10 min 30 min	1 1.271 0.9135	Tukey's Multiple Comparison Test	Con vs. 10 min Con vs. 30 min 10 min vs. 30 min	-0.2715 0.0865 0.3580	0.4581 0.9019 0.2495	ns ns ns

2.3.3 β-arrestin 2 is required to activate ERK1/2 signaling in the limbic structures of the brain

To determine if β-arrestin 2 is responsible for the ERK1/2 activation in the tested brain regions (**Figure 2.3 g-k**), we injected 20 mg/kg of SNC80 in the β-arrestin 2 KO mice (**Figure 2.4 a**) and measured levels of ERK1/2 activation in the five brain regions tested in **Figure 2.3**. While, SNC80 still strongly activated ERK1/2 in the striatum and the nucleus accumbens of the β-arrestin 2 KO mice (**Figure 2.4 b-c**; see **Table 2.3** for one-way ANOVA and post-hoc multiple comparison), we did not observe significant SNC80-induced ERK1/2 activation in the amygdala, the ventral hippocampus and the dorsal hippocampus of these KO mice (**Figure 2.4 d-f**; see **Table 2.3** for one-way ANOVA and post-hoc multiple comparison).

2.3.4 β-arrestin 2 is required to activate ERK1/2 signaling in the limbic structures of the brain

We next assessed if the anxiolytic effects of SNC80 were dependent on ERK1/2 activation. We administered wild-type mice with SL327, a MEK1/2 inhibitor that indirectly prevents ERK1/2 activation, (**Figure 2.5 a**) (Tohgo et al., 2002). We found that SL327 (50 mg/kg, s.c.) ablated the anxiolytic-like effects of SNC80 (20 mg/kg, i.p.) in WT mice (**Figure 2.5 b**; see **Table 2.4** for one-way ANOVA and post-hoc multiple comparison). Thus, SNC80 anxiolytic-like behavior relied on the presence of β-arrestin 2 (**Figure 2.1 d,e**) and MEK/ERK1/2 activation (**Figure 2.5 g-k**). The hippocampus is a brain region associated with anxiety-like behavior in the elevated plus maze (File et al., 2000) and δOR-agonism in the dorsal hippocampus, as well as the amygdala reduces anxiety-like behavior in the open field test (Saitoh et al., 2018; Solati et al., 2010). These published findings agree with our observation of SNC80-induced β-arrestin 2-dependent ERK1/2 activity specifically in these two brain regions (**Figure 2.4 d,e**). Therefore, if the β-arrestin-mediated ERK1/2 signaling in these two regions was critical for the anxiolytic-like effects of SNC80, we would expect ERK1/2 activity to be abolished in these regions in the mice co-treated with SNC80 and SL327. Indeed, we found that SL327 effectively decreased SNC80-induced ERK1/2 activity in the dorsal hippocampus and the amygdala (**Figure 2.5 c,d**, see **Table 2.4** for detailed statistics).

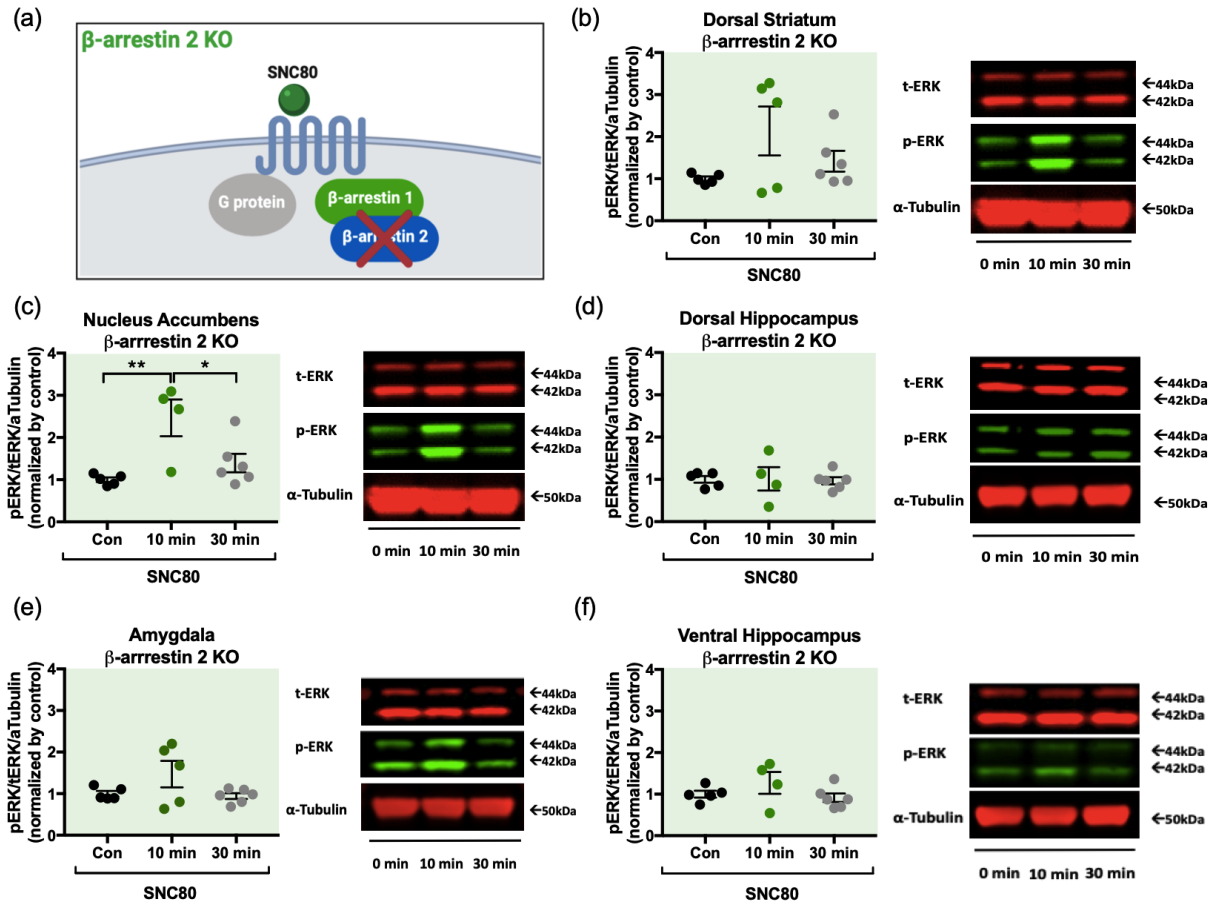

Figure 2.4 ERK1/2 activation in the amygdala and the dorsal hippocampus are β-arrestin 2 dependent

(a) Schematic diagram of the cellular context in β-arrestin 2 genetic KO mice. SNC80 (20 mg/kg, i.p.) induced ERK1/2 activation in the dorsal striatum (**b**) and nucleus accumbens (**c**). β-arrestin 2 KO ablated the SNC80-induced ERK1/2 activation in the dorsal hippocampus (**d**) and the amygdala (**e**) with no effects in the ventral hippocampus. **(f)** Representative Western blot images are shown tothe right of the related bar graph. (Significance was analyzed by one-way ANOVA followed by a Tukey's multiple comparison; *p < 0.05, **p<0.01; all values are shown as individual data points ± S.E.M.)

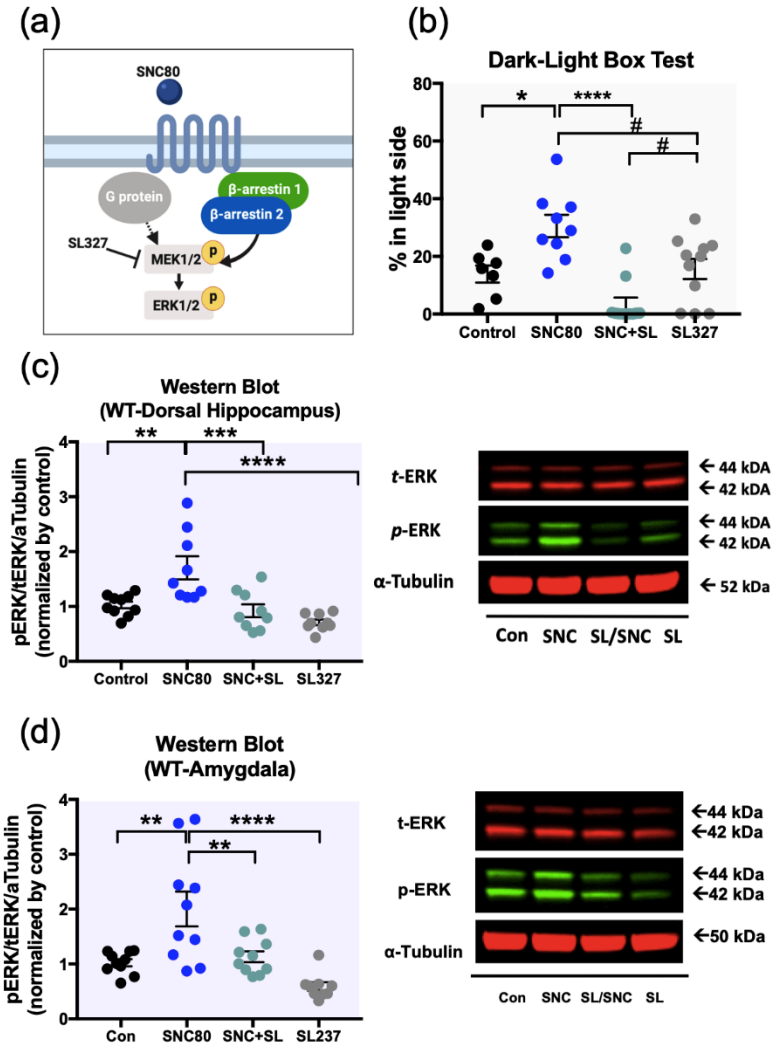

Figure 2.5 ERK1/2 is required for the anxiolytic-like effects induced by SNC80

(a) A schematic diagram of SL327 induced inhibition of SNC80 mediated ERK1/2 signaling. **(b)** SL327 (50 mg/kg, s.c.), attenuated the anxiolytic-like effects of SNC80 (20 mg/kg i.p.) in WT mice (control: n=8, SNC80: n=12, SNC+SL: n=12, SL327: n=12). **(c-d)** SL327 significantly inhibited SNC80-induced ERK1/2 phosphorylation in the dorsal hippocampus and the amygdala (Significance was calculated by one-way ANOVA followed by a Sidak's or Tukey's multiple comparison; *p<0.05, **p<0.01, ***p<0.001, ****p<0.0001, #p<0.05; all values are shown as individual data points ± S.E.M.; SNC+SL means SNC80+SL327 and SL means SL327).

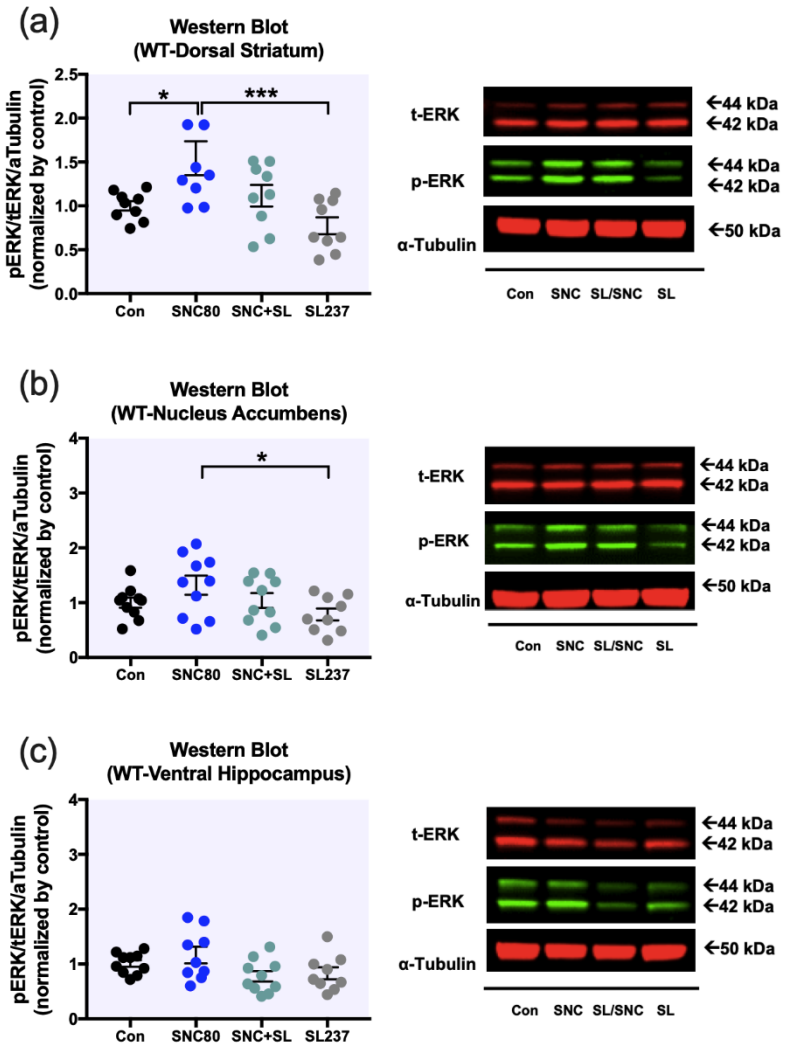

Figure 2.6 SNC80-induced ERK1/2 activation is partly affected by SL327 in the striatal regions of the brain

SL327 (50 mg/kg, s.c.), attenuated SNC80-induced ERK1/2 phosphorylation in the striatum **(a)** and similar trends were observed in the nucleus accumbens **(b)**. **(c)** Yet, no change was observed in the ventral hippocampus similar to Figure 2m. (Significance was calculated by one-way ANOVA followed by a Sidak's or Tukey's multiple comparison; *p<0.05, ***p<0.001; all values are shown as individual data points ± S.E.M.; SNC+SL means SNC80+SL327 and SL means SL327).

Table 2.4. Statistical analysis of anxiety-like behavior and ERK1/2 expression levels upon administration of SNC80 in the presence/absence of SL327 in WT mouse brain

Statistical differences of anxiety-like behavior and ERK1/2 expression levels in WT mouse brain shown in Figure 2.5 and Figure 2.6. Significance between groups was calculated by one-way ANOVA followed by a Tukey's multiple comparison (*p<0.05, **p<0.01, ***p<0.001, and ns=not significant).

Subfigure	Behavior test or Brain region	Genotype	Drug	# of samples	Test	F-value	p-value	Group	Mean	Post hoc analysis	Group Comparison	Mean Diff.	p-value	Significance
Figure 2.5-b	Dar-light box test	WT	SNC80 (20 mg/kg, i.p) or SL327 (50 mg/kg s.c.)	Con: 7 SNC80: 9 SNC+SL: 11 SL327: 11	One-Way ANOVA test	F (3, 34) = 12.35	P<0.0001	Control SNC80 SNC+SL327 SL327	13.88 30.53 3.418 15.64	Tukey's Multiple Comparison Test	Control vs. SNC80	-16.6400	0.0109	*
											Control vs. SNC+SL327	10.4600	0.1496	ns
											Control vs. SL327	-1.7550	0.9830	ns
											SNC80 vs. SNC+SL327	27.1100	<0.0001	****
											SNC80 vs. SL327	14.8900	0.0106	*
											SNC+SL327 vs. SL327	-12.2200	0.0325	*
Figure 2.5-c	Dorsal Hippocampus	WT	SNC80 (20 mg/kg, i.p) or SL327 (50 mg/kg s.c.)	Con: 10 SNC80: 9 SNC+SL: 9 SL327: 9	One-Way ANOVA test	F (3, 33) = 11.68	P<0.0001	Control SNC80 SNC+SL327 SL327	1 1.706 0.9214 0.7122	Tukey's Multiple Comparison Test	Control vs. SNC80	-0.6767	0.0024	**
											Control vs. SNC+SL327	0.1076	0.9247	ns
											Control vs. SL327	0.3169	0.2790	ns
											SNC80 vs. SNC+SL327	0.7843	0.0006	***
											SNC80 vs. SL327	0.9936	<0.0001	****
											SNC+SL327 vs. SL327	0.2092	0.6459	ns
Figure 2.5-d	Amygdala	WT	SNC80 (20 mg/kg, i.p) or SL327 (50 mg/kg s.c.)	Con: 10 SNC80: 10 SNC+SL: 10 SL327: 9	One-Way ANOVA test	F (3, 35) = 10.9	P<0.0001	Control SNC80 SNC+SL327 SL327	1 2.003 1.133 0.5908	Tukey's Multiple Comparison Test	Control vs. SNC80	-0.9798	0.0021	**
											Control vs. SNC+SL327	-0.1093	0.9713	ns
											Control vs. SL327	0.4325	0.3442	ns
											SNC80 vs. SNC+SL327	0.8705	0.0069	**
											SNC80 vs. SL327	1.4120	<0.0001	****
											SNC+SL327 vs. SL327	0.5419	0.1677	ns
Figure 2.6-a	Dorsal Striatum	WT	SNC80 (20 mg/kg, i.p) or SL327 (50 mg/kg s.c.)	Con: 9 SNC80: 9 SNC+SL: 9 SL327: 9	One-Way ANOVA test	F (3, 32) = 6.421	P=0.0016	Control SNC80 SNC+SL327 SL327	1 1.543 1.115 0.7734	Tukey's Multiple Comparison Test	Control vs. SNC80	-0.5429	0.0247	*
											Control vs. SNC+SL327	-0.1155	0.9180	ns
											Control vs. SL327	0.2266	0.5960	ns
											SNC80 vs. SNC+SL327	0.4274	0.1032	ns
											SNC80 vs. SL327	0.7694	0.0009	***
											SNC+SL327 vs. SL327	0.3420	0.2490	ns
Figure 2.6-b	Nucleus Accumbens	WT	SNC80 (20 mg/kg, i.p) or SL327 (50 mg/kg s.c.)	Con: 10 SNC80: 10 SNC+SL: 10 SL327: 9	One-Way ANOVA test	F (3, 35) = 2.672	P=0.0624	Control SNC80 SNC+SL327 SL327	1 1.319 1.04 0.7877	Tukey's Multiple Comparison Test	Control vs. SNC80	-0.3193	0.3248	ns
											Control vs. SNC+SL327	-0.0404	0.9963	ns
											Control vs. SL327	0.2123	0.6809	ns
											SNC80 vs. SNC+SL327	0.2790	0.4427	ns
											SNC80 vs. SL327	0.5316	0.0394	*
											SNC+SL327 vs. SL327	0.2526	0.5501	ns
Figure 2.6-c	Ventral Hippocampus	WT	SNC80 (20 mg/kg, i.p) or SL327 (50 mg/kg s.c.)	Con: 10 SNC80: 9 SNC+SL: 10 SL327: 9	One-Way ANOVA test	F (3, 34) = 2.734	P=0.0588	Control SNC80 SNC+SL327 SL327	1 1.164 0.7771 0.8315	Tukey's Multiple Comparison Test	Control vs. SNC80	-0.1522	0.7419	ns
											Control vs. SNC+SL327	0.2347	0.3879	ns
											Control vs. SL327	0.1803	0.6299	ns
											SNC80 vs. SNC+SL327	0.3869	0.0655	ns
											SNC80 vs. SL327	0.3325	0.1549	ns
											SNC+SL327 vs. SL327	-0.0545	0.9833	ns

2.3.5 Fear-potentiated startle behavior is correlated with ERK1/2 activity but is not mediated by β-arrestin 2

Besides reducing anxiety-like behavior, δOR activation can also alleviate conditioned fear-related behavior (Saitoh et al., 2004; Sugiyama et al., 2019). Based on our results and previous studies, we hypothesized that SNC80 may similarly reduce fear-related behavior through a mechanism that involves β-arrestin 2. To measure conditioned fear, we utilized a mouse behavior paradigm of fear-potentiated startle (FPS) (**Figure 2.7 a**). In WT mice (**Figure 2.7 b**), we noted that SNC80 (20 mg/kg, i.p.) significantly reduced startle responses to the unconditioned 'noise' cue as well as to the conditioned 'light+noise' cue (**Figure 2.7 c**; see **Table 2.5** for two-way ANOVA and post-hoc multiple comparison). The reduction produced by 'light+noise' is larger than the reduction produced by 'noise', and thus these reductions result in a significant reduction in % FPS response (**Figure 2.7 d**; p-value is indicated in figure legends). To our surprise, we found that SNC80 was equally effective in reducing % FPS responses in β-arrestin 2 KO mice (**Figure 2.7 e,f**; see **Table 2.5** for two-way ANOVA and post-hoc multiple comparison; **Figure 2.7 g**; p-value is indicated in figure legends). While SNC80 is a very efficacious recruiter of β-arrestin, it still also fully activates Gi protein signaling (Chiang et al., 2016; Robins, Chiang, Mores, et al., 2018). Thus, we next hypothesized that the observed fear-reducing effects of SNC80 could be mediated through G_i protein signaling. To address this hypothesis, we utilized a δOR selective agonist, TAN67, which is a poor recruiter of β-arrestin (**Figure 2.7 f**), and considered G_i protein-biased (Chiang et al., 2016; Robins, Chiang, Mores, et al., 2018). However, when we administered TAN67 (25 mg/kg, i.p.) to our WT mice (**Figure 2.7 h**), TAN67 did not significantly change startle to the noise yet produced an increasing trend of startle to the light+noise stimuli (**Fig. 2.7 i**; see **Table 2.5** for two-way ANOVA and post-hoc multiple comparison), which resulted in a significant increase in %FPS (**Figure 2.7 j**; p-value is indicated in figure legends). The lack of a direct effect of TAN67 on noise-alone startle is in agreement with our previous finding that TAN67 did not change basal anxiety-like behavior in the elevated plus maze and dark-light transition test (van Rijn et al., 2010). Interestingly, our Western blot analysis of ERK1/2 activities in WT mice revealed that this G_i protein-biased agonist, TAN67, decreased ERK1/2 phosphorylation in the dorsal striatum, the nucleus accumbens, the dorsal hippocampus and the amygdala (**Figure 2.8 a-d**). In the ventral hippocampus, TAN67 did not alter ERK1/2 activity (**Figure 2.8 e**), which was similar to the lack

of ERK1/2 modulation by SNC80 in this region (**Figure 2.3 k**) and may be indicative of low δOR expression in the ventral region as previously described (Mansour et al., 1987).

2.3.6 Potential roles for ERK1/2 and β-arrestin 1 in the modulation of conditioned-fear behavior

Our results suggest that SNC80 reduces conditioned fear through a mechanism that does not involve β-arrestin 2 or G protein signaling. Therefore, we next hypothesized that the effect may be mediated by β-arrestin 1 instead. However, SNC80 is known to induce severe seizures in β-arrestin 1 KO mice (Vicente-Sanchez et al., 2018), preventing us from testing the FPS response of SNC80 in this strain. Instead, we measured SNC80-induced ERK1/2 phosphorylation in the β-arrestin 1 KO mice. In comparison to WT mice (**Figure 2.3 g-k**), genetic knockout of β-arrestin 1 prevented SNC80-mediated ERK1/2 phosphorylation in the dorsal striatum and nucleus accumbens (**Figure 2.8 f-g**; see **Table 2.6** for one-way ANOVA and post-hoc multiple comparison). In the amygdala and dorsal hippocampus of β-arrestin 1 KO mice, SNC80 did increase ERK1/2 phosphorylation (**Figure 2.8 h-i**), but in contrast to the response observed in WT mice, the activation was sustained for at least 30 minutes. Additionally, we observed the same trend in the ventral hippocampus (**Figure 2.8 j**), a region where we had observed no δOR agonist-mediated modulation of ERK1/2 in WT mice (**Figure 2.3 k** and **Figure 2.8 e**). Thus, we hypothesized that the increased ERK1/2 in these regions is most likely a result of seizure activity and not necessarily a result of δOR-mediated effects.

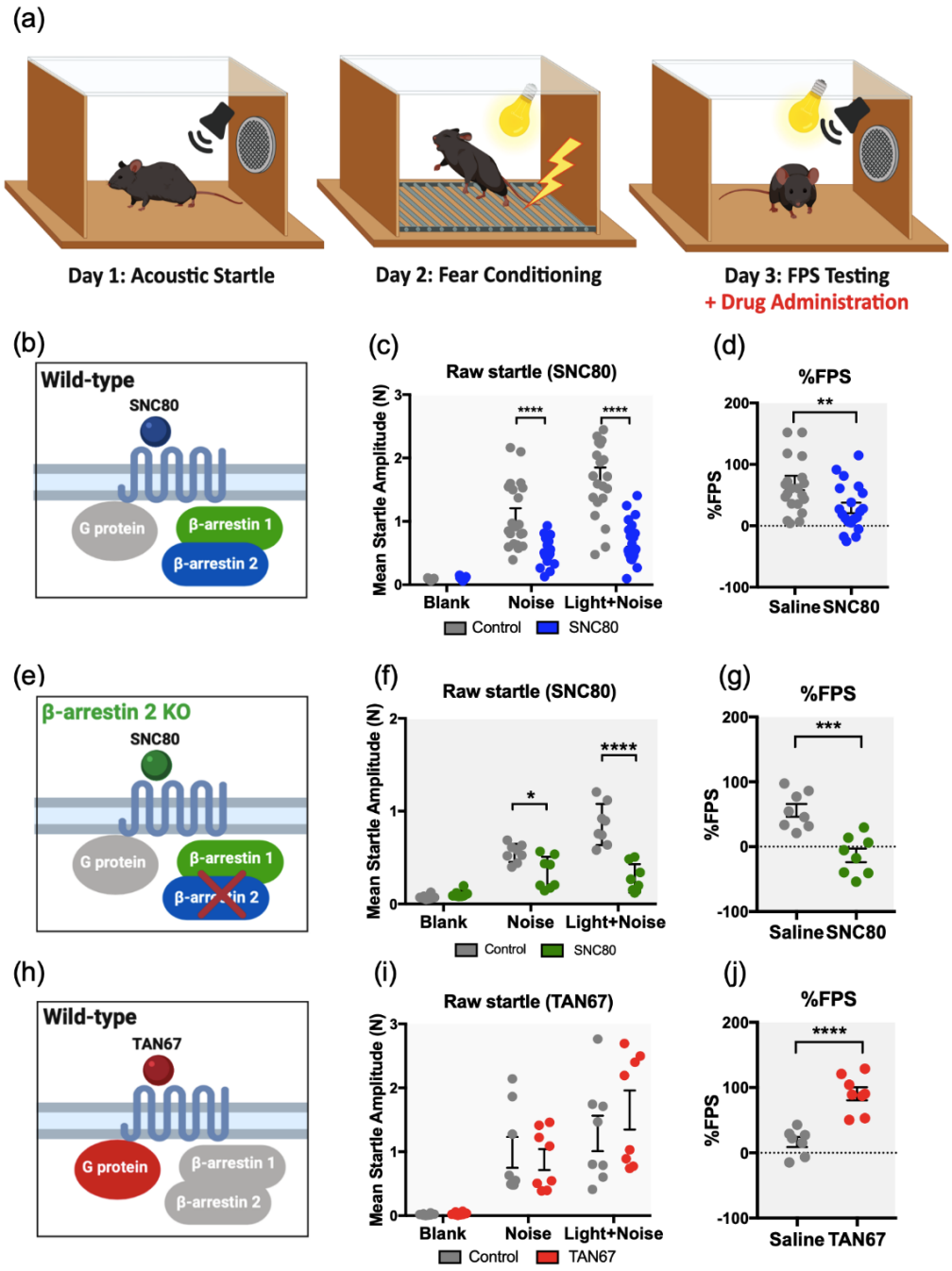

Figure 2.7 Unique modulation of fear-potentiated startle (FPS) by a β-arrestin-biased and G protein-biased δOR agonist

(a) Schematic representation of the three-day experimental paradigm of the fear potentiated startle test; drugs were administered prior to the tests on the third day (See **Figure 2.12** for Day 1 acoustic startle test). **(b-d)** SNC80 (n=21) reduced raw startle amplitudes to noise or light+noise and % FPS during the FPS test in WT mice. **(e-g)** SNC80 also reduced raw startle amplitudes to noise and light+noise as well as % FPS in β-arrestin 2 KO mice (n=8). **(h-j)** Yet, G protein-biased agonist, TAN67, increased % FPS in WT mice (n=8) (Significance was measured by two-way ANOVA followed by a Tukey's multiple comparison for (c, f, i) or unpaired t-test for (d, g, j); for (d) p=0.0085; for (g) p=0.0003; for (j) p<0.0001; *p < 0.05, **p<0.01, ***p < 0.001, ****p < 0.0001; all values are shown as individual data points ± S.E.M.).

Table 2.5. Statistical analysis of fear-related behavior upon systemic administration of SNC80 or TAN67 in WT and β-arrestin 2 KO mice

Statistical differences of fear-related behaviors in WT or β-arrestin 2 KO mice shown in Figure 2.7. Significance between groups was calculated by two-way ANOVA followed by a Bonferroni's multiple comparison (*p<0.05, ****p<0.0001, and ns=not significant).

Subfigure	Behavior test	Genotype	Drug	# of samples	Test	Source of Variation	F-value	p-value	Post hoc analysis	Group Comparison	Mean Diff.	p-value	Significance
Figure 2.7-c	Fear potentiated startle test	WT	SNC80 (20 mg/kg, i.p.)	Control: 21 SNC80: 21	Two-Way ANOVA test	Interaction Stimulation factor Drug factor	F(2,120) = 20.42 F(2,120) = 92.8 F(1,120) = 63.99	<0.0001 <0.0001 <0.0001	Bonferroni's Multiple Comparison Test	Blank: Con vs. SNC80 Noise: Con vs. SNC80 Noise+Light: Con vs. SNC80	-0.0126 0.5879 1.0310	>0.9999 <0.0001 <0.0001	ns **** ****
Figure 2.7-f	Fear potentiated startle test	βarr2 KO	SNC80 (20 mg/kg, i.p.)	Control: 8 SNC80: 8	Two-Way ANOVA test	Interaction Stimulation factor Drug factor	F(2,42) = 20.22 F(2,42) = 51.52 F(1,42) = 40.4	<0.0001 <0.0001 <0.0001	Bonferroni's Multiple Comparison Test	Blank: Con vs. SNC80 Noise: Con vs. SNC80 Noise+Light: Con vs. SNC80	-0.0355 0.2139 0.5812	>0.9999 0.0103 <0.0001	ns * ****
Figure 2.7-i	Fear potentiated startle test	WT	TAN67 (25 mg/kg, i.p.)	Control:8 TAN67: 8	Two-Way ANOVA test	Interaction Stimulation factor Drug factor	F(2,42) = 0.7245 F(2,42) = 25.06 F(1,42) = 0.2754	0.4905 <0.0001 0.6025	Bonferroni's Multiple Comparison Test	Blank: Con vs. SNC80 Noise: Con vs. SNC80 Noise+Light: Con vs. SNC80	-0.0113 0.1123 -0.3665	>0.9999 >0.9999 0.6493	ns ns ns

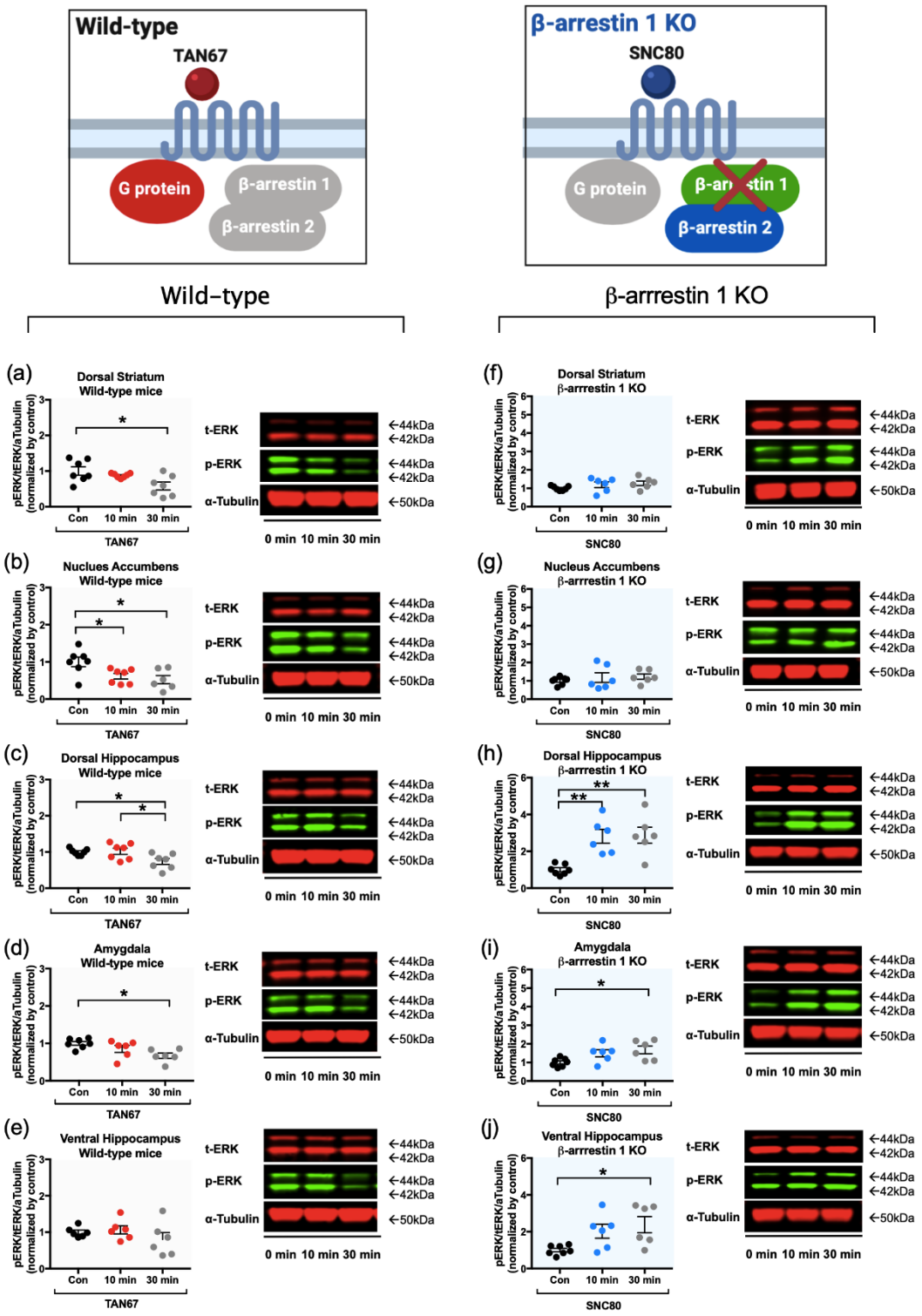

Figure 2.8 Differential roles for G protein and β-arrestin 1 in δOR agonist-induced ERK1/2 activation

Figure 2.8 continued (a-e) The G protein-biased δOR agonist TAN67 (25 mg/kg, i.p.), decreased the basal ERK1/2 activity in all tested brain regions of wild-type mice. Representative Western blot images are depicted next to each related bar graph. **(f-j)**. Systemic administration of SNC80 (20 mg/kg, i.p.) did not activate ERK1/2 in the striatal regions of β-arrestin 1 KO mice but resulted in persistent ERK1/2 activation in the dorsal and ventral hippocampus and amygdala (Significance was analyzed by one-way ANOVA followed by a Tukey's multiple comparison; *$p < 0.05$, **$p<0.01$; all values are shown as individual data points ± S.E.M.).

Table 2.6. Statistical analysis of ERK1/2 expression levels upon time-series administration of TAN67 in WT mouse and SNC80 in β-arrestin 1 KO mouse brain

Statistical differences of ERK1/2 expression levels in WT and β-arrestin 1 KO mouse brain shown in Figure 2.8. Significance between groups was calculated by one-way ANOVA followed by a Tukey's multiple comparison (*p<0.05, **p<0.01, and ns=not significant).

Subfigure	Brain region	Genotype	Drug	# of samples	Test	F-value	p-value	Group	Mean	Post hoc analysis	Group Comparison	Mean Diff.	p-value	Significance
Figure 2.8-a	Dorsal Striatum	WT	TAN67 (25 mg/kg, i.p)	Con: 7 10 min: 7 30 min: 7	One-Way ANOVA test	F (2, 18) = 5.276	P=0.0157	Con 10 min 30 min	1 0.8769 0.5824	Tukey's Multiple Comparison Test	Con vs. 10 min Con vs. 30 min 10 min vs. 30 min	0.1231 0.4176 0.2945	0.6279 0.0142 0.0931	ns * ns
Figure 2.8-b	Nucleus Acumbens	WT	TAN67 (25 mg/kg, i.p)	Con: 7 10 min: 7 30 min: 6	One-Way ANOVA test	F (2, 17) = 5.701	P=0.0127	Con 10 min 30 min	1 0.6152 0.5227	Tukey's Multiple Comparison Test	Con vs. 10 min Con vs. 30 min 10 min vs. 30 min	0.3848 0.4773 0.0925	0.0447 0.0161 0.8190	* * ns
Figure 2.8-c	Dorsal Hippocampus	WT	TAN67 (25 mg/kg, i.p)	Con: 7 10 min: 7 30 min: 7	One-Way ANOVA test	F (2, 18) = 5.09	P=0.0177	Con 10 min 30 min	1 1.021 0.739	Tukey's Multiple Comparison Test	Con vs. 10 min Con vs. 30 min 10 min vs. 30 min	-0.0207 0.2610 0.2817	0.9759 0.0410 0.0266	ns * *
Figure 2.8-d	Amygdala	WT	TAN67 (25 mg/kg, i.p)	Con: 7 10 min: 6 30 min: 6	One-Way ANOVA test	F (2, 16) = 5.455	P=0.0156	Con 10 min 30 min	1 0.851 0.6697	Tukey's Multiple Comparison Test	Con vs. 10 min Con vs. 30 min 10 min vs. 30 min	0.1490 0.3303 0.1813	0.3216 0.0118 0.2189	ns * ns
Figure 2.8-e	Ventral Hippocampus	WT	TAN67 (25 mg/kg, i.p)	Con: 6 10 min: 6 30 min: 6	One-Way ANOVA test	F (2, 15) = 1.092	P=0.3607	Con 10 min 30 min	1 1.063 0.8009	Tukey's Multiple Comparison Test	Con vs. 10 min Con vs. 30 min 10 min vs. 30 min	-0.0628 0.1991 0.2618	0.9388 0.5426 0.3582	ns ns ns
Figure 2.8-f	Dorsal Striatum	βarr1 KO	SNC80 (20 mg/kg, i.p)	Con: 7 10 min: 6 30 min: 6	One-Way ANOVA test	F (2,16) = 1.62	P=0.2288	Con 10 min 30 min	1 1.191 1.271	Tukey's Multiple Comparison Test	Con vs. 10 min Con vs. 30 min 10 min vs. 30 min	-0.1907 -0.2710 -0.0803	0.4580 0.2226 0.8743	ns ns ns
Figure 2.8-g	Nucleus Acumbens	βarr1 KO	SNC80 (20 mg/kg, i.p)	Con: 7 10 min: 6 30 min: 6	One-Way ANOVA test	F (2,16) = 0.5181	P=0.6053	Con 10 min 30 min	1 1.179 1.232	Tukey's Multiple Comparison Test	Con vs. 10 min Con vs. 30 min 10 min vs. 30 min	-0.1791 -0.2319 -0.0528	0.7426 0.6112 0.9759	ns ns ns
Figure 2.8-h	Dorsal Hippocampus	βarr1 KO	SNC80 (20 mg/kg, i.p)	Con: 5 10 min: 4 30 min: 6	One-Way ANOVA test	F (2,16) = 11.48	P=0.0008	Con 10 min 30 min	1 2.812 2.874	Tukey's Multiple Comparison Test	Con vs. 10 min Con vs. 30 min 10 min vs. 30 min	-1.8120 -1.8740 -0.0625	0.0027 0.0020 0.9902	** ** ns
Figure 2.8-i	Amygdala	βarr1 KO	SNC80 (20 mg/kg, i.p)	Con: 7 10 min: 6 30 min: 6	One-Way ANOVA test	F (2,16) = 4.668	P=0.0253	Con 10 min 30 min	1 1.498 1.67	Tukey's Multiple Comparison Test	Con vs. 10 min Con vs. 30 min 10 min vs. 30 min	-0.4981 -0.6695 -0.1714	0.1080 0.0261 0.7564	ns * ns
Figure 2.8-j	Ventral Hippocampus	βarr1 KO	SNC80 (20 mg/kg, i.p)	Con: 7 10 min: 6 30 min: 6	One-Way ANOVA test	F (2,16) = 5.097	P=0.0194	Con 10 min 30 min	1 2.024 2.377	Tukey's Multiple Comparison Test	Con vs. 10 min Con vs. 30 min 10 min vs. 30 min	-1.0240 -1.3770 -0.3530	0.0907 0.0201 0.7372	ns * ns

2.4 Discussion

2.4.1 Summary of the findings

Here, we investigated the hypothesis that β-arrestin can modulate anxiety- and conditioned fear-related behavior via downstream MAPK activation. By utilizing G protein- and β-arrestin-biased δOR agonists together with β-arrestin-isoform selective knockout mice, we discovered that G protein, β-arrestin 1, and β-arrestin 2 uniquely modulated ERK1/2 activity resulting in differential outcomes in mouse models of anxiety/fear-related behavior. Our results suggest that the reduction in anxiety-like behavior by SNC80 required the presence of β-arrestin 2 as well as activation of ERK1/2. Distinctly in the dorsal hippocampus, we found that ERK1/2 activation was β-arrestin 2-dependent (**Figure 2.9 a**). Notably, G protein-biased signaling by TAN67 reduced ERK1/2 phosphorylation and was correlated with increased FPS (**Figure 2.9 b**). We found that SNC80-induced ERK1/2 activation in the nucleus accumbens and the dorsal striatum required β-arrestin 1, which may be part of the mechanism for SNC80 to decrease FPS (**Figure 2.9 c**).

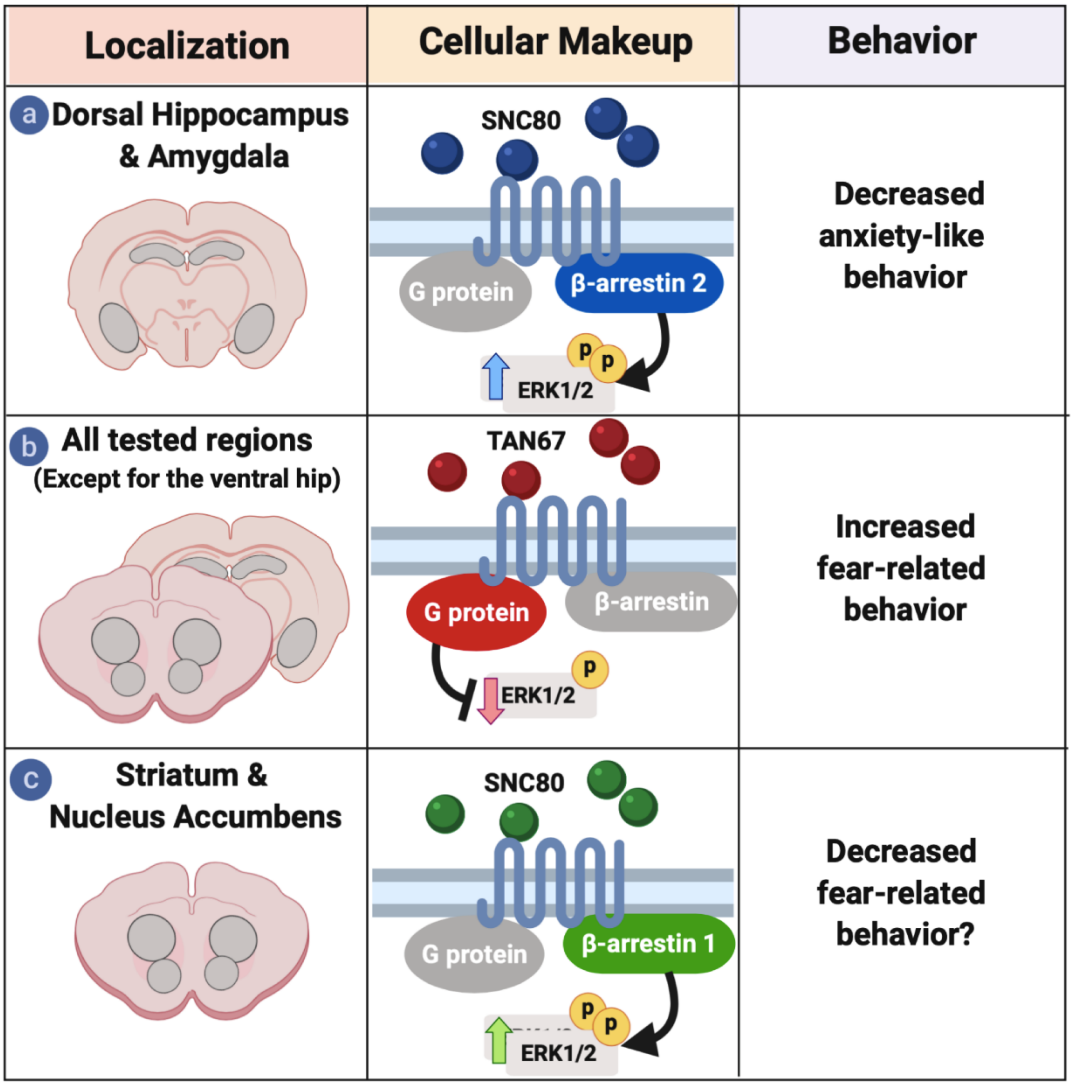

Figure 2.9 Graphical summary

δOR agonists differentially induce ERK1/2 activation in a β-arrestin isoform specific manner to modulate anxiety- and conditioned fear-related behaviors. SNC80 induced β-arrestin 2-mediated ERK1/2 activation (Cellular Makeup) in the hippocampus and amygdala (Localization) decreased anxiety-like behavior **(a)**, whereas an increase in conditioned fear-related behavior (Behavior) by TAN67 can be linked to decreased ERK1/2 activity in all tested brain regions except for the ventral hippocampus **(b)**. Decreased FPS could not be correlated with G protein or β-arrestin 2 signaling, but may involve β-arrestin -1 dependent ERK1/2 signaling in the dorsal striatum and nucleus accumbens **(c)**.

2.4.2 Differential roles for β-arrestin isoforms in neuropsychiatric behavior

The β-arrestin proteins were discovered in quick succession (Attramadal et al., 1992; Lohse et al., 1990). Surprisingly, despite the availability of genetic KO mice for each isoform (Bohn et al., 1999; Conner et al., 1997). Studies investigating β-arrestin in the CNS have largely focused on β-arrestin 2 and have generally neglected β-arrestin 1 (Latapy & Beaulieu, 2013; Whalen et al., 2011). A potential reason for the preference of studying β-arrestin 2 may be that when the β-arrestin 2 knockout mice were generated their first utilization was to highlight the proteins' involvement with the CNS-mediated adverse effects of μ-opioid receptor agonism (Bohn et al., 2000; Raehal et al., 2005). Researchers have only recently begun to utilize β-arrestin 1 KO mice to study various neurological disorders. In 2016, Pradhan *et al.* found that different δOR agonists either preferentially recruited β-arrestin 1 leading to δOR degradation or recruited β-arrestin 2 causing δOR resensitization (Pradhan et al., 2016). A study in 2017 found that amphetamine-induced hyperlocomotion was amplified in β-arrestin 1 KO mice, but attenuated in β-arrestin 2 KO mice (Zurkovsky et al., 2017), further emphasizing the importance of studying both β-arrestin isoforms.

As mentioned, our study further identified that SNC80-induced anxiolytic-like effects were β-arrestin 2-dependent. However, β-arrestin 2 KO mice still exhibited the fear-reducing effect of SNC80, which could suggest a potential role for β-arrestin 1 in the modulation of fear-related behavior. Particularly, we also noted that β-arrestin 1 KO abolished SNC80-induced ERK1/2 activation in the striatum and nucleus accumbens. Our findings were in line with the extensive *in-situ* hybridization studies on differential β-arrestin isoform levels in neonatal and postnatal rats (Gurevich et al., 2002, 2004) and studies showing relatively high β-arrestin 1 and low β-arrestin 2 expressions in the striatal regions (Attramadal et al., 1992; Bjork et al., 2008; Gurevich et al., 2002). In contrast, SNC80-induced ERK1/2 activation in the dorsal hippocampus and amygdala was β-arrestin 2-dependent, which agreed with reports of stronger expression of this isoform in those areas (Attramadal et al., 1992; Bjork et al., 2008). Unfortunately, we were limited in our ability to assess whether SNC80-induced reduction in FPS would be attenuated in β-arrestin 1 KO mice, as SNC80 produces severe seizures in these mice (Vicente-Sanchez et al., 2018), a phenomenon we have also observed ourselves and found to be accompanied by strong and persistent ERK1/2 activation in the dorsal hippocampus. Further investigation of the roles of β-arrestin 1 in neuropsychiatric behavior may be feasible using a conditional knockout approach; currently

conditional β-arrestin 2 knockout mice already exist (Huang et al., 2018), but conditional β-arrestin 1 knockout mice have not yet been reported.

2.4.3 A unique role for Gi protein signaling and ERK1/2 signaling in conditioned fear-related behavior

In contrast to the β-arrestin-mediated activation of ERK1/2, we found that selectively activating the G protein pathway of the δOR using TAN67, a known weak recruiter of β-arrestin 1 and 2 (Chiang et al., 2016) (**Figure 2.6**) decreased ERK1/2 activation, including in the striatum and the amygdala, and was associated with increased FPS. This result is in agreement with the observation and that blocking $G_{i/o}$ protein signaling using pertussis toxin in the basolateral amygdala reduced FPS (Melia et al., 1992) and parallels finding that TAN67 did not reduce unconditioned anxiety-like behavior in naïve mice (van Rijn et al., 2010). Additionally, a study in ovariectomized mice found that estradiol benzoate, an anxiogenic estradiol prodrug (Morgan & Pfaff, 2002), decreased ERK in the hippocampus (Anchan et al., 2014), which supports our finding that decreased ERK1/2 is correlated with increased fear. It is noteworthy that both G_i protein and β-arrestin can activate ERK1/2 albeit via different mechanisms (Goldsmith & Dhanasekaran, 2007; Gutkind, 2000). One explanation for our observation is that TAN67 competes with the endogenous δOR agonist Leu-enkephalin, which is a much more efficacious recruiter of β-arrestin (Chiang et al., 2016) (**Figure 2.10**). Importantly, based on observations of enhanced anxiety-like behavior in preproenkephalin KO mice, Leu-enkephalin has anxiolytic-like effects by itself (Kung et al., 2010; Ragnauth et al., 2001), which is in line with reports that the δOR antagonist, naltrindole, is anxiogenic (Narita et al., 2006). As a weak β-arrestin recruiter, TAN67 would attenuate any baseline Leu-enkephalin-induced β-arrestin-mediated ERK1/2 activity (**Figure 2.11**). In contrast, because SNC80 is a stronger β-arrestin recruiter than Leu-enkephalin, it will elevate basal ERK1/2 activity produced by endogenous opioids. This hypothesis would also explain why SNC80-induced ERK1/2 activation is quite variable and produces on average only a two-fold increase.

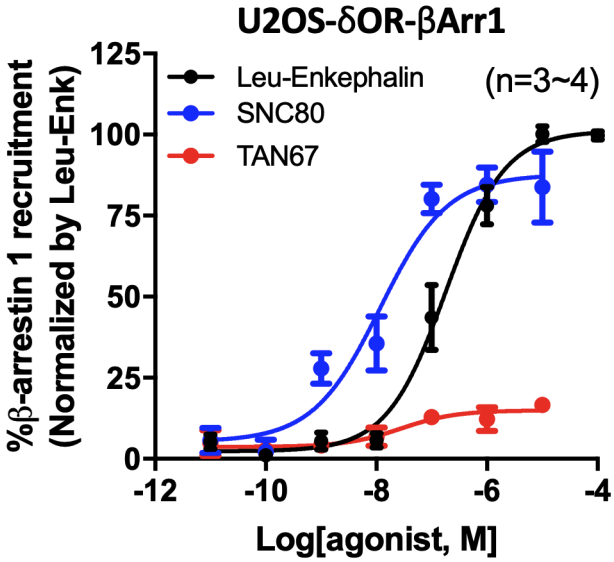

Figure 2.10 β-arrestin 1 recruitment levels by G-protein-biased (TAN67), β-arrestin-biased (SNC80), and non-biased (Leu-Enk) δOR agonist in U2OS-δOR-βArr1 cells

10 μM TAN67, 10 μM SNC80, 10 μM leucine-enkephalin (leu-enk) were administered during the cellular assay and their β-arrestin 1 recruiment levels were tested in a dose-dependent manner. SNC80 revealed the highest efficacy of recruiment and TAN67 showed the lowest. (All recruiment levels were normalized by leu-enk and 10 μM leu-enk was normalized as 100 %).

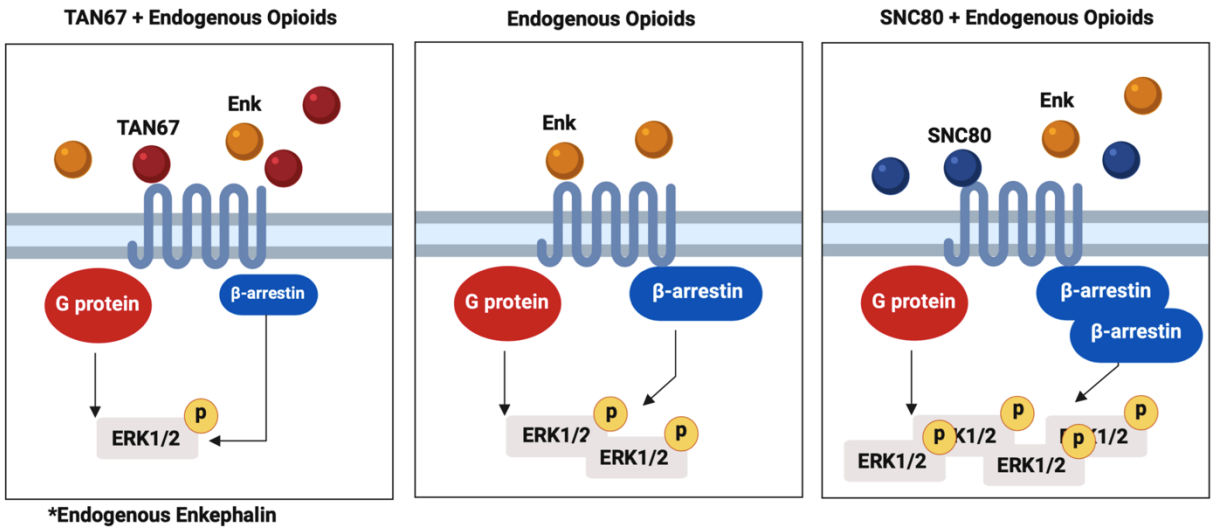

Figure 2.11 A diagram respresenting the pharmacological competition between two biased agonists and an endogenous opioid in relations to their ability to modulate ERK1/2 signaling

Unlike with cells, the brain has endogenous opioids that bind to δOR. As endogenous opioids such as Leu-Enk, an analog of endogenous opioids, have better ability to recruit β-arrestin proteins than TAN67 as shown in Fig. S3, δOR is less likely to recruit β-arrestin and potentially activate less ERK1/2 upon administration of TAN67 in the brain. Likewise, SNC80, which has a better ability to recruit β-arrestin proteins than Leu-Enk, recruits more β-arrestins via δOR and potentially activates more ERK1/2 upon administration of SNC80 in the brain (Right). Yet, it is notworthy that SNC80 and TAN67 have comparable levels of G protein-mediated response (Chiang et al., 2016).

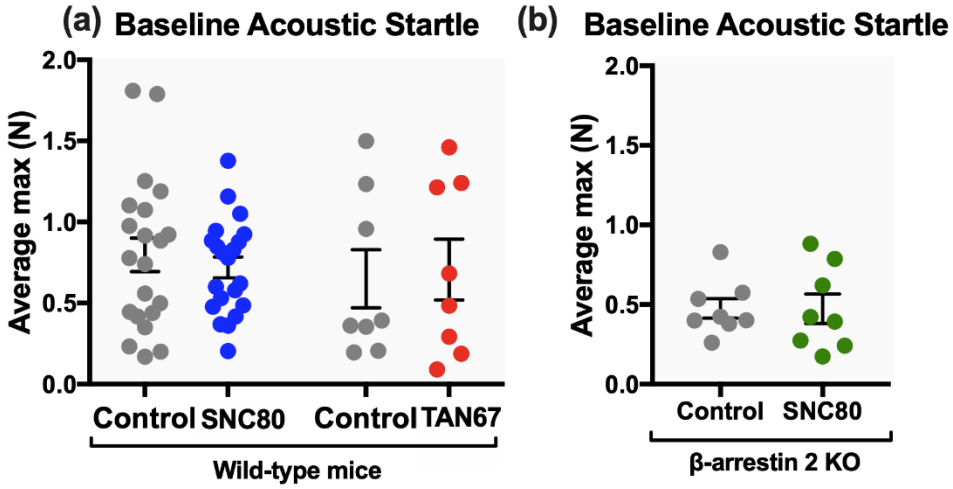

Figure 2.12 Mice groups for FPS tests were counterbalanced based on baseline acoustic startle response

No significance was observed between groups of control *vs.* SNC80 or control *vs.* TAN67 of WT mice **(a)** and control *vs.* SNC80 of β-arrestin 2 KO mice **(b)** (All values are shown as individual data points ± S.E.M.).

2.4.4 β-arrestin serves as a scaffold for a range of kinases and effectors

In our study, we found that δOR agonism strongly activates ERK1/2 compared to the other tested MAPKs, p38 and JNK, and that the ERK1/2 activity induced by SNC80 was negatively correlated with FPS. Other GPCRs, besides the δOR, may also require β-arrestin-dependent ERK1/2 signaling for modulation of fear. Specifically, in the infralimbic prefrontal cortex, β-adrenergic receptor activation can promote the extinction of contextual fear memory (Do-Monte et al., 2010). In a recent study, it was shown that in this same brain region β-arrestin 2-dependent ERK1/2 activation was required for β-adrenergic receptor agonists to stimulate extinction learning of cocaine-induced reward memories (Huang et al., 2018). β-arrestin 2-mediated signaling in the CNS is not exclusive to ERK1/2 signaling; following κOR activation, β-arrestin 2 can scaffold with p38 as part of a potential mechanism for the aversive effects of κOR agonists (Bruchas et al., 2007). A β-arrestin 2 scaffold of AKT, GSK3β and PP2A has been proposed as a mechanism for stabilizing mood (O'Brien et al., 2011), highlighting that β-arrestin signaling is also not limited to MAPKs. In fact, because β-arrestin 1, in contrast to β-arrestin 2, contains a nuclear translocation sequence (Hoeppner et al., 2012), this enables it to enter the nucleus and regulate gene transcription (Kang et al., 2005; Shi et al., 2007). While in this study we report δORs require β-arrestin-dependent ERK1/2 signaling for reduction in anxiety-like behavior, it is certainly possible that other GPCRs may engage different intracellular signaling pathways following β-arrestin recruitment.

2.4.5 Fear- and anxiety-like behaviors rely on shared but distinct neural circuits

In our study, we observed that β-arrestin 2-dependent ERK1/2 activity in the dorsal hippocampus was associated with reduced anxiety-like behavior. Generally, CA1 regions of the ventral hippocampus are associated with responding to contextually-conditioned anxiogenic stimuli than dorsal CA1 regions (Fanselow & Dong, 2010; Jimenez et al., 2018), whereas the dorsal hippocampus is involved with cognitive functions, including exploration, navigation and memory (Kheirbek et al., 2013). Still, our finding that δOR signaling in the dorsal hippocampus is connected to the anxiolytic-like effects of SNC80, agrees with a study showing that intra-dorsal CA1 injection of the δOR antagonist naltrindole is anxiogenic (Solati et al., 2010). Additionally, the anxiolytic-like effects of SNC80 may also involve β-arrestin 2-dependent ERK1/2 signaling in the amygdala, a region more commonly associated innate anxiety-like behavior (Felix-Ortiz et al.,

2013; Tye et al., 2011). The BLA also plays an important role in fear conditioning (Janak & Tye, 2015), including FPS (Terburg et al., 2018). The BLA receives dopaminergic inputs from the ventral tegmental area and projects to the nucleus accumbens. It has been proposed that dopaminergic signaling in the BLA is important for cue-dependent fear-conditioning, such as FPS (Fadok et al., 2009) and that the BLA to nucleus accumbens projection is critical for consolidation of memories associated with aversive effects such as foot shock (Fadok et al., 2010; LaLumiere et al., 2005).

Our finding that ERK1/2 activation in the striatal regions was ablated in β-arrestin 1 KO mice points to a role for striatal β-arrestin 1-mediated ERK1/2 signaling in the modulation of the expression of conditioned fear-related behavior. Processing and executing emotional behaviors in tasks such as the elevated plus maze and FPS tests engages multiple overlapping, yet distinct, brain regions and circuits involved in memory retrieval, locomotion, decision making, reward, and mood (Janak & Tye, 2015). Further studies with circuit-based approaches are necessary to assess the role of biased signaling pathways in the acquisition and expression of conditioned fear-related behavior.

2.4.6 Beneficial roles of β-arrestin signaling

For the longest time, β-arrestin 2 has been associated solely with adverse effects of opioid activation, including tolerance, constipation, respiratory depression, aversion and alcohol use (Raehal & Bohn, 2011; Raehal et al., 2005; van Rijn et al., 2010). These studies fueled a drive to develop G protein-biased opioids to treat pain and other disorders with an improved therapeutic window (Manglik et al., 2016; Mores et al., 2019). Yet, recently a number of studies have started to push back against this narrative (Austin Zamarripa et al., 2018; Hill et al., 2018; Kliewer et al., 2019). Clearly, β-arrestin signaling is not inherently negative as the therapeutic effects of lithium and fluoxetine seem to depend on β-arrestin 2 (David et al., 2009). The increased propensity for β-arrestin 1 KO mice to experience SNC80-induced seizure points to a potential beneficial role for this isoform in maintaining seizure threshold, which could be of use in the treatment of epilepsy. In this study, we provide additional insights regarding potential therapeutic benefits of β-arrestin signaling in reducing anxiety-like behavior. Providing adequate relief of chronic pain is not trivial, partly because it is often associated with negative affect (Corder et al., 2019; Massaly et al., 2019) including anxiety, which may exacerbate pain (al Absi & Rokke, 1991). δOR agonists have been proposed as potential treatment for chronic pain disorders (Pradhan et al., 2011), partly because

they have the ability to not only provide analgesia, but also treat comorbid anxiety and depression (Perrine et al., 2006; Saitoh et al., 2004; van Rijn et al., 2010). However, our results would argue that developing G protein-biased δOR agonists may produce drugs that are suboptimal for the treatment of complex chronic pain; our findings suggest such a drug would not alleviate co-morbid fear and anxiety, but potentially even worsen these symptoms. Thus, our study results argue in favor of a reassessment of drug development efforts that seek solely to identify G protein-biased drugs. Instead, we propose that efforts should be directed towards the development of drugs with finely tuned bias and, if possible, towards development of molecules that are biased against a single β-arrestin isoform rather than both isoforms.

2.4.7 Conclusion

Overall, our results begin to reveal the complex- and context-specific nature of GPCR biased signaling in modulation of fear-related and anxiety-like behavior. These results expand our current understanding of therapeutic effects of β-arrestin signaling in mood disorders, which ultimately may aid development of more efficacious pharmacological treatment options for these disorders.

CHAPTER 3. COMMONLY USED ANESTHESIA/EUTHANASIA METHODS FOR BRAIN COLLECTION DIFFERENTIALLY IMPACT MAPK ACTIVITY IN MALE AND FEMALE C57BL/6 MICE

This chapter is comprised of data that has been peer-reviewed and published in Frontiers in Cellular Neuroscience (Ko, Mulia, et al., 2019).

3.1 Introduction

The classical MAPK is a family of three protein kinases, specifically ERK1/2, JNK, and p38 kinases. MAPKs have many functions including in the central nervous system where they can regulate neuronal proliferation, differentiation, and apoptosis through phosphorylation and activation of subsequent protein kinases (Johnson & Lapadat, 2002; Sweatt, 2001). MAPKs are expressed in the soma, dendrites, and axons of neurons (Flood et al., 1998) as well as in glia and are integral in glioma formation and neurodegeneration (Cheng et al., 2013; Koistinaho & Koistinaho, 2002; Stariha & Kim, 2001). MAPKs can be phosphorylated following activation of receptor tyrosine kinases as well as G protein-coupled receptors, which can occur indirectly by cross-talk with receptor tyrosine kinases or more directly via protein kinase A and C signaling pathways (Kim & Choi, 2015; Marinissen & Gutkind, 2001; Wetzker & Bohmer, 2003). As part of the signaling transduction cascade of these receptors, MAPKs regulate behavioral performance such as fear conditioning and spatial learning (Besnard et al., 2014), and long-term synaptic plasticity in the brain (Thomas & Huganir, 2004), drug addiction (Lu et al., 2006), anxiety-like and depressive-like behavior (Duman et al., 2007; Huang & Lin, 2006; Wefers et al., 2012) signifying the importance of studying MAPK signaling pathways in various neuropsychiatric disorders. Interestingly, MAPKs have been found to scaffold with β-arrestin proteins (Shenoy & Lefkowitz, 2011) and linked for example to the aversive properties of κ-opioid receptor drugs (Bruchas & Chavkin, 2010; Ehrich et al., 2015).

Many studies investigating MAPK function in relation to neuropsychiatric disorders or drug efficacy rely on immunohistochemistry or immunoblotting that require brain extraction. However, the process of tissue collection may directly impact MAPK signaling and obscure any changes induced by a drug or disorder under investigation. Ketamine, which is often used in combination with xylazine to anesthetize animals prior to brain collection, is known to modulate MAPK

signaling (Reus et al., 2014). Another commonly used strategy for brain isolation is the anesthetic isoflurane, which may induce neuroinflammation and increase JNK phosphorylation (Altay et al., 2014). A third method, euthanasia by carbon dioxide asphyxiation, induces a hypoxic state and leading to activation of MAPK signal processes of cell survival (Risbud et al., 2005). Fourthly, a rapid decapitation without anesthesia may trigger a stress response, and modulate MAPK signaling in the prefrontal cortex and the hippocampus (Meller et al., 2003).

Given the possibility of false negative results, due to potentially high basal MAPK activity caused by the different modes of anesthesia/euthanasia, it is imperative to evaluate to what extent the choice of anesthesia/euthanasia can influence baseline MAPK activity. Thus, we assessed activation of ERK1/2, JNK and p38 by Western blot using brain tissue collected from adult male and female C57BL/6 mice isolated following the four aforementioned anesthesia/euthanasia methods: ketamine/xylazine, carbon dioxide asphyxiation, isoflurane, and decapitation. For this investigation, we selectively isolated five brain regions, specifically the prefrontal cortex, the nucleus accumbens, the striatum, the dorsal hippocampus, and the amygdala, that are known for their roles in neuropsychiatric disorders. This is the first study to present the impact of different anesthesia/euthanasia methods in MAPK signaling pathway of the adult male and female mice brain. The findings provide crucial information to researchers who are seeking the optimal anesthesia/euthanasia methods for their neuropsychological and pharmacological studies.

3.2 Materials and methods

3.2.1 Animals

We utilized naïve C57BL/6 mice purchased from Envigo (Indianapolis, IN, USA). Young adult (7-week-old) male and female mice were group housed in ventilated Plexiglas cages (three mice per cage) on a reversed 12-hour dark-light cycle (lights off at 10:00, lights on at 22:00, and used for experimental procedures when they reached 8-9-week-old (20±2g). Unless it is stated otherwise, 3 mice per group were used to test the molecular changes in the brain. Naïve mice groups were randomly assigned to each group. No animal was excluded from the study. All mice handling was performed by one scientist (MJK) to avoid stress induced by multiple handlers. Mice were maintained at ambient temperature (21°C) with ad libitum access to standard rodent diet and pathogen free reverse-osmosis water in an animal housing facility recognized by the Association

for Assessment and Accreditation of Laboratory Animal Care. This study was carried out in accordance with the ARRIVE guidelines (Kilkenny et al., 2012) and the recommendations of the National Institutes of Health Guide for the Care and Use of Laboratory Animals. The protocol (#1605001408 by RMvR) was approved by the Purdue University Institutional Animal Care and Use Committee.

3.2.2 Anesthesia/Euthanasia Methods

The mice brains were collected in a separate suite at the same time of the day during their active cycle following four different anesthesia and euthanasia methods: **1) Ketamine/Xylazine:** mice were decapitated 45 minutes following an intraperitoneal injection of 100 mg/kg (#VINB-KET0-7021, Henry Schein Animal Health, Dublin, OH) with 10 mg/kg xylazine hydrocholoride supplement (#X1251-1G, Sigma-Aldrich, St. Louis, MO), **2) Isoflurane:** mice were placed in a plexiglas chamber with 5 % isoflurane, USP (#NDC 13985-046-60, VetOne, Boise, ID) for five minutes, and decapitated when fully sedated, as measured by a lack of active paw reflex, **3) Carbon Dioxide Asphyxiation:** mice were placed in a new cage with corn cob bedding, and immediately euthanized by displacement of air with 100 % carbon dioxide, within 5 minutes and decapitated for tissue collection, **4) Decapitation:** mice were gently restrained and decapitated in a new cage to minimize the exposure to blood from conspecific mice.

3.2.3 Tissue collection and sample preparation

The mice brains were rapidly removed and coronally sliced in brain matrix (#RBMS-205C, Kent scientific, Torrington, CT). Sliced brains were flash-frozen with dry-iced chilled (-40°C) 2-methylbutane (#03551-4, Fisher Scientific, Waltham, MA). The prefrontal cortex (Bregma = +2 mm to +5 mm), the dorsal hippocampus and the amygdala (Bregma = -2 mm to -1 mm), the striatum and the nucleus accumbens (Bregma = +0.5 mm to +1.5 mm) were collected using 1 mm biopsy punch (#15110-10, Miltex, Plainsboro, NJ) based on Elsevier® The mouse brain in stereotaxic coordinates. The punches, which targeted a specific brain region, collected a majority of the tissue, but its adjacent tissues were not completely excluded. For instance, the punches for the dorsal hippocampus collected a majority of the dorsal dentate gyrus and CA3 with limited lateral ventricle regions but did not collect the ventral hippocampal regions. Collected tissues were mixed with RIPA buffer and 1x protease inhibitor (#1861280, Fisher Scientific) and homogenized

with a Wheaton® tissue grinder (#357535 & 357537, DWK Life Sciences, Millville, NJ). Additional Sample homogenization was performed using an ultrasonic disruption on ice (Level 3, 1-second per pulse, and 10 pulses total) using a probe-type sonicator (#XL-2000, Qsonica, Newtown, CT), and centrifuged at 12,000 rpm, 4 °C for 20 minutes. Supernatant of the samples were quantified using the BSA assay (#5000006, Biorad, Hercules, CA) for further preparation for the Western blot. Samples were prepared with 4 x Laemmli (#1610747, Biorad) and boiled at 98 °C for 5 minutes prior to loading.

3.2.4 SDS-Page and Western blot

10 μg/20 ul samples were loaded in each well of NuPage 4-12 % Bis-Tris gradient gels (#NP0336BOX, Fisher Scientific) and transferred to nitrocellulose transfer membranes (#1620115, BioRad). The membrane was blocked in LiCor blocking buffer overnight at 4 °C, and probed with the appropriate primary antibodies ERK1/2 (1:2000, Cell Signaling 4696S, Lot: #22), pERK1/2 (1:2000, Santa Cruz 7976-R, Lot: #C1113), p38 (1:2000, Bioss 0637R, Lot: #AE020601), pp38 (1:500, Cell Signaling 9216S, Lot: #27), JNK (1:2000, Cell Signaling 9252S, Lot: #17), pJNK (1:2000, Santa Cruz 6254, Lot: #B2117), and α-Tubulin (1:2000, Santa Cruz 5286, Lot: #G3117) for 1 hour at room temperature. All membranes were washed in TBS based 0.1 % Tween 20 solution (#9416, Sigma-Aldrich), and further probed with corresponding LiCor Near-infrared fluorescent secondary antibodies (1:5000, LiCor 926-68020 Lot: #C60824-02, LiCor 926-32211 Lot: #C61103-06) for 2 hours at room temperature. All membranes were washed in TBS based 0.1 % Tween 20 solution and scanned using a LiCor Odyssey® CLx Scanner. The total-form protein, the phspho-form protein, and the α-Tubulin were from the same membrane to reduce the impact of potential variability. Each band of the blots was cut based on their size (e.g. 42/44 kDa for ERK1/2 and 50 kDa for α-Tubulin). Proteins that shared the same size were stained simultaneously using different hosts of their primary antibodies and their corresponding near-intrared fluorescent secondary antibodies. Furthermore, to improve the scientific rigor, both total-form protein (e.g. ERK1/2 and α-Tubulin) were utilized as an internal loading control to normalize the phospho-form protein (e.g. pERK1/2). For instance, pERK1/2 expression levels were divided by ERK1/2, which was previously normalized by α-Tubulin expression levels.

3.2.5 Statistics

All data are presented as means ± standard error of the mean (SEM). The relatively small SEM between samples allowed for the minimum group size of three animals. For the Western blot, all data was measured and quantified by ImageJ, and analyzed by one-way ANOVA. The post-hoc analysis was conducted with the Tukey's multiple comparisons unless it is stated otherwise. For sex difference, 2-way ANOVA was used to test for differences in means for sex effects and interaction (sex x drug) effects, and Tukey's multiple comparisons were used to compare each group when significant differences were found. All data was evaluated using GraphPad Prism 7 (GraphPad Software, La Jolla, CA).

3.3 Results

3.3.1 The use of different general anesthesia and euthanasia methods has a strong impact on extracellular signal-regulated kinase 1 and 2 (ERK1/2) activity

Five different brain regions including the prefrontal cortex, the striatum, the nucleus accumbens, the amygdala, and the hippocampus were collected with tissue puncture and further analyzed using the Western blot (**Figure 3.1**). In all five-brain regions of male mice, one-way ANOVA analysis revealed statistically significant differences in ERK1/2 phosphorylation between euthanasia methods (**Figure 3.2 a-r**; prefrontal cortex: $F_{3, 8} = 14.47$, $p=0.001$; striatum: $F_{3, 20} = 11.74$, $p=0.0001$; nucleus accumbens: $F_{3, 8} = 12.88$, $p=0.002$; hippocampus: $F_{3, 20} = 6.63$, $p=0.003$; amygdala: $F_{3, 8} = 12.62$, $p=0.002$). Similar results were obtained in the female brain (**Figure 3.2 c-t**; prefrontal cortex: $F_{3, 8} = 9.923$, $p=0.005$; striatum: $F_{3, 20} = 22.56$, $p<0.0003$; nucleus accumbens: $F_{3, 8} = 13.04$, $p=0.002$; hippocampus: $F_{3, 20} = 16.18$, $p=0.02$; amygdala: $F_{3, 8} = 23.03$, $p=0.0003$). Especially, decapitation and isoflurane led to statistically significant increases in ERK1/2 phosphorylation relative to carbon dioxide asphyxiation in both males and females (**Figure 3.2 a-r** for males; **Figure 3.2 c-t** for females; see **Table 3.1** for post-hoc multiple comparison). Mice euthanized with ketamine/xylazine displayed stronger ERK1/2 activity than carbon dioxide asphyxiation in the male hippocampus (**Figure 3.2 m, n**), the female striatum (**Figure 3.2 g, h**), the female hippocampus (**Figure 3.2 o, p**), and the female amygdala (**Figure 3.2 s, t**). Mice euthanized with isoflurane showed more pronounced ERK1/2 activity than ketamine/xyalzine in the male prefrontal cortex (**Figure 3.2 a, b**), the male striatum (**Figure 3.2 e, f**), the female prefrontal cortex (**Figure 3.2 c, d**), the female striatum (**Figure 3.2 g, h**), and the female nucleus

accumbens (**Figure 3.2 k, l**; see **Table 3.1** for post-hoc multiple comparison). Especially, to increase the reproducibility and scientific rigor of the study, we performed two separate studies using the same paradigm in selected brain regions such as the male and female striatum and hippocampus (**Figure 3.6**). In both trials, we observed similar trends of ERK1/2 activation in general (**Figure 3.6**; see **Table 3.5** for post-hoc multiple comparison), further supporting the reproducibility of the paradigm.

3.3.2 Impact of different general anesthesia and euthanasia methods on c-Jun N-terminal kinase activity

Of the five tested brain regions, statistically significant differences in JNK phosphorylation between euthanasia methods were only observed in the male striatum (**Figure 3.3 e, f**; One-way ANOVA, $F_{3, 8} = 4.399$, p=0.04), the male nucleus accumbens (**Figure 3.3 i, j**; $F_{3, 8} = 5.765$, p=0.02), the female nucleus accumbens (**Figure 3.3 k, l**; $F_{3, 8} = 4.345$, p=0.04), the female amygdala (**Figure 3.3 s, t**; $F_{3, 8} = 7.982$, p=0.009). However, for the other brain regions we did not find any statistical significant differences between euthanasia methods in males (**Figure 3.3 a, b** for the prefrontal cortex, $F_{3, 8} = 1.898$, p=0.2; **Figure 3.3 m, n** for the hippocampus, $F_{3, 8} = 1.641$, p=0.26; **Figure 3.3 q, r** for the amygdala, $F_{3, 8} = 2.832$, p=0.1) nor in females (**Figure 3.3 k, l** for the prefrontal cortex, $F_{3, 8} = 2.162$, p=0.17; **Figure 3.3 g, h** for the striatum, $F_{3, 8} = 1.906$, p=0.2; **Figure 3.3 o, p** for the hippocampus). Furthermore, decapitation showed a statistical significant increase in JNK activity compared to carbon dioxide asphyxiation in the male striatum (**Figure 3.3 e, f**), the male nucleus accumbens (**Figure 3.3 i, j**), the female nucleus accumbens (**Figure 3.3 k, l**), and the female amygdala (**Figure 3.3 s, t**; see **Table 3.2** for post-hoc multiple comparison). Relative to carbon dioxide asphyxiation, ketamine/xylazine usage also produced a statistically significant increase in JNK levels in the male nucleus accumbens (**Figure 3.3 i, j**) and the female amygdala (**Figure 3.3 s, t**; see supplementary table for post-hoc multiple comparison). In the female amygdala, a significant increase in JNK levels in response to isoflurane was observed compared to carbon dioxide asphyxiation (**Figure 3.3 s, t**; see **Table 3.2** for post-hoc multiple comparison).

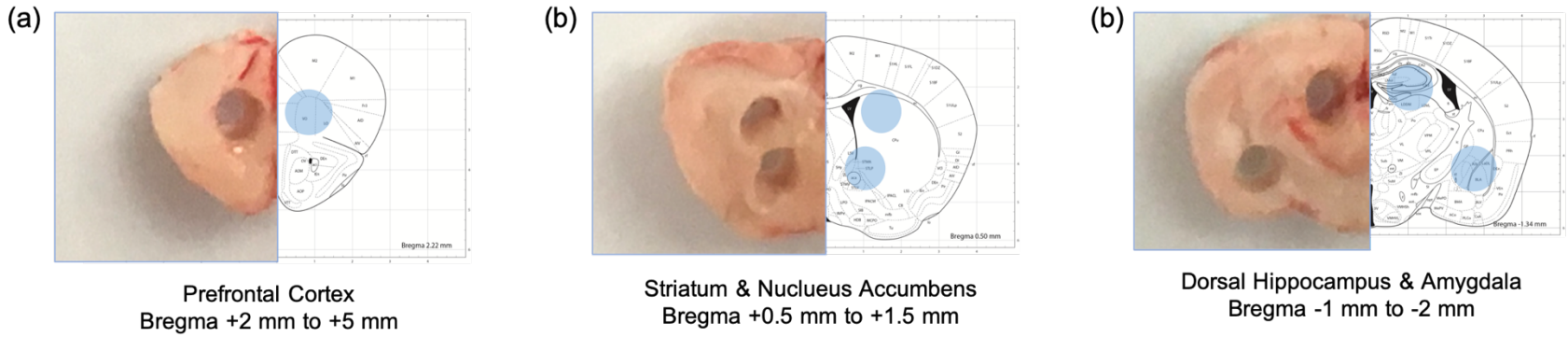

Figure 3.1 Schematic diagrams of collected brain tissues

Specific brain regions were isolated from brain tissue sections using disposable punches. (a) The prefrontal cortex (Bregma +2 mm to +5 mm), (b) The striatum & the nucleus accumbens (Bregma + 0.5 mm to +1.5 mm), and (c) The dorsal hippocampus (Bregma -1 mm to -2 mm).

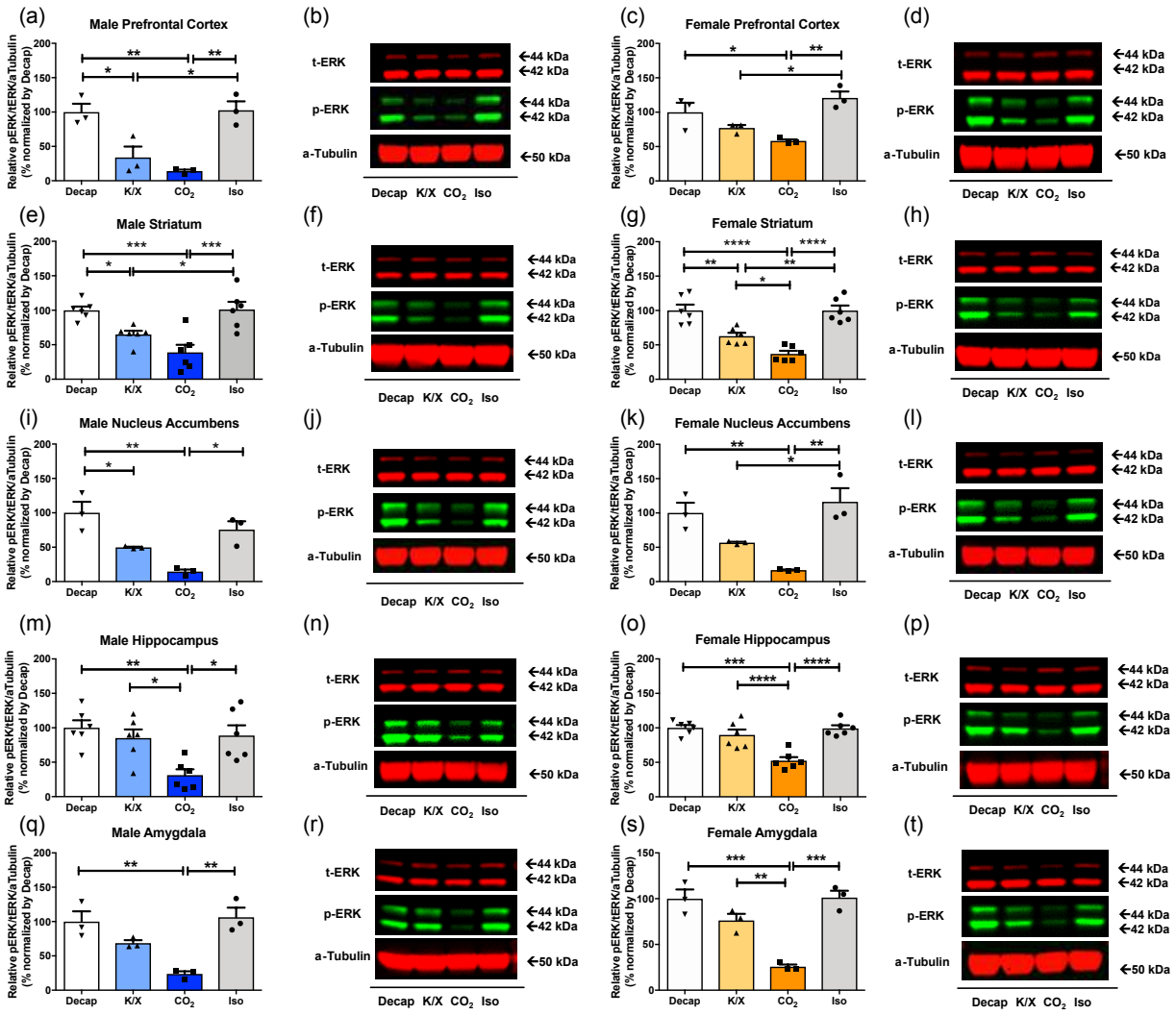

Figure 3.2 ERK1/2 expression levels to different anesthesia/euthanasia methods in the adult male and female mice brain

To test the impact of different anesthetic/euthanasia in MAPK activity, ERK1/2 expression levels were analyzed by the Western blot following the different anesthetic/euthanasia procedures in the male prefrontal cortex (a, b), the male striatum (e, f), the male nucleus accumbens (i, j), the male hippocampus (m, n), the male amygdala (q, r), as well as in the female prefrontal cortex (c, d), the female striatum (g, h), the female nucleus accumbens (k, l), the female hippocampus (o, p), and the female amygdala (s, t). Representative western blot images were presented next to corresponding bar graphs. All data was represented as mean ± SEM, and analyzed with one-way ANOVA with Tukey's multiple comparison (*$p < 0.05$, ** $p < 0.01$, *** $p < 0.001$). For abbreviation, 'iso' represents isoflurane; 'CO2' represents carbon dioxide asphyxiation; 'K/X' represents ketamine and xylazine administration; 'Decap' represents decapitation without anesthesia.

Table 3.1. Statistical analysis of ERK1/2 expression levels in the brain by different anesthetic and euthanasia methods

Statistical differences of ERK1/2 expression levels in mouse brain shown in Figure 3.2. Significance between groups was calculated by one-way ANOVA followed by a Tukey's multiple comparison (*p<0.05, **p<0.01, ***p<0.001, ***p<0001, and ns=not significant).

ERK1/2	# of samples	Test	F-value	p-value	Group	Mean	Post hoc analysis	Group Comparison	Mean Diff.	p-value	Significance
Figure 3.2-a (Prefrontal cortex-M)	**3**	**One-Way ANOVA test**	F (3, 8) = 14.47	P=0.0013	Iso CO2 K/X Decap	102.7 14.03 33.96 100	Tukey's Multiple Comparison Tes	Iso vs. CO2	88.6300	0.0034	**
								Iso vs. K/X	68.7100	0.0151	*
								Iso vs. Decap	2.6650	0.9985	ns
								CO2 vs. K/X	-19.9200	0.6546	ns
								CO2 vs. Decap	-85.9700	0.0041	**
								K/X vs. Decap	-66.0400	0.0187	*
Figure 3.2-c (Prefrontal cortex-F)	**3**	**One-Way ANOVA test**	F (3, 8) = 9.923	P=0.0045	Iso CO2 K/X Decap	120.8 58.18 77.04 100	Tukey's Multiple Comparison Tes	Iso vs. CO2	62.6100	0.0040	**
								Iso vs. K/X	43.7500	0.0296	*
								Iso vs. Decap	20.7900	0.3827	ns
								CO2 vs. K/X	-18.8600	0.4582	ns
								CO2 vs. Decap	-41.8200	0.0368	*
								K/X vs. Decap	-22.9600	0.3085	ns
Figure 3.2-e (Striatum-M)	**6**	**One-Way ANOVA test**	F (3, 20) = 11.74	P=0.0001	Iso CO2 K/X Decap	101.1 38.87 64.86 100	Tukey's Multiple Comparison Tes	Iso vs. CO2	62.2200	0.0004	***
								Iso vs. K/X	36.2200	0.0389	*
								Iso vs. Decap	1.0850	0.9998	ns
								CO2 vs. K/X	-26.0000	0.1884	ns
								CO2 vs. Decap	-61.1300	0.0004	***
								K/X vs. Decap	-35.1400	0.0466	*
Figure 3.2-g (Striatum-F)	**6**	**One-Way ANOVA test**	F (3, 20) = 22.56	P<0.0001	Iso CO2 K/X Decap	99.99 36.91 62.71 100	Tukey's Multiple Comparison Tes	Iso vs. CO2	63.0800	<0.0001	****
								Iso vs. K/X	37.2800	0.0031	**
								Iso vs. Decap	-0.0071	>0.9999	ns
								CO2 vs. K/X	-25.7900	0.0489	*
								CO2 vs. Decap	-63.0900	<0.0001	****
								K/X vs. Decap	-37.2900	0.0031	**
Figure 3.2-i (Nucleus Accumbens-M)	**3**	**One-Way ANOVA test**	F (3, 8) = 12.88	P=0.0020	Iso CO2 K/X Decap	75.52 14.51 49.67 100	Tukey's Multiple Comparison Tes	Iso vs. CO2	61.0100	0.0122	*
								Iso vs. K/X	25.8500	0.3425	ns
								Iso vs. Decap	-24.4800	0.3840	ns
								CO2 vs. K/X	-35.1600	0.1464	ns
								CO2 vs. Decap	-85.4900	0.0016	**
								K/X vs. Decap	-50.3300	0.0334	*
Figure 3.2-k (Nucleus Accumbens-F)	**3**	**One-Way ANOVA test**	F (3, 8) = 13.04	P=0.0019	Iso CO2 K/X Decap	116.2 16.77 56.74 100	Tukey's Multiple Comparison Tes	Iso vs. CO2	99.4500	0.0021	**
								Iso vs. K/X	59.4900	0.0384	*
								Iso vs. Decap	16.2200	0.7931	ns
								CO2 vs. K/X	-39.9700	0.1825	ns
								CO2 vs. Decap	-83.2300	0.0063	**
								K/X vs. Decap	-43.2600	0.1410	ns
Figure 3.2-m (Hippocampus-M)	**6**	**One-Way ANOVA test**	F (3, 20) = 6.63	P=0.0027	Iso CO2 K/X Decap	88.77 31.24 85.04 100	Tukey's Multiple Comparison Tes	Iso vs. CO2	57.5300	0.0135	*
								Iso vs. K/X	3.7300	0.9960	ns
								Iso vs. Decap	-11.2300	0.9084	ns
								CO2 vs. K/X	-53.8000	0.0218	*
								CO2 vs. Decap	-68.7600	0.0030	**
								K/X vs. Decap	-14.9600	0.8112	ns
Figure 3.2-o (Hippocampus-F)	**6**	**One-Way ANOVA test**	F (3, 20) = 16.18	P<0.0001	Iso CO2 K/X Decap	99.22 52.46 89.52 100	Tukey's Multiple Comparison Tes	Iso vs. CO2	46.7600	<0.0001	****
								Iso vs. K/X	9.6990	0.6151	ns
								Iso vs. Decap	-0.7762	0.9996	ns
								CO2 vs. K/X	-37.0700	0.0007	***
								CO2 vs. Decap	-47.5400	<0.0001	****
								K/X vs. Decap	-10.4800	0.5557	ns
Figure 3.2-q (Amygdala-M)	**3**	**One-Way ANOVA test**	F (3, 8) = 12.62	P=0.0021	Iso CO2 K/X Decap	106.2 23.74 68.64 100	Tukey's Multiple Comparison Tes	Iso vs. CO2	82.5000	0.0026	**
								Iso vs. K/X	37.6000	0.1336	ns
								Iso vs. Decap	6.2430	0.9742	ns
								CO2 vs. K/X	-44.9000	0.0674	ns
								CO2 vs. Decap	-76.2600	0.0042	**
								K/X vs. Decap	-31.3600	0.2352	ns
Figure 3.2-s (Amygdala-F)	**3**	**One-Way ANOVA test**	F (3, 8) = 23.03	P=0.0003	Iso CO2 K/X Decap	101.1 25.73 76.23 100	Tukey's Multiple Comparison Tes	Iso vs. CO2	75.4100	0.0004	***
								Iso vs. K/X	24.9100	0.1553	ns
								Iso vs. Decap	1.1380	0.9995	ns
								CO2 vs. K/X	-50.5000	0.0055	**
								CO2 vs. Decap	-74.2700	0.0004	***
								K/X vs. Decap	-23.7700	0.1805	ns

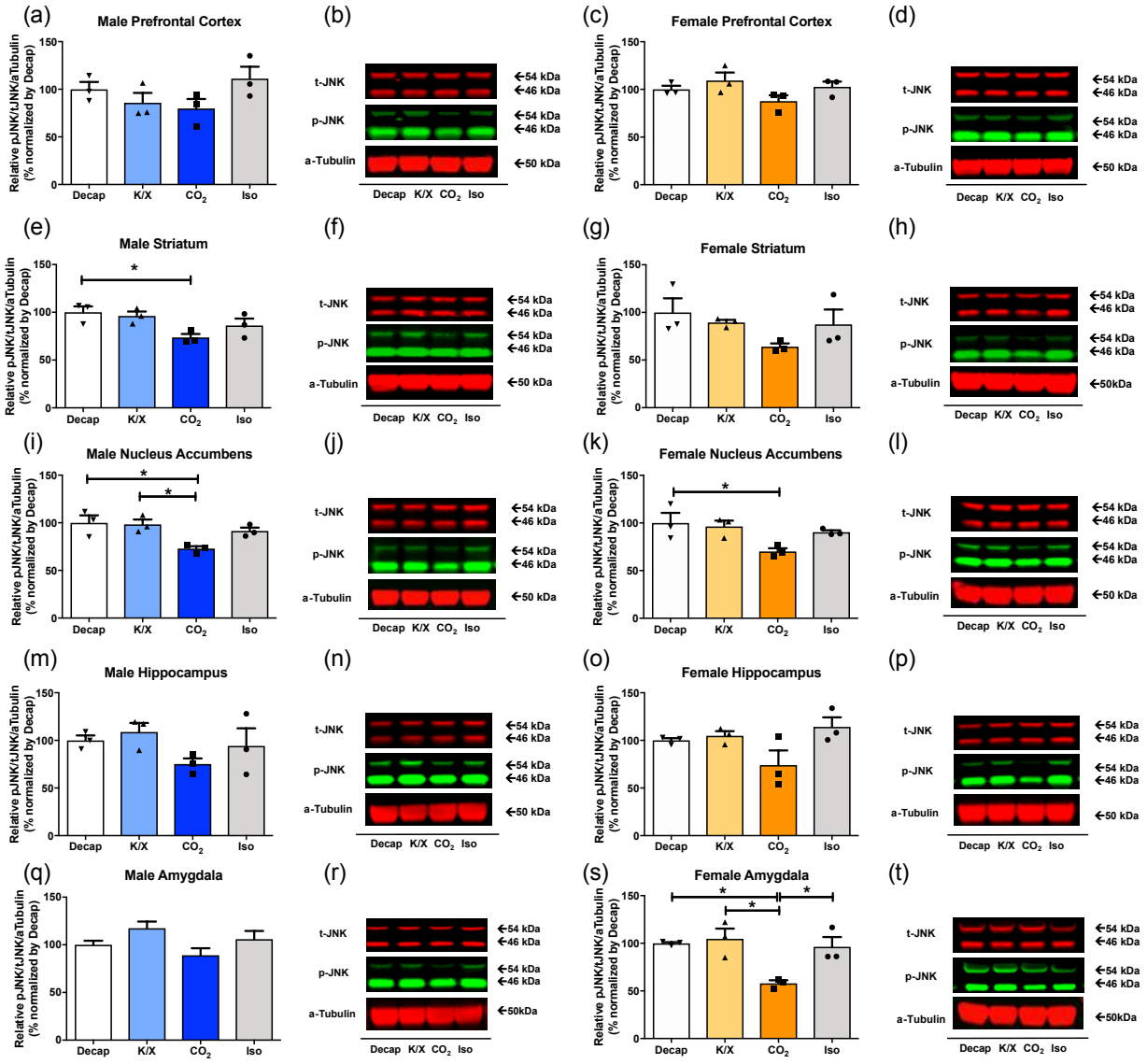

Figure 3.3 JNK expression levels to different anesthesia/euthanasia methods in the adult male and female mice brain

JNK expression levels were analyzed by the Western blot following the different anesthetic/euthanasia procedures in the male prefrontal cortex (a, b), the male striatum (e, f), the male nucleus accumbens (i, j), the male hippocampus (m, n), the male amygdala (q, r), as well as in the female prefrontal cortex (c, d), the female striatum (g, h), the female nucleus accumbens (k, l), the female hippocampus (o, p), and the female amygdala (s, t). Each group has three replicates for statistial analysis. Representative western blot images were presented next to corresponding bar graphs. All data was represented as mean ± SEM, and analyzed with one-way ANOVA with Tukey's multiple comparison (*$p < 0.05$).

Table 3.2. Statistical analysis of JNK expression levels in the brain by different anesthetic and euthanasia methods

Statistical differences of JNK expression levels in mouse brain shown in Figure 3.3. Significance between groups was calculated by one-way ANOVA followed by a Tukey's multiple comparison (*p<0.05, and ns=not significant).

JNK	# of samples	Test	F-value	p-value	Group	Mean	Post hoc analysis	Group Comparison	Mean Diff.	p-value	Significance
Figure 3.3-a (Prefrontal cortex-M)	3	One-Way ANOVA test	F (3, 8) = 1.898	P=0.2084	Iso CO2 K/X Decap	111.2 79.74 85.83 100	Tukey's Multiple Comparison Tes	Iso vs. CO2	31.4800	0.2128	ns
								Iso vs. K/X	25.3900	0.3628	ns
								Iso vs. Decap	11.2200	0.8651	ns
								CO2 vs. K/X	-6.0870	0.9737	ns
								CO2 vs. Decap	-20.2600	0.5368	ns
								K/X vs. Decap	-14.1700	0.7675	ns
Figure 3.3-c (Prefrontal cortex-F)	3	One-Way ANOVA test	F (3, 8) = 2.162	P=0.1705	Iso CO2 K/X Decap	102.7 87.72 109.3 100	Tukey's Multiple Comparison Tes	Iso vs. CO2	14.9400	0.3748	ns
								Iso vs. K/X	-6.6810	0.8663	ns
								Iso vs. Decap	2.6580	0.9893	ns
								CO2 vs. K/X	-21.6200	0.1368	ns
								CO2 vs. Decap	-12.2800	0.5261	ns
								K/X vs. Decap	9.3390	0.7135	ns
Figure 3.3-e (Striatum-M)	3	One-Way ANOVA test	F (3, 8) = 4.399	P=0.0417	Iso CO2 K/X Decap	86.14 73.66 96.16 100	Tukey's Multiple Comparison Tes	Iso vs. CO2	12.4800	0.4436	ns
								Iso vs. K/X	-10.0200	0.6088	ns
								Iso vs. Decap	-13.8600	0.3625	ns
								CO2 vs. K/X	-22.4900	0.0841	ns
								CO2 vs. Decap	-26.3400	0.0425	*
								K/X vs. Decap	-3.8430	0.9605	ns
Figure 3.3-g (Striatum-F)	3	One-Way ANOVA test	F (3, 8) = 1.906	P=0.2071	Iso CO2 K/X Decap	87.48 64.11 89.49 100	Tukey's Multiple Comparison Tes	Iso vs. CO2	23.3800	0.4762	ns
								Iso vs. K/X	-2.0070	0.9992	ns
								Iso vs. Decap	-12.5200	0.8495	ns
								CO2 vs. K/X	-25.3900	0.4122	ns
								CO2 vs. Decap	-35.8900	0.1736	ns
								K/X vs. Decap	-10.5100	0.9027	ns
Figure 3.3-i (Nucleus Accumbens-M)	3	One-Way ANOVA test	F (3, 8) = 5.765	P=0.0213	Iso CO2 K/X Decap	91.41 72.99 98.33 100	Tukey's Multiple Comparison Tes	Iso vs. CO2	18.4200	0.1291	ns
								Iso vs. K/X	-6.9200	0.7801	ns
								Iso vs. Decap	-8.5920	0.6552	ns
								CO2 vs. K/X	-25.3400	0.0340	*
								CO2 vs. Decap	-27.0100	0.0247	*
								K/X vs. Decap	-1.6720	0.9954	ns
Figure 3.3-k (Nucleus Accumbens-F)	3	One-Way ANOVA test	F (3, 8) = 4.345	P=0.0429	Iso CO2 K/X Decap	90.35 70.08 96.32 100	Tukey's Multiple Comparison Tes	Iso vs. CO2	20.2700	0.1924	ns
								Iso vs. K/X	-5.9720	0.9093	ns
								Iso vs. Decap	-9.6490	0.7184	ns
								CO2 vs. K/X	-26.2500	0.0768	ns
								CO2 vs. Decap	-29.9200	0.0433	*
								K/X vs. Decap	-3.6770	0.9759	ns
Figure 3.3-m (Hippocampus-M)	3	One-Way ANOVA test	F (3, 8) = 1.641	P=0.2556	Iso CO2 K/X Decap	94.25 75.19 108.8 100	Tukey's Multiple Comparison Tes	Iso vs. CO2	19.0600	0.6364	ns
								Iso vs. K/X	-14.5500	0.7923	ns
								Iso vs. Decap	-5.7500	0.9821	ns
								CO2 vs. K/X	-33.6100	0.2200	ns
								CO2 vs. Decap	-24.8100	0.4402	ns
								K/X vs. Decap	8.8000	0.9411	ns
Figure 3.3-o (Hippocampus-F)	3	One-Way ANOVA test	F (3, 8) = 3.2	P=0.0837	Iso CO2 K/X Decap	114.2 74.07 104.8 100	Tukey's Multiple Comparison Tes	Iso vs. CO2	40.0900	0.0710	ns
								Iso vs. K/X	9.3400	0.8988	ns
								Iso vs. Decap	14.1600	0.7306	ns
								CO2 vs. K/X	-30.7500	0.1856	ns
								CO2 vs. Decap	-25.9300	0.2960	ns
								K/X vs. Decap	4.8190	0.9836	ns
Figure 3.3-q (Amygdala-M)	3	One-Way ANOVA test	F (3, 8) = 2.832	P=0.1063	Iso CO2 K/X Decap	105.9 89.1 117.4 100	Tukey's Multiple Comparison Tes	Iso vs. CO2	16.8400	0.3851	ns
								Iso vs. K/X	-11.4900	0.6677	ns
								Iso vs. Decap	5.9380	0.9299	ns
								CO2 vs. K/X	-28.3300	0.0819	ns
								CO2 vs. Decap	-10.9000	0.7008	ns
								K/X vs. Decap	17.4300	0.3588	ns
Figure 3.3-s (Amygdala-F)	3	One-Way ANOVA test	F (3, 8) = 7.982	P=0.0087	Iso CO2 K/X Decap	96.32 57.97 104.7 100	Tukey's Multiple Comparison Tes	Iso vs. CO2	38.3600	0.0300	*
								Iso vs. K/X	-8.4180	0.8601	ns
								Iso vs. Decap	-3.6800	0.9852	ns
								CO2 vs. K/X	-46.7700	0.0105	*
								CO2 vs. Decap	-42.0300	0.0188	*
								K/X vs. Decap	4.7380	0.9696	ns

3.3.3 Different general anesthesia and euthanasia methods do not impact p38 kinase activity

No statistical difference between euthanasia methods were observed in p38 activity in males (**Figure 3.4 a, b** for the prefrontal cortex, $F_{3, 8} = 0.1404$, p=0.9; **Figure 3.4 e, f** for the striatum, $F_{3, 8} = 0.008209$, p=1,0; **Figure 3.4 i, j** for the nucleus accumbens, $F_{3, 8} = 0.4954$, p=0.7; **Figure 3.4 m, n** for the hippocampus, $F_{3, 8} = 1.146$, p=0.4; **Figure 3.4 q, r** for the amygdala, $F_{3, 8} = 0.429$, p=0.7; see **Table 3.3** for post-hoc multiple comparison) or in females (**Figure 3.4 c, d** for the prefrontal cortex, $F_{3, 8} = 1.91$, p=0.2; **Figure 3.4 g, h** for the striatum, $F_{3, 8} = 2.528$, p=0.13; **Figure 3.4 k, l** for the nucleus accumbens, $F_{3, 8} = 0.2177$, p=0.9; **Figure 3.4 o, p** for the hippocampus, $F_{3, 8} = 0.37$, p=0.78; **Figure 3.4 s, t** for the amygdala, $F_{3, 8} = 1.451$, p=0.3; see **Table 3.3** for post-hoc multiple comparison).

3.3.4 No sex difference of ERK1/2 activity levels to different general euthanasia methods was observed in the hippocampus and the striatum of both sexes

To investigate if different euthanasia methods impacted MAPK activity across sexes, we tested the ERK1/2 activity to four euthanasia methods in the hippocampus and the striatum of male and female mice. Using 2-way ANOVA, we observed no significant sex effects for ERK1/2 activity between different anesthesia/euthanasia methods in the striatum (**Figure 3.5 a**; $F_{3, 16} = 0.1196$, p=0.9473), and the hippocampus (**Figure 3.5 b**; $F_{3, 15} = 0.1157$, p=9495 see **Table 3.4** for post-hoc multiple comparison).

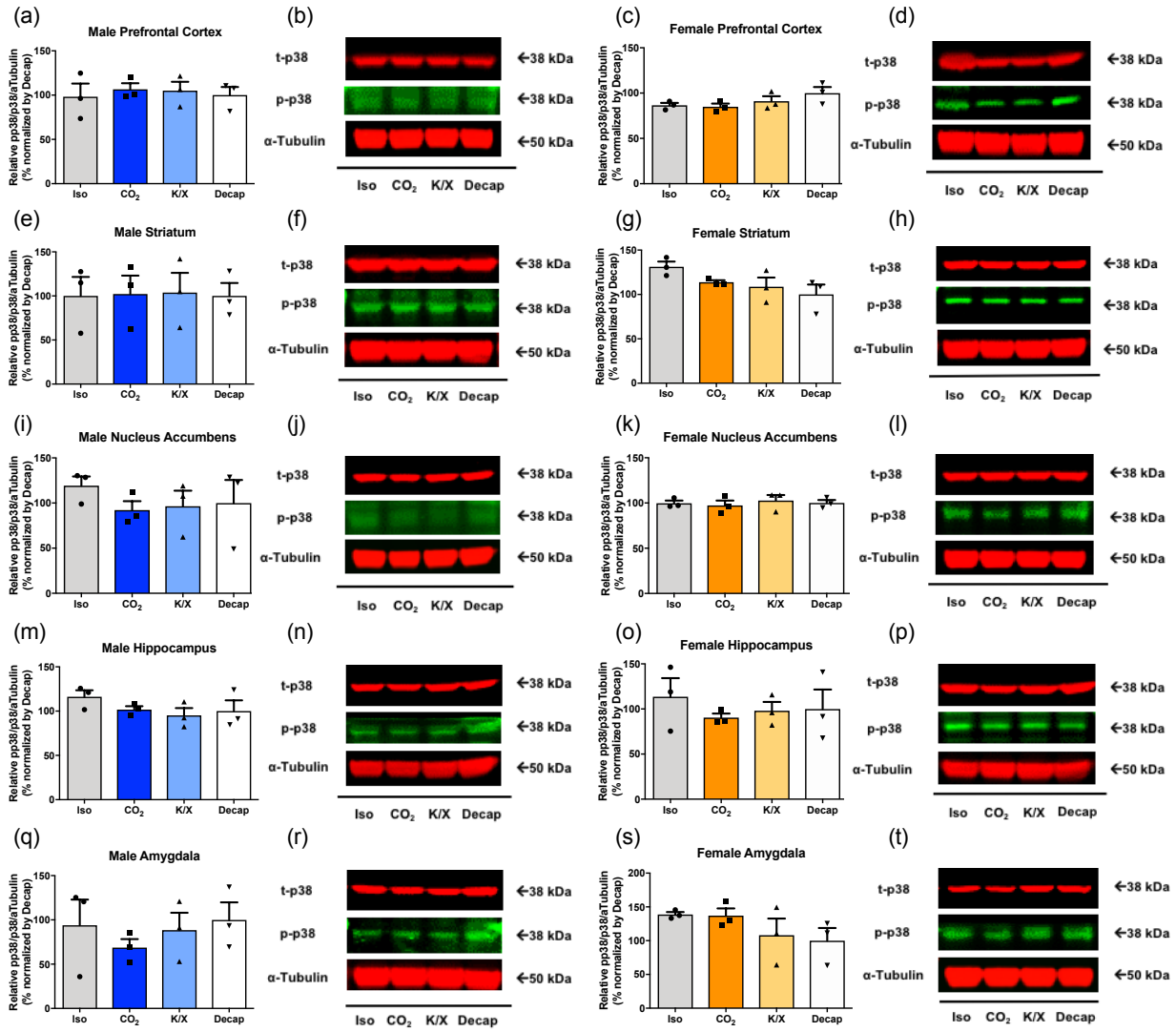

Figure 3.4 p38 expression levels to different anesthesia/euthanasia methods in the adult male and female mice brain

p38 expression levels were analyzed by the Western blot following the different anesthetic/euthanasia procedures in the male prefrontal cortex (a, b), the male striatum (e, f), the male nucleus accumbens (i, j), the male hippocampus (m, n), the male amygdala (q, r), as well as in the female prefrontal cortex (c, d), the female striatum (g, h), the female nucleus accumbens (k, l), the female hippocampus (o, p), and the female amygdala (s, t). Each group has three replicates for statistial analysis. Representative western blot images were presented next to corresponding bar graphs. All data was represented as mean ± SEM, and analyzed with one-way ANOVA.

Table 3.3. Statistical analysis of p38 expression levels in the brain by different anesthetic and euthanasia methods

Statistical differences of p38 expression levels in mouse brain shown in Figure 3.4. Significance between groups was calculated by one-way ANOVA followed by a Tukey's multiple comparison (*p<0.05, **p<0.01, ***p<0.001, ***p<0001, and ns=not significant)

p38	# of samples	Test	F-value	p-value	Group	Mean	Post hoc analysis	Group Comparison	Mean Diff.	p-value	Significance
Figure 3.4-a (Prefrontal cortex-M)	3	One-Way ANOVA test	F (3, 8) = 0.1404	P=0.9330	Iso CO2 K/X Decap	98.23 106.6 105 100	Tukey's Multiple Comparison Tes	Iso vs. CO2 Iso vs. K/X Iso vs. Decap CO2 vs. K/X CO2 vs. Decap K/X vs. Decap	-8.3600 -6.7800 -1.7740 1.5800 6.5860 5.0060	0.9421 0.9675 0.9994 0.9995 0.9700 0.9863	ns ns ns ns ns ns
Figure 3.4-c (Prefrontal cortex-F)	3	One-Way ANOVA test	F (3, 8) = 1.91	P=0.2065	Iso CO2 K/X Decap	86.51 84.98 91.07 100	Tukey's Multiple Comparison Tes	Iso vs. CO2 Iso vs. K/X Iso vs. Decap CO2 vs. K/X CO2 vs. Decap K/X vs. Decap	1.5250 -4.5610 -13.4900 -6.0860 -15.0200 -8.9310	0.9959 0.9092 0.2809 0.8150 0.2104 0.5921	ns ns ns ns ns ns
Figure 3.4-e (Striatum-M)	3	One-Way ANOVA test	F (3, 8) = 0.008209	P=0.9989	Iso CO2 K/X Decap	100.1 102.2 103.8 100	Tukey's Multiple Comparison Tes	Iso vs. CO2 Iso vs. K/X Iso vs. Decap CO2 vs. K/X CO2 vs. Decap K/X vs. Decap	-2.1480 -3.6950 0.0757 -1.5470 2.2230 3.7710	0.9998 0.9991 >0.9999 >0.9999 0.9998 0.9991	ns ns ns ns ns ns
Figure 3.4-g (Striatum-F)	3	One-Way ANOVA test	F (3, 8) = 2.528	P=0.1309	Iso CO2 K/X Decap	131.2 113.8 108.6 100	Tukey's Multiple Comparison Tes	Iso vs. CO2 Iso vs. K/X Iso vs. Decap CO2 vs. K/X CO2 vs. Decap K/X vs. Decap	17.3200 22.5300 31.1600 5.2010 13.8300 8.6310	0.4891 0.2897 0.1065 0.9688 0.6528 0.8789	ns ns ns ns ns ns
Figure 3.4-i (Nucleus Accumbens-M)	3	One-Way ANOVA test	F (3, 8) = 0.4954	P=0.6955	Iso CO2 K/X Decap	119.2 92.22 96.39 100	Tukey's Multiple Comparison Tes	Iso vs. CO2 Iso vs. K/X Iso vs. Decap CO2 vs. K/X CO2 vs. Decap K/X vs. Decap	27.0000 22.8300 19.2200 -4.1630 -7.7770 -3.6140	0.6853 0.7791 0.8521 0.9980 0.9873 0.9987	ns ns ns ns ns ns
Figure 3.4-k (Nucleus Accumbens-F)	3	One-Way ANOVA test	F (3, 8) = 0.2177	P=0.8814	Iso CO2 K/X Decap	99.75 97.35 102.7 100	Tukey's Multiple Comparison Tes	Iso vs. CO2 Iso vs. K/X Iso vs. Decap CO2 vs. K/X CO2 vs. Decap K/X vs. Decap	2.3950 -2.9070 -0.2512 -5.3020 -2.6470 2.6560	0.9823 0.9693 >0.9999 0.8496 0.9764 0.9762	ns ns ns ns ns ns
Figure 3.4-m (Hippocampus-M)	3	One-Way ANOVA test	F (3, 8) = 1.146	P=0.3879	Iso CO2 K/X Decap	116.2 101.7 95.16 100	Tukey's Multiple Comparison Tes	Iso vs. CO2 Iso vs. K/X Iso vs. Decap CO2 vs. K/X CO2 vs. Decap K/X vs. Decap	14.4600 21.0100 16.1700 6.5510 1.7090 -4.8420	0.6378 0.3572 0.5583 0.9444 0.9989 0.9760	ns ns ns ns ns ns
Figure 3.4-o (Hippocampus-F)	3	One-Way ANOVA test	F (3, 8) = 0.37	P=0.7769	Iso CO2 K/X Decap	113.6 90.39 98.05 100	Tukey's Multiple Comparison Tes	Iso vs. CO2 Iso vs. K/X Iso vs. Decap CO2 vs. K/X CO2 vs. Decap K/X vs. Decap	23.1700 15.5000 13.5500 -7.6660 -9.6130 -1.9470	0.7359 0.8975 0.9278 0.9852 0.9718 0.9997	ns ns ns ns ns ns
Figure 3.4-q (Amygdala-M)	3	One-Way ANOVA test	F (3, 8) = 0.429	P=0.7378	Iso CO2 K/X Decap	93.94 68.73 88.39 100	Tukey's Multiple Comparison Tes	Iso vs. CO2 Iso vs. K/X Iso vs. Decap CO2 vs. K/X CO2 vs. Decap K/X vs. Decap	25.2100 5.5420 -6.0640 -19.6700 -31.2700 -11.6100	0.8240 0.9974 0.9966 0.9047 0.7164 0.9774	ns ns ns ns ns ns
Figure 3.4-s (Amygdala-F)	3	One-Way ANOVA test	F (3, 8) = 1.451	P=0.2988	Iso CO2 K/X Decap	138.7 137.1 108.1 100	Tukey's Multiple Comparison Tes	Iso vs. CO2 Iso vs. K/X Iso vs. Decap CO2 vs. K/X CO2 vs. Decap K/X vs. Decap	1.6120 30.6600 38.7200 29.0500 37.1100 8.0650	0.9999 0.5791 0.4006 0.6176 0.4336 0.9847	ns ns ns ns ns ns

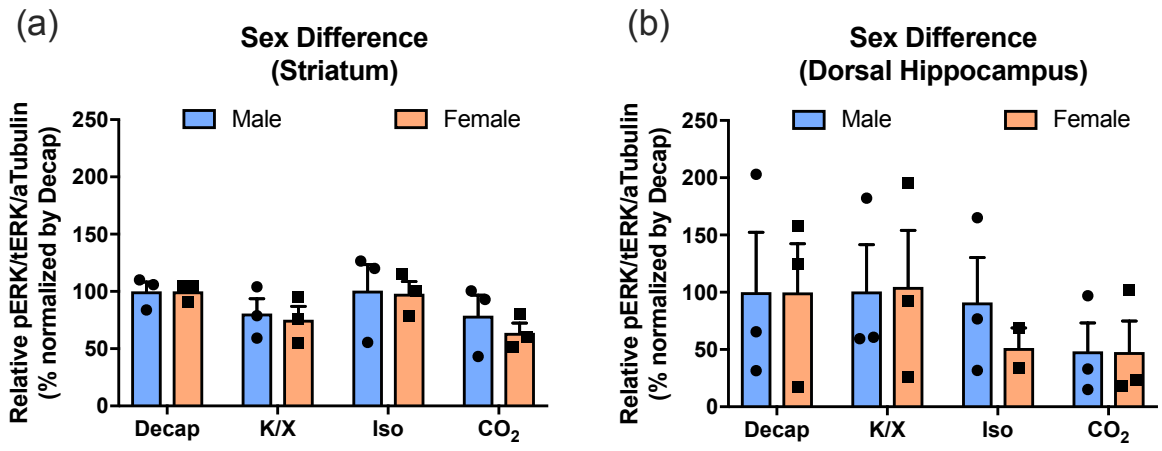

Figure 3.5 No sex difference of ERK1/2 activation in response to different anesthesia/euthanasia methods in selected brain regions

MAPK activity were normalized to those observed in the carbon dioxide group, and relative levels were analyzed using 2-way ANOVA in the striatum **(a)**, the dorsal hippocampus **(b)**, the hippocampus for ERK1/2 activity. Representative western blot images were presented in Figure 2. All data was represented as mean ± SEM, and analyzed with 2-way ANOVA with Tukey's multiple comparison.

Table 3.4. Statistical analysis of ERK1/2 expression levels to different anesthetic and euthanasia methods in the male and female mice brain

Statistical differences of ERK1/2 expression levels in male and female mice brain shown in Figure 3.5. Significance between groups was calculated by two-way ANOVA followed by a Tukey's multiple comparison (ns=not significant)

ERK1/2	Test	Effect	F value	p-value	Post hoc analysis		Significance
Figure 3.5-a (Striatum)	**2-Way ANOVA**	**Sex x Drug effect**	F (3, 16) = 0.1196	P=0.9473	Tukey's Multiple Comparisons Test	CO2: Male vs. Female	ns
		Drug effect	F (3, 16) = 2.432	P=0.1028		Iso: Male vs. Female	ns
		Sex effect	F (1, 16) = 0.3795	P=0.5465		K/X: Male vs. Female	ns
						Decap: Male vs. Female	ns
Figure 3.5-b (Hippocampus)	**2-Way ANOVA**	**Sex x Drug effect**	F (3, 15) = 0.1157	P=0.9495	Tukey's Multiple Comparisons Test	CO2: Male vs. Female	ns
		Drug effect	F (3, 15) = 0.8593	P=0.4835		Iso: Male vs. Female	ns
		Sex effect	F (1, 15) = 0.1019	P=0.7539		K/X: Male vs. Female	ns
						Decap: Male vs. Female	ns

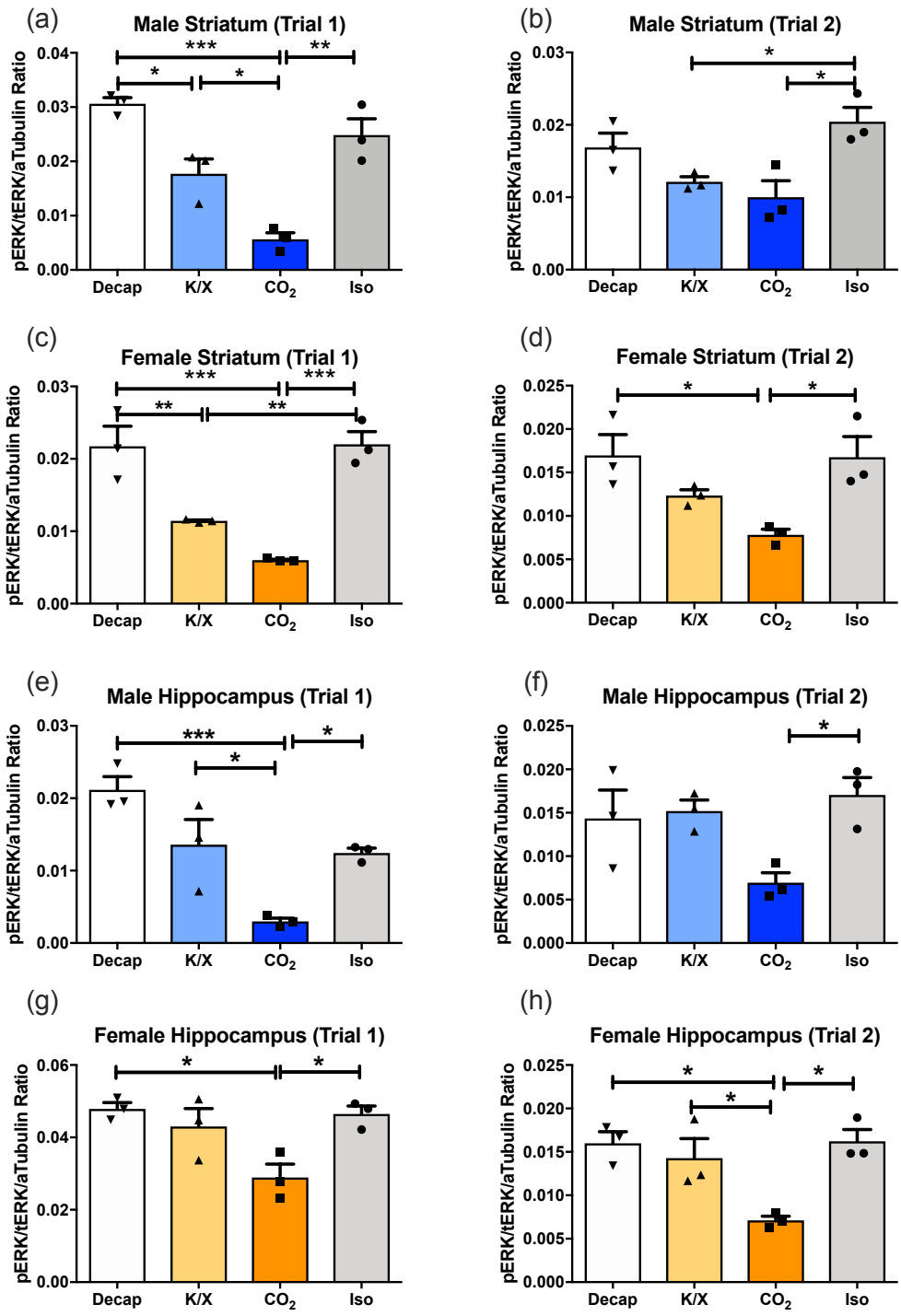

Figure 3.6 Reproducibility of the experimental paradigm

Reproducibility of the experimental paradigm was tested in selected brain regions using the same four anesthetic and euthanasia methods. To increase the scientific rigor and reproducibility, ERK1/2 activation in the male striatum **(a, b)**, the female striatum **(c, d)**, the male hippocampus **(e, f)**, and the female hippocampus **(g, h)** to different euthanasia methods were tested in two separate trials.

Table 3.5. Statistical analysis of reproducibility of experimental paradigm

Statistical differences of ERK1/2 expression levels in mouse brain shown in Figure 3.6 (combined data is in Figure 3.1). Significance between groups was calculated by one-way ANOVA followed by a Tukey's multiple comparison (*p<0.05, **p<0.01,*** p<0.001,and ns=not significant).

ERK1/2	# of samples	Test	F-value	p-value	Group	Mean	Post hoc analysis	Group Comparison	Mean Diff.	p-value	Significance
Supplemental Figure 3.1-a (Striatum-M Trial 1)	**3**	**One-Way ANOVA test**	F (3, 8) = 23.94	P=0.0002	Iso CO2 K/X Decap	0.02484 0.005637 0.01771 0.03061	Tukey's Multiple Comparison Tes	Iso vs. CO2	0.0192	0.0012	**
								Iso vs. K/X	0.0071	0.1793	ns
								Iso vs. Decap	-0.0058	0.3167	ns
								CO2 vs. K/X	-0.0121	0.0194	*
								CO2 vs. Decap	-0.0250	0.0002	***
								K/X vs. Decap	-0.0129	0.0137	*
Supplemental Figure 3.1-b (Striatum-M Trial 2)	**3**	**One-Way ANOVA test**	F (3, 8) = 6.617	P=0.0147	Iso CO2 K/X Decap	0.02045 0.01002 0.01214 0.01689	Tukey's Multiple Comparison Tes	Iso vs. CO2	0.0104	0.0158	*
								Iso vs. K/X	0.0083	0.0489	*
								Iso vs. Decap	0.0036	0.5460	ns
								CO2 vs. K/X	-0.0021	0.8436	ns
								CO2 vs. Decap	-0.0069	0.1072	ns
								K/X vs. Decap	-0.0048	0.3227	ns
Supplemental Figure 3.1-c (Striatum-F Trial 1)	**3**	**One-Way ANOVA test**	F (3, 8) = 23.16	P=0.0003	Iso CO2 K/X Decap	0.02201 0.006021 0.01144 0.02174	Tukey's Multiple Comparison Tes	Iso vs. CO2	0.0160	0.0006	***
								Iso vs. K/X	0.0106	0.0081	**
								Iso vs. Decap	0.0003	0.9994	ns
								CO2 vs. K/X	-0.0054	0.1697	ns
								CO2 vs. Decap	-0.0157	0.0006	***
								K/X vs. Decap	-0.0103	0.0094	**
Supplemental Figure 3.1-d (Striatum-F Trial 2)	**3**	**One-Way ANOVA test**	F (3, 8) = 6.101	P=0.0183	Iso CO2 K/X Decap	0.01675 0.007827 0.01235 0.01697	Tukey's Multiple Comparison Tes	Iso vs. CO2	0.0089	0.0285	*
								Iso vs. K/X	0.0044	0.3495	ns
								Iso vs. Decap	-0.0002	0.9997	ns
								CO2 vs. K/X	-0.0045	0.3281	ns
								CO2 vs. Decap	-0.0091	0.0253	*
								K/X vs. Decap	-0.0046	0.3139	ns
Supplemental Figure 3.1-e (Hippocampus-M Trial 1)	**3**	**One-Way ANOVA test**	F (3, 8) = 13.94	P=0.0015	Iso CO2 K/X Decap	0.01244 0.002983 0.0136 0.02116	Tukey's Multiple Comparison Tes	Iso vs. CO2	0.0095	0.0408	*
								Iso vs. K/X	-0.0012	0.9752	ns
								Iso vs. Decap	-0.0087	0.0587	ns
								CO2 vs. K/X	-0.0106	0.0231	*
								CO2 vs. Decap	-0.0182	0.0009	***
								K/X vs. Decap	-0.0076	0.1047	ns
Supplemental Figure 3.1-f (Hippocampus-M Trial 2)	**3**	**One-Way ANOVA test**	F (3, 8) = 4.46	P=0.0403	Iso CO2 K/X Decap	0.01704 0.006945 0.01519 0.01435	Tukey's Multiple Comparison Tes	Iso vs. CO2	0.0101	0.0379	*
								Iso vs. K/X	0.0019	0.9213	ns
								Iso vs. Decap	0.0027	0.8022	ns
								CO2 vs. K/X	-0.0082	0.0914	ns
								CO2 vs. Decap	-0.0074	0.1357	ns
								K/X vs. Decap	0.0008	0.9916	ns
Supplemental Figure 3.1-g (Hippocampus-F Trial 1)	**3**	**One-Way ANOVA test**	F (3, 8) = 6.554	P=0.0151	Iso CO2 K/X Decap	0.04649 0.02895 0.04298 0.04789	Tukey's Multiple Comparison Tes	Iso vs. CO2	0.0175	0.0263	*
								Iso vs. K/X	0.0035	0.8817	ns
								Iso vs. Decap	-0.0014	0.9906	ns
								CO2 vs. K/X	-0.0140	0.0733	ns
								CO2 vs. Decap	-0.0189	0.0177	*
								K/X vs. Decap	-0.0049	0.7408	ns
Supplemental Figure 3.1-h (Hippocampus-F Trial 2)	**3**	**One-Way ANOVA test**	F (3, 8) = 8.132	P=0.0082	Iso CO2 K/X Decap	0.01621 0.00711 0.01428 0.01599	Tukey's Multiple Comparison Tes	Iso vs. CO2	0.0091	0.0114	*
								Iso vs. K/X	0.0019	0.8003	ns
								Iso vs. Decap	0.0002	0.9996	ns
								CO2 vs. K/X	-0.0072	0.0391	*
								CO2 vs. Decap	-0.0089	0.0130	*
								K/X vs. Decap	-0.0017	0.8496	ns

3.4 Discussion

The current study evaluated to what degree four commonly used general anesthesia/euthanasia methods to collect brain tissue affect MAPK activity in the naïve and healthy male and female wild-type mice adult brain. Of the four methods (isoflurane, carbon dioxide asphyxiation, ketamine/xylazine, and rapid unanaesthetized decapitation), those brains collected following carbon dioxide asphyxiation showed the lowest ERK1/2 phosphorylation in the prefrontal cortex, the striatum, the nucleus accumbens, the hippocampus, and the amygdala of male and female adult mice. JNK activity showed less pronounced effects in comparison to ERK1/2 activity to different anesthesia/euthanasia methods. More specifically, except for the male striatum, the male and female nucleus accumbens, and the female amygdala, no significant difference was observed in JNK activity between different anesthesia/euthanasia methods. No statistically significant difference between groups was observed in terms of p38 activity. Our findings are in agreement with a previous study investigating the impact of different anesthesia methods on the metabolomics (Overmyer et al., 2015). This study, which however did not study the brain, found that carbon dioxide generally produced few significant changes in the metabolomics, whereas isoflurane, ketamine and pentobarbital produced more significant changes. Our study complements this previous study as similar C57BL/6 mice of comparable age were used, although our experiments were performed during the mice's active cycle (in the dark) and focused on MAPK activity in five brain regions linked to various neuropsychiatric disorders.

Although there are many brain regions that are involved in the modulation of MAPK signaling pathways, we specifically chose the prefrontal cortex, the hippocampus, the amygdala, the nucleus accumbens, and the striatum as these brain regions are some of the most commonly investigated in the field of neuroscience particularly in relation to neuropsychiatric disorders. For example, the hippocampus and the amygdala are important brain regions for anxiety disorder (Bannerman et al., 2004), memory disorder (Bannerman et al., 2004), and may also be involved in attention-deficit and hyperactivity disorder (Onnink et al., 2014), and autistic spectrum disorder (Tottenham et al., 2014). For example, consolidation and extinction fear memory required ERK1/2 in the hippocampus and the basolateral amygdala (Besnard et al., 2014). The striatum and the nucleus accumbens are heavily implicated in substance use disorder (Robbins & Everitt, 2002), Parkinson's disease (Surmeier et al., 2014), and epilepsy (Deransart et al., 2000). Especially,

MAPK signaling pathway in striatal neurons involved in the formation of neuronal plasticity related to addictive behavior (Wang et al., 2004). Furthermore, abnormalities in the prefrontal cortex are also implicated in attention-deficit/hyperactivity disorder (Halperin & Schulz, 2006), autistic spectrum disorder (Courchesne et al., 2011; Morgan et al., 2010), and various mood disorders (Drevets et al., 1997). For instance, MAPK activation mediated by dopaminergic D_1 and D_2 receptors in the prefrontal cortex, which are important for various mood and motor control, is also linked to neuronal plasticity (Goto et al., 2010). Therefore, in order to study the neurochemical basis of these disorders or how drug treatments correct or alter the cellular signaling, it is important to properly assess MAPK activity levels. However, methods used in collecting brain tissue have the propensity to change MAPK activity even in naïve wild-type mice.

In our study, we demonstrated that four anesthetic/euthanasia methods differentially impact three MAPKs. In particular, we used the non-anesthetic decapitation method as our control group, as it does not result in any major pharmacokinetic and pharmacodynamics interactions in the brain. We observed the largest impact of euthanasia method on ERK1/2 activity levels. Relative to carbon dioxide asphyxiation, isoflurane produced strong ERK1/2 activation in all brain regions of both male and female mice. It has been reported that a low dose (0.7%) of isoflurane for a short-term (30 minutes) exposure increased NMDA receptor subtype 2B (NR2B) and its downstream ERK1/2 phosphorylation, but a high dose (1.4%) of isoflurane with a long-term (4 hours) exposure decreased NR2B and ERK1/2 activity as well as increased neuroapoptosis in mice hippocampus (Liu et al., 2014). For this study, we briefly (5 minutes) induced with a 5% isoflurane dose, which may more closely mimic the 30 minutes 0.7% exposure, the condition that increased NR2B and ERK1/2 activity.

We have also observed that decapitation increased ERK1/2 activity relative to carbon dioxide asphyxiation in all tested brain regions of male and female adult mice. These findings appear to be in line with previous reports on stress hormone-induced ERK1/2 activation. Acute stress may play a role in the modulation of stress hormone receptors such as corticotropin releasing hormone (CRH) receptors and glucocorticoid receptors (Meller et al., 2003). Previous studies have shown ERK1/2 activation by acute stress-mediated modulation of stress-related receptors such as CRH receptors and glucocorticoid receptors (Kim et al., 2018; Meller et al., 2003), suggesting the potential implication of stress in ERK1/2 activation.

Systemic administration of ketamine/xylazine also led to significant ERK1/2 activation in the male striatum, the male hippocampus, and the female amygdala compared to carbon dioxide asphyxiation. It is possible that ketamine activated the mammalian target of rapamycin (mTOR) pathway as a NMDA receptor antagonist, which potentially increased ERK1/2 phosphorylation in the brain (Li et al., 2010), explaining the increase of ERK1/2 activity in these brain regions. We also observed that ERK1/2 activity by ketamine/xylazine is significantly lower than either decapitation or isoflurane exposure in some brain regions, it is possible that NR2B-mediated or stress-mediated ERK1/2 activation may impact more potent effects in the activation of ERK1/2 than the systemic administration of ketamine/xylazine. Additionally, we chose 45 minutes time-point considering situations where prolonged surgeries or perfusions are performed. The mixture of 100/10 mg/kg ketamine/xylazine is known to last its anesthetic effects up to 80 minutes with reflex suppressions and produces stable heart rates 40 minutes post-injection in mice (Erhardt et al., 1984; Xu et al., 2007). However, given that the serum ketamine levels are peaked at 10-20 minutes (Ganguly et al., 2018), it is possible that there may be more pronounced ERK1/2 activation an earlier time-point.

Studies have also shown the involvement of JNK activation in the isoflurane-mediated neuroapoptosis in the hippocampus of neonatal rats (Li et al., 2013; Liao et al., 2014). Yet, we only observed that isoflurane increased JNK activation relative to carbon dioxide asphyxiation in the amygdala of female mice. As the previous studies used neonatal rats, it is possible that the differences in age and species between our and their studies underlie the differences in outcome. Additionally, it is also possible that the duration and percentage of isoflurane were not comparable to observe similar trends in JNK activation in our hippocampal sections.

For p38 activity, we originally hypothesized that carbon dioxide asphyxiation similar to a reduced oxygen condition (hypoxic condition) may increase p38 activity, because a deprivation of oxygen supply by ischemia/hypoxia-induced cerebral injury in the brain may induce activation of p38 leading to neuroapoptosis (Bu et al., 2007; Yang et al., 2013). However, we did not observe any changes in p38 activity. This could be partly due to the low intensity of the p38 and p-p38 signal compared to ERK1/2 or JNK. This may either be due to actual low presence of p38 in these regions or relative poor quality of the p38/p-p38 antibodies. Another possibility is that a more prolonged exposure to low oxygen levels may be required to induce p38 activation. Furthermore, given that p38 is an integral MAPK signaling of cellular injury (Hensley et al., 2000), it is also

possible that we were unable to observe clear p38 expression levels, because cellular injury was not severe enough to express p38.

Until the day that we can grow entire mouse brains in culture, and therefore won't need to euthanize animals to obtain brain tissue, it is unclear what truly baseline MAPK activity is. Currently, we are unable to claim if isoflurane increased ERK1/2 phosphorylation or carbon dioxide asphyxiation decreased ERK1/2 activity. However, because there are mechanistic rationales for how isoflurane and ketamine can induce activation of MAPK pathways (Reus et al., 2014), the most logical hypothesis is that the observed MAPK levels obtained from carbon dioxide exposed mice are closest to the actual baseline of MAPK activity in adult mice brains.

We also explored sex as an independent variable. While a previous study found that sex hormones impacts MAPK activity through a mechanism involving Tropomyosin-Related Kinase B (TrkB) receptors (Carbone & Handa, 2013), we did not observe sex effects in selected brain regions such as the hippocampus and the striatum. In our study, we did not take the estrous cycle into consideration, and thus it is also possible that the different estrous cycle of the females could have weakened the observed sex effects.

One limitation of our study is that we only used a single mouse strain, specifically the C57BL/6 strain, but given that the C57BL/6 strain is one of the most commonly employed strains in various neurological studies, the findings should still be broadly informative for researchers aiming to optimize brain tissue collections for investigation of MAPK activity. Another potential limitation is that we used only healthy and drug-naïve mice. Mice suffering from specific neurological conditions or undergoing drug treatments may become more or less susceptible to one or more of the different anesthesia/euthanasia methods, and thus caution is advised when extrapolating our results to diseased or drug-treated animals. Yet, we are encouraged by the similarity of our finding compared to the metabolomics study of these methods (Overmyer et al., 2015). Additionally, it is noteworthy that we did not exclude the blood as a potential source of MAPK since lymphocytes in the blood can contribute to the production of cytokines and further activate MAPK signaling through tyrosine kinase (Grace et al., 2014). However, given our significant changes in response to the selected anesthetic methods even in presence of blood, the impact of anesthetics may be more pronounced than the potential impact of the blood. Finally, considering different pharmacokinetic profiles of the pharmacological agents that we used in our experimental paradigm, our findings may be limited to the dosage and time-point that we used in

our paradigm. Still, our experimental results serve as the foundation to the scientific community and allow further advances and optimizations in pharmacological manipulations of MAPK signaling studies in the brain.

Overall, our results demonstrated that euthanasia by carbon dioxide asphyxiation prior to brain tissue collection provides minimal naïve MAPK activation. Based on our findings, we recommend the usage of carbon dioxide asphyxiation as the method of choice for terminal euthanasia for brain tissue collection. Furthermore, for procedures such as transcardiac perfusion for immunohistochemistry or stereotaxic surgery that require a prolonged anesthetic method, we would recommend a systemic administration of ketamine/xylazine over the use of isoflurane. However, we would also recommend careful consideration on the selection of detailed dosages and time-points of the drug administration to serve the objective of the experiments. Overall, our findings offer vital information for researchers who are seeking methods to optimize brain collection to investigate MAPK activity to reduce the risk of false negative results.

CHAPTER 4. A CRITICAL EVALUATION OF TRPA1-MEDIATED LOCOMOTOR BEHAVIOR IN ZEBRAFISH AS A SCREENING TOOL FOR NOVEL ANTI-NOCICEPTIVE DRUG DISCOVERY

This chapter is comprised of data that has been peer-reviewed and published in Scientific Reports (Ko, Ganzen, et al., 2019). Figures 4.12 and 4.13 were produced by Logan Ganzen and Emre Coskun, all others were produced by Mee Jung Ko (or Arbaaz Mukadam under supervision of Mee Jung Ko).

4.1 Introduction

Nociception plays an active role in the defense against injury; however, persisting pain may become maladaptive and significantly impact an individual's daily activity and the quality of life. Chronic pain, defined as unrelieved and persistent lasts longer than 3 months, is usually treated by non-steroidal anti-inflammatory drugs (NSAIDs), anticonvulsants, tricyclic antidepressants, and opioids. Despite these treatment options, many patients still complain that their pain is insufficiently managed (Dowell et al., 2016). Additionally, opioid-based therapeutics have recently been demoted to third- and fourth-line treatment options for chronic pain per the guidelines of the Center for Disease Control and Prevention due to their addictive potentials, thereby further limiting the number of effective therapies. Thus, a critical need exists to identify novel pain targets and develop better analgesics for chronic pain.

An untapped analgesic target for chronic pain is the Transient Receptor Potential subfamily A1 (TRPA1) channel (Chen & Hackos, 2015; Nassini et al., 2014). TRPA1 channels are calcium-permissive cation channels targeted by thermal (Story et al., 2003; Tominaga, 2007), mechanical (Corey et al., 2004; Petrus et al., 2007), and noxious chemical stimuli such as allyl isothiocyanate (AITC), acrolein, cinnamaldehyde, allicin, and formalin (Bautista et al., 2005; Due et al., 2014; McNamara et al., 2007). Pharmacological inhibition of TRPA1 channels inhibited complete Freund's Adjuvant (CFA)-induced mechanical allodynia in wild-type mice, but not in TRPA1-deficient mice (Petrus et al., 2007). Oral administration of the TRPA1 antagonist, HC-030031, increased paw withdrawal threshold in a spinal nerve ligation model of neuropathic pain (Eid et al., 2008). Yet, drug development targeting TRPA1 is still in its infancy, and thus far no TRPA1 ligand has been approved by the Food and Drug Administration. This may be in part because using

the rodent models to establish *in vivo* efficacy of drug candidates can be very expensive and time-consuming.

The limitations associated with using a mouse model early in the drug discovery process motivated us to search for an alternative animal model that could expedite the process of validating *in vivo* TRPA1 ligand efficacy. Zebrafish have long been used as a preclinical vertebrate model organism for testing pharmacodynamics (absorption, distribution, metabolism and excretion), and pharmacokinetics of novel drugs (Zon & Peterson, 2005). The low cost, rapid development and high fecundity of zebrafish makes it ideal as a drug-screening tool. Several behavior models of neurological and neuropsychiatric-like behavior have been created in zebrafish that mimic those established for rodents, such as conditioned place preference (Bretaud et al., 2007) and anxiety-like behavior (Mathur & Guo, 2011). Increased zebrafish locomotor behavior has also been previously observed by both thermal and chemical activation of TRPA1 channels (Curtright et al., 2015; Stevens et al., 2018). Fortunately, TRPA1 channels are relatively conserved across species ranging from planarians to humans (Arenas et al., 2017), and the peripheral and central nociceptive systems of zebrafish are similar to many vertebrates such as mice and humans (Gonzalez-Nunez et al., 2013; Marron Fdez de Velasco et al., 2009; Taylor et al., 2017). However, in slight contrast to humans and rodents, the zebrafish genome encodes two TRPA1 genes: *trpa1a,* and *trpa1b* (which will be called zTRPA1a and zTRPA1b in this study) (Prober et al., 2008). To establish TRPA1 agonist-induced zebrafish hyperlocomotor activity as a drug screening tool, it is important to characterize the pharmacology of TRPA1 agonists and antagonists between these two paralogs.

We hypothesize that hyperlocomotion induced by the activation of zebrafish TRPA1 can serve as a phenotypic screen for novel anti-nociceptive drug discovery. To address our hypothesis, we investigated if locomotor behavior of zebrafish larvae adheres to TRPA1 channel pharmacology. We measured calcium influx of TRPA1 channels in HEK293 cells transiently expressing mouse TRPA1, zebrafish TRPA1a, or zebrafish TRPA1b in response to TRPA1 ligands. The mouse TRPA1 pharmacology in HEK293 cells and nocifensive behavior in mice were also examined upon TPRA1 activation to support the face validity of the zebrafish model. Finally, we evaluated dose-dependent changes of nocifensive swimming behavior in zebrafish larvae following the exposure to TRPA1 ligands.

4.2 Materials and methods

4.2.1 Animals

Zebrafish (*Danio rerio*): Wild-type zebrafish of the AB line were utilized for all behavioral experiments. Adult and larval zebrafish were maintained on a 14hr/10hr light/dark cycle. They were maintained and bred using standard procedure <https://zfin.org/zf_info/zfbook/zfbk.html>. Larval zebrafish were reared until 5 days post-fertilization (dpf) in E3 media <https://zfin.org/zf_info/zfbook/chapt1/1.3.html> in an incubator at 28°C. E3 media was changed daily, and healthy embryos were kept for experiments.

Mice (*Mus musculus*): We utilized WT C57BL/6 mice purchased from Envigo (Indianapolis, IN, USA). Total sixteen adult male mice (8-9 weeks, 22±2g) were housed in four ventilated Plexiglas cages (4 mice per cage). Four mice were tested in each group. It is noteworthy that some sex-differences to painful stimuli have been found in mice (Kwan et al., 2006). However, since the primary focus of this manuscript relates to zebrafish, which does not reach sexual maturity until 6-12 weeks post-fertilization (Parichy et al., 2009), we did not test female mice. Mice are maintained at temperature (21°C) in an animal housing facility accredited by the Association for Assessment and Accreditation of Laboratory Animal Care with a reversed 12-hour dark-light cycle (lights off at 1000, lights on at 2200). This study was carried out in accordance with the recommendations of the National Institutes of Health Guide for the Care and Use of Laboratory Animals. The protocol (#1201000592 by Y.F.L. for Zebrafish, and #1605001408 by R.M.vR for mice) was approved by the Purdue University Institutional Animal Care and Use Committee.

4.2.2 Cell culture

HEK293 cells (#CRL-1573, ATCC, VA, USA) were cultured in DMEM media (#11995-065, Sigma-Aldrich, MO, USA) with 10 % Fetal Bovine Serum (#F0926-500ML, Thermo Fisher, MA, USA). The cells were maintained in a 37°C incubator with consistent 5% CO_2. They were seeded in a clear 6 well flat bottom cell culture plates (#07-200-83, Corning ®, Thermo Fisher) with 500,000 cells/2 ml/well for transfection, in serum-free Opti-MEM (#31985070, Gibco®, Thermo Fisher). These cells were transfected with pcDNA3.1-mTRPA1 (#MR227099, OriGene, MD, USA), pcDNA3.1-zTRPA1a, or pcDNA3.1-zTRPA1b (a gift from Dr. David Prober) using X-tremeGENE^{TM} 9 (#6365809001, Sigma-Aldrich). After 24 hours, the transfected cells were

dislodged with trypsin, resuspended in Opti-MEM, and seeded 25,000 cells/25 µl/well in 384-well black polystyrene microplates (#82051-296, VWR, PA, USA) for testing calcium signaling the following day. Experiments were carried out with the approval of the Institutional Biohazard Committee (#13-013-16).

4.2.3 FLIPR calcium signaling assay

Twenty-five µl calcium sensitive Fluorescent Imaging Plate Reader (FLIPR) Calcium 6 assay dye (#R8190, Molecular Devices, CA, USA) was added to each well of a 384-well plate containing HEK293 cells transiently expressing mTRPA1, zTRPA1a, and zTRPA1b, respectively. The cells were incubated for an hour prior to the recording of intracellular calcium levels in a FlexStation3 Multi-Mode Microplate Reader (#R8190, Molecular Devices) as previously described (van Rijn et al., 2013). All compounds were diluted in calcium buffer made with 1x HBSS (#14025-092, Thermo Fisher), 20 mM HEPES (#15630-080, Thermo Fisher), and 2.5 mM Probenecid (#P8761, Sigma-Aldrich). For agonist studies, ASP7663 (#5178, Tocris, Bristol, UK) was diluted in 1 % DMSO-containing calcium buffer at desired concentrations and was added during the recording. The TRPA1 antagonists HC-030031 (#2896, Tocris), TCS-5861528 (#3938, Tocris), and A-967079 (#4716, Tocris) were diluted in calcium buffer, and 5 µl of 10x solutions were added 10 minutes prior to the recording. The same amount of DMSO (1%) was added to all control groups to maintain similar DMSO levels with the experimental groups. During the assay, the cells were challenged by a 5x ASP7663 solution or 1% DMSO solution at the 20 seconds time point, and both solutions were diluted in calcium buffer. Relative fluorescence units (RFU) were measured for 120 seconds period by the Flexstation. Area under the curve (AUC) was further evaluated from individual calcium influx data (**Figures 4.1 and 4.2**) to plot does-response curve of antagonists. For each specific antagonist concentration we plotted Log(dose ratio-1) against the antagonist concentration in a Schild plot. The dose ratio (A'/A) equals the EC_{50} of the agonist (ASP7665) in the presence of a concentration of the antagonist (A') divided by the EC_{50} of the agonist in the absence of antagonist (A). The x-intercept of the Schild plot was used to identify the antagonist-receptor affinity (pA_2).

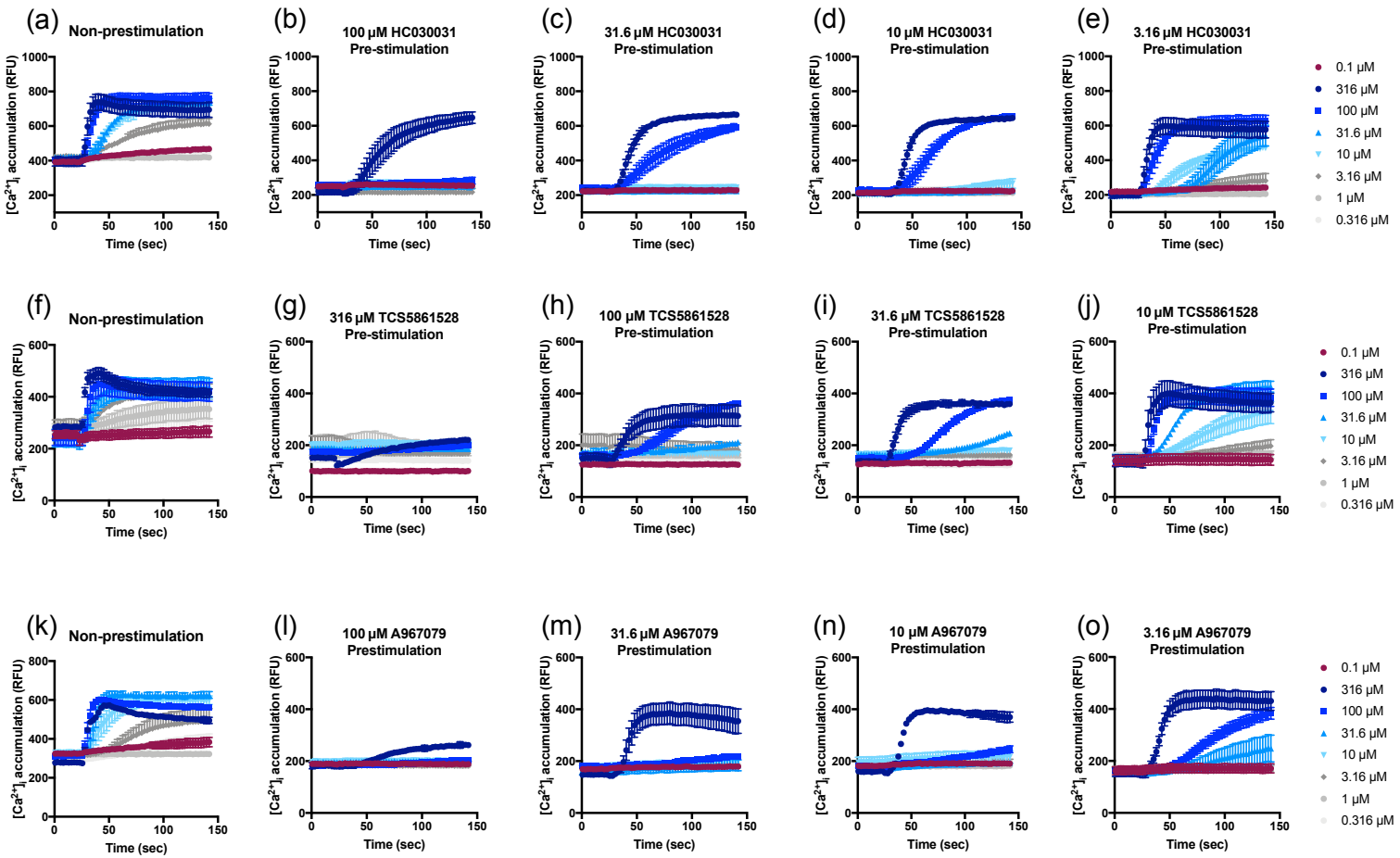

Figure 4.1 Calcium influx to TRPA1 antagonists in HEK293 cells transiently expressing mTRPA1

(a, f, k) Intracellular calcium levels of HEK293 cells transiently expressing mTRPA1 to ASP7663 with half-log dilutions. **(b-e)** ASP7663 dose-response calcium influx to HC-030031 with half-log dilutions. **(g-j)** ASP7663 dose-response calcium influx to TCS5861528 with half-log dilutions. **(l-o)** ASP7663 dose-response calcium influx to A967079 with half-log dilutions. The AUC of the RFU was further analyzed in Figure 4.3.

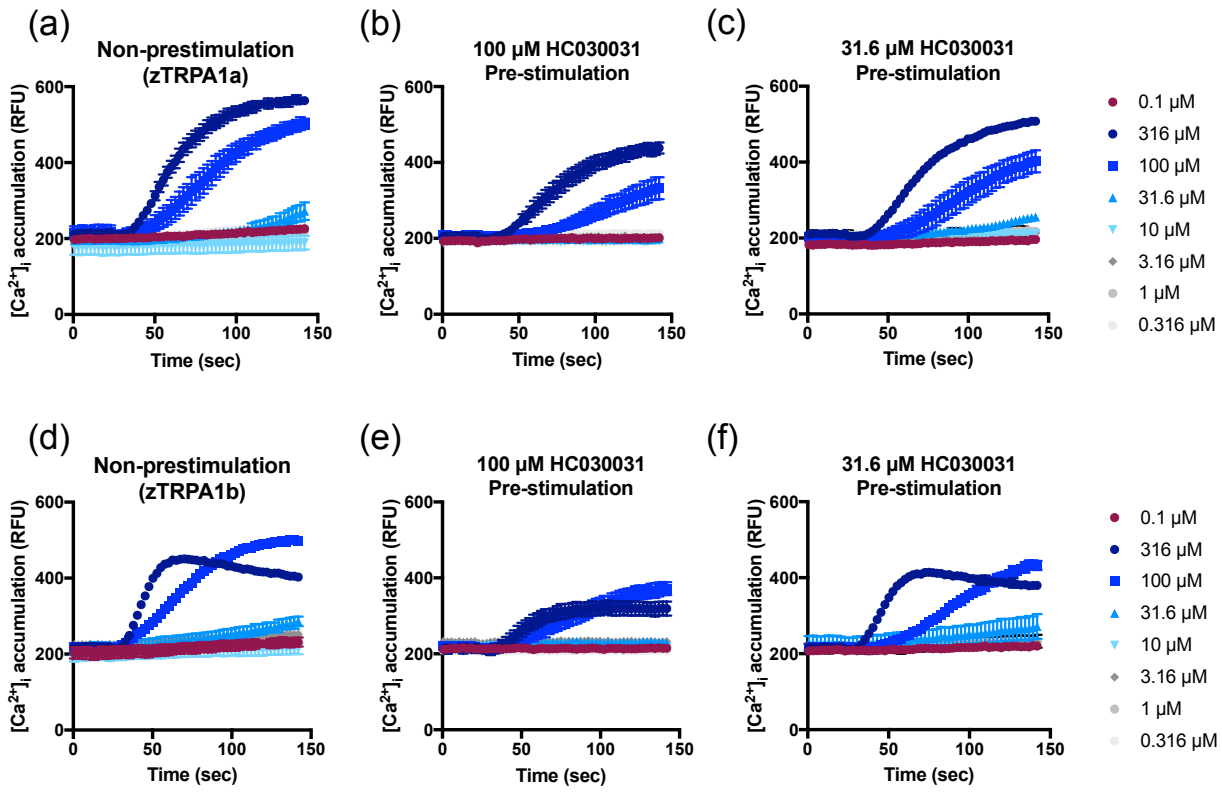

Figure 4.2 Calcium influx to HC-030031 in HEK293 cells transiently expressing zTRPA1a and zTRPA1b

(a, b) Intracellular calcium levels of HEK293 cells transiently expressing zTRPA1a and zTRPA1b respectively to ASP7663 with half-log dilutions. **(b,c)** ASP7663 dose-response calcium influx in zTRPA1a to HC-030031 with a full-log dilution. **(e,f)** ASP7663 dose-response calcium influx in zTRPA1b to HC-030031 with a full-log dilution. The AUC of the RFU was further analyzed in Figure 4.5.

4.2.4 Von Frey Test

Von Frey filaments (2.44 (0.04g) - 4.31 (2g)) and a grid platform (#58011 and #57816, Stoelting, WI, USA) were used to test mechanical hypersensitivity of mice. A modified up-and-down method was utilized as previously described (van Rijn et al., 2012). Immediately after measuring the baseline, the mice were injected with 100 mg/kg HC-030031 (p.o., diluted in 5 % DMSO, 0.5 % methylcellulose in saline), whereas the control group mice were injected with the appropriate vehicle solution (5 % DMSO, 0.5 % methylcellulose in saline). Thirty minutes after the first injection, mice were systemically administered 1 mg/kg ASP7663 (i.p., diluted in 1 % DMSO in saline), or vehicle (1 % DMSO in saline). Drug-induced mechanical hypersensitivity was measured 30 minutes after the second injection. Pre- and post-drug responses were represented as mean ± SEM.

4.2.5 Zebrafish Locomotor Tracking Assay

In the behavioral experiments, one 5 dpf zebrafish was placed in 250 µL of fish media per well of a 96-well plate (UNIPLATE Collection and Analysis Microplate, 96-Well 7701-1651). For each experimental condition, a group of 8 larvae (1 column) was used. Larvae were acclimated to the wells for 300 seconds after which an 8-channel pipette was used to simultaneously dispense 250 µL of 2x concentration of the TRPA1 agonist ASP7663 in fish media into each well. Locomotor activity was subsequently tracked and quantified (as distance travelled) for 300 additional seconds utilizing the Zebrabox system from ViewPoint Behavior Technology (Civrieux, France). For TRPA1 antagonist testing, larvae in the 96-well plate were pretreated with 1x concentration of antagonist in 250 µL E3 media for 20 minutes. Then, 250 µL of 2x TRPA1 agonist was added directly to this solution, and the resulting behavior was recorded as described above.

4.2.6 Statistics

All data are presented as means ± standard error of the mean (SEM). For our *in vitro* statistical analysis, area under curve (AUC) of calcium relative fluorescence units (RFU) was measured to plot dose-response curves, which were further analyzed by nonlinear regression analysis. Mean RFU of the first 10 seconds was used as a baseline of the AUC. EC_{50} values of the dose-response curves were further used to plot Schild curves, and the curves were analyzed with linear regression analysis. For the mice von Frey test, mechanical thresholds were analyzed with two-way ANOVA

followed by a Bonferonni test for multiple comparison analysis. For the zebrafish behavior test, the data from the first five seconds following drug administration were excluded, as zebrafish displacement during that period was highly influenced by liquid dispensing. AUC of all curves were measured and analyzed by one-way ANOVA. The post-hoc analysis was conducted with the Tukey's or Dunnett's multiple comparisons unless it stated otherwise. A value of y=0 in the graph was used as a baseline of the AUC. For our time-course average displacement graph, we used 2nd degree polynomial smoothing for a better representation; however, we used data before smoothing for all statistical analysis and quantification. All *in vitro* and *in vivo* data were evaluated using GraphPad Prism 7 (GraphPad Software, La Jolla, CA) unless it stated otherwise.

4.3 Results

4.3.1 Two TRPA1 agonists have similar potency but different kinetics to mouse TRPA1

To test previously known TRPA1 channel agonists, we analyzed dose-response curves of ASP7663 and AITC in mouse TRPA1 (mTRPA1)-transfected HEK293 cells. The potency of the two agonists were measured based on AUC of individual calcium accumulation in **Figure 4.3 b and c**. Based on the dose-response curve analysis, AITC and ASP7663 displayed similar potency at mTRPA1 (**Figure 4.3 a**, ASP7663: pEC_{50} = 5.16 ± 0.16, 6.8 μM, n=8; AITC: pEC_{50}=5.24 ± 0.3, 5.8 μM, n=5; unpaired t-test *p*=0.8106). The recorded potency for ASP7663 is ~10-fold weaker than previously reported in a similar FLIPR-based calcium assay (Kojima et al., 2014). Interestingly, we noticed that at 316 μM ASP7663 produced a more persistent calcium influx compared to AITC up to 120 seconds (Dark blue line, **Figure 4.3 b and c**). The calcium influx around 40-50 seconds was particularly decreased upon application of AITC in mTRPA1 (**Figure 4.3 c**). Furthermore, we have also found that ASP7663 could elicit calcium responses in non-transfected HEK293 cells with ASP7663. The potency for this unknown off-target effect was pEC_{50} = 4.27 ± 0.03 (54.1 μM n=3), and thus a log unit lower than the TRPA1 response (**Figure 4.4**). The off-target calcium response also appeared to have slower kinetics similar to AITC (Compare **Figure 4.3 c** with **Figure 4.4 b**).

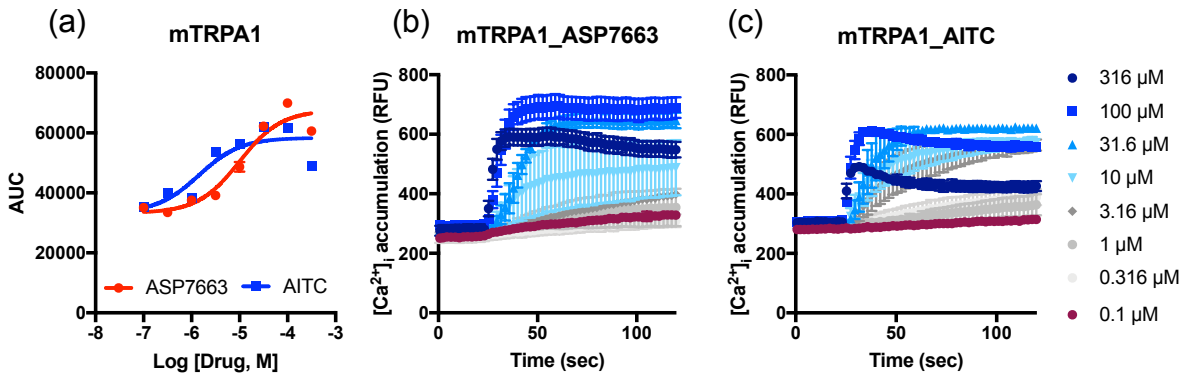

Figure 4.3 Potency of TRPA1 agonists (ASP7663 and AITC) in mTRPA1-transfected HEK293 cells.

(a) Dose-response curve of ASP7663 and AITC in mTRPA1-transfected HEK293 cells. (b,c) RFU of ASP7663 and AITC was measured to plot the dose response calcium influx in (a).

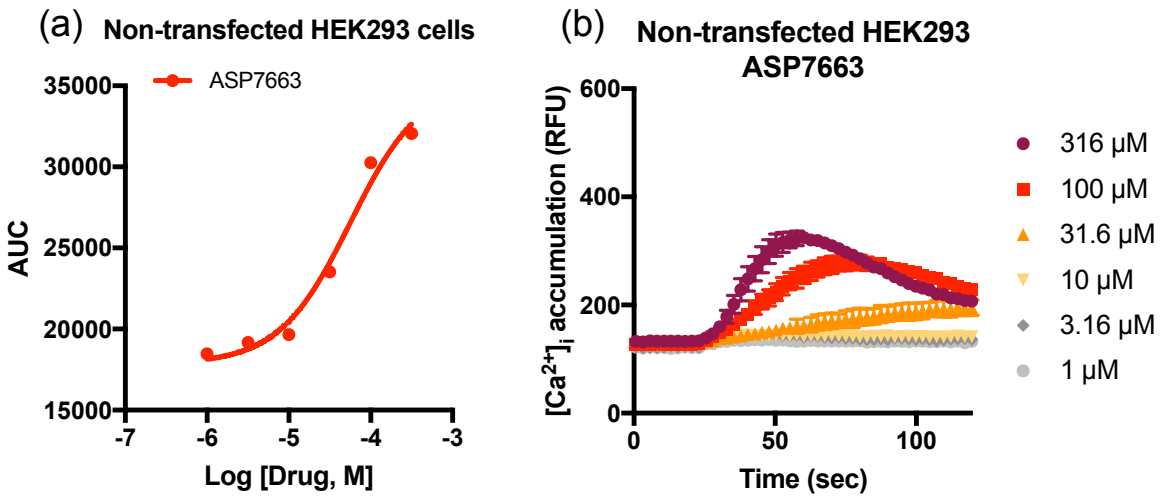

Figure 4.4 Potential off-target effect of ASP7663 in non-transfected HEK293 cells

(a) Dose-response curve of ASP7663 in non-transfected HEK293 cells (ASP7663: pEC50 = 4.57 ± 0.29, n=3). RFU of ASP7663 dose response calcium influx in non-transfected HEK293 (b). (a) was measured by AUC of the RFU.

4.3.2 TRPA1 antagonists inhibit ASP7663-induced calcium influx to mTRPA1

The majority of TRPA1 studies use AITC to activate TRPA1 channels. However, given the unique kinetics observed in **Figure 4.3 c** and its potential ability to activate other TRP channels (Gees et al., 2013; Janssens et al., 2016), we decided to use the TRPA1 agonists ASP7663, which is supposedly more selective (Kojima et al., 2014). First, we chose to assess the ability of the TRPA1 agonist ASP7663 and the TRPA1 antagonists HC-030031, TCS-5861528, and A-967076 to induce or prevent calcium mobilization, respectively. HEK293 cells transiently expressing mTRPA1 channels were exposed to the TRPA1 agonist ASP7663 and intracellular calcium levels were fluorescently measured using the FLIPR-based calcium assay. The TRPA1 antagonists, HC-030031 and TCS-5861528, which are structurally very similar, shifted the ASP7663 dose-response curve towards the right in a dose-dependent manner (**Figure 4.5 a and b**). The pA_2 of HC-030031 was 5.65 ± 0.2 (2.2 µM, n=4, **Figure 4.5 d**), and the pA_2 of TCS-5861528 was 5.34 ± 0.2 (4.6 µM, n=4, **Figure 4.5 e**), indicating similar antagonist-channel affinities. A-967076 also shifted the ASP7663 dose-response curve towards the right (**Figure 4.5 c**), and the pA2 of A-967076 was 7.0 ± 0.3 (0.09 µM, n=3, **Figure 4.5 f**). We found that HC-030031 and TCS-5861528 exhibit lower antagonist-channel affinities than A-967076 (One-way ANOVA, $F_{2,10}$=12.52, p=0.0019, HC-030031 vs. A-967076 p=0.0094, TCS-5861528 vs. A-967076 p=0.0024 with Tukey's multiple comparison). Individual calcium traces for ASP7663 in the presence of the antagonists are presented in **Figure 4.1**. We did not observe any calcium influx with HC-030031 in non-transfected HEK293 cells (**Figure 4.6 a and b**) or an off-target effect in mTPRA1-transfected HEK293 cells (**Figure 4.6 c and d**). These results validate the use of ASP7663 to activate mTRPA1 to induce a calcium response and confirm the affinity of the TRPA1 antagonists for mTPRA1.

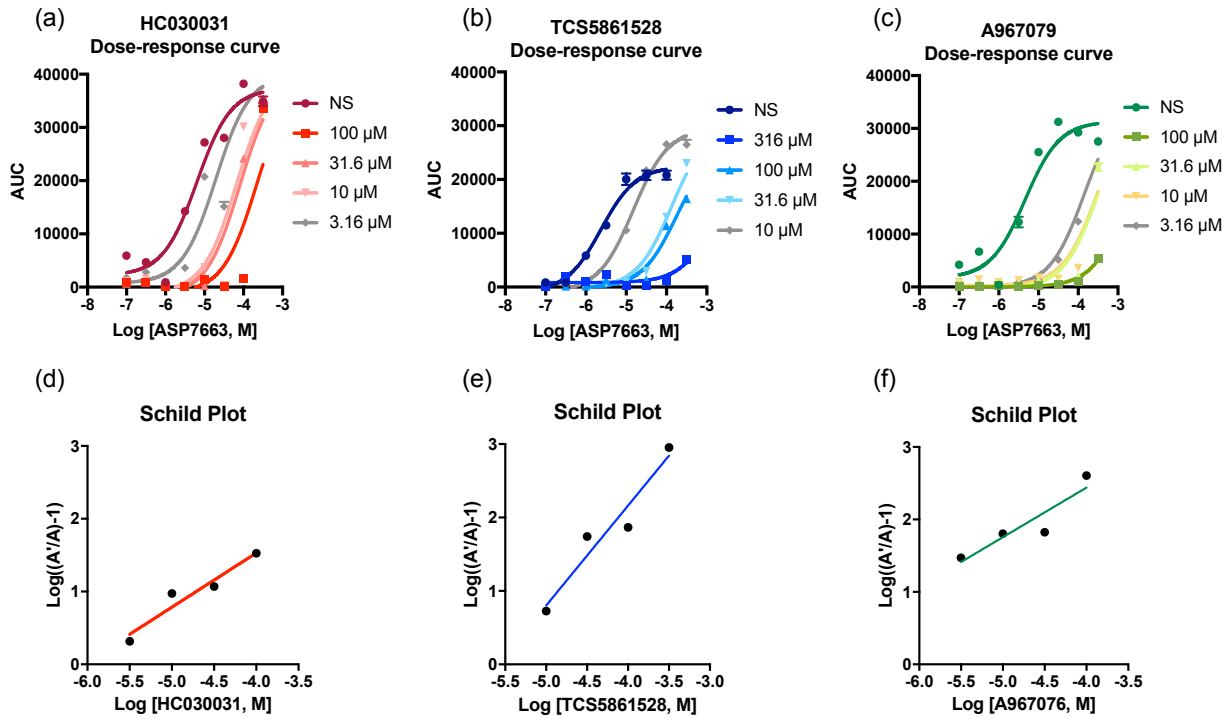

Figure 4.5 TRPA1 antagonists dose-dependently attenuate ASP7663-mediated TRPA1 calcium influx in mTRPA1-transfected HEK293 cells

(a–c) Representative dose-response curve of TRPA1 agonist ASP7663 in the absence or presence of three TRPA1 antagonists, HC-030031, TCS-5861528, and A-907076. Note the shift in the dose response curve of ASP7663 towards the right with increasing concentration of the antagonist. (d–f) Schild plot for the three TRPA1 antagonists HC-030031, TCS-5861528, and A-967076. Representative curves are shown.

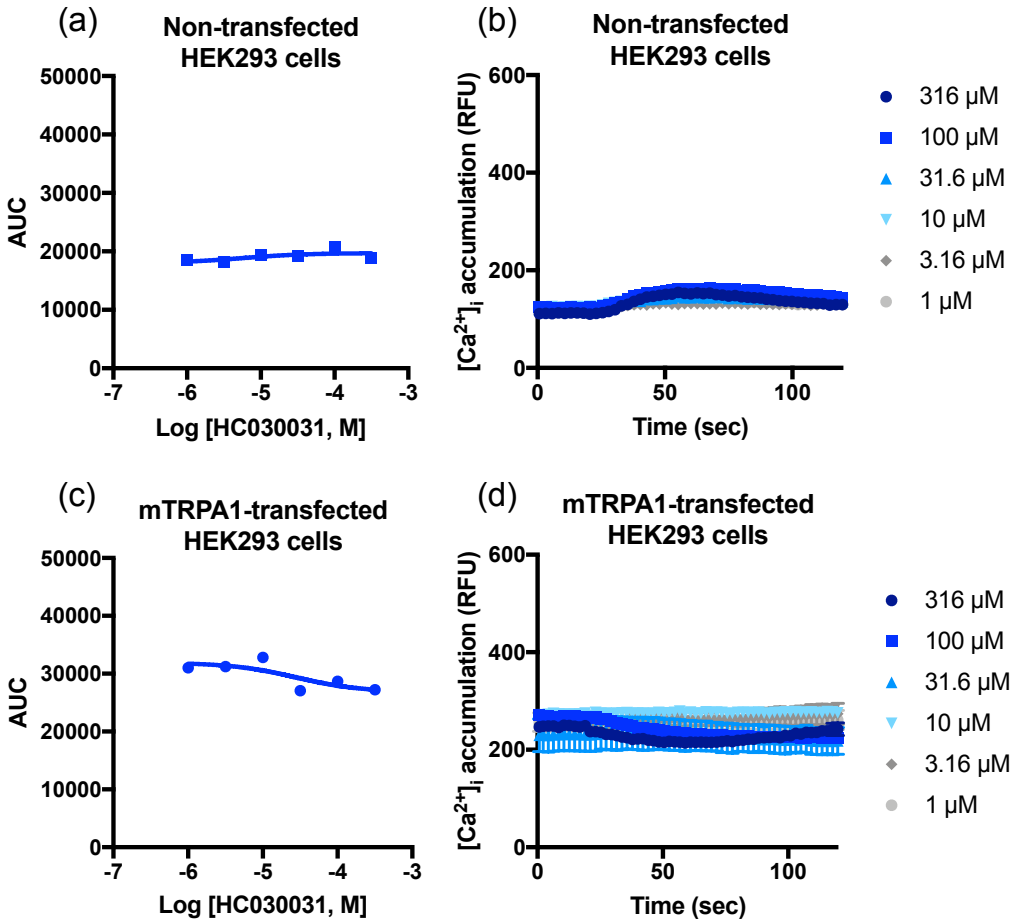

Figure 4.6 Calcium influx to HC-030031 in non-transfected or mTRPA1 transfected HEK293 cells

Dose response intracellular calcium levels of HC030031 in non-transfected HEK293 cells **(a)** and mTRPA1-transfected HEK293 cells **(c).** RFU of HC030031 dose response calcium influx in non-transfected HEK293 **(b, d)**. (a, c) were measured by AUC of the RFU. (mTRPA1: pIC50 = 5.77 ± 0.21, n=4).

4.3.3 HC-030031 blocked ASP7663-induced mechanical hypersensitivity in mice

Having confirmed that the TRPA1 compounds are functional *in vitro*, we next determined whether TRPA1 activation using ASP7663 would result in a painful response and whether this effect would be blocked by a TRPA1 antagonist in C57BL/6 mice. Intraperitoneal administration of a previously determined effective dose of ASP7663 (1 mg/kg) significantly decreased mechanical thresholds of von Frey filaments as evaluated by two-way ANOVA, (**Figure 4.7**, Effect of pre-drug x post-drug: $F_{1,18}$=1.522, p=0.2332; Group effects: $F_{2,18}$=4.426, p=0.0273). Bonferroni's multiple comparison further indicated statistical significance between pre- and post-drug mechanical thresholds in the mice administered with ASP7663 (p=0.0034), suggesting that ASP7663 administration increased mechanical sensation and nocifensive behavior. Based on a previous study (Kojima et al., 2014), we used an oral administered dose of HC-030031 (100 mg/kg) to block the ASP7663-mediated mechanical hypersensitivity (p>0.99). Bonferroni's multiple comparison did not show a statistical significance between pre- and post-drug mechanical thresholds in the mice administered vehicle (p=0.8692 after unpaired t-test, **Figure 4.8**) or HC-030031 (p=0.97 after Bonferroni multiple comparison, **Figure 4.7**).

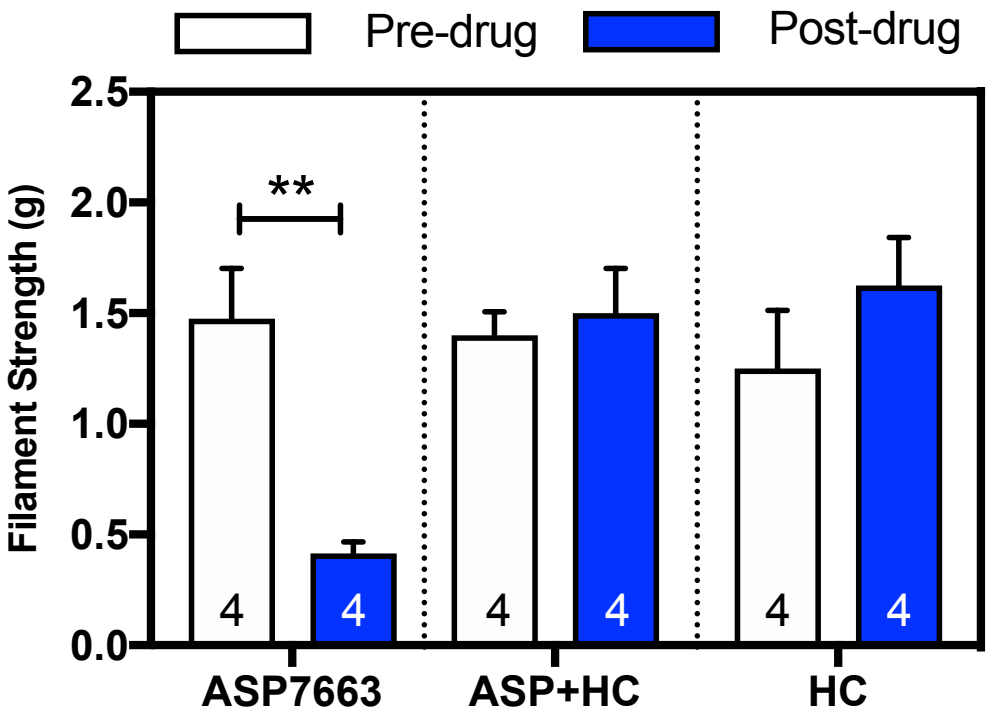

Figure 4.7 HC-030031 blocked ASP7663-induced mechanical hypersensitivity in C57BL/6 mice

Mechanical sensitivity was measured in C57BL/6 mice pre- and post-drug administration (n = 4 per treatment) in response to von Frey filament stimulation. Systemic administration of HC-030031 (100 mg/kg, p.o.) blocked mechanical hypersensitivity induced by ASP7663 (1 mg/kg, i.p.). (Two-way ANOVA, Effect of pre-drug x post-drug: $F_{1,18} = 1.522$, $p = 0.2332$; Group effects: $F_{2,18} = 4.426$, $p = 0.0273$; After Bonferroni's multiple comparison, Pre-ASP7663 vs. Post-ASP7663: *$p = 0.0034$).

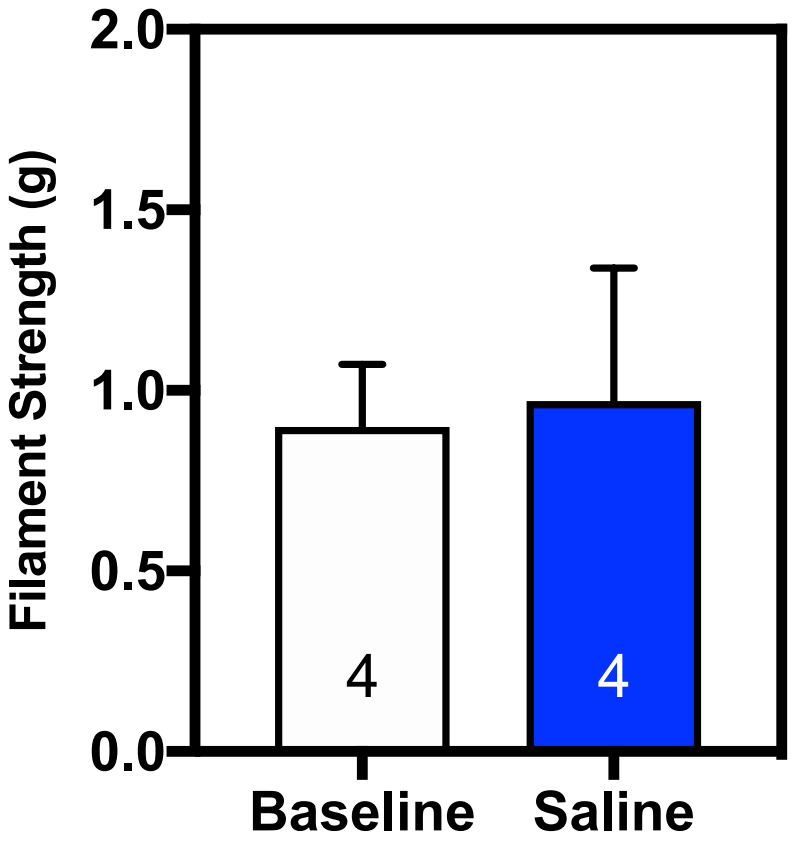

Figure 4.8 Mechanical hypersensitivity was not changed by saline injection in C57BL/6 mice

Mechanical sensitivity was measured in C57BL/6 mice pre- and post-saline administration (n=4 per treatment) in response to von Frey filament stimulation. (Unpaired t-test, p=0.8692).

4.3.4 ASP7663 and AITC have similar potency to two zebrafish TRPA1 paralogs but lower potency than mTRPA1

We also analyzed dose-response curves of ASP7663 and AITC in zebrafish TRPA1a (zTRPA1a), or zebrafish TRPA1b (zTRPA1b)-transfected HEK293 cells. Dose-response curve of the two agonists (**Figure 4.9 a and d**) was plotted based on the area under the curve (AUC) of individual calcium accumulation in **Figure 4.9 b, c, e and f**. In line with our previous observation in mTRPA1, ASP7663 and AITC displayed similar potency to zTRPA1a (**Figure 4.9 a**, ASP7663: pEC_{50}= 3.9 ± 0.18, 118 µM, n=7; AITC: EC_{50}=4.6 ± 0.4, 26.6 µM, n=4; unpaired t test p=0.1333) and zTRPA1b (**Figure 4.9 d**, ASP7663: EC_{50}= 4.0 ± 0.15, 99 µM, n=7; AITC: EC_{50}=4.5 ± 0.5, 35.4 µM, n=4; unpaired t test p=0.2855). Similar slow kinetics with mTRPA1 to 316 µM AITC was observed especially in zTRPA1b (**Figure 4.9 f**). Overall, the ASP7663 potency at zTPRA1 paralogs was significantly lower than at mTRPA1 (One-way ANOVA, $F_{2,19}$=18.72, p<0.0001, mTRPA1 vs. zTRPA1a p<0.0001, mTRPA1 vs. zTRPA1b p=0.0002) but no statistical significance to AITC was observed (One-way ANOVA, $F_{2,10}$=1.226, p=0.3341, mTRPA1 vs. zTRPA1a p=0.4770, mTRPA1 vs. zTRPA1b p=0.3625). However, we did not find any significant potency difference for the TRPA1 agonists between zTRPA1 paralogs (ASP7663: zTRPA1a vs. zTRPA1b p=0.9466, AITC: zTRPA1a vs. zTRPA1b p=0.9749).

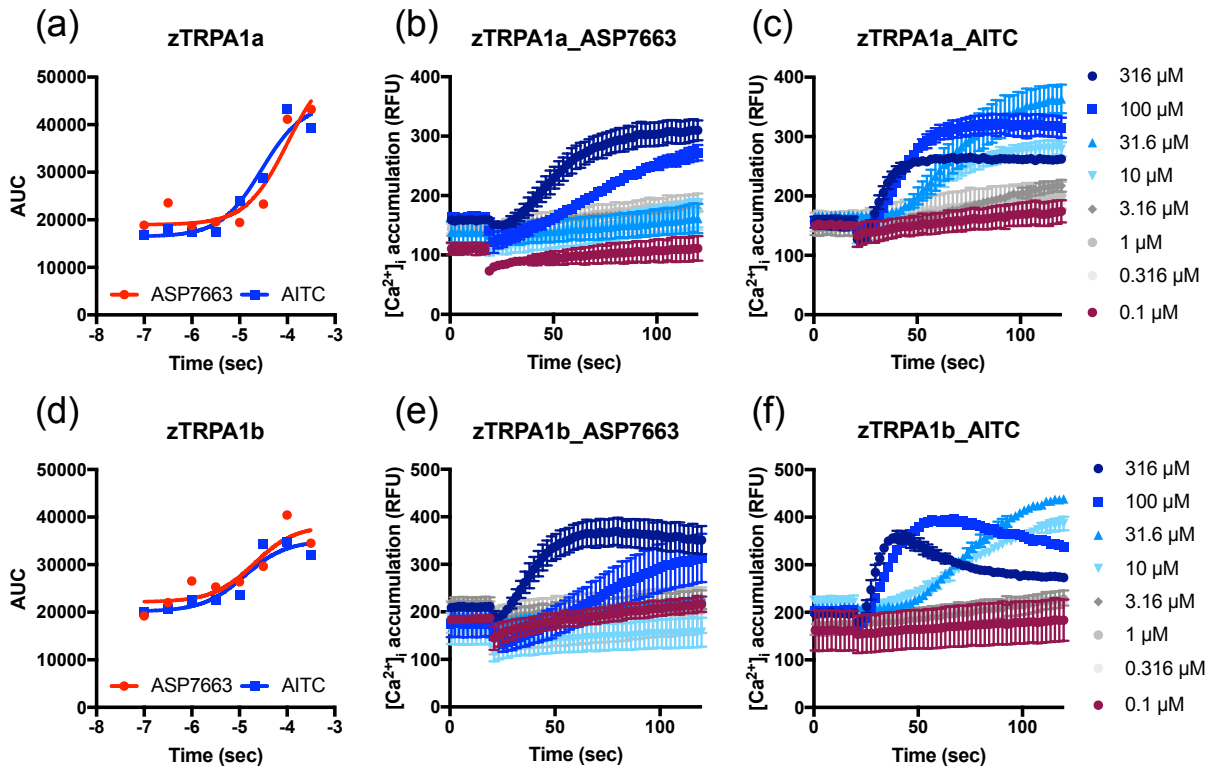

Figure 4.9 Potency of ASP7663 and AITC in HEK293 cells transfected with zTRPA1a or zTRPA1b.

Dose-response curve of ASP7663 and AITC in zTRPA1a-transfected (a), and zTRPA1b-transfected (d) HEK293 cells. The dose response calcium influx in zTRPA1a-transfected (b,c), and zTRPA1b-transfected (e,f) HEK293 cells was measured by RFU of ASP7663 and AITC

4.3.5 HC-030031 inhibited ASP7663-induced calcium influx of zebrafish TRPA1a and TRPA1b in a dose-dependent manner

After establishing that ASP7663 is a pain-inducing agonist whose effects can be blocked by the TRPA1 antagonist HC-030031, our next step was to pharmacologically characterize these two compounds at the two zebrafish TRPA1 paralogs in transfected HEK 293 cells as we had done for the mTRPA1. Despite the presence of an off-target effect for ASP7663 in non-transfected HEK293 cells (**Figure 4.4**), HC-030031 was able to inhibit ASP7663-mediated calcium influx in HEK293 cells transfected with zTRPA1a (pA_2=4.6 ± 0.2, 26.8 μM, n=3, **Figure 4.10 a and c**) or with zTRPA1b (pA_2=4.6 ± 0.3, 27.1 μM, n=3, **Figure 4.10 b and d**, individual calcium traces of the dose-response curves are presented in **Figure 4.2**). As for the zTRPA1, we noticed that 316 μM HC-030031 could produce an influx of intracellular calcium (**Figure 4.11**) in transfected, but not un-transfected cells. Our results suggest that the potency of ASP7663 and efficacy of HC030031 are similar between two zTRPA1 paralogs and that at high concentrations HC-030031 may activate TRPA1.

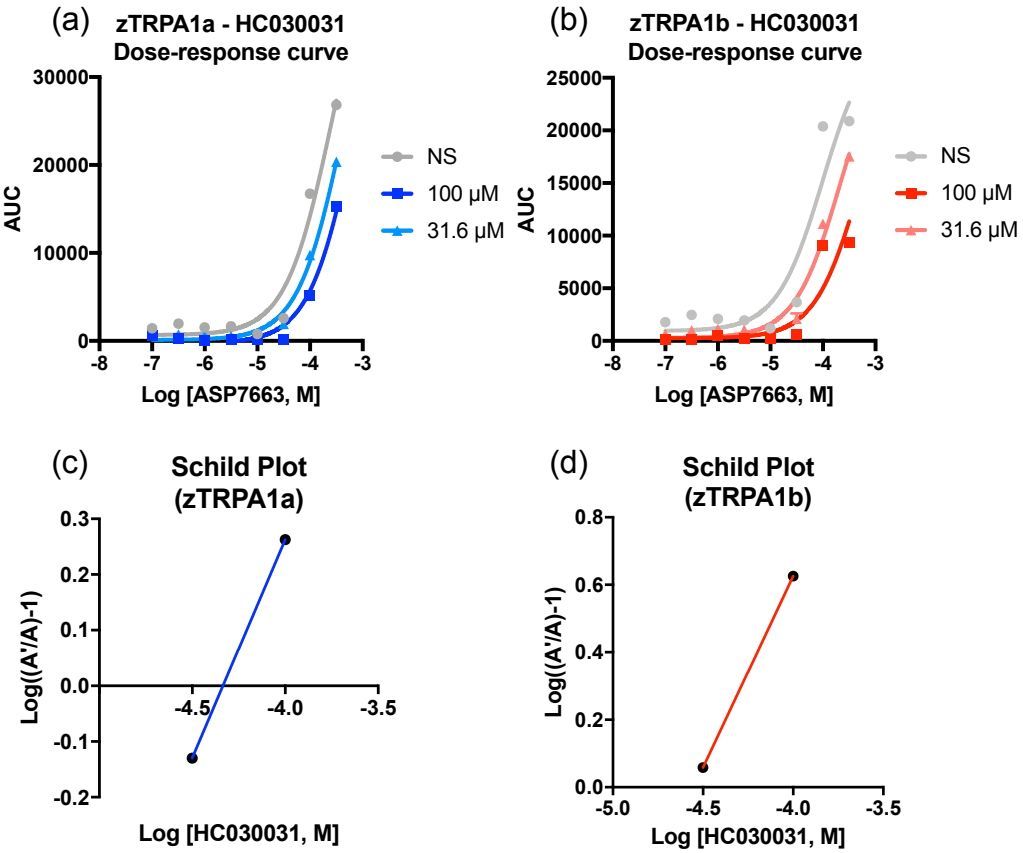

Figure 4.10 HC-030031 dose-dependently attenuates ASP7663 activation of zTRPA1a and zTRPA1b in transfected HEK293 cells.

(a, b) Dose-response curve of TRPA1 agonist ASP7663 in the absence or presence of HC-030031. Note the shift in the dose-response curve of ASP7663 towards the right with increasing concentration of the antagonist. **(c,d)** Schild plot for the HC-030031 at zTRPA1a and zTRPA1b. Representative curves are shown.

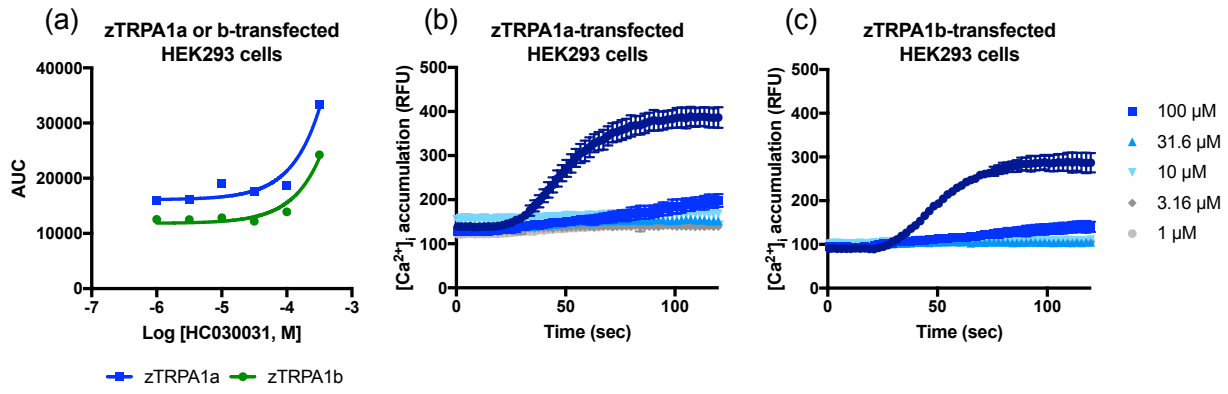

Figure 4.11 HC030031 works as weak agonist at high concentration.

(a) Dose-response curve of HC030031 in zTRPA1a-transfected (Blue), and zTRPA1b-transfected (Green) HEK293 cells (zTRPA1a: pEC50 = 4.9 ± 0.6, n=3; zTRPA1b: Non-determinant, n=3). Relative Fluorescent Unit (RFU) of HC030031 dose response calcium influx in zTRPA1a-transfected (b), and zTRPA1b-transfected (c) HEK293 cells. (a) was measured by area under the curve (AUC) of the RFU.

4.3.6 TRPA1 agonist-induced nociceptive-like swimming behavior in 5 days post-fertilization (dpf) zebrafish larvae

With the acquired knowledge that ASP7663 and HC-030031 pharmacology show little differences between the zTRPA1 paralogs, we next determined whether we could elicit a TRPA1-mediated behavioral response in zebrafish larvae using TRPA1 agonists. We selected 5 dpf zebrafish larvae as they display a repertoire of locomotor behaviors and are easily detected by motion tracking software (Ganzen et al., 2017; Kalueff et al., 2013). Additionally, at this age zebrafish will express both TRPA1 paralogs, as previous studies by Prober *et al.* showed that during development zebrafish expressed TRPA1a as early as 72 hours post-fertilization (hpf) and TRPA1b as early as 30 hpf (Prober et al., 2008). Larvae were exposed to two TRPA1 agonists, AITC (100 μM) and ASP7663 (100 μM), and the swimming behavior was tracked. Increased locomotor activity in zebrafish larva in response to TRPA1 agonists including AITC (mustard oil), acrolein and 4-hydroxynonenal may be interpreted as a nocifensive-like escape behavior in response to a noxious stimulus (Prober et al., 2008). AITC elicited an acute and rapid swimming behavior immediately upon treatment (**Figure 4.12 a and b**; One-way ANOVA, $F_{2, 5} = 491$ $p<0.0001$; E3 vs. ASP7663 $p<0.0001$; E3 vs. AITC $p<0.01$; ASP7663 vs. AITC $p<0.0001$ with Tukey's multiple comparison). In contrast to AITC, ASP7663 induced a slower and more sustained swimming behavior. To determine the dose-dependency of the ASP7663 behavior, larvae were exposed to three additional half-log dilutions of ASP7663 and AUC was analyzed based on the displacement (locomotion) graph (**Figure 4.12 c and d**; One-way ANOVA, $F_{4, 10} = 697$, $p<0.0001$, E3 vs. 3.16 μM $p<0.0001$, E3 vs. 10 μM $p<0.0001$, E3 vs. 31.6 μM $p=0.429$, E3 vs. 100 μM $p<0.0001$, 3.16 μM vs. 10 μM $p<0.05$, 3.16 μM vs. 31.6 μM $p<0.0001$, 3.16 μM vs. 100 μM $p<0.0001$, 10 μM vs. 31.6 μM $p<0.0001$, 10 μM vs. 100 μM $p<0.0001$, 31.6 μM vs. 100 μM $p<0.0001$ with Tukey's multiple comparison). Surprisingly, we observed what appears to be a dose dependent depression of locomotor activity at low ASP7663, which reverses to hyperlocomotor activity around 10 μM to 31.6 μM.

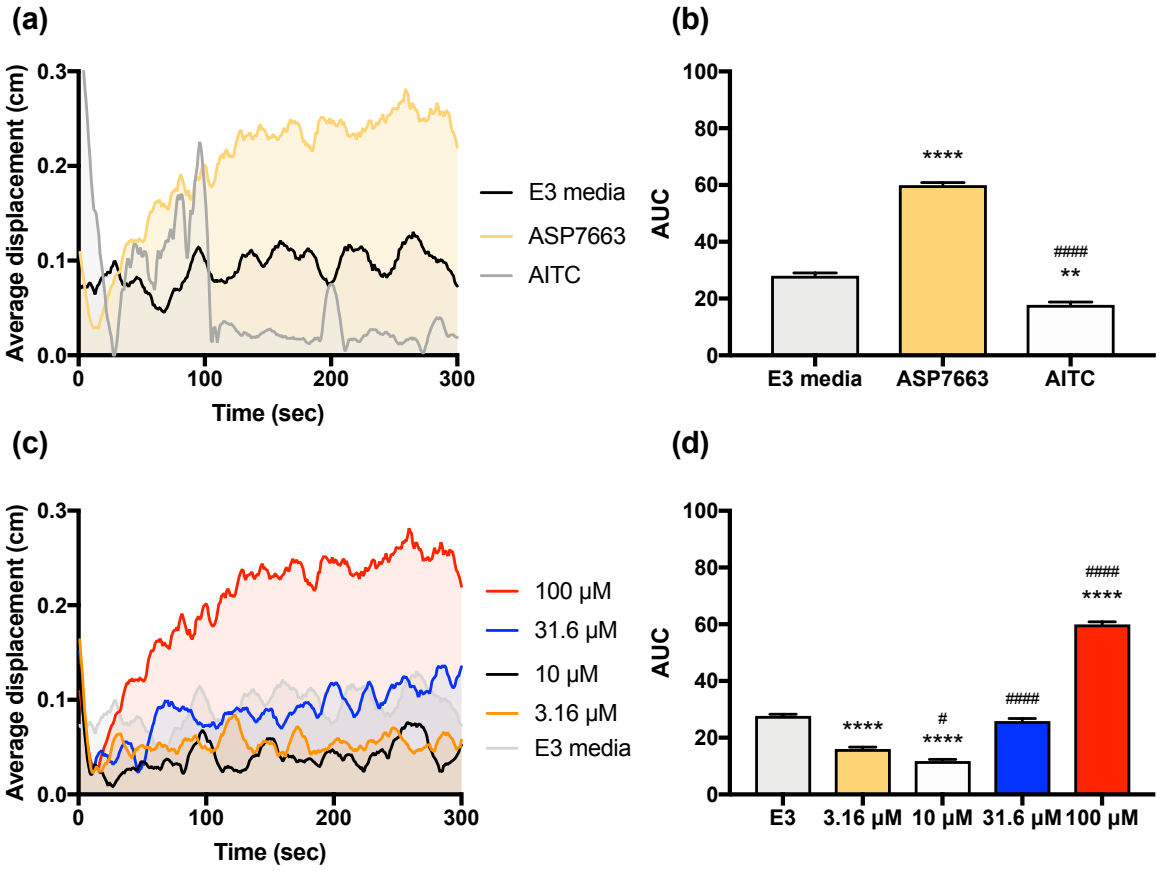

Figure 4.12 Increased locomotor response of zebrafish larvae to TRPA1 agonists.

(a) Displacement graph of average zebrafish locomotion in response to 100 µM ASP7663, 100 µM AITC or E3 media. Zebrafish larvae at 5dpf are exposed to the TRPA1 agonist at 0 sec. Solid line indicates average distance travelled of 3 biological replicates (n = 8 larvae for each replicate, (a)). Area under the curve was further analyzed in **(b). (c)** Displacement graph of average zebrafish locomotion in response to four series half-log dilutions of TRPA1 agonist ASP7663 and E3 media. Zebrafish larvae at 5 dpf are exposed to the TRPA1 agonist at 0 sec. Solid line indicates average distance travelled of 3 biological replicates (n = 8 larvae for each replicate). **(d)** Area under the curve was further quantified from graph (c). ((b) One-way ANOVA, $F_{2, 5} = 491$ $p<0.0001$; E3 vs. ASP7663 ****$p<0.0001$; E3 vs. AITC **$p<0.01$; ASP7663 vs. AITC ##$p<0.01$ after Tukey's multiple comparison). ((d) One-way ANOVA, $F_{2, 6} = 385.1$, $p<0.0001$; E3 vs. 10 µM: ****$p<0.0001$; E3 vs. 3.16 µM: ****$p<0.0001$; E3 vs. 100 µM: ****$p<0.0001$; 3.16 µM vs. 10 µM: #$p<0.05$; 3.16 µM vs. 31.6 µM: ####$p<0.0001$; 3.16 µM vs. 100 µM: ####$p<0.0001$ after Tukey's post-hoc comparison). Data produced by Logan Ganzen and Emre Koskun.

4.3.7 TRPA1 antagonist pretreatment prevented TRPA1-mediated nocifensive-like locomotor behavior in zebrafish

We next assessed if a TRPA1 antagonist could block the ASP7663-induced nocifensive-like behavior in the zebrafish model. Pre-incubation with HC-30031 (10 μM) significantly (ASP7663 vs. ASP+HC, $p<0.0001$) inhibited the nocifensive locomotor behavior mediated by ASP7663 (100 μM) administration (**Figure 4.13 a and b**; One-way ANOVA, $F_{3, 8} = 214.3$, $p<0.0001$, E3 vs. ASP $p<0.0001$, E3 vs. ASP+HC $p<0.01$, E3 vs. HC $p<0.0001$, ASP vs. ASP+HC $p<0.0001$, ASP vs. HC $p<0.000$, ASP+HC vs. HC $p=0.0012$ after Sidak's multiple comparison). Position tracking of the locomotor behavior of a single representative larva 5 minutes after experimental treatment is further illustrated in **Figure 4.13 c**. In the traces, black lines indicate a swimming velocity below 0.6 cm/sec, green lines indicate a swimming velocity between 0.6cm/sec and 1.0cm/sec, and red lines indicate a swimming velocity exceeding 1.0 cm/sec. To control for any behavior the antagonists may cause in the zebrafish larvae, we tested zebrafish behavior upon exposure to 10 μM HC-030031 alone. This exposure increased swimming behavior over baseline (E3 vs. HC-030031 $p<0.0001$). Even though this single treatment of HC-030031 enhanced the swimming behavior, its pre-treatment inhibited TRPA1-induced nocifensive swimming behavior.

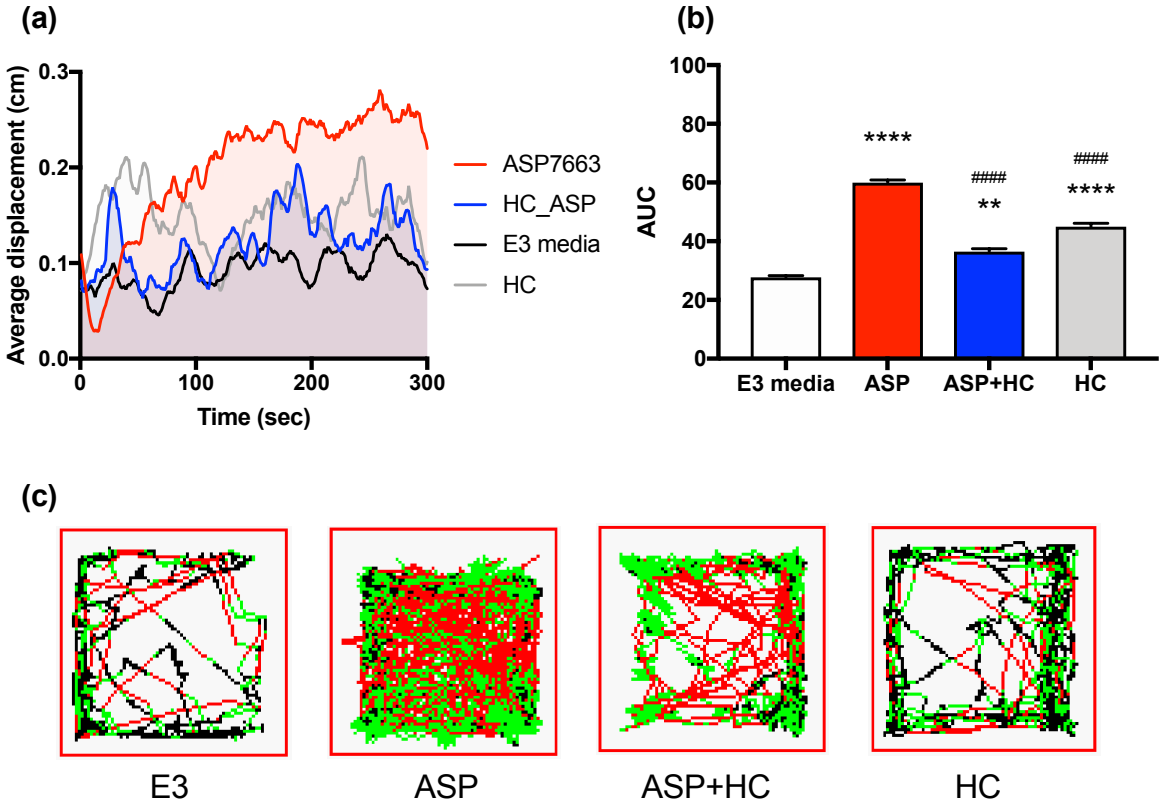

Figure 4.13 Locomotor response of zebrafish larvae to ASP7663 in presence or absence of HC-030031.

(a) To determine if TRPA1 antagonists can block ASP7663-mediated channel stimulation, zebrafish were pre-treated with antagonists 10 μM HC-030031 for 20 minutes before challenged with ASP7663. HC-030031 application was able to block ASP7663-mediated locomotor behavior. Solid line indicates average distance travelled of 3 biological replicates (n = 8 larvae for each replicate). (b) Area under the curve was further quantified from graph (a). (c) Representative displacement graph of (a,b). In the traces, black lines indicate a swimming velocity below 0.6 cm/sec, green lines indicate a swimming velocity between 0.6 cm/sec and 1.0 cm/sec, and red lines indicate a swimming velocity exceeding 1.0 cm/sec. ((b) One-way ANOVA, F3, 8 = 214.3, $p < 0.0001$; E3 vs. ASP: ****$p < 0.0001$; E3 vs. ASP + HC: ** $p < 0.01$; E3 vs. HC: ****$p < 0.0001$; ASP vs. ASP + HC: ####$p < 0.0001$; ASP vs. HC ####$p < 0.000$; ASP + HC vs. HC &&$p = 0.0012$ after Sidak's multiple comparison). Data produced by Logan Ganzen and Emre Koskun.

4.4 Discussion

Although TRPA1 channels are being considered as a novel target for the development of new chronic pain treatments (Moran et al., 2011), there currently are no U.S. Food and Drug Administration approved TRPA1 ligands. Therefore, it is imperative to better characterize TRPA1 pharmacology across different animal species to facilitate drug development and translation of anti-nociceptive TRPA1 drugs for clinical use. Preclinical rodent models are one of the most popular vertebrate models used in drug discovery. One of the biggest hurdles in drug development is showing *in vivo* efficacy. Generally, rodents are used for *in vivo* validation once a lead compound has been generated. Unsurprisingly, much of the physiological and behavioral effects of TRPA1 channels thus far have been established in rodents (Gerlai, 2010; Petrus et al., 2007). Only the best-hit compounds identified in cellular screening assays are moved forward for *in vivo* validation because it would be prohibitive to utilize rodent models to phenotypically screen hundreds of novel anti-nociceptive hits due to the time and cost required for rodent studies. The ability to screen drugs in a 96-well plate format using zebrafish larvae highlights the strength of zebrafish as an alternative *in vivo* model for drug discovery. Utilizing zebrafish models has various benefits in the field of drug discovery by providing large phenotype-based screening with its rapid embryonic development (Zon & Peterson, 2005). Various behavioral assays of zebrafish have been established for novel drug developments, including for retinal degeneration for example (Ganzen et al., 2017). Zebrafish can also be used to investigate nociceptive-like phenotypes (S. Chen et al., 2016; Taylor et al., 2017) as well as analgesic effects of drugs (Curtright et al., 2015). A study by Prober *et al.* showed that TRPA1-mediated locomotion can be utilized as distinct characteristic for the nocifensive behavior in zebrafish (Prober et al., 2008). In this study, we presented a detailed *in vitro* and *in vivo* pharmacological characterization of mouse and zebrafish TRPA1 using selective agonists and antagonists. Specifically, we demonstrated that activation of TRPA1 increased locomotor behavior of zebrafish in a dose-dependent manner, which was blocked by the TRPA1 antagonist/partial agonist HC-030031. This finding was in line with the ability of HC-030031 to inhibit ASP7663-mediated mechanical sensitivity in mice.

In comparison to mouse TRPA1, zebrafish has two TRPA1 paralogs due to genome duplication, which may have distinct pharmacology and anatomy. Although one study has reported that the zTRAP1a has higher sensitivity to chemical irritant such as AITC than zTRPA1b (Oda et

al., 2016), our study strongly indicates that the zTRPA1 paralogs acted similarly *in vitro*, as we observed similar potencies for ASP7663 and affinities for HC-030031 at both zTRPA1 paralogs. However, *in vivo*, zTRPA1a expression is limited to the posterior vagal sensory ganglia while zTRPA1b is expressed in all cranial ganglia (Prober et al., 2008), which may preclude exogenous agonists from reaching zTRPA1a. Additionally, knockout studies of zTRPA1b reveal loss of sensitivity to the agonist AITC (Esancy et al., 2018; Prober et al., 2008), indicating that zTRPA1b is solely responsible for the locomotor behavior.

For the zTRPA1 paralogs, we particularly found that maximal response of ASP7663 was reduced in response to increasing doses of HC-030031 (**Figure 4.10**) while also shifting the EC_{50} values of ASP7663. This finding suggests that HC-030031 may interact with the zTRPA1 paralogs as a competitive or negative allosteric modulator. The Schild slopes for HC-030031 at the zTRPA1 paralogs were lower than 1 (zTRPA1a: 0.84 ± 0.22, n=3, zTRPA1b: 0.83 ± 0.05, n=2), which is a textbook definition of competitive interaction (Colquhoun, 2007). The limitation of the low potency of ASP7663 at the zTRPA1 paralogs is exemplified by our ability to test only two doses of HC-030031 to draw the Schild plot, where it is recommended to test five different antagonist concentrations. Having only two concentration data points limits our ability to definitively calculate pA2 values for the antagonist and determine the slope. This is in line with a potential limitation of using ASP7663 in zebrafish given that the potency of ASP7663 and affinity for HC-030031 was lower at the zTRPA1 paralogs in comparison to mTRPA1. Discovery or development of a stronger TRPA1-selective agonist, such as crotalphine (Bressan et al., 2016), could be beneficial in replacing ASP7663 for future screening efforts with a larger range of detection and will help provide better quality pA_2 calculation.

We further suggest that the observed hyperlocomotion in zebrafish is TRPA1-mediated. First, TRPA1-mediated hyperlocomotion has been previously reported by others (Prober et al., 2008; Stevens et al., 2018). Second, both AITC, although briefly, and ASP7663 produce hyperlocomotion, and both agonists increase calcium signaling *in vitro* via TRPA1. Third, ASP7663-induced hyperlocomotion was attenuated by administration of HC-030031. Fourth, HC-030031 increases calcium release in HEK293 cells at a high concentration, and a high dose of HC-030031 *in vivo* produces significant hyperlocomotion albeit weaker than ASP7663 (**Figure 4.13 b**). An unexpected observation, however, was that at low doses (3.16 and 10 μM) ASP7663 induced hypolocomotion in zebrafish (**Figure 4.12 c and d**), but hyperlocomotor activity at higher

concentration (31.6 and 100 μM). We currently do not have an explanation for the hypolocomotion, but this may be a potent off-target effect in zebrafish (**Figure 4.4**) that is masked by hyperlocomotion once TRPA1 is activated. Furthermore, our observation that the TRPA1 antagonist HC-030031 may have some partial agonistic effects is novel.

The nocifensive behavior in zebrafish was initially demonstrated using mustard oil (Eilers et al., 2010), which contains the TRPA1 agonist AITC. AITC has been shown to also activate TRPM8 (Janssens et al., 2016) and TRPV1 (Gees et al., 2013), and thus it would be suboptimal to use this agonist to screen for TRPA1-selective antagonists. However, given the fact that zebrafish lack TRPM8 channels (S. Chen et al., 2016), selectivity may be less of a concern in this species. A different concern is that AITC activation of TRPA1 channel has been shown to lead to rapid TRPA1 desensitization and internalization (Akopian et al., 2007; Kistner et al., 2016; Raisinghani et al., 2011), a feature we observe also in the calcium assay for this agonist (**Figure 4.9 f**, see particularly at 316 μM) and in zebrafish (see **Figure 4.12 a** at 100 seconds AITC). In our hands, AITC has similar potency with the TRPA1-selective agonist ASP7663, but we found no indication of rapid desensitization for ASP7663. The lack of rapid desensitization by ASP7663 was a reason for us to choose this agonist to investigate the pharmacological profiles of mouse and zebrafish TRPA1 channels in both *in vivo* model systems. The *in vitro* desensitization profile of AITC may correlate with its *in vivo* profile, where a short initial bout of AITC-induced hyperlocomotion is followed by a rapid decline in locomotor activity. In contrast, application of ASP7663 in zebrafish larvae showed more prolonged agonist-mediated locomotor behavior than AITC (**Figure 4.10 a and b**). At the high concentration of HC-030031 at which we observe calcium influx, the kinetic profile resembles that of ASP7663 and similarly HC-030031 produces a moderate but persistent increase in locomotor activity, suggesting that HC-030031 does not rapidly desensitize zTRPA1.

The TRPA1 agonist ASP7663 also produced mechanical hypersensitivity in mice (**Figure 4.7**), a widely used nociception model, and was blocked by the TRPA1 antagonist HC-030031. This finding mimics our observations using the same agonist and antagonist in zebrafish locomotor behavior (**Figures 4.12 and 4.13**). A study by Stevens *et al.* previously found that HC-030031 was able to inhibit locomotor responses in zebrafish larvae induced by the TRPA1 agonist acrolein (Stevens et al., 2018) and further support the face validity of the zebrafish model.

In addition to the finding that ASP7663-induced nocifensive-like behavior, we found similarities in ASP7663-mediated calcium influx from both zebrafish and mouse TRPA1 channels.

In mTRPA1, ASP7663 dose-dependently induced calcium signaling, and TRPA1 antagonists attenuated this influx. Of the three antagonists, HC-030031 and TCS-5861528 had lower antagonist-channel affinities compared to A-967076 (**Figure 4.5**). This is in agreement with published characterization of A-967076 interaction with rat TRPA1 in which the antagonist has an IC_{50} of 0.289 μM, and A-967076 was found to be about 25-fold stronger than HC-030031 (Chen et al., 2011).

We also noted some off-target effects in our HEK293 cells; specifically, ASP7663 showed calcium influx at high concentration (316 μM) in non-transfected HEK293 cells. It is possible that the agonist may interact with endogenous calcium channels in HEK293 cells (Bugaj et al., 2005). Nonetheless, it is important to note that the potency of ASP7663 was much lower in non-transfected HEK293 compared with HEK293 transfected with mTRPA1 and we were able to block the intracellular calcium release using TRPA1 antagonists for both the mTRPA1 and the zTRPA1 paralogs. The existence of an off-target effect, however, may explain why we did not obtain a perfect slope for the Schild plots for the TRPA1 antagonists.

Overall, our critical analysis of currently commercialized TRPA1 agonists and antagonists in mouse TRPA1 and the two zebrafish TRPA1 paralogs have found similarities in line with previous published observations particularly in agonist-mediated hyperalgesia in mice and hyperlocomotion in zebrafish. However, our study revealed several novel findings. First, the kinetics of calcium release and zebrafish hyperlocomotion were not identical between TRPA1 agonists. Second, both HEK293 cells and zebrafish may exhibit non-TRPA1 targets that respond to the TRPA1 agonist ASP7663. Third, the TRPA1 antagonist HC-030031 may activate TRPA1 *in vitro* and *in vivo* at high enough concentrations. Finally, the potency of TPRA1 agonists and antagonists appears to be stronger for mTRPA1 than the zTRPA1 paralogs. Taken together, we propose that TRPA1-mediated hyperlocomotion in zebrafish has the potential to be a useful phenotypic assay to for TRPA1 drug screening and discovery. As for all compound screening, secondary assays will still be required to assess channel-ligand pharmacology including receptor desensitization, potential off-target effects of a ligand, and an ability of a ligand to serve as an antagonist, partial agonist, or a full agonist.

CHAPTER 5. DISCUSSION

5.1 Cellular mechanisms of G protein signaling in synaptic transmission

Chapter 2 of the present thesis clearly suggests that δORs are capable of modulating emotional behaviors through their unique signaling pathways. My data suggests that this modulation is mediated by β-arrestin 2 for anxiety, and potentially by β-arrestin 1 for fear (**Figure 2.9**). This β-arrestin signaling is believed to be rather slow modulation (Shenoy et al., 2006), yet behavioral effects observed in Chapter 2 appeared to be engaged within 30 minutes of post-systemic administration of drugs. Then how is the behavior mediated by β-arrestin signaling? A potential mechanism by which β-arrestin mediates behaviors may be linked to β-arrestin-mediated ion channel modulation instead of solely through β-arrestin-scaffolded intracellular signaling pathways. In the discussion, I will expand on potential ways in which δOR signaling may modify ion channels, what is known about GPCR-mediated modulation of ion channels via G protein or β-arrestin, and finally preliminary data I have generated suggesting δORs-TRPA1 crosstalk (**Figure 5.1**), which does not relate to anxiety, but highlights potential mechanisms of δOR biased signaling and neuronal activity.

All three (μ, δ, κ) opioid receptors can interact with ion channels through their heterotrimetic G protein (see Chapter 1.2.1). Earlier hints of this came from observations on modulation of postsynaptic currents and intrinsic membrane conductance by opioid peptide (Grudt & Williams, 1995; Thompson et al., 1993). Specifically, those studies observed that activation of μORs modulates inhibitory postsynaptic current as well as potassium conductance of neurons respectively in the hippocampus and the spinal cord where μORs are heavily expressed (Grudt & Williams, 1995; Thompson et al., 1993). Many years later, it was shown that the change in potassium conductance was accomplished by the $G_{\beta\gamma}$-mediated activation of GIRKs following MOR stimulation (Ikeda et al., 2003).

Modulation of GIRK or Ca_v channels are relatively well-established mechanisms by which opioid receptors alter neuronal excitation. Yet, an alternative mechanism by which opioid receptors modulate neuronal excitation is to induce long-term potentiation (LTP) and long-term depression (LTD), a type of synaptic plasticity. Commonly, LTP is first produced by increased activation of postsynaptic N-methyl-D-aspartate (NMDA) receptors. Subsequent calcium influx

through NMDAR further results in activation of Ca^{2+}/calmodulin-dependent protein kinase II (CaMKII). Activated CaMKII initiates downstream signaling cascades that ultimately increase AMPA receptor synthesis and synaptic AMPA receptor expression (Herring & Nicoll, 2016). On the other hand, LTD is a reversal of LTD in that reduced activation of postsynaptic NMDA receptors triggers CaMKII phosphatase, calcineurin, and protein phosphatase 1, resulting in decreases in AMPA protein synthesis (Luscher & Malenka, 2012). Opioid receptors including μORs and δORs have been shown to induce LTP/LTD and alter synaptic plasticity (Bramham & Sarvey, 1996). This is well-exemplified by a study that demonstrated high frequency-induced LTP in the hippocampal pathways was inhibited by a μOR antagonist CTAP, and δOR antagonists BNTX and naltrindole (Bramham & Sarvey, 1996). Activation of δORs has been also involved in modulation of synaptic plasticity in the striatum (Jiang & North, 1992). Similar to the GIRK and Ca_v, these instances have been linked to G_i signaling, decrease in cAMP by G_i protein is thought to alter the phosphorylation status of glutamatergic receptors, GABA receptors, and Ca_v, and ultimately leading to changes in synaptic plasticity (Francois & Scherrer, 2018).

In the perspective of synaptic transmission, δORs have been shown to actively engage in vesicle release that can further affect synaptic plasticity. Bao *et al.* demonstrated that activation of δORs triggers Ca^{2+} release from IP_3-sensitive intracellular storages, which ultimately result in excitatory neuropeptide release in dorsal root ganglion neurons (Bao et al., 2003). Other GPCRs have been implicated in modulation of synaptic transmission, and thus to what degree this extends to other GPCRs would be worth investigating. In other G_i-coupled receptors, it has been suggested that $G_{\beta\gamma}$ can interact with synaptotagmin, a part of the presynaptic Soluble N-Ethylmaleimide-Sensitive Factor Attachment Protein Receptor (SNARE) complex and modulate vesicle release in the presynaptic terminals (Yoon et al., 2007). Yet, it is unclear if δORs are also adopting this mechanism of action, and further studies are required in order to understand underlying mechanisms by which δORs modulate synaptic transmission. More importantly, it would be crucial to investigate to what degree β-arrestin may contribute to modulation of ion channel activity and synaptic plasticity and I will discuss this in the following section.

5.2 Cellular mechanisms of β-arrestin signaling in synaptic transmission

The previous section provided examples of G protein-mediated modulation of synaptic transmission in the brain. In fact, GPCRs-mediated synaptic transmission is not restricted to G

protein complex, and accumulating evidence also suggests that β-arrestin signaling is involved in the modulation of synaptic transmission (Beaulieu et al., 2005). Studies presented in Chapter 2 clearly demonstrated therapeutic potentials of β-arrestin signaling in emotional behaviors. However, does β-arrestin signaling also mediate synaptic transmission for behavioral modulation as does G protein-mediated signaling? To answer this question on β-arrestin signaling in synaptic transmission, I will provide examples of how β-arrestin signaling modulate synaptic transmission in various GPCRs that are implicated in neurological disorders. Unfortunately, only few studies have investigated β-arrestin-mediated synaptic transmission at opioid receptors, and thus the present section will discuss various GPCRs that have shown β-arrestin-mediated synaptic transmission in the brain.

GPCRs, in particular, also have a profound role in the modulation of the LTPs in the brain (Betke et al., 2012), which leads to an open question if β-arrestin plays a role in the modulation of LTP. For the past decade, a series of studies have reported new roles of β-arrestin in NMDA receptor function at synaptic levels (G. Chen et al., 2016; Pontrello et al., 2012). NMDA receptors are located at excitatory glutamate synapses and involved in activity-dependent synaptic plasticity in the postsynaptic terminals. Although activation of NMDA receptor does not necessarily lead to LTP, NMDA receptors play a profound role in the induction of LTP (Malenka & Nicoll, 1993). A late phase of LTP involves gene transcription and new protein synthesis, and this process contributes to long-lasting memory formation (Malenka & Nicoll, 1999). One example is fear memories; the process of fear learning including acquisition and even extinction requires LTP in the amygdala as well as in the hippocampus (Johansen et al., 2011). Given the importance of NMDA receptors in LTP, it is worth exploring to what degree β-arrestin have been associated with NMDA receptors. Genetic studies of β-arrestin proteins have further implicated that β-arrestin signaling plays a critical role in NMDA receptor function (G. Chen et al., 2016; Mittal et al., 2017). These studies have revealed that the two isoforms have unique effects with β-arrestin 2 knockout mice exhibiting increased NMDA current in spinal lamina (G. Chen et al., 2016), and β-arrestin 1 knockout mice exhibiting decreased currents in nucleus accumbens (Mittal et al., 2017). Therefore, since δORs function are closely regulated by β-arrestin 1 and 2, it is certainly possible that β-arrestin modulation of NMDA receptor could be impacted by δOR-β-arrestin signaling. A study by Pontrello *et al.* has shown more detailed mechanisms by which NMDA receptors are modulated by β-arrestin 2 signaling (Pontrello et al., 2012). Upon activation of NMDA receptor in the

hippocampus, subsequent calcium signaling dephosphorylates downstream cofilin, which is required for dendrite remodeling. In this study, β-arrestin 2 plays a key role in transferring cofilin to the dendrite for remodeling, and dysregulated dendrite remodeling resulted in impaired LTD and spatial memory, suggesting that the mechanisms by which β-arrestin 2 modulate NMDA-mediated synaptic plasticity may be indirect (Pontrello et al., 2012).

Besides β-arrestin-mediated modulation of synaptic transmission through NMDA receptors, studies have also demonstrated that opioid receptors such as μORs and δORs can engage with TRP channels through β-arrestin proteins. As previously introduced in Chapter 1.2.2, a series of studies by Rowan *et al.* demonstrated that both μORs and δORs can interact with calcium-permeable TRPV1 channels in primary sensory neurons, and this crosstalk was mediated by β-arrestin 2 isoform (Rowan, Bierbower, et al., 2014; Rowan, Szteyn, et al., 2014). To further evaluate the crosstalk between δORs and another TRP channels, TRPA1 channels, which was implicated in modulating synaptic transmission in primary sensory neurons (Kosugi et al., 2007), a preliminary study presented in **Figure 5.1** further examined a crosstalk between δORs and TRPA1 channels in HEK293 cells transiently expressing δORs and TRPA1 channels and measured TRPA1 agonist, ASP7663, mediated calcium influx in presence or absence of δORs agonists (SNC80 and TAN67). In this preliminary study, a pre-stimulation of a strong β-arrestin recruiter, SNC80, potentiated the calcium influx mediated by ASP7663, compared to a weak β-arrestin recruiter, TAN67 (**Figure 5.1 a and b**). Furthermore, these effects were not observed in non-transfected HEK239 cells (**Figure 5.1 c**), indicating a role of β-arrestin in the crosstalk between TRPA1 and δORs. To further determine 1) detailed signaling pathways involved in the crosstalk between TRPA1 and δORs, 2) the effects of β-arrestin 1 or 2 in the crosstalk, and 3) neural mechanisms underlying the synaptic transmission mediated by TRPA1 channels, future experiments that incorporate pharmacological inhibitors of downstream signaling pathways, gene silencing technique for β-arrestin 1 or 2 isoform, and brain slice recording with distinct neural circuits would provide additional insights on underlaying mechanisms. Together with these insights, it is expected that the *in vivo* tools evaluated in Chapter 4 would be able to contribute to facilitating preclinical phase of drug developments that may potentially target the crosstalk between δORs and TRPA1 channels by phenotypically screening opioid ligands in a high-throughput manner.

Altogether, evidence clearly suggests that β-arrestin can modulate ion channel activity and through that impact neuronal excitability, which would be at a pace that might explain the

relatively fast behavioral responses observed with the β-arrestin preferring agonist, SNC80. It is important to note that the two β-arrestin isoforms differentially affect plasticity at synaptic levels, and thus further studies would be required to fully elucidate the unique role of two β-arrestin isoforms in distinct behavioral modulation.

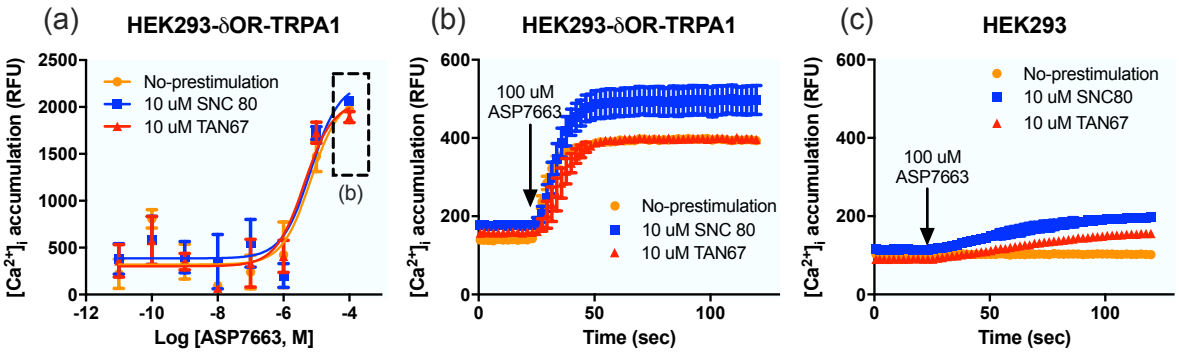

Figure 5.1 TRPA channel is modulated by activation of δORs via synthetic agonist, SNC80.

To evaluate crosstalk between TRPA1 channels and δORs, HEK293 cells were pre-stimulated with δORs agonists including SNC80 and TAN67 and calcium influx by TRPA1 channels were evaluated by FLIPR-based calcium assay. (a) EC50 curves of ASP7663 with pre-stimulation of SNC80, TAN67, assay buffer (indicated as no-prestimulation). (b) Time-course calcium influx upon activaiton of TRPA1 in HEK293 cells stably expressing δORs and TRPA1 channels with SNC80 or TAN67 pre-stimulation. (c) Time-course calcium influx upon activation of TRPA1 in non-transfected HEK293 cells with SNC80 or TAN67 pre-stimulation.

5.3 Spatiotemporal dynamics of ERK1/2 signaling by GPCRs

The present thesis is primarily focused on ERK1/2 signaling located in whole cells including cytoplasm and nucleus. Yet, given that increased nuclear translocation and activation of ERK1/2 is linked to gene transcription (Chambard et al., 2007), it would be crucial to discuss a potential implication of ERK1/2 in specific intracellular compartment. It is noteworthy that nuclear translocation of ERK1/2 can further impact the pathophysiology of various neurological disorders or behavioral changes, which include fear conditioning and spatial learning (Besnard et al., 2014), and long-term synaptic plasticity in the brain (Thomas & Huganir, 2004), drug addiction (Lu et al., 2006), anxiety-like and depressive-like behavior (Duman et al., 2007; Huang & Lin, 2006; Wefers et al., 2012). These examples further signify the importance of investigating the spatial profile of ERK1/2 activation and if this is correlated to distinct pathophysiological or behavioral phenotypes.

As previously mentioned in Chapter 1.3.1, activation of ERK1/2 is primarily mediated by either RTKs or two secondary effectors of GPCRs: G protein or β-arrestin (Lefkowitz & Shenoy, 2005). Accumulating studies have suggested that spatial (cytosol *vs.* nucleus) profile of ERK1/2 is associated with temporal (transient *vs.* persistent) profiles of ERK1/2. Ahn and colleagues first demonstrated that G protein mediates transient (~2-3 min) activation of ERK1/2 in the cytosols and nucleus in HEK293 cells expressing Angiotensin II receptor and β2-adrenergic receptors. Intriguingly, when G protein is ablated via pharmacological inhibitor, β-arrestin signaling promotes more persistent (~30 min) activation of ERK1/2 in the cytosols, suggesting differential temporal dynamics of ERK1/2 modulated by G protein and β-arrestin signaling (Ahn et al., 2004; Gesty-Palmer et al., 2006; Shenoy et al., 2006). However, further studies have implicated that the temporal dynamics heavily rely on cell and receptor types, in that studies suggested that β-arrestin can initiate a rapid and transient activation of ERK1/2 in HEK293 cells expressing vasopressin receptors (Ren et al., 2005), or sustained nuclear translocation of ERK1/2 in HEK293 cells expressing μ-opioid receptors (μOR) (Zheng et al., 2008). As previously described, ERK1/2 signaling is involved in a critical role in various behavioral modulation, and it is important to understand 'where' (spatial) and 'when' (temporal) ERK1/2 signaling is activated in distinct cellular context.

Despite the importance, investigating the spatiotemporal dynamics of ERK1/2 is challenging because: 1) spatiotemporal dynamics are highly cell and receptor type specific, and thus it requires studies in distinct receptor type in specific cellular context such as δORs expressing neuronal cell

lines, 2) a lack of in vivo tools to investigate real-time ERK1/2 activation in an organism makes it difficult to correlate the ERK1/2 activation profile with distinct pathophysiological or behavioral profile. Future studies that can identify correlation between real-time spatiotemporal dynamics of ERK1/2 and a unique disease status would provide great insights to the field.

5.4 Molecular mechanisms of ERK1/2 in synaptic plasticity and fear conditioning

Activation of ERK1/2 can affect various cellular functions ranging from cell differentiation to gene transcription. G protein and β-arrestin both activate ERK1/2 signaling, while it has been suggested that kinetics of β-arrestin-mediated ERK1/2 is much slower and persistent than G protein-mediated ERK1/2 (Shenoy et al., 2006). Not only have different temporal dynamics of ERK1/2 activation been observed, but different spatial locations of ERK1/2 activation have been suggested. As described in Chapter 5.3, studies have suggested that G protein activates ERK1/2 in the cytoplasm and nucleus, whereas β-arrestin activates ERK1/2 in the cytoplasm in HEK293 cells expressing Angiotensin II receptor and β2-adrenergic receptors (Ahn et al., 2004; Gesty-Palmer et al., 2006; Shenoy et al., 2006). The different spatiotemporal profiles make it plausible that the target of ERK1/2 may similarly differ. I will next discuss different downstream targets of ERK1/2 and different locations of activation, which may provide new hypotheses on how G-protein and β-arrestin may impact intracellular signaling pathways and subsequent gene transcription.

Earlier studies have found that ERK1/2 signaling is required for LTP in hippocampal and cortical neurons (Di Cristo et al., 2001; English & Sweatt, 1997). Upon postsynaptic calcium entry in neurons, CaMKII triggered by calcium entry stimulate AC (Impey et al., 1999). Subsequent production of cAMP can activate downstream Rap1 and Raf1 in series, which ultimately activates ERK1/2 (Impey et al., 1999). Activation of ERK1/2 can be critical in that nuclear translocation can further allow gene transcriptional potential protein synthesis required for LTP (Impey et al., 1999). Activation of transcriptional factors such as ETS transcription factor-1 (Elk-1) or cAMP response element-binding protein (CREB) has been implicated as a mechanism by which ERK1/2 mediates long-term synaptic plasticity (**Figure 1.5**) (S. Davis et al., 2000). Nuclear phosphorylation of Elk-1 by ERK1/2 activation can bind to serum response element (SRE) in the promoter regions of target genes including c-fos and immediate early genes (IEGs) (Besnard et al., 2011). An alternative pathway for ERK1/2 to indirectly modulate gene transcription is via downstream kinase such as ribosomal protein kinase (RSK) family. Upon activation of RSK by

ERK1/2, RSK translocate to the nucleus and further phosphorylate a downstream transcriptional factor, CREB (De Cesare et al., 1998; Ginty et al., 1994). Subsequent binding of CREB in CRE promotor region also mediates c-fos and other IEGs induction (West & Greenberg, 2011). Neuronal c-fos and IEGs encode critical neuronal functions including other transcriptional factors for protein synthesis, growth factors, metabolic enzymes, cytoskeletal proteins, and proteins required for plasticity, and thus provide critical roles in the overall mechanisms for synaptic plasticity (Lanahan & Worley, 1998). For instance, studies have also demonstrated that the c-fos and IEGs are required for NMDA-dependent synaptic plasticity (Fleischmann et al., 2003), spatial memory formation (Vann et al., 2000), contextual and cued fear conditioning memory retrieval (Hall et al., 2001), and contextual fear memory extinction (Mamiya et al., 2009). Although the present thesis did not cover the downstream targets of ERK1/2 in the perspective of emotional regulation, above accumulating studies clearly show the connection between ERK1/2 signaling in behaviors potentially through downstream gene transcription and subsequent neuronal/synaptic modulation. The present thesis, especially Chapter 2, clearly suggests that the two signaling pathways differentially modulate emotional behaviors. Furthermore, I have briefly discussed that differential molecular and cellular mechanisms of synaptic transmission and spatiotemporal activation of ERK1/2 by two distinct GPCR signaling pathways in previous sections. Thereby, it is possible that G protein- and β-arrestin-mediated pathways may differentially modulate behaviors through differential transcriptional modulation as well as subsequent synaptic transmission. Future studies with interdisciplinary approaches would be able to provide more insights on this topic.

5.5 Conclusion

Overall, the present thesis investigated signaling by membrane proteins (specifically δORs and TRPA1) in the perspective of anxiety, fear, and pain. In Chapter 2, I demonstrated that δORs are an interesting novel target for the development anti-anxiety therapeutics. A key finding was the importance of β-arrestin 2 signaling in the therapeutic efficacy of the anxiolytic drug. This stands in contrast with recent findings in the opioid field that promote G protein signaling for treating pain. Thus, my findings suggest that careful consideration should be given to using G protein-biased analgesics in patients with co-morbid mood disorders as it may be difficult to treat both disorders effectively with a signal biased opioid drug. The findings in Chapter 2 targeting δORs

also showed a beneficial role of β-arrestin signaling in mood regulation, but they are particularly intriguing in that two β-arrestin isoforms regulate different types of mood behaviors such as anxiety- and fear-related behaviors. This unique observation was also followed by distinct ERK1/2 activities in the brain. β-arrestin 1 increases ERK1/2 activation in the basal ganglia, whereas β-arrestin 2 increases ERK1/2 activation in the limbic regions of the brain. These results prompt further stratification of biased drugs into β-arrestin isoform-biased drugs to precisely treat a specific disorder. In addition to ERK1/2 activities by β-arrestin signaling, Chapter 3 briefly examined MAP kinase activities sensitive to various anesthetic methods. Given that many research paradigms heavily rely on anesthetic methods to record, monitor, and screen neural activities, the studies carry significance in providing guidelines towards robust and unbiased experimental design. Finally, the current thesis also discussed GPCR-mediated ion channel modulation. As described in Chapter 1.2, TRP channels, in particular, are attractive alternative targets for chronic pain syndrome in that they can crosstalk with various opioid receptors potentially through β-arrestin signaling of GPCRs. In Chapter 4, I provided further support for TRPA1 as a therapeutic target for chronic pain and helped develop a high-throughput screen in zebrafish to identify novel TRPA1 antagonists with analgesic efficacy. Moreover, I presented a first hint of novel opioid ligand crosstalk with TRPA1 channels. Whether this crosstalk is synergistic or antagonistic is still unclear, but it highlights the importance of providing in depth investigations of complex pharmacology of GPCRs and ion channel signaling transduction, as such insight would accelerate the development process of novel drugs that can treat pain and possible pain that is co-morbid with anxiety disorders.

REFERENCES

Adolphs, R., Tranel, D., Damasio, H., & Damasio, A. (1994, Dec 15). Impaired recognition of emotion in facial expressions following bilateral damage to the human amygdala. *Nature, 372*(6507), 669-672. https://doi.org/10.1038/372669a0

Ahn, S., Shenoy, S. K., Wei, H., & Lefkowitz, R. J. (2004, Aug 20). Differential kinetic and spatial patterns of beta-arrestin and G protein-mediated ERK activation by the angiotensin II receptor. *J Biol Chem, 279*(34), 35518-35525. https://doi.org/10.1074/jbc.M405878200

Akimova, E., Lanzenberger, R., & Kasper, S. (2009, Oct 1). The serotonin-1A receptor in anxiety disorders. *Biol Psychiatry, 66*(7), 627-635. https://doi.org/10.1016/j.biopsych.2009.03.012

Akopian, A. N., Ruparel, N. B., Jeske, N. A., & Hargreaves, K. M. (2007, Aug 15). Transient receptor potential TRPA1 channel desensitization in sensory neurons is agonist dependent and regulated by TRPV1-directed internalization. *J Physiol, 583*(Pt 1), 175-193. https://doi.org/10.1113/jphysiol.2007.133231

al Absi, M., & Rokke, P. D. (1991, Jul). Can anxiety help us tolerate pain? *Pain, 46*(1), 43-51. https://doi.org/10.1016/0304-3959(91)90032-s

Allen, J. A., Yost, J. M., Setola, V., Chen, X., Sassano, M. F., Chen, M., Peterson, S., Yadav, P. N., Huang, X. P., Feng, B., Jensen, N. H., Che, X., Bai, X., Frye, S. V., Wetsel, W. C., Caron, M. G., Javitch, J. A., Roth, B. L., & Jin, J. (2011, Nov 8). Discovery of beta-arrestin-biased dopamine D2 ligands for probing signal transduction pathways essential for antipsychotic efficacy. *Proc Natl Acad Sci U S A, 108*(45), 18488-18493. https://doi.org/10.1073/pnas.1104807108

Altay, O., Suzuki, H., Hasegawa, Y., Ostrowski, R. P., Tang, J., & Zhang, J. H. (2014, Feb). Isoflurane on brain inflammation. *Neurobiol Dis, 62*, 365-371. https://doi.org/10.1016/j.nbd.2013.09.016

Anchan, D., Clark, S., Pollard, K., & Vasudevan, N. (2014, Jan). GPR30 activation decreases anxiety in the open field test but not in the elevated plus maze test in female mice. *Brain Behav, 4*(1), 51-59. https://doi.org/10.1002/brb3.197

Arenas, O. M., Zaharieva, E. E., Para, A., Vasquez-Doorman, C., Petersen, C. P., & Gallio, M. (2017, Dec). Activation of planarian TRPA1 by reactive oxygen species reveals a conserved mechanism for animal nociception. *Nat Neurosci, 20*(12), 1686-1693. https://doi.org/10.1038/s41593-017-0005-0

Atkins, C. M., Selcher, J. C., Petraitis, J. J., Trzaskos, J. M., & Sweatt, J. D. (1998, Nov). The MAPK cascade is required for mammalian associative learning. *Nat Neurosci, 1*(7), 602-609. https://doi.org/10.1038/2836

Attramadal, H., Arriza, J. L., Aoki, C., Dawson, T. M., Codina, J., Kwatra, M. M., Snyder, S. H., Caron, M. G., & Lefkowitz, R. J. (1992, Sep 5). Beta-arrestin2, a novel member of the arrestin/beta-arrestin gene family. *J Biol Chem, 267*(25), 17882-17890. https://www.ncbi.nlm.nih.gov/pubmed/1517224

Austin Zamarripa, C., Edwards, S. R., Qureshi, H. N., Yi, J. N., Blough, B. E., & Freeman, K. B. (2018, Nov 1). The G-protein biased mu-opioid agonist, TRV130, produces reinforcing and antinociceptive effects that are comparable to oxycodone in rats. *Drug Alcohol Depend, 192*, 158-162. https://doi.org/10.1016/j.drugalcdep.2018.08.002

Bannerman, D. M., Rawlins, J. N., McHugh, S. B., Deacon, R. M., Yee, B. K., Bast, T., Zhang, W. N., Pothuizen, H. H., & Feldon, J. (2004, May). Regional dissociations within the hippocampus--memory and anxiety. *Neurosci Biobehav Rev, 28*(3), 273-283. https://doi.org/10.1016/j.neubiorev.2004.03.004

Bao, L., Jin, S. X., Zhang, C., Wang, L. H., Xu, Z. Z., Zhang, F. X., Wang, L. C., Ning, F. S., Cai, H. J., Guan, J. S., Xiao, H. S., Xu, Z. Q., He, C., Hokfelt, T., Zhou, Z., & Zhang, X. (2003, Jan 9). Activation of delta opioid receptors induces receptor insertion and neuropeptide secretion. *Neuron, 37*(1), 121-133. https://doi.org/10.1016/s0896-6273(02)01103-0

Barrenha, G. D., & Chester, J. A. (2007, Jul). Genetic correlation between innate alcohol preference and fear-potentiated startle in selected mouse lines. *Alcohol Clin Exp Res, 31*(7), 1081-1088. https://doi.org/10.1111/j.1530-0277.2007.00396.x

Basbaum, A. I., Bautista, D. M., Scherrer, G., & Julius, D. (2009, Oct 16). Cellular and molecular mechanisms of pain. *Cell, 139*(2), 267-284. https://doi.org/10.1016/j.cell.2009.09.028

Bautista, D. M., Movahed, P., Hinman, A., Axelsson, H. E., Sterner, O., Hogestatt, E. D., Julius, D., Jordt, S. E., & Zygmunt, P. M. (2005, Aug 23). Pungent products from garlic activate the sensory ion channel TRPA1. *Proc Natl Acad Sci U S A, 102*(34), 12248-12252. https://doi.org/10.1073/pnas.0505356102

Beaulieu, J. M., Marion, S., Rodriguiz, R. M., Medvedev, I. O., Sotnikova, T. D., Ghisi, V., Wetsel, W. C., Lefkowitz, R. J., Gainetdinov, R. R., & Caron, M. G. (2008, Jan 11). A beta-arrestin 2 signaling complex mediates lithium action on behavior. *Cell, 132*(1), 125-136. https://doi.org/10.1016/j.cell.2007.11.041

Beaulieu, J. M., Sotnikova, T. D., Marion, S., Lefkowitz, R. J., Gainetdinov, R. R., & Caron, M. G. (2005, Jul 29). An Akt/beta-arrestin 2/PP2A signaling complex mediates dopaminergic neurotransmission and behavior. *Cell, 122*(2), 261-273. https://doi.org/10.1016/j.cell.2005.05.012

Belcheva, M. M., Clark, A. L., Haas, P. D., Serna, J. S., Hahn, J. W., Kiss, A., & Coscia, C. J. (2005, Jul 29). Mu and kappa opioid receptors activate ERK/MAPK via different protein kinase C isoforms and secondary messengers in astrocytes. *J Biol Chem, 280*(30), 27662-27669. https://doi.org/10.1074/jbc.M502593200

Benemei, S., Nicoletti, P., Capone, J. G., & Geppetti, P. (2009, Feb). CGRP receptors in the control of pain and inflammation. *Curr Opin Pharmacol, 9*(1), 9-14. https://doi.org/10.1016/j.coph.2008.12.007

Besnard, A., Galan-Rodriguez, B., Vanhoutte, P., & Caboche, J. (2011). Elk-1 a transcription factor with multiple facets in the brain. *Front Neurosci, 5*, 35. https://doi.org/10.3389/fnins.2011.00035

Besnard, A., Laroche, S., & Caboche, J. (2014, Jan). Comparative dynamics of MAPK/ERK signalling components and immediate early genes in the hippocampus and amygdala following contextual fear conditioning and retrieval. *Brain Struct Funct, 219*(1), 415-430. https://doi.org/10.1007/s00429-013-0505-y

Betke, K. M., Wells, C. A., & Hamm, H. E. (2012, Mar). GPCR mediated regulation of synaptic transmission. *Prog Neurobiol, 96*(3), 304-321. https://doi.org/10.1016/j.pneurobio.2012.01.009

Bjork, K., Rimondini, R., Hansson, A. C., Terasmaa, A., Hyytia, P., Heilig, M., & Sommer, W. H. (2008, Jul). Modulation of voluntary ethanol consumption by beta-arrestin 2. *FASEB J, 22*(7), 2552-2560. https://doi.org/10.1096/fj.07-102442

Bohn, L. M., Gainetdinov, R. R., Lin, F. T., Lefkowitz, R. J., & Caron, M. G. (2000, Dec 7). Mu-opioid receptor desensitization by beta-arrestin-2 determines morphine tolerance but not dependence. *Nature, 408*(6813), 720-723. https://doi.org/10.1038/35047086

Bohn, L. M., Lefkowitz, R. J., Gainetdinov, R. R., Peppel, K., Caron, M. G., & Lin, F. T. (1999, Dec 24). Enhanced morphine analgesia in mice lacking beta-arrestin 2. *Science, 286*(5449), 2495-2498. https://doi.org/10.1126/science.286.5449.2495

Bond, R. A., Lucero Garcia-Rojas, E. Y., Hegde, A., & Walker, J. K. L. (2019). Therapeutic Potential of Targeting ss-Arrestin. *Front Pharmacol, 10*, 124. https://doi.org/10.3389/fphar.2019.00124

Borst, J. G., & Sakmann, B. (1996, Oct 3). Calcium influx and transmitter release in a fast CNS synapse. *Nature, 383*(6599), 431-434. https://doi.org/10.1038/383431a0

Bourin, M., & Hascoet, M. (2003, Feb 28). The mouse light/dark box test. *Eur J Pharmacol, 463*(1-3), 55-65. https://doi.org/10.1016/s0014-2999(03)01274-3

Bourinet, E., Altier, C., Hildebrand, M. E., Trang, T., Salter, M. W., & Zamponi, G. W. (2014, Jan). Calcium-permeable ion channels in pain signaling. *Physiol Rev, 94*(1), 81-140. https://doi.org/10.1152/physrev.00023.2013

Bramham, C. R., & Sarvey, J. M. (1996, Dec 15). Endogenous activation of mu and delta-1 opioid receptors is required for long-term potentiation induction in the lateral perforant path: dependence on GABAergic inhibition. *J Neurosci, 16*(24), 8123-8131. https://www.ncbi.nlm.nih.gov/pubmed/8987837

Bressan, E., Touska, F., Vetter, I., Kistner, K., Kichko, T. I., Teixeira, N. B., Picolo, G., Cury, Y., Lewis, R. J., Fischer, M. J., Zimmermann, K., & Reeh, P. W. (2016, Nov). Crotalphine desensitizes TRPA1 ion channels to alleviate inflammatory hyperalgesia. *Pain, 157*(11), 2504-2516. https://doi.org/10.1097/j.pain.0000000000000669

Bretaud, S., Li, Q., Lockwood, B. L., Kobayashi, K., Lin, E., & Guo, S. (2007, May 25). A choice behavior for morphine reveals experience-dependent drug preference and underlying neural substrates in developing larval zebrafish. *Neuroscience, 146*(3), 1109-1116. https://doi.org/10.1016/j.neuroscience.2006.12.073

Brownstein, M. J. (1993, Jun 15). A brief history of opiates, opioid peptides, and opioid receptors. *Proc Natl Acad Sci U S A, 90*(12), 5391-5393. https://doi.org/10.1073/pnas.90.12.5391

Bruchas, M. R., & Chavkin, C. (2010, Jun). Kinase cascades and ligand-directed signaling at the kappa opioid receptor. *Psychopharmacology (Berl), 210*(2), 137-147. https://doi.org/10.1007/s00213-010-1806-y

Bruchas, M. R., Land, B. B., Aita, M., Xu, M., Barot, S. K., Li, S., & Chavkin, C. (2007, Oct 24). Stress-induced p38 mitogen-activated protein kinase activation mediates kappa-opioid-dependent dysphoria. *J Neurosci, 27*(43), 11614-11623. https://doi.org/10.1523/JNEUROSCI.3769-07.2007

Bruchas, M. R., Macey, T. A., Lowe, J. D., & Chavkin, C. (2006, Jun 30). Kappa opioid receptor activation of p38 MAPK is GRK3- and arrestin-dependent in neurons and astrocytes. *J Biol Chem, 281*(26), 18081-18089. https://doi.org/10.1074/jbc.M513640200

Bu, X., Huang, P., Qi, Z., Zhang, N., Han, S., Fang, L., & Li, J. (2007, Dec). Cell type-specific activation of p38 MAPK in the brain regions of hypoxic preconditioned mice. *Neurochem Int, 51*(8), 459-466. https://doi.org/10.1016/j.neuint.2007.04.028

Bugaj, V., Alexeenko, V., Zubov, A., Glushankova, L., Nikolaev, A., Wang, Z., Kaznacheyeva, E., Bezprozvanny, I., & Mozhayeva, G. N. (2005, Apr 29). Functional properties of endogenous receptor- and store-operated calcium influx channels in HEK293 cells. *J Biol Chem, 280*(17), 16790-16797. https://doi.org/10.1074/jbc.M500192200

Carbone, D. L., & Handa, R. J. (2013, Jun 3). Sex and stress hormone influences on the expression and activity of brain-derived neurotrophic factor. *Neuroscience, 239*, 295-303. https://doi.org/10.1016/j.neuroscience.2012.10.073

Carola, V., D'Olimpio, F., Brunamonti, E., Mangia, F., & Renzi, P. (2002, Aug 21). Evaluation of the elevated plus-maze and open-field tests for the assessment of anxiety-related behaviour in inbred mice. *Behav Brain Res, 134*(1-2), 49-57. https://www.ncbi.nlm.nih.gov/pubmed/12191791

Cassier, E., Gallay, N., Bourquard, T., Claeysen, S., Bockaert, J., Crepieux, P., Poupon, A., Reiter, E., Marin, P., & Vandermoere, F. (2017, Feb 7). Phosphorylation of beta-arrestin2 at Thr(383) by MEK underlies beta-arrestin-dependent activation of Erk1/2 by GPCRs. *Elife, 6*. https://doi.org/10.7554/eLife.23777

Caterina, M. J., Leffler, A., Malmberg, A. B., Martin, W. J., Trafton, J., Petersen-Zeitz, K. R., Koltzenburg, M., Basbaum, A. I., & Julius, D. (2000, Apr 14). Impaired nociception and pain sensation in mice lacking the capsaicin receptor. *Science, 288*(5464), 306-313. https://doi.org/10.1126/science.288.5464.306

Cavanaugh, D. J., Lee, H., Lo, L., Shields, S. D., Zylka, M. J., Basbaum, A. I., & Anderson, D. J. (2009, Jun 2). Distinct subsets of unmyelinated primary sensory fibers mediate behavioral responses to noxious thermal and mechanical stimuli. *Proc Natl Acad Sci U S A, 106*(22), 9075-9080. https://doi.org/10.1073/pnas.0901507106

Cen, B., Yu, Q., Guo, J., Wu, Y., Ling, K., Cheng, Z., Ma, L., & Pei, G. (2001, Mar). Direct binding of beta-arrestins to two distinct intracellular domains of the delta opioid receptor. *J Neurochem, 76*(6), 1887-1894. https://doi.org/10.1046/j.1471-4159.2001.00204.x

Chambard, J. C., Lefloch, R., Pouyssegur, J., & Lenormand, P. (2007, Aug). ERK implication in cell cycle regulation. *Biochim Biophys Acta, 1773*(8), 1299-1310. https://doi.org/10.1016/j.bbamcr.2006.11.010

Chen, G., Xie, R. G., Gao, Y. J., Xu, Z. Z., Zhao, L. X., Bang, S., Berta, T., Park, C. K., Lay, M., Chen, W., & Ji, R. R. (2016, Aug 19). beta-arrestin-2 regulates NMDA receptor function in spinal lamina II neurons and duration of persistent pain. *Nat Commun, 7*, 12531. https://doi.org/10.1038/ncomms12531

Chen, J., & Hackos, D. H. (2015, Apr). TRPA1 as a drug target--promise and challenges. *Naunyn Schmiedebergs Arch Pharmacol, 388*(4), 451-463. https://doi.org/10.1007/s00210-015-1088-3

Chen, J., Joshi, S. K., DiDomenico, S., Perner, R. J., Mikusa, J. P., Gauvin, D. M., Segreti, J. A., Han, P., Zhang, X. F., Niforatos, W., Bianchi, B. R., Baker, S. J., Zhong, C., Simler, G. H., McDonald, H. A., Schmidt, R. G., McGaraughty, S. P., Chu, K. L., Faltynek, C. R., Kort, M. E., Reilly, R. M., & Kym, P. R. (2011, May). Selective blockade of TRPA1 channel attenuates pathological pain without altering noxious cold sensation or body temperature regulation. *Pain, 152*(5), 1165-1172. https://doi.org/10.1016/j.pain.2011.01.049

Chen, S., Chiu, C. N., McArthur, K. L., Fetcho, J. R., & Prober, D. A. (2016, Feb). TRP channel mediated neuronal activation and ablation in freely behaving zebrafish. *Nat Methods, 13*(2), 147-150. https://doi.org/10.1038/nmeth.3691

Chen, Y., Geis, C., & Sommer, C. (2008, May 28). Activation of TRPV1 contributes to morphine tolerance: involvement of the mitogen-activated protein kinase signaling pathway. *J Neurosci, 28*(22), 5836-5845. https://doi.org/10.1523/JNEUROSCI.4170-07.2008

Cheng, P., Alberts, I., & Li, X. (2013, Dec). The role of ERK1/2 in the regulation of proliferation and differentiation of astrocytes in developing brain. *Int J Dev Neurosci, 31*(8), 783-789. https://doi.org/10.1016/j.ijdevneu.2013.09.008

Chiang, T., Sansuk, K., & van Rijn, R. M. (2016, Jan). beta-Arrestin 2 dependence of delta opioid receptor agonists is correlated with alcohol intake. *Br J Pharmacol, 173*(2), 332-343. https://doi.org/10.1111/bph.13374

Chu Sin Chung, P., Keyworth, H. L., Martin-Garcia, E., Charbogne, P., Darcq, E., Bailey, A., Filliol, D., Matifas, A., Scherrer, G., Ouagazzal, A. M., Gaveriaux-Ruff, C., Befort, K., Maldonado, R., Kitchen, I., & Kieffer, B. L. (2015, Feb 15). A novel anxiogenic role for the delta opioid receptor expressed in GABAergic forebrain neurons. *Biol Psychiatry, 77*(4), 404-415. https://doi.org/10.1016/j.biopsych.2014.07.033

Ciocchi, S., Herry, C., Grenier, F., Wolff, S. B., Letzkus, J. J., Vlachos, I., Ehrlich, I., Sprengel, R., Deisseroth, K., Stadler, M. B., Muller, C., & Luthi, A. (2010, Nov 11). Encoding of conditioned fear in central amygdala inhibitory circuits. *Nature, 468*(7321), 277-282. https://doi.org/10.1038/nature09559

Clapham, D. E., Runnels, L. W., & Strubing, C. (2001, Jun). The TRP ion channel family. *Nat Rev Neurosci, 2*(6), 387-396. https://doi.org/10.1038/35077544

Colquhoun, D. (2007, Dec). Why the Schild method is better than Schild realised. *Trends Pharmacol Sci, 28*(12), 608-614. https://doi.org/10.1016/j.tips.2007.09.011

Conner, D. A., Mathier, M. A., Mortensen, R. M., Christe, M., Vatner, S. F., Seidman, C. E., & Seidman, J. G. (1997, Dec). beta-Arrestin1 knockout mice appear normal but demonstrate altered cardiac responses to beta-adrenergic stimulation. *Circ Res, 81*(6), 1021-1026. https://doi.org/10.1161/01.res.81.6.1021

Corder, G., Ahanonu, B., Grewe, B. F., Wang, D., Schnitzer, M. J., & Scherrer, G. (2019, Jan 18). An amygdalar neural ensemble that encodes the unpleasantness of pain. *Science, 363*(6424), 276-281. https://doi.org/10.1126/science.aap8586

Corey, D. P., Garcia-Anoveros, J., Holt, J. R., Kwan, K. Y., Lin, S. Y., Vollrath, M. A., Amalfitano, A., Cheung, E. L., Derfler, B. H., Duggan, A., Geleoc, G. S., Gray, P. A., Hoffman, M. P., Rehm, H. L., Tamasauskas, D., & Zhang, D. S. (2004, Dec 9). TRPA1 is a candidate for the mechanosensitive transduction channel of vertebrate hair cells. *Nature, 432*(7018), 723-730. https://doi.org/10.1038/nature03066

Courchesne, E., Mouton, P. R., Calhoun, M. E., Semendeferi, K., Ahrens-Barbeau, C., Hallet, M. J., Barnes, C. C., & Pierce, K. (2011, Nov 9). Neuron number and size in prefrontal cortex of children with autism. *JAMA, 306*(18), 2001-2010. https://doi.org/10.1001/jama.2011.1638

Coyle, J. T., & Duman, R. S. (2003, Apr 24). Finding the intracellular signaling pathways affected by mood disorder treatments. *Neuron, 38*(2), 157-160. https://doi.org/10.1016/s0896-6273(03)00195-8

Crawley, J. N. (1985, Spring). Exploratory behavior models of anxiety in mice. *Neurosci Biobehav Rev, 9*(1), 37-44. https://www.ncbi.nlm.nih.gov/pubmed/2858080

Cruz, C. D., & Cruz, F. (2007, Dec). The ERK 1 and 2 pathway in the nervous system: from basic aspects to possible clinical applications in pain and visceral dysfunction. *Curr Neuropharmacol, 5*(4), 244-252. https://doi.org/10.2174/157015907782793630

Curtright, A., Rosser, M., Goh, S., Keown, B., Wagner, E., Sharifi, J., Raible, D. W., & Dhaka, A. (2015). Modeling nociception in zebrafish: a way forward for unbiased analgesic discovery. *PLoS One, 10*(1), e0116766. https://doi.org/10.1371/journal.pone.0116766

Daub, H., Weiss, F. U., Wallasch, C., & Ullrich, A. (1996, Feb 8). Role of transactivation of the EGF receptor in signalling by G-protein-coupled receptors. *Nature, 379*(6565), 557-560. https://doi.org/10.1038/379557a0

David, D. J., Samuels, B. A., Rainer, Q., Wang, J. W., Marsteller, D., Mendez, I., Drew, M., Craig, D. A., Guiard, B. P., Guilloux, J. P., Artymyshyn, R. P., Gardier, A. M., Gerald, C., Antonijevic, I. A., Leonardo, E. D., & Hen, R. (2009, May 28). Neurogenesis-dependent and -independent effects of fluoxetine in an animal model of anxiety/depression. *Neuron, 62*(4), 479-493. https://doi.org/10.1016/j.neuron.2009.04.017

Davis, J. B., Gray, J., Gunthorpe, M. J., Hatcher, J. P., Davey, P. T., Overend, P., Harries, M. H., Latcham, J., Clapham, C., Atkinson, K., Hughes, S. A., Rance, K., Grau, E., Harper, A. J., Pugh, P. L., Rogers, D. C., Bingham, S., Randall, A., & Sheardown, S. A. (2000, May 11). Vanilloid receptor-1 is essential for inflammatory thermal hyperalgesia. *Nature, 405*(6783), 183-187. https://doi.org/10.1038/35012076

Davis, S., Vanhoutte, P., Pages, C., Caboche, J., & Laroche, S. (2000, Jun 15). The MAPK/ERK cascade targets both Elk-1 and cAMP response element-binding protein to control long-term potentiation-dependent gene expression in the dentate gyrus in vivo. *J Neurosci, 20*(12), 4563-4572. https://www.ncbi.nlm.nih.gov/pubmed/10844026

De Cesare, D., Jacquot, S., Hanauer, A., & Sassone-Corsi, P. (1998, Oct 13). Rsk-2 activity is necessary for epidermal growth factor-induced phosphorylation of CREB protein and transcription of c-fos gene. *Proc Natl Acad Sci U S A, 95*(21), 12202-12207. https://doi.org/10.1073/pnas.95.21.12202

de la Mora, M. P., Gallegos-Cari, A., Arizmendi-Garcia, Y., Marcellino, D., & Fuxe, K. (2010, Feb 9). Role of dopamine receptor mechanisms in the amygdaloid modulation of fear and anxiety: Structural and functional analysis. *Prog Neurobiol, 90*(2), 198-216. https://doi.org/10.1016/j.pneurobio.2009.10.010

Dellemijn, P. L., & Fields, H. L. (1994, May). Do benzodiazepines have a role in chronic pain management? *Pain, 57*(2), 137-152. https://doi.org/10.1016/0304-3959(94)90217-8

Deransart, C., Riban, V., Le, B., Marescaux, C., & Depaulis, A. (2000). Dopamine in the striatum modulates seizures in a genetic model of absence epilepsy in the rat. *Neuroscience, 100*(2), 335-344. https://www.ncbi.nlm.nih.gov/pubmed/11008171

Deutch, A. Y., & Cameron, D. S. (1992). Pharmacological characterization of dopamine systems in the nucleus accumbens core and shell. *Neuroscience, 46*(1), 49-56. https://doi.org/10.1016/0306-4522(92)90007-o

Di Cristo, G., Berardi, N., Cancedda, L., Pizzorusso, T., Putignano, E., Ratto, G. M., & Maffei, L. (2001, Jun 22). Requirement of ERK activation for visual cortical plasticity. *Science, 292*(5525), 2337-2340. https://doi.org/10.1126/science.1059075

Do-Monte, F. H., Kincheski, G. C., Pavesi, E., Sordi, R., Assreuy, J., & Carobrez, A. P. (2010, Oct). Role of beta-adrenergic receptors in the ventromedial prefrontal cortex during contextual fear extinction in rats. *Neurobiol Learn Mem, 94*(3), 318-328. https://doi.org/10.1016/j.nlm.2010.07.004

Dong, H. W., Petrovich, G. D., & Swanson, L. W. (2001, Dec). Topography of projections from amygdala to bed nuclei of the stria terminalis. *Brain Res Brain Res Rev, 38*(1-2), 192-246. https://www.ncbi.nlm.nih.gov/pubmed/11750933

Dowell, D., Haegerich, T. M., & Chou, R. (2016, Mar 18). CDC Guideline for Prescribing Opioids for Chronic Pain - United States, 2016. *MMWR Recomm Rep, 65*(1), 1-49. https://doi.org/10.15585/mmwr.rr6501e1

Drevets, W. C., Price, J. L., Simpson, J. R., Jr., Todd, R. D., Reich, T., Vannier, M., & Raichle, M. E. (1997, Apr 24). Subgenual prefrontal cortex abnormalities in mood disorders. *Nature, 386*(6627), 824-827. https://doi.org/10.1038/386824a0

Dripps, I. J., & Jutkiewicz, E. M. (2018). Delta Opioid Receptors and Modulation of Mood and Emotion. *Handb Exp Pharmacol, 247*, 179-197. https://doi.org/10.1007/164_2017_42

Due, M. R., Park, J., Zheng, L., Walls, M., Allette, Y. M., White, F. A., & Shi, R. (2014, Mar). Acrolein involvement in sensory and behavioral hypersensitivity following spinal cord injury in the rat. *J Neurochem, 128*(5), 776-786. https://doi.org/10.1111/jnc.12500

Duman, C. H., Schlesinger, L., Kodama, M., Russell, D. S., & Duman, R. S. (2007, Mar 1). A role for MAP kinase signaling in behavioral models of depression and antidepressant treatment. *Biol Psychiatry, 61*(5), 661-670. https://doi.org/10.1016/j.biopsych.2006.05.047

Duvarci, S., Bauer, E. P., & Pare, D. (2009, Aug 19). The bed nucleus of the stria terminalis mediates inter-individual variations in anxiety and fear. *J Neurosci, 29*(33), 10357-10361. https://doi.org/10.1523/JNEUROSCI.2119-09.2009

Ehrich, J. M., Messinger, D. I., Knakal, C. R., Kuhar, J. R., Schattauer, S. S., Bruchas, M. R., Zweifel, L. S., Kieffer, B. L., Phillips, P. E., & Chavkin, C. (2015, Sep 16). Kappa Opioid Receptor-Induced Aversion Requires p38 MAPK Activation in VTA Dopamine Neurons. *J Neurosci, 35*(37), 12917-12931. https://doi.org/10.1523/JNEUROSCI.2444-15.2015

Eid, S. R., Crown, E. D., Moore, E. L., Liang, H. A., Choong, K. C., Dima, S., Henze, D. A., Kane, S. A., & Urban, M. O. (2008, Oct 27). HC-030031, a TRPA1 selective antagonist, attenuates inflammatory- and neuropathy-induced mechanical hypersensitivity. *Mol Pain, 4*, 48. https://doi.org/10.1186/1744-8069-4-48

Eilers, H., Cattaruzza, F., Nassini, R., Materazzi, S., Andre, E., Chu, C., Cottrell, G. S., Schumacher, M., Geppetti, P., & Bunnett, N. W. (2010, Jun). Pungent general anesthetics activate transient receptor potential-A1 to produce hyperalgesia and neurogenic bronchoconstriction. *Anesthesiology, 112*(6), 1452-1463. https://doi.org/10.1097/ALN.0b013e3181d94e00

Eisinger, D. A., & Ammer, H. (2008, Dec). Delta-opioid receptors activate ERK/MAP kinase via integrin-stimulated receptor tyrosine kinases. *Cell Signal, 20*(12), 2324-2331. https://doi.org/10.1016/j.cellsig.2008.09.002

Eisinger, D. A., Ammer, H., & Schulz, R. (2002, Dec 1). Chronic morphine treatment inhibits opioid receptor desensitization and internalization. *J Neurosci, 22*(23), 10192-10200. https://www.ncbi.nlm.nih.gov/pubmed/12451120

Engin, E., & Treit, D. (2007, Sep). The role of hippocampus in anxiety: intracerebral infusion studies. *Behav Pharmacol, 18*(5-6), 365-374. https://doi.org/10.1097/FBP.0b013e3282de7929

English, J. D., & Sweatt, J. D. (1997, Aug 1). A requirement for the mitogen-activated protein kinase cascade in hippocampal long term potentiation. *J Biol Chem, 272*(31), 19103-19106. https://doi.org/10.1074/jbc.272.31.19103

Erbs, E., Faget, L., Scherrer, G., Matifas, A., Filliol, D., Vonesch, J. L., Koch, M., Kessler, P., Hentsch, D., Birling, M. C., Koutsourakis, M., Vasseur, L., Veinante, P., Kieffer, B. L., & Massotte, D. (2015, Mar). A mu-delta opioid receptor brain atlas reveals neuronal co-occurrence in subcortical networks. *Brain Struct Funct, 220*(2), 677-702. https://doi.org/10.1007/s00429-014-0717-9

Erhardt, W., Hebestedt, A., Aschenbrenner, G., Pichotka, B., & Blumel, G. (1984). A comparative study with various anesthetics in mice (pentobarbitone, ketamine-xylazine, carfentanyl-etomidate). *Res Exp Med (Berl), 184*(3), 159-169. https://www.ncbi.nlm.nih.gov/pubmed/6473905

Esancy, K., Condon, L., Feng, J., Kimball, C., Curtright, A., & Dhaka, A. (2018, Mar 21). A zebrafish and mouse model for selective pruritus via direct activation of TRPA1. *Elife, 7*. https://doi.org/10.7554/eLife.32036

Fadok, J. P., Darvas, M., Dickerson, T. M., & Palmiter, R. D. (2010, Sep 15). Long-term memory for pavlovian fear conditioning requires dopamine in the nucleus accumbens and basolateral amygdala. *PLoS One, 5*(9), e12751. https://doi.org/10.1371/journal.pone.0012751

Fadok, J. P., Dickerson, T. M., & Palmiter, R. D. (2009, Sep 9). Dopamine is necessary for cue-dependent fear conditioning. *J Neurosci, 29*(36), 11089-11097. https://doi.org/10.1523/JNEUROSCI.1616-09.2009

Fanselow, M. S., & Dong, H. W. (2010, Jan 14). Are the dorsal and ventral hippocampus functionally distinct structures? *Neuron, 65*(1), 7-19. https://doi.org/10.1016/j.neuron.2009.11.031

Feinstein, J. S., Adolphs, R., Damasio, A., & Tranel, D. (2011, Jan 11). The human amygdala and the induction and experience of fear. *Curr Biol, 21*(1), 34-38. https://doi.org/10.1016/j.cub.2010.11.042

Felix-Ortiz, A. C., Beyeler, A., Seo, C., Leppla, C. A., Wildes, C. P., & Tye, K. M. (2013, Aug 21). BLA to vHPC inputs modulate anxiety-related behaviors. *Neuron, 79*(4), 658-664. https://doi.org/10.1016/j.neuron.2013.06.016

Fendt, M., & Fanselow, M. S. (1999, May). The neuroanatomical and neurochemical basis of conditioned fear. *Neurosci Biobehav Rev, 23*(5), 743-760. https://www.ncbi.nlm.nih.gov/pubmed/10392663

File, S. E., Kenny, P. J., & Cheeta, S. (2000, May). The role of the dorsal hippocampal serotonergic and cholinergic systems in the modulation of anxiety. *Pharmacol Biochem Behav, 66*(1), 65-72. https://doi.org/10.1016/s0091-3057(00)00198-2

Filliol, D., Ghozland, S., Chluba, J., Martin, M., Matthes, H. W., Simonin, F., Befort, K., Gaveriaux-Ruff, C., Dierich, A., LeMeur, M., Valverde, O., Maldonado, R., & Kieffer, B. L. (2000, Jun). Mice deficient for delta- and mu-opioid receptors exhibit opposing alterations of emotional responses. *Nat Genet, 25*(2), 195-200. https://doi.org/10.1038/76061

Fisher, A., Heldman, E., Gurwitz, D., Haring, R., Barak, D., Meshulam, H., Marciano, D., Brandeis, R., Pittel, Z., Segal, M., & et al. (1993, Sep 24). Selective signaling via unique M1 muscarinic agonists. *Ann N Y Acad Sci, 695*, 300-303. https://doi.org/10.1111/j.1749-6632.1993.tb23070.x

Fleischmann, A., Hvalby, O., Jensen, V., Strekalova, T., Zacher, C., Layer, L. E., Kvello, A., Reschke, M., Spanagel, R., Sprengel, R., Wagner, E. F., & Gass, P. (2003, Oct 8). Impaired long-term memory and NR2A-type NMDA receptor-dependent synaptic plasticity in mice lacking c-Fos in the CNS. *J Neurosci, 23*(27), 9116-9122. https://www.ncbi.nlm.nih.gov/pubmed/14534245

Flood, D. G., Finn, J. P., Walton, K. M., Dionne, C. A., Contreras, P. C., Miller, M. S., & Bhat, R. V. (1998, Aug 31). Immunolocalization of the mitogen-activated protein kinases p42MAPK and JNK1, and their regulatory kinases MEK1 and MEK4, in adult rat central nervous system. *J Comp Neurol, 398*(3), 373-392. https://www.ncbi.nlm.nih.gov/pubmed/9714150

Francois, A., & Scherrer, G. (2018). Delta Opioid Receptor Expression and Function in Primary Afferent Somatosensory Neurons. *Handb Exp Pharmacol, 247*, 87-114. https://doi.org/10.1007/164_2017_58

Freedman, N. J., & Lefkowitz, R. J. (1996). Desensitization of G protein-coupled receptors. *Recent Prog Horm Res, 51*, 319-351; discussion 352-313. https://www.ncbi.nlm.nih.gov/pubmed/8701085

Ganguly, S., Panetta, J. C., Roberts, J. K., & Schuetz, E. G. (2018, Jul). Ketamine Pharmacokinetics and Pharmacodynamics Are Altered by P-Glycoprotein and Breast Cancer Resistance Protein Efflux Transporters in Mice. *Drug Metab Dispos, 46*(7), 1014-1022. https://doi.org/10.1124/dmd.117.078360

Ganzen, L., Venkatraman, P., Pang, C. P., Leung, Y. F., & Zhang, M. (2017, Jun 2). Utilizing Zebrafish Visual Behaviors in Drug Screening for Retinal Degeneration. *Int J Mol Sci, 18*(6). https://doi.org/10.3390/ijms18061185

Gaveriaux-Ruff, C., & Kieffer, B. L. (2011, Sep). Delta opioid receptor analgesia: recent contributions from pharmacology and molecular approaches. *Behav Pharmacol, 22*(5-6), 405-414. https://doi.org/10.1097/FBP.0b013e32834a1f2c

Gees, M., Alpizar, Y. A., Boonen, B., Sanchez, A., Everaerts, W., Segal, A., Xue, F., Janssens, A., Owsianik, G., Nilius, B., Voets, T., & Talavera, K. (2013, Sep). Mechanisms of transient receptor potential vanilloid 1 activation and sensitization by allyl isothiocyanate. *Mol Pharmacol, 84*(3), 325-334. https://doi.org/10.1124/mol.113.085548

Gerlai, R. (2010, Apr 12). High-throughput behavioral screens: the first step towards finding genes involved in vertebrate brain function using zebrafish. *Molecules, 15*(4), 2609-2622. https://doi.org/10.3390/molecules15042609

Gesty-Palmer, D., Chen, M., Reiter, E., Ahn, S., Nelson, C. D., Wang, S., Eckhardt, A. E., Cowan, C. L., Spurney, R. F., Luttrell, L. M., & Lefkowitz, R. J. (2006, Apr 21). Distinct beta-arrestin- and G protein-dependent pathways for parathyroid hormone receptor-stimulated ERK1/2 activation. *J Biol Chem, 281*(16), 10856-10864. https://doi.org/10.1074/jbc.M513380200

Ginty, D. D., Bonni, A., & Greenberg, M. E. (1994, Jun 3). Nerve growth factor activates a Ras-dependent protein kinase that stimulates c-fos transcription via phosphorylation of CREB. *Cell, 77*(5), 713-725. https://doi.org/10.1016/0092-8674(94)90055-8

Girnita, L., Shenoy, S. K., Sehat, B., Vasilcanu, R., Vasilcanu, D., Girnita, A., Lefkowitz, R. J., & Larsson, O. (2007, Apr 13). Beta-arrestin and Mdm2 mediate IGF-1 receptor-stimulated ERK activation and cell cycle progression. *J Biol Chem, 282*(15), 11329-11338. https://doi.org/10.1074/jbc.M611526200

Goldberg, D. S., & McGee, S. J. (2011, Oct 6). Pain as a global public health priority. *BMC Public Health, 11*, 770. https://doi.org/10.1186/1471-2458-11-770

Goldsmith, Z. G., & Dhanasekaran, D. N. (2007, May 14). G protein regulation of MAPK networks. *Oncogene, 26*(22), 3122-3142. https://doi.org/10.1038/sj.onc.1210407

Gonzalez-Nunez, V., Jimenez Gonzalez, A., Barreto-Valer, K., & Rodriguez, R. E. (2013, Mar 5). In vivo regulation of the mu opioid receptor: role of the endogenous opioid agents. *Mol Med, 19*, 7-17. https://doi.org/10.2119/molmed.2012.00318

Goto, Y., Yang, C. R., & Otani, S. (2010, Feb 1). Functional and dysfunctional synaptic plasticity in prefrontal cortex: roles in psychiatric disorders. *Biol Psychiatry, 67*(3), 199-207. https://doi.org/10.1016/j.biopsych.2009.08.026

Grace, P. M., Hutchinson, M. R., Maier, S. F., & Watkins, L. R. (2014, Apr). Pathological pain and the neuroimmune interface. *Nat Rev Immunol, 14*(4), 217-231. https://doi.org/10.1038/nri3621

Grudt, T. J., & Williams, J. T. (1995, Jul-Sep). Opioid receptors and the regulation of ion conductances. *Rev Neurosci, 6*(3), 279-286. https://doi.org/10.1515/revneuro.1995.6.3.279

Gurevich, E. V., Benovic, J. L., & Gurevich, V. V. (2002). Arrestin2 and arrestin3 are differentially expressed in the rat brain during postnatal development. *Neuroscience, 109*(3), 421-436. https://www.ncbi.nlm.nih.gov/pubmed/11823056

Gurevich, E. V., Benovic, J. L., & Gurevich, V. V. (2004, Dec). Arrestin2 expression selectively increases during neural differentiation. *J Neurochem, 91*(6), 1404-1416. https://doi.org/10.1111/j.1471-4159.2004.02830.x

Gurwitz, D., Haring, R., Heldman, E., Fraser, C. M., Manor, D., & Fisher, A. (1994, Mar 15). Discrete activation of transduction pathways associated with acetylcholine m1 receptor by several muscarinic ligands. *Eur J Pharmacol, 267*(1), 21-31. https://doi.org/10.1016/0922-4106(94)90220-8

Gutkind, J. S. (2000, Jul 11). Regulation of mitogen-activated protein kinase signaling networks by G protein-coupled receptors. *Sci STKE, 2000*(40), re1. https://doi.org/10.1126/stke.2000.40.re1

Hahn, Y. K., Paris, J. J., Lichtman, A. H., Hauser, K. F., Sim-Selley, L. J., Selley, D. E., & Knapp, P. E. (2016, Aug). Central HIV-1 Tat exposure elevates anxiety and fear conditioned responses of male mice concurrent with altered mu-opioid receptor-mediated G-protein activation and beta-arrestin 2 activity in the forebrain. *Neurobiol Dis, 92*(Pt B), 124-136. https://doi.org/10.1016/j.nbd.2016.01.014

Hall, J., Thomas, K. L., & Everitt, B. J. (2001, Mar 15). Cellular imaging of zif268 expression in the hippocampus and amygdala during contextual and cued fear memory retrieval: selective activation of hippocampal CA1 neurons during the recall of contextual memories. *J Neurosci, 21*(6), 2186-2193. https://www.ncbi.nlm.nih.gov/pubmed/11245703

Halperin, J. M., & Schulz, K. P. (2006, Jul). Revisiting the role of the prefrontal cortex in the pathophysiology of attention-deficit/hyperactivity disorder. *Psychol Bull, 132*(4), 560-581. https://doi.org/10.1037/0033-2909.132.4.560

Hasbi, A., Fan, T., Alijaniaram, M., Nguyen, T., Perreault, M. L., O'Dowd, B. F., & George, S. R. (2009, Dec 15). Calcium signaling cascade links dopamine D1-D2 receptor heteromer to striatal BDNF production and neuronal growth. *Proc Natl Acad Sci U S A, 106*(50), 21377-21382. https://doi.org/10.1073/pnas.0903676106

Haubensak, W., Kunwar, P. S., Cai, H., Ciocchi, S., Wall, N. R., Ponnusamy, R., Biag, J., Dong, H. W., Deisseroth, K., Callaway, E. M., Fanselow, M. S., Luthi, A., & Anderson, D. J. (2010, Nov 11). Genetic dissection of an amygdala microcircuit that gates conditioned fear. *Nature, 468*(7321), 270-276. https://doi.org/10.1038/nature09553

Hauser, A. S., Attwood, M. M., Rask-Andersen, M., Schioth, H. B., & Gloriam, D. E. (2017, Dec). Trends in GPCR drug discovery: new agents, targets and indications. *Nat Rev Drug Discov, 16*(12), 829-842. https://doi.org/10.1038/nrd.2017.178

Heimer, L. (2000, Mar). Basal forebrain in the context of schizophrenia. *Brain Res Brain Res Rev, 31*(2-3), 205-235. https://www.ncbi.nlm.nih.gov/pubmed/10719150

Hensley, K., Robinson, K. A., Gabbita, S. P., Salsman, S., & Floyd, R. A. (2000, May 15). Reactive oxygen species, cell signaling, and cell injury. *Free Radic Biol Med, 28*(10), 1456-1462. https://www.ncbi.nlm.nih.gov/pubmed/10927169

Herlitze, S., Garcia, D. E., Mackie, K., Hille, B., Scheuer, T., & Catterall, W. A. (1996, Mar 21). Modulation of Ca2+ channels by G-protein beta gamma subunits. *Nature, 380*(6571), 258-262. https://doi.org/10.1038/380258a0

Herring, B. E., & Nicoll, R. A. (2016). Long-Term Potentiation: From CaMKII to AMPA Receptor Trafficking. *Annu Rev Physiol, 78*, 351-365. https://doi.org/10.1146/annurev-physiol-021014-071753

Herry, C., Trifilieff, P., Micheau, J., Luthi, A., & Mons, N. (2006, Jul). Extinction of auditory fear conditioning requires MAPK/ERK activation in the basolateral amygdala. *Eur J Neurosci, 24*(1), 261-269. https://doi.org/10.1111/j.1460-9568.2006.04893.x

Hill, R., Disney, A., Conibear, A., Sutcliffe, K., Dewey, W., Husbands, S., Bailey, C., Kelly, E., & Henderson, G. (2018, Jul). The novel mu-opioid receptor agonist PZM21 depresses respiration and induces tolerance to antinociception. *Br J Pharmacol, 175*(13), 2653-2661. https://doi.org/10.1111/bph.14224

Hill, S. J. (2006, Jan). G-protein-coupled receptors: past, present and future. *Br J Pharmacol, 147 Suppl 1*, S27-37. https://doi.org/10.1038/sj.bjp.0706455

Hoeppner, C. Z., Cheng, N., & Ye, R. D. (2012, Mar 16). Identification of a nuclear localization sequence in beta-arrestin-1 and its functional implications. *J Biol Chem, 287*(12), 8932-8943. https://doi.org/10.1074/jbc.M111.294058

Holz, G. G. t., Rane, S. G., & Dunlap, K. (1986, Feb 20-26). GTP-binding proteins mediate transmitter inhibition of voltage-dependent calcium channels. *Nature, 319*(6055), 670-672. https://doi.org/10.1038/319670a0

Holzer, P. (1991, Jun). Capsaicin: cellular targets, mechanisms of action, and selectivity for thin sensory neurons. *Pharmacol Rev, 43*(2), 143-201. https://www.ncbi.nlm.nih.gov/pubmed/1852779

Howard, J., & Bechstedt, S. (2004, Mar 23). Hypothesis: a helix of ankyrin repeats of the NOMPC-TRP ion channel is the gating spring of mechanoreceptors. *Curr Biol, 14*(6), R224-226. https://doi.org/10.1016/j.cub.2004.02.050

Huang, B., Li, Y., Cheng, D., He, G., Liu, X., & Ma, L. (2018, Jan 9). beta-Arrestin-biased beta-adrenergic signaling promotes extinction learning of cocaine reward memory. *Sci Signal, 11*(512). https://doi.org/10.1126/scisignal.aam5402

Huang, T. Y., & Lin, C. H. (2006, Oct 2). Role of amygdala MAPK activation on immobility behavior of forced swim rats. *Behav Brain Res, 173*(1), 104-111. https://doi.org/10.1016/j.bbr.2006.06.009

Ikeda, K., Yoshii, M., Sora, I., & Kobayashi, T. (2003). Opioid receptor coupling to GIRK channels. In vitro studies using a Xenopus oocyte expression system and in vivo studies on weaver mutant mice. *Methods Mol Med, 84*, 53-64. https://doi.org/10.1385/1-59259-379-8:53

Impey, S., Obrietan, K., & Storm, D. R. (1999, May). Making new connections: role of ERK/MAP kinase signaling in neuronal plasticity. *Neuron, 23*(1), 11-14. https://doi.org/10.1016/s0896-6273(00)80747-3

Ivanina, T., Rishal, I., Varon, D., Mullner, C., Frohnwieser-Steinecke, B., Schreibmayer, W., Dessauer, C. W., & Dascal, N. (2003, Aug 1). Mapping the Gbetagamma-binding sites in GIRK1 and GIRK2 subunits of the G protein-activated K+ channel. *J Biol Chem, 278*(31), 29174-29183. https://doi.org/10.1074/jbc.M304518200

Jain, R., Watson, U., Vasudevan, L., & Saini, D. K. (2018). ERK Activation Pathways Downstream of GPCRs. *Int Rev Cell Mol Biol, 338*, 79-109. https://doi.org/10.1016/bs.ircmb.2018.02.003

Janak, P. H., & Tye, K. M. (2015, Jan 15). From circuits to behaviour in the amygdala. *Nature, 517*(7534), 284-292. https://doi.org/10.1038/nature14188

Janssens, A., Gees, M., Toth, B. I., Ghosh, D., Mulier, M., Vennekens, R., Vriens, J., Talavera, K., & Voets, T. (2016, Jul 23). Definition of two agonist types at the mammalian cold-activated channel TRPM8. *Elife, 5*. https://doi.org/10.7554/eLife.17240

Jiang, Z. G., & North, R. A. (1992, Jan). Pre- and postsynaptic inhibition by opioids in rat striatum. *J Neurosci, 12*(1), 356-361. https://www.ncbi.nlm.nih.gov/pubmed/1309576

Jimenez, J. C., Su, K., Goldberg, A. R., Luna, V. M., Biane, J. S., Ordek, G., Zhou, P., Ong, S. K., Wright, M. A., Zweifel, L., Paninski, L., Hen, R., & Kheirbek, M. A. (2018, Feb 7). Anxiety Cells in a Hippocampal-Hypothalamic Circuit. *Neuron, 97*(3), 670-683 e676. https://doi.org/10.1016/j.neuron.2018.01.016

Johansen, J. P., Cain, C. K., Ostroff, L. E., & LeDoux, J. E. (2011, Oct 28). Molecular mechanisms of fear learning and memory. *Cell, 147*(3), 509-524. https://doi.org/10.1016/j.cell.2011.10.009

Johnson, G. L., & Lapadat, R. (2002, Dec 6). Mitogen-activated protein kinase pathways mediated by ERK, JNK, and p38 protein kinases. *Science, 298*(5600), 1911-1912. https://doi.org/10.1126/science.1072682

Kalueff, A. V., Gebhardt, M., Stewart, A. M., Cachat, J. M., Brimmer, M., Chawla, J. S., Craddock, C., Kyzar, E. J., Roth, A., Landsman, S., Gaikwad, S., Robinson, K., Baatrup, E., Tierney, K., Shamchuk, A., Norton, W., Miller, N., Nicolson, T., Braubach, O., Gilman, C. P., Pittman, J., Rosemberg, D. B., Gerlai, R., Echevarria, D., Lamb, E., Neuhauss, S. C., Weng, W., Bally-Cuif, L., Schneider, H., & Zebrafish Neuroscience Research, C. (2013, Mar). Towards a comprehensive catalog of zebrafish behavior 1.0 and beyond. *Zebrafish, 10*(1), 70-86. https://doi.org/10.1089/zeb.2012.0861

Kang, J., Shi, Y., Xiang, B., Qu, B., Su, W., Zhu, M., Zhang, M., Bao, G., Wang, F., Zhang, X., Yang, R., Fan, F., Chen, X., Pei, G., & Ma, L. (2005, Dec 2). A nuclear function of beta-arrestin1 in GPCR signaling: regulation of histone acetylation and gene transcription. *Cell, 123*(5), 833-847. https://doi.org/10.1016/j.cell.2005.09.011

Kerstein, P. C., del Camino, D., Moran, M. M., & Stucky, C. L. (2009, Apr 21). Pharmacological blockade of TRPA1 inhibits mechanical firing in nociceptors. *Mol Pain, 5*, 19. https://doi.org/10.1186/1744-8069-5-19

Kessler, R. C., Berglund, P., Demler, O., Jin, R., Merikangas, K. R., & Walters, E. E. (2005, Jun). Lifetime prevalence and age-of-onset distributions of DSM-IV disorders in the National Comorbidity Survey Replication. *Arch Gen Psychiatry, 62*(6), 593-602. https://doi.org/10.1001/archpsyc.62.6.593

Kheirbek, M. A., Drew, L. J., Burghardt, N. S., Costantini, D. O., Tannenholz, L., Ahmari, S. E., Zeng, H., Fenton, A. A., & Hen, R. (2013, Mar 6). Differential control of learning and anxiety along the dorsoventral axis of the dentate gyrus. *Neuron, 77*(5), 955-968. https://doi.org/10.1016/j.neuron.2012.12.038

Kilkenny, C., Browne, W. J., Cuthill, I. C., Emerson, M., & Altman, D. G. (2012, Apr). Improving bioscience research reporting: the ARRIVE guidelines for reporting animal research. *Osteoarthritis Cartilage, 20*(4), 256-260. https://doi.org/10.1016/j.joca.2012.02.010

Kim, E. K., & Choi, E. J. (2015, Jun). Compromised MAPK signaling in human diseases: an update. *Arch Toxicol, 89*(6), 867-882. https://doi.org/10.1007/s00204-015-1472-2

Kim, J. W., Ko, M. J., Gonzales, E. L., Kang, R. J., Kim, D. G., Kim, Y., Seung, H., Oh, H. A., Eun, P. H., & Shin, C. Y. (2018, Aug 13). Social support rescues acute stress-induced cognitive impairments by modulating ERK1/2 phosphorylation in adolescent mice. *Sci Rep, 8*(1), 12003. https://doi.org/10.1038/s41598-018-30524-4

Kindt, M., Soeter, M., & Vervliet, B. (2009, Mar). Beyond extinction: erasing human fear responses and preventing the return of fear. *Nat Neurosci, 12*(3), 256-258. https://doi.org/10.1038/nn.2271

Kistner, K., Siklosi, N., Babes, A., Khalil, M., Selescu, T., Zimmermann, K., Wirtz, S., Becker, C., Neurath, M. F., Reeh, P. W., & Engel, M. A. (2016, Jun 30). Systemic desensitization through TRPA1 channels by capsazepine and mustard oil - a novel strategy against inflammation and pain. *Sci Rep, 6*, 28621. https://doi.org/10.1038/srep28621

Klee, W. A., Simonds, W. F., Sweat, F. W., Burke, T. R., Jr., Jacobson, A. E., & Rice, K. C. (1982, Dec 13). Identification of a Mr 58 000 glycoprotein subunit of the opiate receptor. *FEBS Lett, 150*(1), 125-128. https://doi.org/10.1016/0014-5793(82)81318-5

Kliewer, A., Schmiedel, F., Sianati, S., Bailey, A., Bateman, J. T., Levitt, E. S., Williams, J. T., Christie, M. J., & Schulz, S. (2019, Jan 21). Phosphorylation-deficient G-protein-biased mu-opioid receptors improve analgesia and diminish tolerance but worsen opioid side effects. *Nat Commun, 10*(1), 367. https://doi.org/10.1038/s41467-018-08162-1

Ko, M. J., Ganzen, L. C., Coskun, E., Mukadam, A. A., Leung, Y. F., & van Rijn, R. M. (2019, Feb 20). A critical evaluation of TRPA1-mediated locomotor behavior in zebrafish as a screening tool for novel anti-nociceptive drug discovery. *Sci Rep, 9*(1), 2430. https://doi.org/10.1038/s41598-019-38852-9

Ko, M. J., Mulia, G. E., & van Rijn, R. M. (2019). Commonly Used Anesthesia/Euthanasia Methods for Brain Collection Differentially Impact MAPK Activity in Male and Female C57BL/6 Mice. *Front Cell Neurosci, 13*, 96. https://doi.org/10.3389/fncel.2019.00096

Koistinaho, M., & Koistinaho, J. (2002, Nov). Role of p38 and p44/42 mitogen-activated protein kinases in microglia. *Glia, 40*(2), 175-183. https://doi.org/10.1002/glia.10151

Kojima, R., Nozawa, K., Doihara, H., Keto, Y., Kaku, H., Yokoyama, T., & Itou, H. (2014, Jan 15). Effects of novel TRPA1 receptor agonist ASP7663 in models of drug-induced constipation and visceral pain. *Eur J Pharmacol, 723*, 288-293. https://doi.org/10.1016/j.ejphar.2013.11.020

Kolodny, A., Courtwright, D. T., Hwang, C. S., Kreiner, P., Eadie, J. L., Clark, T. W., & Alexander, G. C. (2015, Mar 18). The prescription opioid and heroin crisis: a public health approach to an epidemic of addiction. *Annu Rev Public Health, 36*, 559-574. https://doi.org/10.1146/annurev-publhealth-031914-122957

Kosugi, M., Nakatsuka, T., Fujita, T., Kuroda, Y., & Kumamoto, E. (2007, Apr 18). Activation of TRPA1 channel facilitates excitatory synaptic transmission in substantia gelatinosa neurons of the adult rat spinal cord. *J Neurosci, 27*(16), 4443-4451. https://doi.org/10.1523/JNEUROSCI.0557-07.2007

Kramer, H. K., Onoprishvili, I., Andria, M. L., Hanna, K., Sheinkman, K., Haddad, L. B., & Simon, E. J. (2002). Delta opioid activation of the mitogen-activated protein kinase cascade does not require transphosphorylation of receptor tyrosine kinases. *BMC Pharmacol, 2*, 5. https://doi.org/10.1186/1471-2210-2-5

Kung, J. C., Chen, T. C., Shyu, B. C., Hsiao, S., & Huang, A. C. (2010, Apr 21). Anxiety- and depressive-like responses and c-fos activity in preproenkephalin knockout mice: oversensitivity hypothesis of enkephalin deficit-induced posttraumatic stress disorder. *J Biomed Sci, 17*, 29. https://doi.org/10.1186/1423-0127-17-29

Kwan, K. Y., Allchorne, A. J., Vollrath, M. A., Christensen, A. P., Zhang, D. S., Woolf, C. J., & Corey, D. P. (2006, Apr 20). TRPA1 contributes to cold, mechanical, and chemical nociception but is not essential for hair-cell transduction. *Neuron, 50*(2), 277-289. https://doi.org/10.1016/j.neuron.2006.03.042

LaLumiere, R. T., Nawar, E. M., & McGaugh, J. L. (2005, May-Jun). Modulation of memory consolidation by the basolateral amygdala or nucleus accumbens shell requires concurrent dopamine receptor activation in both brain regions. *Learn Mem, 12*(3), 296-301. https://doi.org/10.1101/lm.93205

Lanahan, A., & Worley, P. (1998, Jul-Sep). Immediate-early genes and synaptic function. *Neurobiol Learn Mem, 70*(1-2), 37-43. https://doi.org/10.1006/nlme.1998.3836

Land, B. B., Bruchas, M. R., Schattauer, S., Giardino, W. J., Aita, M., Messinger, D., Hnasko, T. S., Palmiter, R. D., & Chavkin, C. (2009, Nov 10). Activation of the kappa opioid receptor in the dorsal raphe nucleus mediates the aversive effects of stress and reinstates drug seeking. *Proc Natl Acad Sci U S A, 106*(45), 19168-19173. https://doi.org/10.1073/pnas.0910705106

Langley, J. N. (1905). On the reaction of cells and of nerve-endings to certain poisons, chiefly as regards the reaction of striated muscle to nicotine and to curari. *The Journal of physiology, 33*(4-5), 374-413.

Latapy, C., & Beaulieu, J. M. (2013). beta-Arrestins in the central nervous system. *Prog Mol Biol Transl Sci, 118*, 267-295. https://doi.org/10.1016/B978-0-12-394440-5.00011-5

LeDoux, J. E. (2000). Emotion circuits in the brain. *Annu Rev Neurosci, 23*, 155-184. https://doi.org/10.1146/annurev.neuro.23.1.155

Lefkowitz, R. J. (2013, Jun 17). A brief history of G-protein coupled receptors (Nobel Lecture). *Angew Chem Int Ed Engl, 52*(25), 6366-6378. https://doi.org/10.1002/anie.201301924

Lefkowitz, R. J., Pierce, K. L., & Luttrell, L. M. (2002, Nov). Dancing with different partners: protein kinase a phosphorylation of seven membrane-spanning receptors regulates their G protein-coupling specificity. *Mol Pharmacol, 62*(5), 971-974. https://doi.org/10.1124/mol.62.5.971

Lefkowitz, R. J., Rajagopal, K., & Whalen, E. J. (2006, Dec 8). New roles for beta-arrestins in cell signaling: not just for seven-transmembrane receptors. *Mol Cell, 24*(5), 643-652. https://doi.org/10.1016/j.molcel.2006.11.007

Lefkowitz, R. J., & Shenoy, S. K. (2005, Apr 22). Transduction of receptor signals by beta-arrestins. *Science, 308*(5721), 512-517. https://doi.org/10.1126/science.1109237

Lewis, M. M., Watts, V. J., Lawler, C. P., Nichols, D. E., & Mailman, R. B. (1998, Jul). Homologous desensitization of the D1A dopamine receptor: efficacy in causing desensitization dissociates from both receptor occupancy and functional potency. *J Pharmacol Exp Ther, 286*(1), 345-353. https://www.ncbi.nlm.nih.gov/pubmed/9655879

Li, N., Lee, B., Liu, R. J., Banasr, M., Dwyer, J. M., Iwata, M., Li, X. Y., Aghajanian, G., & Duman, R. S. (2010, Aug 20). mTOR-dependent synapse formation underlies the rapid antidepressant effects of NMDA antagonists. *Science, 329*(5994), 959-964. https://doi.org/10.1126/science.1190287

Li, Y., Li, H., Liu, X., Bao, G., Tao, Y., Wu, Z., Xia, P., Wu, C., Li, B., & Ma, L. (2009, Dec 22). Regulation of amygdalar PKA by beta-arrestin-2/phosphodiesterase-4 complex is critical for fear conditioning. *Proc Natl Acad Sci U S A, 106*(51), 21918-21923. https://doi.org/10.1073/pnas.0906941106

Li, Y., Wang, F., Liu, C., Zeng, M., Han, X., Luo, T., Jiang, W., Xu, J., & Wang, H. (2013, Jun 17). JNK pathway may be involved in isoflurane-induced apoptosis in the hippocampi of neonatal rats. *Neurosci Lett, 545*, 17-22. https://doi.org/10.1016/j.neulet.2013.04.008

Liao, Z., Cao, D., Han, X., Liu, C., Peng, J., Zuo, Z., Wang, F., & Li, Y. (2014, Aug). Both JNK and P38 MAPK pathways participate in the protection by dexmedetomidine against isoflurane-induced neuroapoptosis in the hippocampus of neonatal rats. *Brain Res Bull, 107*, 69-78. https://doi.org/10.1016/j.brainresbull.2014.07.001

Liu, C. H., Gong, Z., Liang, Z. L., Liu, Z. X., Yang, F., Sun, Y. J., Ma, M. L., Wang, Y. J., Ji, C. R., Wang, Y. H., Wang, M. J., Cui, F. A., Lin, A., Zheng, W. S., He, D. F., Qu, C. X., Xiao, P., Liu, C. Y., Thomsen, A. R., Joseph Cahill, T., 3rd, Kahsai, A. W., Yi, F., Xiao, K. H., Xue, T., Zhou, Z., Yu, X., & Sun, J. P. (2017, Feb 9). Arrestin-biased AT1R agonism induces acute catecholamine secretion through TRPC3 coupling. *Nat Commun, 8*, 14335. https://doi.org/10.1038/ncomms14335

Liu, J., Wang, P., Zhang, X., Zhang, W., & Gu, G. (2014). Effects of different concentration and duration time of isoflurane on acute and long-term neurocognitive function of young adult C57BL/6 mouse. *Int J Clin Exp Pathol, 7*(9), 5828-5836. https://www.ncbi.nlm.nih.gov/pubmed/25337224

Liu, X., Ma, L., Li, H. H., Huang, B., Li, Y. X., Tao, Y. Z., & Ma, L. (2015, Apr 7). beta-Arrestin-biased signaling mediates memory reconsolidation. *Proc Natl Acad Sci U S A, 112*(14), 4483-4488. https://doi.org/10.1073/pnas.1421758112

Lohse, M. J., Benovic, J. L., Codina, J., Caron, M. G., & Lefkowitz, R. J. (1990, Jun 22). beta-Arrestin: a protein that regulates beta-adrenergic receptor function. *Science, 248*(4962), 1547-1550. https://doi.org/10.1126/science.2163110

Lomazzo, E., Bindila, L., Remmers, F., Lerner, R., Schwitter, C., Hoheisel, U., & Lutz, B. (2015, Jan). Therapeutic potential of inhibitors of endocannabinoid degradation for the treatment of stress-related hyperalgesia in an animal model of chronic pain. *Neuropsychopharmacology, 40*(2), 488-501. https://doi.org/10.1038/npp.2014.198

Loonen, A. J., & Ivanova, S. A. (2015). Circuits regulating pleasure and happiness: the evolution of reward-seeking and misery-fleeing behavioral mechanisms in vertebrates. *Front Neurosci, 9*, 394. https://doi.org/10.3389/fnins.2015.00394

Lu, L., Koya, E., Zhai, H., Hope, B. T., & Shaham, Y. (2006, Dec). Role of ERK in cocaine addiction. *Trends Neurosci, 29*(12), 695-703. https://doi.org/10.1016/j.tins.2006.10.005

Lujan, R., Marron Fernandez de Velasco, E., Aguado, C., & Wickman, K. (2014, Jan). New insights into the therapeutic potential of Girk channels. *Trends Neurosci, 37*(1), 20-29. https://doi.org/10.1016/j.tins.2013.10.006

Luscher, C., & Malenka, R. C. (2012, Jun 1). NMDA receptor-dependent long-term potentiation and long-term depression (LTP/LTD). *Cold Spring Harb Perspect Biol, 4*(6). https://doi.org/10.1101/cshperspect.a005710

Luttrell, L. M., & Miller, W. E. (2013). Arrestins as regulators of kinases and phosphatases. In *Progress in molecular biology and translational science* (Vol. 118, pp. 115-147). Elsevier.

Lutz, P. E., & Kieffer, B. L. (2013, Mar). Opioid receptors: distinct roles in mood disorders. *Trends Neurosci, 36*(3), 195-206. https://doi.org/10.1016/j.tins.2012.11.002

Malenka, R. C., & Nicoll, R. A. (1993, Dec). NMDA-receptor-dependent synaptic plasticity: multiple forms and mechanisms. *Trends Neurosci, 16*(12), 521-527. https://doi.org/10.1016/0166-2236(93)90197-t

Malenka, R. C., & Nicoll, R. A. (1999, Sep 17). Long-term potentiation--a decade of progress? *Science, 285*(5435), 1870-1874. https://doi.org/10.1126/science.285.5435.1870

Mamiya, N., Fukushima, H., Suzuki, A., Matsuyama, Z., Homma, S., Frankland, P. W., & Kida, S. (2009, Jan 14). Brain region-specific gene expression activation required for reconsolidation and extinction of contextual fear memory. *J Neurosci, 29*(2), 402-413. https://doi.org/10.1523/JNEUROSCI.4639-08.2009

Manglik, A., Lin, H., Aryal, D. K., McCorvy, J. D., Dengler, D., Corder, G., Levit, A., Kling, R. C., Bernat, V., Hubner, H., Huang, X. P., Sassano, M. F., Giguere, P. M., Lober, S., Da, D., Scherrer, G., Kobilka, B. K., Gmeiner, P., Roth, B. L., & Shoichet, B. K. (2016, Sep 8). Structure-based discovery of opioid analgesics with reduced side effects. *Nature, 537*(7619), 185-190. https://doi.org/10.1038/nature19112

Mansour, A., Khachaturian, H., Lewis, M. E., Akil, H., & Watson, S. J. (1987, Aug). Autoradiographic differentiation of mu, delta, and kappa opioid receptors in the rat forebrain and midbrain. *J Neurosci, 7*(8), 2445-2464. https://www.ncbi.nlm.nih.gov/pubmed/3039080

Mansour, A., Khachaturian, H., Lewis, M. E., Akil, H., & Watson, S. J. (1988, Jul). Anatomy of CNS opioid receptors. *Trends Neurosci, 11*(7), 308-314. https://doi.org/10.1016/0166-2236(88)90093-8

Maren, S. (2001). Neurobiology of Pavlovian fear conditioning. *Annu Rev Neurosci, 24*, 897-931. https://doi.org/10.1146/annurev.neuro.24.1.897

Marinissen, M. J., & Gutkind, J. S. (2001, Jul). G-protein-coupled receptors and signaling networks: emerging paradigms. *Trends Pharmacol Sci, 22*(7), 368-376. https://www.ncbi.nlm.nih.gov/pubmed/11431032

Marron Fdez de Velasco, E., Law, P. Y., & Rodriguez, R. E. (2009, Sep). Mu opioid receptor from the zebrafish exhibits functional characteristics as those of mammalian mu opioid receptor. *Zebrafish, 6*(3), 259-268. https://doi.org/10.1089/zeb.2009.0594

Martin, K. C., Michael, D., Rose, J. C., Barad, M., Casadio, A., Zhu, H., & Kandel, E. R. (1997, Jun). MAP kinase translocates into the nucleus of the presynaptic cell and is required for long-term facilitation in Aplysia. *Neuron, 18*(6), 899-912. https://www.ncbi.nlm.nih.gov/pubmed/9208858

Martini, L., & Whistler, J. L. (2007, Oct). The role of mu opioid receptor desensitization and endocytosis in morphine tolerance and dependence. *Curr Opin Neurobiol, 17*(5), 556-564. https://doi.org/10.1016/j.conb.2007.10.004

Masri, B., Salahpour, A., Didriksen, M., Ghisi, V., Beaulieu, J. M., Gainetdinov, R. R., & Caron, M. G. (2008, Sep 9). Antagonism of dopamine D2 receptor/beta-arrestin 2 interaction is a common property of clinically effective antipsychotics. *Proc Natl Acad Sci U S A, 105*(36), 13656-13661. https://doi.org/10.1073/pnas.0803522105

Massaly, N., Copits, B. A., Wilson-Poe, A. R., Hipolito, L., Markovic, T., Yoon, H. J., Liu, S., Walicki, M. C., Bhatti, D. L., Sirohi, S., Klaas, A., Walker, B. M., Neve, R., Cahill, C. M., Shoghi, K. I., Gereau, R. W. t., McCall, J. G., Al-Hasani, R., Bruchas, M. R., & Moron, J. A. (2019, May 8). Pain-Induced Negative Affect Is Mediated via Recruitment of The Nucleus Accumbens Kappa Opioid System. *Neuron, 102*(3), 564-573 e566. https://doi.org/10.1016/j.neuron.2019.02.029

Mathur, P., & Guo, S. (2011, Jun 1). Differences of acute versus chronic ethanol exposure on anxiety-like behavioral responses in zebrafish. *Behav Brain Res, 219*(2), 234-239. https://doi.org/10.1016/j.bbr.2011.01.019

McDonald, A. J. (1982a, Jul 10). Cytoarchitecture of the central amygdaloid nucleus of the rat. *J Comp Neurol, 208*(4), 401-418. https://doi.org/10.1002/cne.902080409

McDonald, A. J. (1982b, Dec 10). Neurons of the lateral and basolateral amygdaloid nuclei: a Golgi study in the rat. *J Comp Neurol, 212*(3), 293-312. https://doi.org/10.1002/cne.902120307

McDonald, A. J. (1985, Jan 21). Immunohistochemical identification of gamma-aminobutyric acid-containing neurons in the rat basolateral amygdala. *Neurosci Lett, 53*(2), 203-207. https://doi.org/10.1016/0304-3940(85)90186-7

McFadzean, I., Mullaney, I., Brown, D. A., & Milligan, G. (1989, Aug). Antibodies to the GTP binding protein, Go, antagonize noradrenaline-induced calcium current inhibition in NG108-15 hybrid cells. *Neuron, 3*(2), 177-182. https://www.ncbi.nlm.nih.gov/pubmed/2560391

McKay, M. M., & Morrison, D. K. (2007, May 14). Integrating signals from RTKs to ERK/MAPK. *Oncogene, 26*(22), 3113-3121. https://doi.org/10.1038/sj.onc.1210394

McNamara, C. R., Mandel-Brehm, J., Bautista, D. M., Siemens, J., Deranian, K. L., Zhao, M., Hayward, N. J., Chong, J. A., Julius, D., Moran, M. M., & Fanger, C. M. (2007, Aug 14). TRPA1 mediates formalin-induced pain. *Proc Natl Acad Sci U S A, 104*(33), 13525-13530. https://doi.org/10.1073/pnas.0705924104

Melia, K. R., Falls, W. A., & Davis, M. (1992, Jul 3). Involvement of pertussis toxin sensitive G-proteins in conditioned fear-potentiated startle: possible involvement of the amygdala. *Brain Res, 584*(1-2), 141-148. https://www.ncbi.nlm.nih.gov/pubmed/1515934

Meller, E., Shen, C., Nikolao, T. A., Jensen, C., Tsimberg, Y., Chen, J., & Gruen, R. J. (2003, Jul 25). Region-specific effects of acute and repeated restraint stress on the phosphorylation of mitogen-activated protein kinases. *Brain Res, 979*(1-2), 57-64. https://www.ncbi.nlm.nih.gov/pubmed/12850571

Mittal, N., Minasyan, A., Romaneschi, N., Hakimian, J. K., Gonzalez-Fernandez, G., Albert, R., Desai, N., Mendez, I. A., Schallert, T., Ostlund, S. B., & Walwyn, W. (2017). Beta-arrestin 1 regulation of reward-motivated behaviors and glutamatergic function. *PLoS One, 12*(10), e0185796. https://doi.org/10.1371/journal.pone.0185796

Mochida, S. (2019, May 6). Presynaptic Calcium Channels. *Int J Mol Sci, 20*(9). https://doi.org/10.3390/ijms20092217

Moran, M. M., McAlexander, M. A., Biro, T., & Szallasi, A. (2011, Aug 1). Transient receptor potential channels as therapeutic targets. *Nat Rev Drug Discov, 10*(8), 601-620. https://doi.org/10.1038/nrd3456

Mores, K. L., Cummins, B. R., Cassell, R. J., & van Rijn, R. M. (2019). A Review of the Therapeutic Potential of Recently Developed G Protein-Biased Kappa Agonists. *Front Pharmacol, 10*, 407. https://doi.org/10.3389/fphar.2019.00407

Morgan, J. T., Chana, G., Pardo, C. A., Achim, C., Semendeferi, K., Buckwalter, J., Courchesne, E., & Everall, I. P. (2010, Aug 15). Microglial activation and increased microglial density observed in the dorsolateral prefrontal cortex in autism. *Biol Psychiatry, 68*(4), 368-376. https://doi.org/10.1016/j.biopsych.2010.05.024

Morgan, M. A., & Pfaff, D. W. (2002, Apr 15). Estrogen's effects on activity, anxiety, and fear in two mouse strains. *Behav Brain Res, 132*(1), 85-93. https://doi.org/10.1016/s0166-4328(01)00398-9

Morrison, D. K., & Davis, R. J. (2003). Regulation of MAP kinase signaling modules by scaffold proteins in mammals. *Annu Rev Cell Dev Biol, 19*, 91-118. https://doi.org/10.1146/annurev.cellbio.19.111401.091942

Moser, M. B., & Moser, E. I. (1998). Functional differentiation in the hippocampus. *Hippocampus, 8*(6), 608-619. https://doi.org/10.1002/(SICI)1098-1063(1998)8:6<608::AID-HIPO3>3.0.CO;2-7

Narita, M., Kaneko, C., Miyoshi, K., Nagumo, Y., Kuzumaki, N., Nakajima, M., Nanjo, K., Matsuzawa, K., Yamazaki, M., & Suzuki, T. (2006, Apr). Chronic pain induces anxiety with concomitant changes in opioidergic function in the amygdala. *Neuropsychopharmacology, 31*(4), 739-750. https://doi.org/10.1038/sj.npp.1300858

Nassini, R., Materazzi, S., Benemei, S., & Geppetti, P. (2014). The TRPA1 channel in inflammatory and neuropathic pain and migraine. *Rev Physiol Biochem Pharmacol, 167*, 1-43. https://doi.org/10.1007/112_2014_18

O'Brien, W. T., Huang, J., Buccafusca, R., Garskof, J., Valvezan, A. J., Berry, G. T., & Klein, P. S. (2011, Sep). Glycogen synthase kinase-3 is essential for beta-arrestin-2 complex formation and lithium-sensitive behaviors in mice. *J Clin Invest, 121*(9), 3756-3762. https://doi.org/10.1172/JCI45194

Oakley, R. H., Laporte, S. A., Holt, J. A., Caron, M. G., & Barak, L. S. (2000, Jun 2). Differential affinities of visual arrestin, beta arrestin1, and beta arrestin2 for G protein-coupled receptors delineate two major classes of receptors. *J Biol Chem, 275*(22), 17201-17210. https://doi.org/10.1074/jbc.M910348199

Oda, M., Kurogi, M., Kubo, Y., & Saitoh, O. (2016, Mar). Sensitivities of Two Zebrafish TRPA1 Paralogs to Chemical and Thermal Stimuli Analyzed in Heterologous Expression Systems. *Chem Senses, 41*(3), 261-272. https://doi.org/10.1093/chemse/bjv091

Oka, T., Tsumori, T., Yokota, S., & Yasui, Y. (2008, Dec). Neuroanatomical and neurochemical organization of projections from the central amygdaloid nucleus to the nucleus retroambiguus via the periaqueductal gray in the rat. *Neurosci Res, 62*(4), 286-298. https://doi.org/10.1016/j.neures.2008.10.004

Onnink, A. M., Zwiers, M. P., Hoogman, M., Mostert, J. C., Kan, C. C., Buitelaar, J., & Franke, B. (2014, Mar). Brain alterations in adult ADHD: effects of gender, treatment and comorbid depression. *Eur Neuropsychopharmacol, 24*(3), 397-409. https://doi.org/10.1016/j.euroneuro.2013.11.011

Overmyer, K. A., Thonusin, C., Qi, N. R., Burant, C. F., & Evans, C. R. (2015). Impact of anesthesia and euthanasia on metabolomics of mammalian tissues: studies in a C57BL/6J mouse model. *PLoS One, 10*(2), e0117232. https://doi.org/10.1371/journal.pone.0117232

Parichy, D. M., Elizondo, M. R., Mills, M. G., Gordon, T. N., & Engeszer, R. E. (2009, Dec). Normal table of postembryonic zebrafish development: staging by externally visible anatomy of the living fish. *Dev Dyn, 238*(12), 2975-3015. https://doi.org/10.1002/dvdy.22113

Pavlov, P. I. (2010, Jul). Conditioned reflexes: An investigation of the physiological activity of the cerebral cortex. *Ann Neurosci, 17*(3), 136-141. https://doi.org/10.5214/ans.0972-7531.1017309

Paxinos, G., & Franklin, K. B. (2004). *The mouse brain in stereotaxic coordinates*. Gulf professional publishing.

Pearson, J. (2012, Jun 19). Associative learning: Pavlovian conditioning without awareness. *Curr Biol, 22*(12), R495-496. https://doi.org/10.1016/j.cub.2012.04.042

Peirs, C., & Seal, R. P. (2016, Nov 4). Neural circuits for pain: Recent advances and current views. *Science, 354*(6312), 578-584. https://doi.org/10.1126/science.aaf8933

Perrine, S. A., Hoshaw, B. A., & Unterwald, E. M. (2006, Apr). Delta opioid receptor ligands modulate anxiety-like behaviors in the rat. *Br J Pharmacol, 147*(8), 864-872. https://doi.org/10.1038/sj.bjp.0706686

Petrus, M., Peier, A. M., Bandell, M., Hwang, S. W., Huynh, T., Olney, N., Jegla, T., & Patapoutian, A. (2007, Dec 17). A role of TRPA1 in mechanical hyperalgesia is revealed by pharmacological inhibition. *Mol Pain, 3*, 40. https://doi.org/10.1186/1744-8069-3-40

Pezze, M. A., & Feldon, J. (2004, Dec). Mesolimbic dopaminergic pathways in fear conditioning. *Prog Neurobiol, 74*(5), 301-320. https://doi.org/10.1016/j.pneurobio.2004.09.004

Pezze, M. A., Feldon, J., & Murphy, C. A. (2002, Apr). Increased conditioned fear response and altered balance of dopamine in the shell and core of the nucleus accumbens during amphetamine withdrawal. *Neuropharmacology, 42*(5), 633-643. https://doi.org/10.1016/s0028-3908(02)00022-9

Pierce, K. L., & Lefkowitz, R. J. (2001, Oct). Classical and new roles of beta-arrestins in the regulation of G-protein-coupled receptors. *Nat Rev Neurosci, 2*(10), 727-733. https://doi.org/10.1038/35094577

Pierce, K. L., Premont, R. T., & Lefkowitz, R. J. (2002, Sep). Seven-transmembrane receptors. *Nat Rev Mol Cell Biol, 3*(9), 639-650. https://doi.org/10.1038/nrm908

Pontrello, C. G., Sun, M. Y., Lin, A., Fiacco, T. A., DeFea, K. A., & Ethell, I. M. (2012, Feb 14). Cofilin under control of beta-arrestin-2 in NMDA-dependent dendritic spine plasticity, long-term depression (LTD), and learning. *Proc Natl Acad Sci U S A, 109*(7), E442-451. https://doi.org/10.1073/pnas.1118803109

Por, E. D., Bierbower, S. M., Berg, K. A., Gomez, R., Akopian, A. N., Wetsel, W. C., & Jeske, N. A. (2012, Oct 26). beta-Arrestin-2 desensitizes the transient receptor potential vanilloid 1 (TRPV1) channel. *J Biol Chem, 287*(44), 37552-37563. https://doi.org/10.1074/jbc.M112.391847

Pradhan, A. A., Befort, K., Nozaki, C., Gaveriaux-Ruff, C., & Kieffer, B. L. (2011, Oct). The delta opioid receptor: an evolving target for the treatment of brain disorders. *Trends Pharmacol Sci, 32*(10), 581-590. https://doi.org/10.1016/j.tips.2011.06.008

Pradhan, A. A., Perroy, J., Walwyn, W. M., Smith, M. L., Vicente-Sanchez, A., Segura, L., Bana, A., Kieffer, B. L., & Evans, C. J. (2016, Mar 23). Agonist-Specific Recruitment of Arrestin Isoforms Differentially Modify Delta Opioid Receptor Function. *J Neurosci, 36*(12), 3541-3551. https://doi.org/10.1523/JNEUROSCI.4124-15.2016

Prober, D. A., Zimmerman, S., Myers, B. R., McDermott, B. M., Jr., Kim, S. H., Caron, S., Rihel, J., Solnica-Krezel, L., Julius, D., Hudspeth, A. J., & Schier, A. F. (2008, Oct 1). Zebrafish TRPA1 channels are required for chemosensation but not for thermosensation or mechanosensory hair cell function. *J Neurosci, 28*(40), 10102-10110. https://doi.org/10.1523/JNEUROSCI.2740-08.2008

Raehal, K. M., & Bohn, L. M. (2011, Jan). The role of beta-arrestin2 in the severity of antinociceptive tolerance and physical dependence induced by different opioid pain therapeutics. *Neuropharmacology, 60*(1), 58-65. https://doi.org/10.1016/j.neuropharm.2010.08.003

Raehal, K. M., Walker, J. K., & Bohn, L. M. (2005, Sep). Morphine side effects in beta-arrestin 2 knockout mice. *J Pharmacol Exp Ther, 314*(3), 1195-1201. https://doi.org/10.1124/jpet.105.087254

Ragnauth, A., Schuller, A., Morgan, M., Chan, J., Ogawa, S., Pintar, J., Bodnar, R. J., & Pfaff, D. W. (2001, Feb 13). Female preproenkephalin-knockout mice display altered emotional responses. *Proc Natl Acad Sci U S A, 98*(4), 1958-1963. https://doi.org/10.1073/pnas.041598498

Rainnie, D. G., Mania, I., Mascagni, F., & McDonald, A. J. (2006, Sep 1). Physiological and morphological characterization of parvalbumin-containing interneurons of the rat basolateral amygdala. *J Comp Neurol, 498*(1), 142-161. https://doi.org/10.1002/cne.21049

Raisinghani, M., Zhong, L., Jeffry, J. A., Bishnoi, M., Pabbidi, R. M., Pimentel, F., Cao, D. S., Evans, M. S., & Premkumar, L. S. (2011, Sep). Activation characteristics of transient receptor potential ankyrin 1 and its role in nociception. *Am J Physiol Cell Physiol, 301*(3), C587-600. https://doi.org/10.1152/ajpcell.00465.2010

Rajagopal, S., Rajagopal, K., & Lefkowitz, R. J. (2010, May). Teaching old receptors new tricks: biasing seven-transmembrane receptors. *Nat Rev Drug Discov, 9*(5), 373-386. https://doi.org/10.1038/nrd3024

Ranjan, R., Gupta, P., & Shukla, A. K. (2016, Apr 4). GPCR Signaling: beta-arrestins Kiss and Remember. *Curr Biol, 26*(7), R285-288. https://doi.org/10.1016/j.cub.2016.02.056

Rankovic, Z., Brust, T. F., & Bohn, L. M. (2016, Jan 15). Biased agonism: An emerging paradigm in GPCR drug discovery. *Bioorg Med Chem Lett, 26*(2), 241-250. https://doi.org/10.1016/j.bmcl.2015.12.024

Reiter, E., & Lefkowitz, R. J. (2006, May-Jun). GRKs and beta-arrestins: roles in receptor silencing, trafficking and signaling. *Trends Endocrinol Metab, 17*(4), 159-165. https://doi.org/10.1016/j.tem.2006.03.008

Ren, X. R., Reiter, E., Ahn, S., Kim, J., Chen, W., & Lefkowitz, R. J. (2005, Feb 1). Different G protein-coupled receptor kinases govern G protein and beta-arrestin-mediated signaling of V2 vasopressin receptor. *Proc Natl Acad Sci U S A, 102*(5), 1448-1453. https://doi.org/10.1073/pnas.0409534102

Reus, G. Z., Vieira, F. G., Abelaira, H. M., Michels, M., Tomaz, D. B., dos Santos, M. A., Carlessi, A. S., Neotti, M. V., Matias, B. I., Luz, J. R., Dal-Pizzol, F., & Quevedo, J. (2014, Aug). MAPK signaling correlates with the antidepressant effects of ketamine. *J Psychiatr Res, 55*, 15-21. https://doi.org/10.1016/j.jpsychires.2014.04.010

Richards, E. M., Mathews, D. C., Luckenbaugh, D. A., Ionescu, D. F., Machado-Vieira, R., Niciu, M. J., Duncan, W. C., Nolan, N. M., Franco-Chaves, J. A., Hudzik, T., Maciag, C., Li, S., Cross, A., Smith, M. A., & Zarate, C. A., Jr. (2016, Mar). A randomized, placebo-controlled pilot trial of the delta opioid receptor agonist AZD2327 in anxious depression. *Psychopharmacology (Berl), 233*(6), 1119-1130. https://doi.org/10.1007/s00213-015-4195-4

Risbud, M. V., Guttapalli, A., Albert, T. J., & Shapiro, I. M. (2005, Nov 15). Hypoxia activates MAPK activity in rat nucleus pulposus cells: regulation of integrin expression and cell survival. *Spine (Phila Pa 1976),* *30*(22), 2503-2509. https://www.ncbi.nlm.nih.gov/pubmed/16284587

Ritter, S. L., & Hall, R. A. (2009, Dec). Fine-tuning of GPCR activity by receptor-interacting proteins. *Nat Rev Mol Cell Biol, 10*(12), 819-830. https://doi.org/10.1038/nrm2803

Robbins, T. W., & Everitt, B. J. (2002, Nov). Limbic-striatal memory systems and drug addiction. *Neurobiol Learn Mem, 78*(3), 625-636. https://www.ncbi.nlm.nih.gov/pubmed/12559840

Robins, M. T., Chiang, T., Berry, J. N., Ko, M. J., Ha, J. E., & van Rijn, R. M. (2018). Behavioral Characterization of beta-Arrestin 1 Knockout Mice in Anxiety-Like and Alcohol Behaviors. *Front Behav Neurosci, 12*, 54. https://doi.org/10.3389/fnbeh.2018.00054

Robins, M. T., Chiang, T., Mores, K. L., Alongkronrusmee, D., & van Rijn, R. M. (2018). Critical Role for Gi/o-Protein Activity in the Dorsal Striatum in the Reduction of Voluntary Alcohol Intake in C57Bl/6 Mice. *Front Psychiatry, 9*, 112. https://doi.org/10.3389/fpsyt.2018.00112

Rosenblum, A., Marsch, L. A., Joseph, H., & Portenoy, R. K. (2008, Oct). Opioids and the treatment of chronic pain: controversies, current status, and future directions. *Exp Clin Psychopharmacol, 16*(5), 405-416. https://doi.org/10.1037/a0013628

Rowan, M. P., Bierbower, S. M., Eskander, M. A., Szteyn, K., Por, E. D., Gomez, R., Veldhuis, N., Bunnett, N. W., & Jeske, N. A. (2014). Activation of mu opioid receptors sensitizes transient receptor potential vanilloid type 1 (TRPV1) via beta-arrestin-2-mediated cross-talk. *PLoS One, 9*(4), e93688. https://doi.org/10.1371/journal.pone.0093688

Rowan, M. P., Szteyn, K., Doyle, A. P., Gomez, R., Henry, M. A., & Jeske, N. A. (2014, Aug 1). beta-arrestin-2-biased agonism of delta opioid receptors sensitizes transient receptor potential vanilloid type 1 (TRPV1) in primary sensory neurons. *Mol Pain, 10*, 50. https://doi.org/10.1186/1744-8069-10-50

Rozenfeld, R., & Devi, L. A. (2007, Aug). Receptor heterodimerization leads to a switch in signaling: beta-arrestin2-mediated ERK activation by mu-delta opioid receptor heterodimers. *FASEB J, 21*(10), 2455-2465. https://doi.org/10.1096/fj.06-7793com

Saitoh, A., Kimura, Y., Suzuki, T., Kawai, K., Nagase, H., & Kamei, J. (2004, Jul). Potential anxiolytic and antidepressant-like activities of SNC80, a selective delta-opioid agonist, in behavioral models in rodents. *J Pharmacol Sci, 95*(3), 374-380. https://www.ncbi.nlm.nih.gov/pubmed/15272214

Saitoh, A., Suzuki, S., Soda, A., Ohashi, M., Yamada, M., Oka, J. I., Nagase, H., & Yamada, M. (2018, Jan 15). The delta opioid receptor agonist KNT-127 in the prelimbic medial prefrontal cortex attenuates veratrine-induced anxiety-like behaviors in mice. *Behav Brain Res, 336*, 77-84. https://doi.org/10.1016/j.bbr.2017.08.041

Schlessinger, J. (2000, Oct 13). Cell signaling by receptor tyrosine kinases. *Cell, 103*(2), 211-225. https://doi.org/10.1016/s0092-8674(00)00114-8

Schmid, C. L., & Bohn, L. M. (2009, Mar). Physiological and pharmacological implications of beta-arrestin regulation. *Pharmacol Ther, 121*(3), 285-293. https://doi.org/10.1016/j.pharmthera.2008.11.005

Seger, R., & Krebs, E. G. (1995, Jun). The MAPK signaling cascade. *FASEB J, 9*(9), 726-735. https://www.ncbi.nlm.nih.gov/pubmed/7601337

Shah, B. H., & Catt, K. J. (2004, Jan). GPCR-mediated transactivation of RTKs in the CNS: mechanisms and consequences. *Trends Neurosci, 27*(1), 48-53. https://doi.org/10.1016/j.tins.2003.11.003

Shenoy, S. K., Drake, M. T., Nelson, C. D., Houtz, D. A., Xiao, K., Madabushi, S., Reiter, E., Premont, R. T., Lichtarge, O., & Lefkowitz, R. J. (2006, Jan 13). beta-arrestin-dependent, G protein-independent ERK1/2 activation by the beta2 adrenergic receptor. *J Biol Chem, 281*(2), 1261-1273. https://doi.org/10.1074/jbc.M506576200

Shenoy, S. K., & Lefkowitz, R. J. (2011, Sep). beta-Arrestin-mediated receptor trafficking and signal transduction. *Trends Pharmacol Sci, 32*(9), 521-533. https://doi.org/10.1016/j.tips.2011.05.002

Shi, Y., Feng, Y., Kang, J., Liu, C., Li, Z., Li, D., Cao, W., Qiu, J., Guo, Z., Bi, E., Zang, L., Lu, C., Zhang, J. Z., & Pei, G. (2007, Aug). Critical regulation of CD4+ T cell survival and autoimmunity by beta-arrestin 1. *Nat Immunol, 8*(8), 817-824. https://doi.org/10.1038/ni1489

Shin, L. M., & Liberzon, I. (2010, Jan). The neurocircuitry of fear, stress, and anxiety disorders. *Neuropsychopharmacology, 35*(1), 169-191. https://doi.org/10.1038/npp.2009.83

Shukla, A. K., Kim, J., Ahn, S., Xiao, K., Shenoy, S. K., Liedtke, W., & Lefkowitz, R. J. (2010, Sep 24). Arresting a transient receptor potential (TRP) channel: beta-arrestin 1 mediates ubiquitination and functional down-regulation of TRPV4. *J Biol Chem, 285*(39), 30115-30125. https://doi.org/10.1074/jbc.M110.141549

Shukla, A. K., Xiao, K., & Lefkowitz, R. J. (2011, Sep). Emerging paradigms of beta-arrestin-dependent seven transmembrane receptor signaling. *Trends Biochem Sci, 36*(9), 457-469. https://doi.org/10.1016/j.tibs.2011.06.003

Siehler, S. (2009, Sep). Regulation of RhoGEF proteins by G12/13-coupled receptors. *Br J Pharmacol, 158*(1), 41-49. https://doi.org/10.1111/j.1476-5381.2009.00121.x

Soergel, D. G., Subach, R. A., Burnham, N., Lark, M. W., James, I. E., Sadler, B. M., Skobieranda, F., Violin, J. D., & Webster, L. R. (2014, Sep). Biased agonism of the mu-opioid receptor by TRV130 increases analgesia and reduces on-target adverse effects versus morphine: A randomized, double-blind, placebo-controlled, crossover study in healthy volunteers. *Pain, 155*(9), 1829-1835. https://doi.org/10.1016/j.pain.2014.06.011

Solati, J., Zarrindast, M. R., & Salari, A. A. (2010, Dec). Dorsal hippocampal opioidergic system modulates anxiety-like behaviors in adult male Wistar rats. *Psychiatry Clin Neurosci, 64*(6), 634-641. https://doi.org/10.1111/j.1440-1819.2010.02143.x

Stariha, R. L., & Kim, S. U. (2001, Mar 15). Protein kinase C and mitogen-activated protein kinase signalling in oligodendrocytes. *Microsc Res Tech, 52*(6), 680-688. https://doi.org/10.1002/jemt.1052

Stevens, J. S., Padilla, S., DeMarini, D. M., Hunter, D. L., Martin, W. K., Thompson, L. C., Gilmour, M. I., Hazari, M. S., & Farraj, A. K. (2018, Feb 1). Zebrafish Locomotor Responses Reveal Irritant Effects of Fine Particulate Matter Extracts and a Role for TRPA1. *Toxicol Sci, 161*(2), 290-299. https://doi.org/10.1093/toxsci/kfx217

Story, G. M., Peier, A. M., Reeve, A. J., Eid, S. R., Mosbacher, J., Hricik, T. R., Earley, T. J., Hergarden, A. C., Andersson, D. A., Hwang, S. W., McIntyre, P., Jegla, T., Bevan, S., & Patapoutian, A. (2003, Mar 21). ANKTM1, a TRP-like channel expressed in nociceptive neurons, is activated by cold temperatures. *Cell, 112*(6), 819-829. https://www.ncbi.nlm.nih.gov/pubmed/12654248

Strange, B. A., Witter, M. P., Lein, E. S., & Moser, E. I. (2014, Oct). Functional organization of the hippocampal longitudinal axis. *Nat Rev Neurosci, 15*(10), 655-669. https://doi.org/10.1038/nrn3785

Strungs, E. G., & Luttrell, L. M. (2014). Arrestin-dependent activation of ERK and Src family kinases. *Handb Exp Pharmacol, 219*, 225-257. https://doi.org/10.1007/978-3-642-41199-1_12

Sturm, V., Lenartz, D., Koulousakis, A., Treuer, H., Herholz, K., Klein, J. C., & Klosterkotter, J. (2003, Dec). The nucleus accumbens: a target for deep brain stimulation in obsessive-compulsive- and anxiety-disorders. *J Chem Neuroanat, 26*(4), 293-299. https://www.ncbi.nlm.nih.gov/pubmed/14729131

Sugiyama, A., Yamada, M., Furuie, H., Gotoh, L., Saitoh, A., Nagase, H., Oka, J. I., & Yamada, M. (2019, Mar). Systemic administration of a delta opioid receptor agonist, KNT-127, facilitates extinction learning of fear memory in rats. *J Pharmacol Sci, 139*(3), 174-179. https://doi.org/10.1016/j.jphs.2019.01.002

Surmeier, D. J., Graves, S. M., & Shen, W. (2014, Dec). Dopaminergic modulation of striatal networks in health and Parkinson's disease. *Curr Opin Neurobiol, 29*, 109-117. https://doi.org/10.1016/j.conb.2014.07.008

Swanson, L. W., & Cowan, W. M. (1977, Mar 1). An autoradiographic study of the organization of the efferent connections of the hippocampal formation in the rat. *J Comp Neurol, 172*(1), 49-84. https://doi.org/10.1002/cne.901720104

Sweatt, J. D. (2001, Jan). The neuronal MAP kinase cascade: a biochemical signal integration system subserving synaptic plasticity and memory. *J Neurochem, 76*(1), 1-10. https://www.ncbi.nlm.nih.gov/pubmed/11145972

Szallasi, A., & Blumberg, P. M. (1999, Jun). Vanilloid (Capsaicin) receptors and mechanisms. *Pharmacol Rev, 51*(2), 159-212. https://www.ncbi.nlm.nih.gov/pubmed/10353985

Takahashi, L. K. (2001, Dec). Role of CRF(1) and CRF(2) receptors in fear and anxiety. *Neurosci Biobehav Rev, 25*(7-8), 627-636. https://www.ncbi.nlm.nih.gov/pubmed/11801288

Tasken, K., & Aandahl, E. M. (2004, Jan). Localized effects of cAMP mediated by distinct routes of protein kinase A. *Physiol Rev, 84*(1), 137-167. https://doi.org/10.1152/physrev.00021.2003

Taylor, J. C., Dewberry, L. S., Totsch, S. K., Yessick, L. R., DeBerry, J. J., Watts, S. A., & Sorge, R. E. (2017, May 15). A novel zebrafish-based model of nociception. *Physiol Behav, 174*, 83-88. https://doi.org/10.1016/j.physbeh.2017.03.009

Terburg, D., Scheggia, D., Triana Del Rio, R., Klumpers, F., Ciobanu, A. C., Morgan, B., Montoya, E. R., Bos, P. A., Giobellina, G., van den Burg, E. H., de Gelder, B., Stein, D. J., Stoop, R., & van Honk, J. (2018, Oct 18). The Basolateral Amygdala Is Essential for Rapid Escape: A Human and Rodent Study. *Cell, 175*(3), 723-735 e716. https://doi.org/10.1016/j.cell.2018.09.028

Thathiah, A., Horre, K., Snellinx, A., Vandewyer, E., Huang, Y., Ciesielska, M., De Kloe, G., Munck, S., & De Strooper, B. (2013, Jan). beta-arrestin 2 regulates Abeta generation and gamma-secretase activity in Alzheimer's disease. *Nat Med, 19*(1), 43-49. https://doi.org/10.1038/nm.3023

Thomas, G. M., & Huganir, R. L. (2004, Mar). MAPK cascade signalling and synaptic plasticity. *Nat Rev Neurosci, 5*(3), 173-183. https://doi.org/10.1038/nrn1346

Thompson, S. M., Capogna, M., & Scanziani, M. (1993, Jun). Presynaptic inhibition in the hippocampus. *Trends Neurosci, 16*(6), 222-227. https://doi.org/10.1016/0166-2236(93)90160-n

Tohgo, A., Pierce, K. L., Choy, E. W., Lefkowitz, R. J., & Luttrell, L. M. (2002, Mar 15). beta-Arrestin scaffolding of the ERK cascade enhances cytosolic ERK activity but inhibits ERK-mediated transcription following angiotensin AT1a receptor stimulation. *J Biol Chem, 277*(11), 9429-9436. https://doi.org/10.1074/jbc.M106457200

Tominaga, M. (2007). Nociception and TRP channels. *Handb Exp Pharmacol*(179), 489-505. https://doi.org/10.1007/978-3-540-34891-7_29

Tominaga, M., Caterina, M. J., Malmberg, A. B., Rosen, T. A., Gilbert, H., Skinner, K., Raumann, B. E., Basbaum, A. I., & Julius, D. (1998, Sep). The cloned capsaicin receptor integrates multiple pain-producing stimuli. *Neuron, 21*(3), 531-543. https://doi.org/10.1016/s0896-6273(00)80564-4

Tottenham, N., Hertzig, M. E., Gillespie-Lynch, K., Gilhooly, T., Millner, A. J., & Casey, B. J. (2014, Jan). Elevated amygdala response to faces and gaze aversion in autism spectrum disorder. *Soc Cogn Affect Neurosci, 9*(1), 106-117. https://doi.org/10.1093/scan/nst050

Tovote, P., Fadok, J. P., & Luthi, A. (2015, Jun). Neuronal circuits for fear and anxiety. *Nat Rev Neurosci, 16*(6), 317-331. https://doi.org/10.1038/nrn3945

Treede, R. D., Rief, W., Barke, A., Aziz, Q., Bennett, M. I., Benoliel, R., Cohen, M., Evers, S., Finnerup, N. B., First, M. B., Giamberardino, M. A., Kaasa, S., Kosek, E., Lavand'homme, P., Nicholas, M., Perrot, S., Scholz, J., Schug, S., Smith, B. H., Svensson, P., Vlaeyen, J. W., & Wang, S. J. (2015, Jun). A classification of chronic pain for ICD-11. *Pain, 156*(6), 1003-1007. https://doi.org/10.1097/j.pain.0000000000000160

Tye, K. M., Prakash, R., Kim, S. Y., Fenno, L. E., Grosenick, L., Zarabi, H., Thompson, K. R., Gradinaru, V., Ramakrishnan, C., & Deisseroth, K. (2011, Mar 17). Amygdala circuitry mediating reversible and bidirectional control of anxiety. *Nature, 471*(7338), 358-362. https://doi.org/10.1038/nature09820

Tzingounis, A. V., von Zastrow, M., & Yudowski, G. A. (2010, Dec 7). {Beta}-blocker drugs mediate calcium signaling in native central nervous system neurons by {beta}-arrestin-biased agonism. *Proc Natl Acad Sci U S A, 107*(49), 21028-21033. https://doi.org/10.1073/pnas.1004169107

Urban, J. D., Clarke, W. P., von Zastrow, M., Nichols, D. E., Kobilka, B., Weinstein, H., Javitch, J. A., Roth, B. L., Christopoulos, A., Sexton, P. M., Miller, K. J., Spedding, M., & Mailman, R. B. (2007, Jan). Functional selectivity and classical concepts of quantitative pharmacology. *J Pharmacol Exp Ther, 320*(1), 1-13. https://doi.org/10.1124/jpet.106.104463

Urs, N. M., Gee, S. M., Pack, T. F., McCorvy, J. D., Evron, T., Snyder, J. C., Yang, X., Rodriguiz, R. M., Borrelli, E., Wetsel, W. C., Jin, J., Roth, B. L., O'Donnell, P., & Caron, M. G. (2016, Dec 13). Distinct cortical and striatal actions of a beta-arrestin-biased dopamine D2 receptor ligand reveal unique antipsychotic-like properties. *Proc Natl Acad Sci U S A, 113*(50), E8178-E8186. https://doi.org/10.1073/pnas.1614347113

van Rijn, R. M., Brissett, D. I., & Whistler, J. L. (2010, Oct). Dual efficacy of delta opioid receptor-selective ligands for ethanol drinking and anxiety. *J Pharmacol Exp Ther, 335*(1), 133-139. https://doi.org/10.1124/jpet.110.170969

van Rijn, R. M., Brissett, D. I., & Whistler, J. L. (2012, Feb 1). Emergence of functional spinal delta opioid receptors after chronic ethanol exposure. *Biol Psychiatry, 71*(3), 232-238. https://doi.org/10.1016/j.biopsych.2011.07.015

van Rijn, R. M., Harvey, J. H., Brissett, D. I., DeFriel, J. N., & Whistler, J. L. (2013, Jan). Novel screening assay for the selective detection of G-protein-coupled receptor heteromer signaling. *J Pharmacol Exp Ther, 344*(1), 179-188. https://doi.org/10.1124/jpet.112.198655

Vann, S. D., Brown, M. W., Erichsen, J. T., & Aggleton, J. P. (2000, Apr 1). Fos imaging reveals differential patterns of hippocampal and parahippocampal subfield activation in rats in response to different spatial memory tests. *J Neurosci, 20*(7), 2711-2718. https://www.ncbi.nlm.nih.gov/pubmed/10729352

Vardanyan, A., Wang, R., Vanderah, T. W., Ossipov, M. H., Lai, J., Porreca, F., & King, T. (2009, Mar). TRPV1 receptor in expression of opioid-induced hyperalgesia. *J Pain, 10*(3), 243-252. https://doi.org/10.1016/j.jpain.2008.07.004

Vicente-Sanchez, A., Dripps, I. J., Tipton, A. F., Akbari, H., Akbari, A., Jutkiewicz, E. M., & Pradhan, A. A. (2018, Jul). Tolerance to high-internalizing delta opioid receptor agonist is critically mediated by arrestin 2. *Br J Pharmacol, 175*(14), 3050-3059. https://doi.org/10.1111/bph.14353

Villalba, M., Bockaert, J., & Journot, L. (1997, Jan 1). Pituitary adenylate cyclase-activating polypeptide (PACAP-38) protects cerebellar granule neurons from apoptosis by activating the mitogen-activated protein kinase (MAP kinase) pathway. *J Neurosci, 17*(1), 83-90. https://www.ncbi.nlm.nih.gov/pubmed/8987738

Walker, D. L., & Davis, M. (2002, Nov). Quantifying fear potentiated startle using absolute versus proportional increase scoring methods: implications for the neurocircuitry of fear and anxiety. *Psychopharmacology (Berl), 164*(3), 318-328. https://doi.org/10.1007/s00213-002-1213-0

Wang, D., Tawfik, V. L., Corder, G., Low, S. A., Francois, A., Basbaum, A. I., & Scherrer, G. (2018, Apr 4). Functional Divergence of Delta and Mu Opioid Receptor Organization in CNS Pain Circuits. *Neuron, 98*(1), 90-108 e105. https://doi.org/10.1016/j.neuron.2018.03.002

Wang, J. Q., Tang, Q., Parelkar, N. K., Liu, Z., Samdani, S., Choe, E. S., Yang, L., & Mao, L. (2004, Feb). Glutamate signaling to Ras-MAPK in striatal neurons: mechanisms for inducible gene expression and plasticity. *Mol Neurobiol, 29*(1), 1-14. https://doi.org/10.1385/MN:29:1:01

Wefers, B., Hitz, C., Holter, S. M., Trumbach, D., Hansen, J., Weber, P., Putz, B., Deussing, J. M., de Angelis, M. H., Roenneberg, T., Zheng, F., Alzheimer, C., Silva, A., Wurst, W., & Kuhn, R. (2012). MAPK signaling determines anxiety in the juvenile mouse brain but depression-like behavior in adults. *PLoS One, 7*(4), e35035. https://doi.org/10.1371/journal.pone.0035035

West, A. E., & Greenberg, M. E. (2011, Jun 1). Neuronal activity-regulated gene transcription in synapse development and cognitive function. *Cold Spring Harb Perspect Biol, 3*(6). https://doi.org/10.1101/cshperspect.a005744

Wetzker, R., & Bohmer, F. D. (2003, Aug). Transactivation joins multiple tracks to the ERK/MAPK cascade. *Nat Rev Mol Cell Biol, 4*(8), 651-657. https://doi.org/10.1038/nrm1173

Whalen, E. J., Rajagopal, S., & Lefkowitz, R. J. (2011, Mar). Therapeutic potential of beta-arrestin- and G protein-biased agonists. *Trends Mol Med, 17*(3), 126-139. https://doi.org/10.1016/j.molmed.2010.11.004

Whistler, J. L., & von Zastrow, M. (1998, Aug 18). Morphine-activated opioid receptors elude desensitization by beta-arrestin. *Proc Natl Acad Sci U S A, 95*(17), 9914-9919. https://doi.org/10.1073/pnas.95.17.9914

Wilden, U., Wust, E., Weyand, I., & Kuhn, H. (1986, Oct 27). Rapid affinity purification of retinal arrestin (48 kDa protein) via its light-dependent binding to phosphorylated rhodopsin. *FEBS Lett, 207*(2), 292-295. https://doi.org/10.1016/0014-5793(86)81507-1

Wisler, J. W., DeWire, S. M., Whalen, E. J., Violin, J. D., Drake, M. T., Ahn, S., Shenoy, S. K., & Lefkowitz, R. J. (2007, Oct 16). A unique mechanism of beta-blocker action: carvedilol stimulates beta-arrestin signaling. *Proc Natl Acad Sci U S A, 104*(42), 16657-16662. https://doi.org/10.1073/pnas.0707936104

Witherow, D. S., Garrison, T. R., Miller, W. E., & Lefkowitz, R. J. (2004, Jun 8). beta-Arrestin inhibits NF-kappaB activity by means of its interaction with the NF-kappaB inhibitor IkappaBalpha. *Proc Natl Acad Sci U S A, 101*(23), 8603-8607. https://doi.org/10.1073/pnas.0402851101

Xiao, K., McClatchy, D. B., Shukla, A. K., Zhao, Y., Chen, M., Shenoy, S. K., Yates, J. R., 3rd, & Lefkowitz, R. J. (2007, Jul 17). Functional specialization of beta-arrestin interactions revealed by proteomic analysis. *Proc Natl Acad Sci U S A, 104*(29), 12011-12016. https://doi.org/10.1073/pnas.0704849104

Xu, Q., Ming, Z., Dart, A. M., & Du, X. J. (2007, May-Jun). Optimizing dosage of ketamine and xylazine in murine echocardiography. *Clin Exp Pharmacol Physiol, 34*(5-6), 499-507. https://doi.org/10.1111/j.1440-1681.2007.04601.x

Yamamoto, K., Hashimoto, K., Nakano, M., Shimohama, S., & Kato, N. (2002). A distinct form of calcium release down-regulates membrane excitability in neocortical pyramidal cells. *Neuroscience, 109*(4), 665-676. https://doi.org/10.1016/s0306-4522(01)00486-9

Yang, S., Ben-Shalom, R., Ahn, M., Liptak, A. T., van Rijn, R. M., Whistler, J. L., & Bender, K. J. (2016, Aug 9). beta-Arrestin-Dependent Dopaminergic Regulation of Calcium Channel Activity in the Axon Initial Segment. *Cell Rep, 16*(6), 1518-1526. https://doi.org/10.1016/j.celrep.2016.06.098

Yang, S., Zhou, G., Liu, H., Zhang, B., Li, J., Cui, R., & Du, Y. (2013). Protective effects of p38 MAPK inhibitor SB202190 against hippocampal apoptosis and spatial learning and memory deficits in a rat model of vascular dementia. *Biomed Res Int, 2013*, 215798. https://doi.org/10.1155/2013/215798

Yoon, E. J., Gerachshenko, T., Spiegelberg, B. D., Alford, S., & Hamm, H. E. (2007, Nov). Gbetagamma interferes with Ca2+-dependent binding of synaptotagmin to the soluble N-ethylmaleimide-sensitive factor attachment protein receptor (SNARE) complex. *Mol Pharmacol, 72*(5), 1210-1219. https://doi.org/10.1124/mol.107.039446

Zahm, D. S., & Heimer, L. (1990, Dec 15). Two transpallidal pathways originating in the rat nucleus accumbens. *J Comp Neurol, 302*(3), 437-446. https://doi.org/10.1002/cne.903020302

Zhang, J., Ferguson, S. S., Barak, L. S., Aber, M. J., Giros, B., Lefkowitz, R. J., & Caron, M. G. (1997). Molecular mechanisms of G protein-coupled receptor signaling: role of G protein-coupled receptor kinases and arrestins in receptor desensitization and resensitization. *Receptors Channels, 5*(3-4), 193-199. https://www.ncbi.nlm.nih.gov/pubmed/9606723

Zheng, H., Loh, H. H., & Law, P. Y. (2008, Jan). Beta-arrestin-dependent mu-opioid receptor-activated extracellular signal-regulated kinases (ERKs) Translocate to Nucleus in Contrast to G protein-dependent ERK activation. *Mol Pharmacol, 73*(1), 178-190. https://doi.org/10.1124/mol.107.039842

Zon, L. I., & Peterson, R. T. (2005, Jan). In vivo drug discovery in the zebrafish. *Nat Rev Drug Discov, 4*(1), 35-44. https://doi.org/10.1038/nrd1606

Zurkovsky, L., Sedaghat, K., Ahmed, M. R., Gurevich, V. V., & Gurevich, E. V. (2017, Jul 15). Arrestin-2 and arrestin-3 differentially modulate locomotor responses and sensitization to amphetamine. *Neuropharmacology, 121*, 20-29. https://doi.org/10.1016/j.neuropharm.2017.04.021

VITA

Mee Jung Ko was born May, 14th 1990 to Dr. Young Tae Ko and Yun Ja Woo in Seoul, Korea. After her graduation from Hyewha girls' senior high school in 2009, she attended Konkuk University in Seoul, Korea where she graduated with a Bachelor of Science in Biological Sciences in 2013. Upon graduation, she joined Dr. Chan-Young Shin's laboratory at Konkuk University and pursued her Master of Science in Neuroscience. In Dr. Shin's lab, she investigated molecular mechanisms of pro-social behavior in stress-mediated behavioral dysfunction, and she was also involved in numerous projects developing novel therapeutics for excitatory and inhibitory imbalance in mice models of autistic spectrum disorders. In 2015, she started her predoctoral training at Purdue University Interdisciplinary Life Science Ph.D. Program (PULSe) with a focus on integrative neuroscience. In the following year, she joined Dr. Richard M. van Rijn's laboratory, where she later obtained her Doctor of Philosophy in Medicinal Chemistry and Molecular Pharmacology. In Dr. van Rijn's lab, she investigated molecular and cellular mechanisms of G protein-coupled receptor signaling in the modulation of anxiety, fear, and pain. These studies were published in multiple peer-reviewed journals and preprints including Scientific Reports, Frontiers in Cellular Neuroscience, and BioRxiv, and part of the studies was supported by the Collaborative Research Award from Purdue Institute for Integrative Neuroscience and the Purdue Research Foundation Grant. During her predoctoral training, she was also awarded multiple travel awards including A.H. Ismail Interdisciplinary Program Doctoral Research Travel Award, Chaney Graduate Student Travel Award, Helmsley Scholarship, and numerous travel awards from academic societies to attend national and international conferences. With these supports, she also attended Ion Channels in Synaptic & Neural Circuit Physiology course at the Cold Spring Harbor Laboratory to gain insights on neurophysiology. Besides her career in research, she gave multiple lectures in undergraduate/graduate-level courses and mentored numerous undergraduate students in the lab, and her passion for teaching was recognized by the Outstanding Graduate Student in Teaching Award from the Office of Interdisciplinary Graduate Program at Purdue University.

PUBLICATIONS

MJ Ko, T Chiang, AA Mukadam, GE Mulia, AM Gutridge, JA Chester, RM van Rijn, (2019) β-arrestin-dependent ERK signaling positively correlates with reduced anxiety-like and conditioned fear-related behavior in mice, BioRxiv

MJ Ko, RM van Rijn, (2019) Response: Commentary: Commonly used anesthesia/euthanasia methods differentially impact MAPK signaling pathway in C57BL/6 male and female mice, Frontiers in Cellular Neuroscience

MJ Ko†, GE Mulia†, RM van Rijn, (2019) Commonly used anesthesia/euthanasia methods differentially impact MAPK signaling pathway in C57BL/6 male and female mice, Frontiers in Cellular Neuroscience (†Equal Contribution)

MJ Ko†, LC Ganzen†, E Coskun, YF Leung, RM van Rijn, (2019) A critical evaluation of TRPA1-mediated locomotor behavior in zebrafish as a screening tool for novel anti-nociceptive drug discovery, Scientific Report (†Equal Contribution)

AM Gutridge, MT Robins, RJ Cassell, R Uprety, KL Mores, **MJ Ko**, S Majumdar, RM van Rijn, (2019) G protein-biased kratom-alkaloids and synthetic carfentanil-amide opioids as potential treatments for alcohol use disorder, British Journal of Pharmacology

JW Kim, K Park, RJ Kang, EL Gonzales, HA Oh, H Seung, **MJ Ko**, JH Cheung, CH Chung, CY Shin, (2019) Gene-environmental interaction produces mutual offsetting effects on social impairments in animal models of autism, Scientific Report

JW Kim†, **MJ Ko**†, EL Gonzales†, RJ Kang, DG Kim, Y Kim, H Seung, HA Oh, PH Eun, CS Shin, (2018) Social interaction rescues acute stress-induced cognitive impairments by modulating ERK1/2 phosphorylation in adolescent mice, Scientific Report (†Equal Contribution)

MT Robins, T Chiang, JN Berry, **MJ Ko**, J Ha, RM van Rijn, (2018) Behavioral characterization of β-arrestin 1 knockout mice in anxiety-like and alcohol behaviors, Frontiers in Behavioral Neuroscience

JW Kim, K Park, RJ Kang, EL Gonzales, DK Kim, H Seung, HA Oh, **MJ Ko**, KJ Kwon, KC Kim, SH Lee, CH Chung, CY Shin (2018) Pharmacological modulation of AMPA receptor rescues social impairments in animal models of autism, Neuropsychopharmacology

JW Kim, HA Oh, SH Lee, KC Kim, PH Eun, **MJ Ko**, EL Gonzales, H Seung, S Kim, GH Bahn, CY Shin, (2018) T-type calcium channels are required to maintain viability of neural progenitor cells, Biomolecules & Therapeutics

JW Kim, H Seung, KC Kim, EL Gonzalesa, HA Oh, SM Yang, **MJ Ko**, SH Han, S Banerjee, CY Shin, (2017) Agmatine rescues autistic behaviors in the valproic acid-induced animal model of autism, Neuropharmacology

EL Gonzales, JH Jang, DF Mabunga, JW Kim, **MJ Ko**, KS Cho, JH Ryu, GH Bahn, M Hong, HJ Kim, JH Cheong, CY Shin, (2016) Supplementation of Korean Red Ginseng improves behavior deviations in adolescent mice models of Autism, Food and Nutrition Research

CS Choi, P Kim, JH Park, EL Gonzales, KC Kim, KS Cho, **MJ Ko**, SM Yang, H Seung, SH Han, JH Ryu, and JH Cheong, (2015) High sucrose consumption during pregnancy induced ADHD-like behavioral phenotypes in mice offspring, Nutritional Biochemistry

YR Lim, IH Kim, S Han, HG Park, **MJ Ko**, YJ Chun, CH Yun, and D Kim, (2015) Functional significances of cytochrome P450 1A2 Allelic Variants, P450 1A2*8, *15, and *16 (R456H, P42R, and R377Q), Biomolecule & Therapeutics

JW Kim, H Seung, KJ Kwon, **MJ Ko**, EJ Lee, HA Oh, CS Choi, KC Kim, EL Gonzales, JS You, DH Choi, J Lee, SH Han, SM Yang, JH Cheong, CY Shin, and GH Bahn, (2014) Subchronic treatment of donepezil rescues impaired social, hyperactive, and stereotypic behavior in valproic acid induced animal model of Autism, PLOS ONE

CS Choi, M Hong, KC Kim, JW Kim, SM Young, H Seung, **MJ Ko**, DH Choi, JS Yoo, CY Shin, and GH Bahn, (2014) Effects of atomoxetine on hyper-locomotive activity of the prenatally valproate exposed rat offspring, Biomolecules & Therapeutics